

UNIVERSITÀ DEGLI STUDI DI NAPOLI “FEDERICO II”

*in consorzio con*

SECONDA UNIVERSITÀ DI NAPOLI  
UNIVERSITÀ “PARTHENOPE” NAPOLI

*in convenzione con*

ISTITUTO PER L’AMBIENTE MARINO COSTIERO – C.N.R.  
STAZIONE ZOOLOGICA “ANTON DOHRN”

Dottorato in Scienze ed Ingegneria del Mare

XXIV ciclo

Tesi di Dottorato

HYDRODYNAMICS AND MORPHODYNAMICS IN THE SWASH ZONE:  
HYDRALAB III LARGE-SCALE EXPERIMENTS

Relatore: Prof. Diego Vicinanza

Co-relatore: Prof. Maurizio Brocchini

Candidato: Ing. Pasquale Contestabile

Il Coordinatore del Dottorato: Prof. Alberto Incoronato  
ANNO 2011

## ABSTRACT

The modelling of swash zone hydrodynamics and sediment transport and the resulting morphodynamics has been an area of very active research over the last decade. However, many details are still to be understood, whose knowledge will be greatly advanced by the collection of high quality data under controlled large-scale laboratory conditions. The advantage of using a large wave flume is that scale effects that affected previous laboratory experiments are minimized.

In this work new large-scale laboratory data from two sets of experiments are presented. Physical model tests were performed in the large-scale wave flumes at the Grosser Wellen Kanal (GWK) in Hannover and at the Catalonia University of Technology (UPC) in Barcelona, within the Hydralab III program.

The tests carried out at the GWK aimed at improving the knowledge of the hydrodynamic and morphodynamic behaviour of a beach containing a buried drainage system. Experiments were undertaken using a set of multiple drains, up to three working simultaneously, located within the beach and at variable distances from the shoreline. The experimental program was organized in series of tests with variable wave energy. While a positive effect was observed under low energy conditions, for medium and high energy conditions the benefit of having the drains operative was not always clear. In any case, it was evident that any positive effect of the drains on the beachface was confined by the position of the cone of depression in the aquifer's surface.

The tests carried out in the large wave flume at UPC had the intent to investigate swash zone under storm conditions. The main aim was to compare beach profile response for monochromatic waves, monochromatic waves plus free long waves, bichromatic waves and random waves. Both erosive and accretive conditions were considered. The experiments suggest that the inclusion of long wave and wave group sediment transport is important for improved nearshore morphological modelling of cross-shore beach profile evolution, and provide a very comprehensive and controlled series of tests for evaluating numerical models. It is suggested that the large change in the beach response between monochromatic conditions and wave group conditions is a result of the increased significant and maximum wave heights in the wave groups, as much as the presence of the forced and free long waves induced by the groupiness. The equilibrium state model concept can provide a heuristic explanation of the influence of the wave groups on the bulk beach profile response if their effective relative fall velocity is larger than that of monochromatic waves with the same incident energy flux.

## THESIS OUTLINE

In Chapter 1 the dominant hydrodynamic forcing and resulting sediment transport mechanisms in the swash zone are identified and local and global hydro-morphodynamic phenomena are introduced. In Chapter 2 major emphasis is placed on illustrating the physical aspects directly considered in the two sets of experiments. Chapters 3 and 4 outline the experimental programs and fundamental results, followed by a more detailed discussion in Chapter 5. A final summary and future perspectives conclude the Thesis.

## KEYWORDS

Swash Zone, Large Wave Flume, Beach Drainage System, Long Waves, Wave Groups, Beach Morphodynamics, Sediment Transport, Surf Beat.

# CONTENTS

<b>1. The Swash Zone System</b>	<b>15</b>
1.1 Introduction	15
1.2 Swash zone boundary conditions	18
1.2.1 Underlying beach condition	21
1.2.2 From surf zone forcing to swash hydrodynamics: the role of inner surf boundary conditions	24
1.3 Superficial SZ Hydrodynamics	30
1.3.1 High- and low-frequency swash motion	30
1.3.2 Internal flow kinematics	37
1.4 Beach groundwater hydrodynamics	38
1.5 Asymmetries in SZ hydro- sediment dynamics	44
1.5.1 Sediment advection as a boundary condition for SZ	45
1.5.2 Uprush hydro-sediment dynamics	48
1.5.3 Backwash hydro-sediment dynamics	53
1.6 Beachface morphodynamics	56
1.6.1 Beachface morphology	56
1.6.2 Morphing feedback processes	59
1.7 Modelling sediment processes in the SZ	61
1.7.1 Water flow through a porous medium	62
1.7.2 Forces on sediment particles	63
1.7.3 The flow-bed interaction	66
1.7.4 Sediment transport models	70
<b>2. Literature review</b>	<b>76</b>
2.1 The Beach Drainage System	76
2.2 Influence of free long waves, bichromatic wave groups and random waves	79
<b>3. Swash zone response induced by different groundwater regimes: large-scale experiments at GWK</b>	<b>84</b>
3.1 Experimental procedure and setup	84
3.1.1 Wave flume and instrumentation	84
3.1.2 Measurement instruments	90
3.1.3 Test program	100
3.1.3.1 Static tests	100
3.1.3.2 Dynamic tests	102
3.2 Pre-processing and data analysis	108
3.2.1 Signal processing	108

3.2.2	Groundwater Hydrodynamics Measurement methods	122
3.2.3	Morphodynamic Measurement methods	125
3.3	Results	126
3.3.1	Hydrodynamic response	126
3.3.1.1	Water table and wave set up	126
3.3.1.2	Hydraulic regime of drains Undertow current profiles	129
3.3.1.3	Wave set up	132
3.3.1.4	Undertow current profiles	133
3.3.1.5	Analysis of surf beat	136
3.3.2	Morphodynamic response	138
3.3.2.1	Morphodynamic analysis under High Energy conditions	138
3.3.2.2	Morphodynamic analysis under Medium Energy conditions	146
3.3.2.3	Morphodynamic analysis under Low Energy conditions	150
<b>4.</b>	<b>Swash Zone Response induced by long waves, wave groups and random waves: large-scale experiments at LIM</b>	<b>154</b>
4.1	Experimental procedure and setup	154
4.1.1	Wave flume and instrumentation	154
4.1.2	Test program	161
4.2	Data analysis	167
4.3	Results	170
4.3.1	Hydrodynamic results	170
4.3.1.1	Waves data	170
4.3.2	Morphodynamic results	172
4.3.2.1	Erosive conditions	172
4.3.2.2	Accretive conditions	178
4.3.2.3	Morphological pattern	181
4.3.3	Sediment dynamic results	184
4.3.3.1	Cross-shore Sediment transport patterns	184
4.3.3.2	Total net sediment transport direction and magnitude	191
<b>5.</b>	<b>Discussion and Conclusions</b>	<b>197</b>
5.1	Discussion	197
5.1.1	Large experiment at GWK	197
5.1.2	Large experiment at CIEM	198
5.1.3	Implication on SZ modeling	202
5.2	Summary of key results and Conclusion	208
	References	212

## Acknowledgements

This large scale experiment at GWK and at CIEM has been supported by European Community's Sixth Framework Programme through the grant to the budget of the Integrated Infrastructure Initiative HYDRALAB III within the Transnational Access Activities, Contract no. 022441.

The Author is grateful to participants from all other partners in the projects carried out at GWK, and particularly to: Paolo Ciavola (Università di Ferrara), Leonardo Damiani (Politecnico di Bari), Paolo Veltri and Francesco Aristodemo (Università della Calabria), Rui Taborda and Ana Silva (University of Lisbon), Gonzalo Malvarez (University Pablo de Olavide), Lincoln Heitman and Charles Lemckert (Griffith University), Mouncef Sedrati and Elisa Fontana (Università di Ferrara), Alessandra Saponieri and Marino L'Abbruzzi (Politecnico di Bari), Vincenzo Ferrante (Seconda Università di Napoli), and Biancamaria Verbeni (Università della Calabria).

The Author also thank the other members of the SUSCO project: Tom Baldock and Hannah Power (University of Queensland, Australia), Maurizio Brocchini and Matteo Postacchini (Università Politecnica delle Marche, Italy), Josè Alsina and Ivan Caceres (UPC, Spain), Peter Frigaard and Thomas Lykke Andersen (Aalborg University, Denmark), Daniel Conley and Peter Ganderton (University of Plymouth, United Kingdom), and Paolo Ciavola (Università di Ferrara, Italy), Quim Sospedra (UPC).

The Author show appreciation for the Technical Staff at the GWK and CIEM for their assistance with planning and running the experiments.

Finally, I am heartily thankful to my supervisor, Prof. Diego Vicinanza (Seconda Università degli Studi di Napoli) whose encouragement, guidance and support from the initial to the final level enabled me to develop this doctoral thesis. I wish to say a special thank you to my co-supervisors Prof. Maurizio Brocchini (Università Politecnica delle Marche) and Prof. Ciavola (Università di Ferrara) for the many useful comments and suggestions provided, and to my colleagues Dr. Vincenzo Ferrante (Seconda Università degli Studi di Napoli) and Dr. Francesco Aristodemo (Università della Calabria) for their continued support.

This thesis would not have been possible without the help and support of my family. Above all, I would like to thank my wife Tiziana for her personal support and great patience at all times. This thesis is dedicated to my son Gianfranco, who has been a great source of motivation and inspiration (especially at night...).

## Declarations

Part of the work presented in this thesis is being published as:

Baldock, T. E., Alsina, J., Cáceres, I., Vicinanza, D., Contestabile, P., Power, H., Sanchez-Arcilla, A. (2011). "Large-scale experiments on beach profile evolution and sediment transport induced by long waves, wave groups and random waves", *Coastal Engineering*, ISSN 0378-3839, vol. 58, pp. 214-227.

Ciavola P., Vicinanza D., Aristodemo F., Contestabile P., (2011). "Large-scale morphodynamic experiments on a Beach Drainage System", *Journal of hydraulic research*, Vol. 49, n. 4, pp. 523-528.

Contestabile, P., Aristodemo, F., Vicinanza, D., Ciavola, P. (2011). "Laboratory study on a beach drainage system", *Coastal Engineering*, ISSN 0378-3839, vol. ??, pp. ???-??? (submitted).

Vicinanza, D., Baldock, T. E., Contestabile, P., Alsina, J., Cáceres, I., Brocchini, M., Conley, D., Andersen, T. L., Frigaard, P., Ciavola, P. (2011). "Swash Zone Response Under Grouping Storm Conditions", *Journal of Hydraulic Research*, ISSN 0022-1686, vol. 00, pp. 1-9.

For any errors or inadequacies that may remain in this work, of course, the responsibility is entirely my own.

# Abbreviations

2D → Two Dimension

3D → Three Dimension

ALT → Altimeter

ADV → Acoustic Doppler Velocimeter

AWG → Acoustic Wave Gauge

\_A → Accretive sea state condition

B\_ → Bichromatic waves

BG → Beach Groundwater

C\_ → Combination waves

ECM → Electromagnetic Currentmeter

\_E → Erosive sea state condition

HE → High Energy sea state condition

LE → Low Energy sea state condition

LFW → Low Frequency Waves

ME → Medium Energy sea state condition

M\_ → Monochromatic waves

NSWE → Nonlinear Shallow Water Equations

OBS → Optical Backscatter Sensor

P → Piezometer

pt → pressure transducer

R\_ → Random waves

SBCs → Shoreline Boundary Conditions

SM63 → Shen and Meyer (1963)

SZ → Swash Zone

WG → Wave Gauges

## List of symbols

$a$  = wave amplitude

$A$  = pump station area

$A_c$  = arbitrary constant

$A_e$  = water particle semi-excursion

$A_L$  = normalised advection lengths

$A_s$  = cross sectional area facing the flow

$b$  = beach width

$B$  = Bagnold's dimensionless parameter

$c$  = local instantaneous sediment concentration

$c_z$  = sediment concentration at a distance  $z$  from the bed

$C$  = efficiency of the bore collapse coefficient

$C_D$  = drag coefficient

$C_f$  = constant friction factor

$C_M$  = extra mass coefficient

$C_0$  = reference sediment concentration at the bed

$d$  = water depth

$d_a$  = aquifer depth

$D$  = particle diameter

$D_s$  = diameter of the related spherical particle

$D_z$  = flow depth

$D_1$  = Schlichting (1979)'s constant

$D_{50}$  = mean sand diameter

$E(t)$  = half of square wave envelope function

$f$  = frequency

$f_p$  = peak frequency

$f_r$  = empirical friction factors

$f_{sw}$  = frequency of the incident bores or swash frequency

$f_w$  = wave friction factors

$F$  = seepage force

$F_g$  = gravity force

$F_p$  = pressure force

$F_{p,x}$  = pressure force in a horizontally accelerated fluid  
 $F_L$  = buoyancy force per unit of volume  
 $g$  = gravity acceleration  
 $G$  = group-based surf-similarity parameter  
 $GF$  = groupiness factor  
 $h$  = hydraulic head  
 $H$  = incident wave height  
 $H_b$  = breaker height  
 $H_B$  = height of the incident bore at the point of collapse  
 $H_h$  = total hydraulic head  
 $H_{rms}$  = root mean square wave height  
 $h_s$  = wave set up  
 $H_s$  = significant wave height  
 $H_{m0}$  = spectral wave height  
 $H_0$  = deep water wave height  
 $I$  = hydraulic gradient  
 $I_l$  = total load sediment transport rate  
 $i_n$  = integer in the range 1-3  
 $I_{wb}$  = immersed weight sediment transport during backwash per unit meter beach width  
 $I_{wu}$  = immersed weight sediment transport during uprush per unit meter beach width  
 $k$  = permeability coefficient  
 $K$  = hydraulic conductivity  
 $k_b$  = backwash sediment transport calibration coefficient  
 $k_u$  = uprush sediment transport calibration coefficient  
 $k_w$  = wave number  
 $L_0$  = deep water wavelength  
 $l_s$  = mixing length scale  
 $M$  = mass  
 $M_s$  = solid fraction  
 $m_0$  = zeroth-order moment of wave power spectrum  
 $n$  = power of exponential function  
 $N$  = number of short waves in the group  
 $N_T$  = total number of sampling values

$N'$  = sampling number between the first and the last zero-upcrossing points of the recording

$N_0$  = Dean parameter

$p$  = phases correlation parameter

$P$  = available fluid power

$p_w$  = dynamic water pressure

$\bar{p}_w$  = mean dynamic water pressure

$P_0$  = offshore mean wave energy flux

$q$  = sediment transport rate

$Q$  = net time-averaged sediment transport

$Q_m$  = mean drained discharge

$r$  = roughness

$R$  = runup height

$Re$  = Reynolds number

$R_s$  = saturated runup height

$s$  = relative density of sediment

$S$  = horizontal swash excursion or swash length

$S_g$  = average sand grain sphericity

$s_p$  = mean wave steepness

$S_p$  = pressure spectra

$s_y$  = specific yield

$t$  = time

$T$  = incident-wave period

$\hat{T}$  = swash period to wave period ratio

$T_b$  = backwash duration

$T_B$  = time it takes the largest wave to reach the shore after breaking

$T_G$  = sum of the periods of the waves in the group

$\hat{T}_G$  = swash-LFW interaction parameter

$t_m$  = mean time between pump cycles

$T_m$  = mean wave period

$T_s$  = swash period

$T_p$  = peak wave period

$T_u$  = uprush duration

$u$  = horizontal component of velocity

$U$  = representative stream velocity  
 $\bar{u}$  = mean horizontal flow velocity  
 $u_b$  = mean backwash velocity  
 $u_{bs}$  = near bed free stream velocity  
 $u_m$  = peak velocity under the wave  
 $u_{max}$  = maximum horizontal flow velocity  
 $u_{min}$  = minimum horizontal flow velocity  
 $u_s$  = instantaneous horizontal sediment velocity  
 $u_u$  = mean uprush velocity  
 $u_*$  = friction velocity  
 $U_0$  = initial speed of the shoreline  
 $U_l$  = infiltration/exfiltration velocity per unit area  
 $v$  = vertical component of velocity  
 $\bar{v}$  = mean vertical flow velocity  
 $V$  = particle volume  
 $V_m$  = mean drained volume  
 $v_{max}$  = maximum vertical flow velocity  
 $v_{min}$  = minimum vertical flow velocity  
 $x (m)$  = horizontal coordinate  
 $x_l$  = lowest rundown during a cycle  
 $x_h$  = highest runup during a cycle  
 $y^*$  = instrument depths  
 $y^*_t$  = beach depths for the specific test  
 $w$  = vertical outflow velocity  
 $w_f$  = vertical fall velocity  
 $w_i^j$  = sediment volume per meter of cross-shore section at step  $j$  between points  $i$  and  $i+1$   
 $W^j$  = sediment volume per meter of cross-shore section at step  $j$   
 $w_{\Delta h}$  = rising velocity  
 $z$  = vertical coordinate  
 $Z_R$  = relative bathymetric variation  
 $z_0$  = bed roughness length  
 $\%inf$  = infiltrated swash volume expressed as a percentage  
 $\alpha$  = energy scale parameter

$a_s$  = vertical amplitude of the shoreline motion  
 $\beta$  = beach slope  
 $\gamma_f$  = peak-enhancement factor  
 $\Gamma$  = dimensionless sediment volume variation  
 $\gamma$  = local wave height to depth ratio  
 $\Delta h$  = water table lowering over static level  
 $\Delta t$  = time difference between measurement intervals or time step  
 $\Delta V$  = net sediment volume variation  
 $\Delta x$  = spatial resolution  
 $\Delta z$  = relative vertical variation of bed level  
 $\Delta z_b$  = difference in bed elevation between measurement intervals  
 $\partial h$  = change in hydraulic head  
 $\partial x$  = change in  $x$  coordinate  
 $\varepsilon$  = Miche parameter  
 $\varepsilon_b$  = Guza and Inman surf scaling parameter  
 $\varepsilon_s$  = eddy diffusivity of the sediment  
 $\acute{\varepsilon}_b$  = bed load efficiencies  
 $\acute{\varepsilon}_s$  = suspended load efficiencies  
 $\zeta_s$  = normalized net sediment transport in swash zone (emerged beach)  
 $\zeta_t$  = normalized net sediment transport in surf/swash zone  
 $\eta$  = wave setup  
 $\eta_{\max}$  = maximum surface elevation  
 $\eta_{\min}$  = minimum surface elevation  
 $\bar{\eta}_w$  = mean surface elevation  
 $\eta_w$  = sea surface elevation  
 $\theta$  = Shields parameter  
 $\theta_c$  = threshold (critical) value for the Shields parameter  
 $\theta_s$  = modified Shields parameter  
 $\theta_w$  = wave phase  
 $\kappa$  = von Karman's constant  
 $\lambda$  = linear sediment concentration  
 $A$  = dimensionless sediment flux  
 $A_{T/2}$  = dimensionless average transport over a half cycle

$\mu_3$  = skewness of surface elevation  
 $\mu_{3,p}$  = skewness of dynamic pressure  
 $\mu_{3,u}$  = skewness of horizontal flow velocity  
 $\mu_{3,v}$  = skewness of vertical flow velocity  
 $\mu_4$  = kurtosis of surface elevation  
 $\mu_{4,p}$  = kurtosis of dynamic pressure  
 $\mu_{4,u}$  = kurtosis of horizontal flow velocity  
 $\mu_{4,v}$  = kurtosis of vertical flow velocity  
 $\nu$  = kinematic viscosity  
 $\xi$  = surf similarity parameter or Iribarren number,  
 $\varphi$  = friction angle  
 $\varphi_r$  = random variable  
 $\pi$  = Pi Greco constant  
 $\rho$  = water density  
 $\sigma$  = spectral width parameter  
 $\sigma_p$  = standard deviation of dynamic pressure  
 $\sigma_u$  = standard deviation of the horizontal flow velocity  
 $\sigma_v$  = standard deviation of the vertical flow velocity  
 $\sigma_w$  = standard deviation of surface elevation  
 $\sigma_\varphi$  = standard deviation of the grain size in  $\psi_d$  units  
 $\zeta$  = porosity  
 $\tau$  = instantaneous bed shear stress  
 $\tau(o)$  = steady bed shear stress  
 $\tau_b$  = bottom shear stress  
 $\psi$  = pressure head  
 $\Psi$  = sediment mobility number  
 $\psi_d$  = negative logarithm to base 2 of  $D_{50}$   
 $\omega$  = angular wave frequency  
 $\Omega$  = effective relative fall velocity parameter  
 $\Omega_e(s)$  = value of  $\Omega$  for equilibrium conditions  
 $\Omega_{max}$  = maximum value of  $\Omega$

# 1. The Swash Zone System

## 1.1 Introduction

Waves reaching a coastline release the majority of their energy and momentum within the surf zone as intense turbulence is generated at the front face of the breaker. However a portion of that energy is converted to potential energy and momentum is transferred to low frequency modes (like LFW, longshore currents, rip-currents, shear waves, etc.) (Brocchini, 2002). The breaking, in fact, drives a shallow flow which approaches the shoreline in the form of runup (Hunt, 1959). This intermittent advance and recede of the shoreline, which expresses the superficial beach response due to final dissipation (or reflection) of individual waves, is termed swash motion or simply swash. The term swash is generally used also to describe the flow within the relatively thin lens of water that moves up and down the beach in connection with the shoreline (e.g., Hughes and Turner, 1999; Butt and Russell, 2000; Elfrink and Baldock, 2002; Masselink and Puleo, 2006). The spatial domain which experiences the swash motion is termed swash zone (SZ hereinafter).

There is no precise definition of the seaward edge of the SZ. Puleo et al., (2000) suggested that the swash starts where the turbulence associated with final wave breaking (bore) begins to influence local sediment transport. Most researcher, however, reference the SZ as the location where the bore associated with this wave breaking intersects the shoreline. In this way the SZ can be defined as either the part of the beach between the wave runup (uprush) and rundown (backwash) around the mean water level (Homan, 1986). The mean position of the shoreline is approximately located where the mean water surface in the surf zone due to wave setup intersects the beachface (Guza and Thornton, 1981; Nielsen, 1989). The shoreline motion about this mean position occurs in relation to waves of varying frequency (wind waves, swell, and infragravity waves) as well as the tide (Guza and Thornton, 1982; Hughes and Turner, 1999; Elfrink and Baldock, 2002). Based on the latter definition, the SZ is well-defined only for monochromatic waves, whereas for real sea states rundown, runup, and setup vary constantly with time. Here, therefore, the swash zone is loosely defined as that part of the beach alternately covered and exposed by uprush and backwash. However, the reference to rundown and runup is commonly accepted for whatever sea state, referring respectively to the minimum and maximum values in a implied time window that includes all sub-tidal frequencies of shoreline oscillation, but is stationary with respect to the tide. The region between the SZ and the location of final wave breaking can be

defined as the zone of bore propagation. On steep reflective beaches this zone may essentially coincide with the SZ, but on intermediate and dissipative beaches they are substantially different. The nature of incident short-wave bores with some remaining group structure (Watson and Peregrine, 1992) and their relationship to processes in the SZ is thus dependent on site-specific conditions, in particular the beach morphodynamic state (Jackson et al., 2004). Indeed, the time scale of swash motion is highly variable and ranges from seconds on calm, steep and reflective beaches (e.g., Hughes et al., 1997a), to minutes on energetic, low-gradient and dissipative beaches (e.g., Butt and Russell, 1999).

SZ flows are responsible for:

- beachface morphodynamics (e.g. Greenwood and Hale, 1980; Sherman et al., 1993; Ciavola et al., 1997);
- overwash and overtopping of barrier islands and coastal defense structures (e.g. Guza and Thornton, 1982; Roos and Battjes, 1994; Fucella and Dolan, 1996, Ciavola et al., 2005; Stockdon et al., 2006 and references therein);
- longshore sediment transport near the shoreline (Bodge and Dean, 1987; Kamphuis, 1991, Van Wellen et al., 2000);
- local scouring at the base of coastal structures placed near the shoreline (Fredsoe and Sumer, 1997, Fucella and Dolan, 1996, Ciavola et al., 2005);
- the burial and dispersal of sediment-bound contaminants (Dolphin et al., 1995).

However, it is now fairly well established that SZ flows are of fundamental importance not only because of their local effects but also because they can affect the entire surf zone dynamics as a whole (e.g., Elfrink and Baldock, 2002; Bellotti and Brocchini, 2005; Masselink and Puleo, 2006; Brocchini and Baldock, 2008). Indeed, the hydro/morpho-dynamic processes of the surf zone and SZ, are strongly linked through feedback processes. This leads that the SZ system cannot be considered in isolation from the surf zone, and vice versa. However, SZ has traditionally received less attention than surf zone. Probably this is partly due to a cultural approach of coastal research, focused on the larger surf zone and its most spectacular wave transformation, the breaking, neglecting the analysis of the SZ, considered as a very narrow strip of lesser importance. Nevertheless, research on the SZ is difficult because of the complexity of the processes themselves (Elfrink and Baldock, 2002) as well as of the highly transient nature of the swash flows and the strongly nonlinear nature of sediment transport processes (Pritchard, 2009). Furthermore, analysis of SZ data is impeded by difficulties in measuring hydrodynamic quantities and sediment transport. In fact, performing

high-quality field measurements is complicated by the intermittent nature of swash flow but also by the various modes of transport involved, including bed load and suspended load, sheet flow and even single-phase flow at the end of the backwash (Hughes et al., 1997b). As a result, since SZ includes the littoral overflow processes, its analysis was initially devoted to the wave runup forecast as primary factor in the coastal structures design (e.g. Guza and Thornton, 1982; Roos and Battjes, 1994). In fact, the roots of the SZ flow study can be traced to attempts since the 60's to expose a parameterization of maximum uprush limit (e.g. Hunt, 1959). Only recently, the renewed attitude for addressing environmental issues has recognized a more important role to the SZ. In fact, short and long term predictions of the beachface are crucial in management, environmental sensitivity assessment and protection, recreational and commercial use of the coastal zone. Swash flow provides the principal mechanism for cross-shore sediment exchange between the subaerial and sub-aqueous zones of the beach (Masselink and Hughes, 1998). Sediment concentrations are often several orders of magnitude higher in the SZ than in the inner-surf zone (Osborne and Rooker, 1999; Beach and Sternberg, 1991). Additional reasons for which SZ processes are important are related to the influence of the SZ dynamics on the ecology of the intertidal zone (McArdle and McLachlan, 1992) and groundwater levels in subaerial littoral beaches (Nielsen, 1999). Finally, the SZ may define legal boundaries (Morton and Speed, 1998). Nowadays, there is the perception that the SZ represents one of the most scientifically challenging marine environments for describing sediment transport (Puleo et al., 2003) and considerable efforts have been made to improve the state of knowledge of swash zone transport processes (see the reviews by; Elfrink and Baldock, 2002; Masselink and Puleo, 2006 ,Brocchini and Baldock, 2008). However, many important aspects remain unclear.

The Thesis presents new large-scale laboratory data from two sets of experiments, both supported by the European Community's Sixth Framework Programme through the Integrated Infrastructure Initiative HYDRALAB III.

The tests carried out at the GWK aimed at improving the knowledge of the hydrodynamic and morphodynamic behaviour of the beach containing a buried drainage system. In order to avoid scale effects, which are still a major source of error when working with sediments, tests were carried out in the large wave flume "Grosser Wellen Kanal" (GWK) of Coastal Research Centre (FZK) of Leibniz University Hannover and Technical University Braunschweig. Due to the fact that there were two proposals submitted for GWK (<http://www.fzk.uni-hannover.de/fzk.html>), HYIII-GWK-05 (Experiments on Sediment Depth

Of Disturbance for beaches under the influence of Drainage Systems - ESDODDS coordinated by P. Ciavola) and HYIII-GWK-06 (Infiltration and exfiltration on the beachface coordinated by L. Damiani) with similar topics, model setup and same rating, the access was shared between these two teams to avoid double supporting. It was decided that one project would concentrate on morphological aspects while the other one would study the hydraulic performance of the system.

The second large-scale model tests were carried out at the Maritime Engineering Laboratory (LIM) at the Catalonia University of Technology (UPC) during July-October 2009. The project, titled: “SUSCO: Swash zone response Under grouping Storm COnditions”, was coordinated by D. Vicinanza. The experiments were designed specifically to compare variations in beach profile evolution between monochromatic waves and unsteady waves with the same mean energy flux. The scope is to derive information on the influence of long waves, bichromatic wave groups and random waves on sediment transport in the surf and swash zones.

## 1.2 Swash zone boundary conditions

The boundary condition forcing the SZ system (as a unique hydro-morphodynamic system) can be referred to as two primary “sources”: the *underlying beach conditions* and the *inner surf zone hydro-sediment dynamics*, both acting over different space-time scale. The underlying beach conditions give account of the local sediment characteristics and of the porewater pressure related to the beach groundwater hydrodynamics. The inner surf zone hydro-sediment dynamics include the in/out coming hydrodynamics (comprising the remaining short-wave group structure following breaking and surf dissipation, the low frequency waves, the amount and structure of bores, the currents, the tidal excursions and the related sediment concentration) and the advection of sediments. The region where the potential effective pickup zone for pre-suspended sediment takes place is defined by the advection length. Figure 1.1 illustrates a simple conceptual scheme to easily describe the main interactions into the SZ system, also in the perspective of modelling purposes. The underlying beach conditions are proposed as the fulcrum of the system because, through the sediment characteristics and the terrestrial watertable level, define the main features for the beach morphology and the beach groundwater dynamics. The forcing of the SZ sediment dynamics

system are represented by the hydrodynamics and by the sediment advection coming from the inner surf zone, respectively discussed in more detail in section 1.2.2 and 1.5.1.

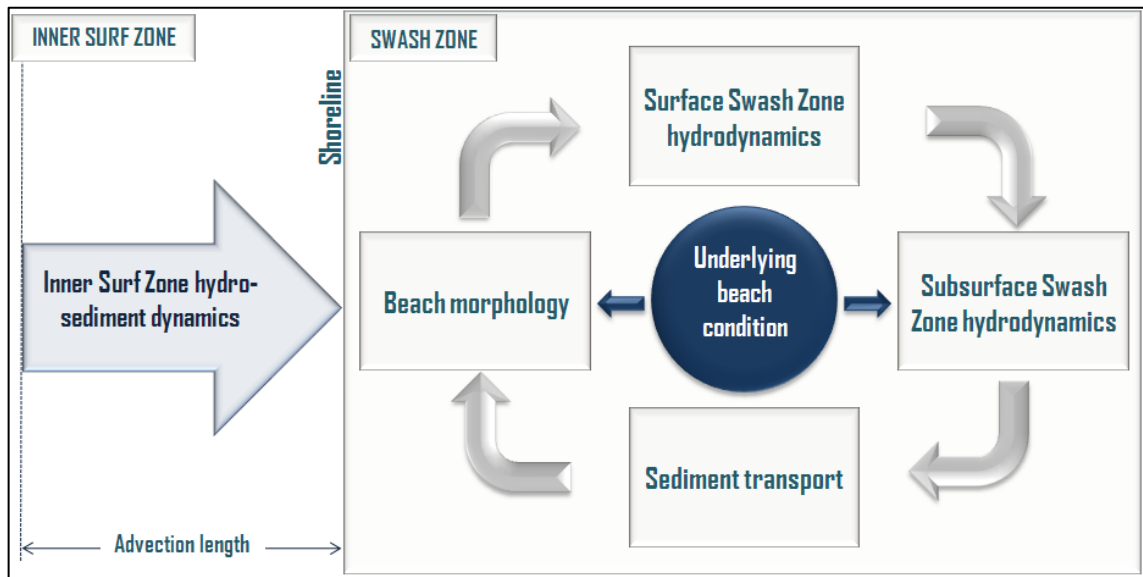


Figure 1.1. Schematic of the SZ system.

This scheme considers changes of beach morphology as an iterative result. Each iteration involves three main steps. First, the main flow patterns in the SZ are derived on the basis of the incoming hydrodynamics from inner surf zone and the exiting beachface morphology. In this phase, also the advection of sediment must be considered as primary factor affecting asymmetry in the SZ sediment dynamics. Secondly, the local sediment transport rates are computed from the SZ flows and sediment characteristics, which interact through the beachface. The SZ flows (tangential and perpendicular to the beach surface) are the results of two mutually interacting systems, the surface and the subsurface SZ (i.e. superficial SZ hydrodynamics and beach groundwater hydrodynamics). Thirdly, the local sediment transport rates allow the calculation of morphological change.

The one-way sequential coupling approach used for this conceptual model makes use of some simplifying assumptions. First, the nearshore hydrodynamics appears not affected by the fluxes across the beachface. This may be justified in simplified modelling approaches, because the pore water flow velocity across the interface of the porous medium is much smaller than the water velocity in the nearshore zone. The second and more critical assumption is that the shape of the beachface is dynamically updated only after the sediment transport calculations. In other words, the beach morphology is not modified during the swash and groundwater flows simulations. Vice versa, both direction and magnitude of the fluxes

across the interface and the swash velocity are not significantly affected by changes in the beachface morphology. Obviously, this assumption might be reasonable under certain conditions (Horn et al., 2007), i.e. when the local slope change induced by erosion/deposition of sediments is small compared to the mean beachface slope. However, this is not always the case. Indeed, when the beachface changes strongly in time, the terms controlling the level of sediment transport (i.e., normal/shear stress balance on the surface) are modified.

A two-way coupling of the three models (hydrodynamics, groundwater flow, sediment profile change) might be required for a dynamic updating of beachface morphology during the flows modeling. Since the time stepping would always be controlled by the stiffest sub-module, the resulting simulation would be extremely demanding in terms of computational time. However, comparison carried out Bakhtyar et al., (2011) between numerical model and experimental observations reported by Ang et al., (2004) and Horn et al. (2007), show that the two-way coupling is not necessary and the simplifications introduced do not strongly affect model simulations.

In the perspective of beachface morphing, many Authors (e.g. Larson et al., 2004; Masselink and Puleo, 2006) define the SZ as the hydrodynamic equivalent of the beachface (often also called foreshore). Although the beachface is the morphologically-active part of the beach that is shaped by the hydrodynamic forces and related sediment transport patterns in the SZ, the beachface does not represent a SZ boundary. In contrast with the surf zone, in which the bottom defines an impermeable boundary, the SZ control volume is not inferiorly defined by the bottom. Thus, the beachface should be treated as an intermediate permeable surface totally included in the SZ, by which are identified a superficial and a subsurface zone, with completely different (but interacting) hydrodynamics.

Hence, when it comes to SZ dynamics, four different dynamics are considered: superficial SZ hydrodynamics (or simply SZ hydrodynamics) (discussed in detail in Section 1.3 and, looking at the factors affecting SZ sediment transport, in Section 1.7), subsurface SZ hydrodynamics (or beach groundwater dynamic) (see Section 1.4), sediment dynamics (in Section 1.5, with specific emphasis on swash asymmetry and 1.7 concerning conceptual aspects for modelling purposes) and co-related beachface morphodynamic (reviewed in Section 1.6).

The objective of this short review is to provide an overview of the cross-shore hydro-sediment dynamic processes and ensuing morphological change in the SZ of natural sandy beaches. In addition, parametric and empirical modelling of cross-shore SZ sediment transport

are discussed. The role of longshore swash flows and the development of three-dimensional beachface morphology are, therefore, not addressed. Further, the review neither focuses on the tidal effect and the stochastic prediction of maximum runup.

### 1.2.1 Underlying beach condition

Elfrink and Baldock (2002) claimed: "...the dominant boundary condition for the swash zone may be considered to be the hydrodynamics of the inner surf zone". Although this point of view can be widely shared for engineering purposes, the basic question summarised by Masselink and Puleo (2006): "Why are some beaches steep and others shallow?", appears to be not adequately solvable by only accounting for the inner surf zone hydrodynamics. Therefore, although sometimes neglected or only implicitly accounted for, more attention should be paid to the conditions of the underlying beach. While detailed models are still being developed, simpler approach to sediment transport have been in use for some time. The most famous of these is the so-called CERC formula. One interesting aspect of the CERC formula is that it works without considering the size of the sand (see "The CERC Formula Paradox, Nielsen (1988b)). However, other classical transport models based on gradient diffusion and the assumption of flat bed, e.g. Deigaard et al., (1986), predict a very strong grain size dependence.

In particular, the role of the grain size appears to be important as it largely affects the hydro-morphodynamics at various scales. Generally speaking, it seems that the influence of the sediment size correlated phenomena on the SZ hydro-morphodynamics, increases with the increase of the grain size. Two main types of conditions describing the underlying beach are to be considered: one associated with the sediment characteristics and a second one related with the undisturbed groundwater level (terrestrial watertable). The latter is simply described in terms of the elevation of the watertable in correspondence of a point sufficiently far from the SZ flows to be taken as "undisturbed". Its effect can be ascribed to the changes in the saturation degree inside the beach.

The sediment characteristics, on the other hand, can be given in terms of many parameters. These are: density, internal friction angle, cohesion, particle size and size sorting, shape, chemical composition, porosity, biological activity (Gourlay, 1992; Horn, 2002). However, when analysing the more practical applications, both cohesion and biological activity can be neglected. Moreover, for a simplified approach, the particle shape, size sorting,

chemical composition and porosity can be substituted by some “global or integral parameters” like the static angle of repose, the hydraulic penetration index and the hydraulic conductivity. All strongly affect the beach stability, albeit with differ modality, and hence they will be treated separately. While no direct function exists to correlate the friction angle to the sediment characteristics, direct empirical relations are available which link the sediment properties to the hydraulic penetration index and to the permeability.

The static angle of repose (or natural slope angle),  $\varphi_s$ , is classically defined as the maximum angle at which the soil will lie in the shape of a static mound without slipping. It is determined by the ratio between the effective normal stress,  $\sigma_e$ , and the maximum sustainable shear stress,  $\tau_{max}$ . The angle  $\varphi_s$  is used to characterize either dry sand or sand which is entirely under water. Unsaturated sand may stand at a much steeper angle because the negative porewater pressure increases the effective normal stress. The angle  $\varphi_s$  increases with the packing material. Generally speaking, the range of  $\varphi_s$  for sandy materials is between 26 and 34 degrees; for example, Hanes and Inman (1985b) suggested a typical value of 31 degrees for beach sand. In other words, it is a stability factor, which directly acts on the beach slope and bed forms, which, in turn, influence the inner surf zone hydro-morphodynamics and the related sediment transport, sediment that is successively advected in the SZ.

The hydrodynamic penetration coefficient affects the fluid drag/stabilization force. Commonly the hydrodynamic penetration coefficient is substituted by the *equivalent Nikuradse roughness* or briefly the hydraulic roughness,  $r$ . In fact, in the modelling purposes, it is generally necessary to apply a simplified description of bed geometry, and in the extreme, often it tries to summarise the bed geometry in terms of a single length. The only bed geometry for which the definition of roughness is obvious is a layer of densely packed spheres for which the roughness equals the grain diameter, i.e.  $r = D_{50}$ . For all other geometries, the definition is indirect. It is found, through indirect experimental measurement of energy dissipation and available friction data, that the roughness of natural sand bed is generally one or two orders of magnitude larger than that of sand paper with the same sand size. In those cases, the great roughness is obviously due to bedforms which generate roughness of the order of their height (Carstens et al., 1969; Lofquist, 1986). The same Authors, however, found that also flat, mobile sand beds (as the beachface) dissipate wave energy at a high rate and thus, in this sense, appear very rough, particularly at high flow intensities. Therefore, flat beds in oscillatory flow generally exhibit roughness values (based on total friction or total energy dissipation rates) of the order 100 to 200 grain diameters. This

is somewhat surprising because the corresponding roughnesses in steady flows are generally one order of magnitude smaller and, therefore, in the different flow history during uprush and backwash should also be taken into account.

The hydraulic conductivity,  $K$ , is the specific discharge per unit hydraulic gradient. It is a coefficient of proportionality which reflects the ease with which a liquid flows and the ease with which a porous medium permits the liquid to pass through it, and relates the mean discharge flowing through a porous substance per unit cross-section to the total gravitational and potential force (Horn, 2002). Hydraulic conductivity should be distinguished from permeability (also referred to as intrinsic or specific permeability), denoted by  $k$ , which is the measure of the ability of a rock, soil or porous substance to transmit fluids and refers only to the characteristics of the porous medium and not to the fluid which passes through it. Many empirical formulas are available to relate the permeability to some measure of the representative grain size. A commonly used formula is that of Kozeny and Carman (1935), in which  $k$  is function of the mean grain size and sorting, as follows:

$$k = 760D_{50}^2 e^{1.31\sigma_\phi} * 9.87 * 10^{-13} \quad [1.1]$$

where  $D_{50}$  is the mean grain size in millimeters,  $\sigma_\phi$  is the standard deviation of the grain size in  $\psi_d$  units ( $\psi_d = -\log_2 D_{50}$ ).

An equivalent method relates the permeability of the sand bed to its porosity,  $\zeta$ , to the average sand grain sphericity,  $S_g$ , and to the diameter of the related spherical particle,  $D_s$ , by the Kozeny–Carman equation:

$$k = \frac{D_s^2 S_g^2 \zeta^3}{150(1 - \zeta^2)} \quad [1.2]$$

The hydraulic conductivity is then given by:

$$K = \frac{kg}{\nu} \quad [1.3]$$

where  $\nu$  is the kinematic viscosity of sea water and  $g$  is acceleration due to gravity.

Sediment suspension under steady flows and wave motion is governed by forces acting on the individual sediment grains. For non-cohesive sands, these forces include gravity, the surface drag force, forces due to pressure gradients in the fluid, the lift force due to flow over the sediment grain and the infiltration force (Obhrai and Nielsen, 2002). Contrasting results are found in the literature. Experiments carried out by Martin (1970), comparing quartz sand (2.65 N/mc) and nickel particles (8.75 N/mc) with similar diameters (0.58 mm), have shown

that the heavier the particles the higher the incipient motion threshold. Experimental observations on the stabilizing force as function of the grain size only and neglecting the density (i.e. by comparing sediments of the same density) have shown an increase in the stabilizing force with the decrease in grain size (and therefore hydraulic conductivity) (Nielsen, 1997, 2001; Horn, 2002). However, Hardisty (1990) and Baldock and Holmes (1997) have shown how the inertial forces may become significant for coarse grain sizes for which Elfrink and Baldock (2002) pointed out that the coarser the sediment, the larger the weight and, hence, the stabilizing force. An explanation for such an apparent contradiction might be that on natural beaches the balance between stabilizing and mobilizing forces on sediment particles is dependent on several factors, which act simultaneously as a whole but with different ways in function of grain size, density and hydraulic conditions.

### 1.2.2 From surf zone forcing to swash hydrodynamics: the role of inner surf boundary conditions

Real sea states are constituted by both short and long (free and bound) waves. Thus, the swash motion is driven by both low frequency infra-gravity motions and short-period bores which collapse at the shoreline and then propagate up the beachface.

Physical modelling of natural sea states has primarily been based on regular and random wave tests. However, only random wave simulations, with a specified wave spectrum, are representative. Hence, following this concept, a diagram showing the transfer of random waves energy into SZ oscillations is depicted in Figure 1.2.

Incident short waves can contribute to both the high- and low frequency oscillations (Elgar et al., 1992; Herbers et al., 1995a; Ruessink, 1998). In the first case, short waves shoal and break in the surf zone and drive *swash component* oscillations at a frequency similar to the incident frequency. In the second case, low frequency oscillations can be addressed to two main components:

- 1) *Wave group component*, driven by wave groups due to breakpoint variation (Shah and Kamphuis, 1996; Baldock and Holmes, 1999);
- 2) *Swash interaction component*, due to both uprush/backwash interactions (Carlson, 1984; Erikson et al., 2005) and bore overtaking/capture (Bradshaw, 1982).

Incident long wave motions are generally manifested as shoreline reflections and observed as a *standing wave component* to the low frequency swash signal (Suhayda, 1974; Huntley, 1976).

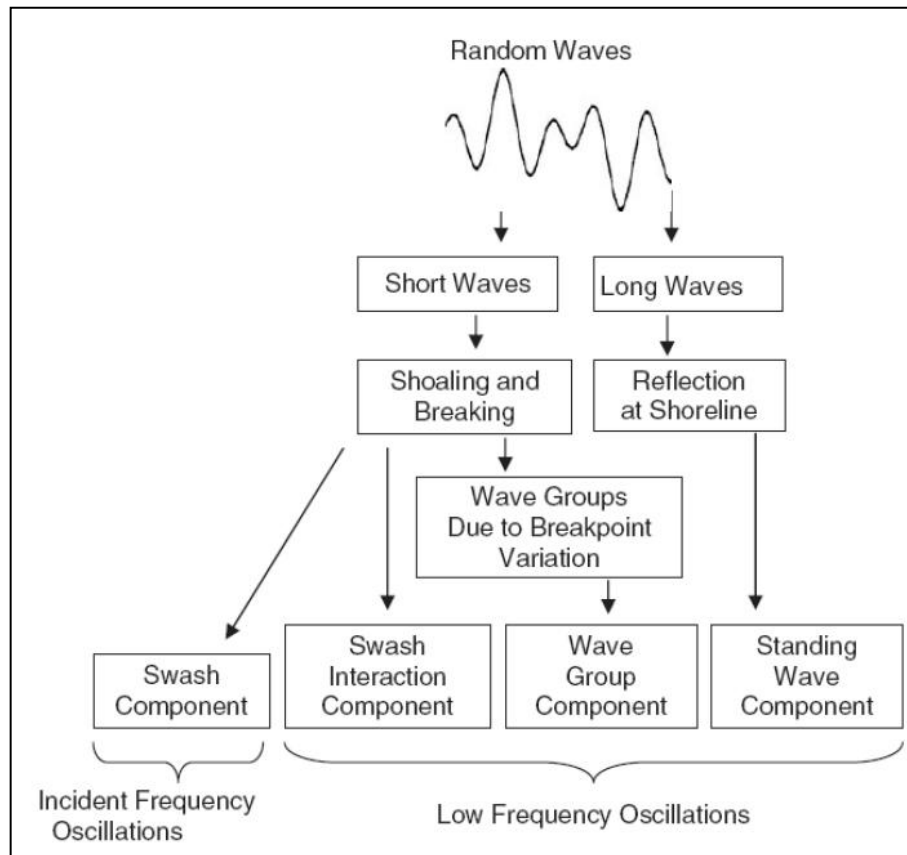


Figure 1.2. Schematic showing transfer of random wave energy into SZ oscillations (adapted from Masselink and Puleo, 2006).

First observations outside the surf zone of the long-period waves were carried out by Munk (1949) and Tucker (1950), and were termed surf beat due to a correlation with variations in the incident short wave height or wave grouping (Longuet-Higgins and Stewart, 1962, 1964; Gallagher, 1971; Symonds et al., 1982; Schaffer, 1993; Lippmann et al., 1997) of high and low waves breaking further shoreward (Munk, 1949; Tucker, 1950). Surf beat is particularly significant in the nearshore zone, since long waves can modify the incident short-wave field (Goda 1975; Peregrine 1983; Dally and Dean 1986) and strongly influence sediment transport patterns. Random wave breaking occurs over a broad range of space-time-scales and considerable uncertainty remains as to which surf-beat mechanisms are important or dominant during more realistic conditions (Battjes 1988; Hamm et al. 1993).

Infragravity energy may propagate cross-shore (leaky waves) (Suhayda, 1974; Guza and Thornton, 1985; Holland et al., 1995; Raubenheimer and Guza, 1996), be refractively trapped (edge waves) (Huntley et al., 1981; Oltman-Shay and Guza, 1987; Herbers et al., 1995b) or induce a mixture of both modes. Finally, low frequency motions include shear waves (Oltman-Shay et al., 1989). Long waves may enhance shoreline erosion (Osborne and Greenwood 1992) and, due to reflection, lead to the formation of longshore bars, beach cusps and more complex morphology (Holman and Bowen 1982; O'Hare and Huntley 1994; Yu and Mei 2000).

Which type of motion dominates the swash depends on the relative magnitudes of short and long wave energy in the inner surf zone, which in turn is dependent on the offshore wave conditions, and hence to a large extent on wave groupiness (List, 1991; Elftink and Baldock, 2002).

To a first approximation, the scale of the dominant wave motion in the inner surf zone is determined by whether the surf zone is saturated (i.e. short wave heights depth limited) or unsaturated (i.e. local wave height independent of depth) (Goda, 1975; Wright and Short, 1984; Raubenheimer and Guza, 1996). The transition between a saturated surf zone and unsaturated surf zone depends primarily on the relative beach slope in the surf which may be approximately defined using the surf similarity parameter or Iribarren number,

$$\xi = \beta / \sqrt{H_0 L_0} \quad [1.4]$$

where  $\beta$ ,  $H_0$  and  $L_0$  are the beach slope, deep water wave height and deep water wavelength respectively and it is assumed that  $\tan(\beta) \approx \beta$ . (Iribarren and Nogales, 1949; Battjes, 1974). The formula, originally developed for monochromatic waves, has been widely applied to random waves substituting the deep water wave height with the spectral deep water significant wave height and computing the deep water wavelength by the spectral peak wave period. The Iribarren number predicts type of breaking wave, from spilling breakers ( $\xi < 0.4$ ), plunging breakers ( $0.4 < \xi < 2$ ) to surging breakers ( $\xi > 2$ ) (Fredsoe and Deigaard, 1992), that are strictly related to beach morphodynamic behaviour. For monochromatic waves, a saturated surf zone typically occurs for  $\xi < 0.5$ , whereas unsaturated conditions tend to occur for  $\xi > 0.5$  (e.g. Battjes, 1974), with slightly different values probably applicable for random waves. Unsaturated surf zone conditions frequently show a dominance of short wave energy in the inner surf zone (Bradshaw, 1980; Wright and Short, 1984; List 1991), with short wave bores reaching the shoreline (Hibberd and Peregrine, 1979; Kobayashi et al., 1989; Hughes,

1992; Baldock et al., 1998; Masselink and Hughes, 1998). In contrast, typical of gently sloping beaches, the hydrodynamics in the inner surf zone may be expected to be dominated by non-breaking low frequency waves (frequently termed infragravity waves) (Huntley et al., 1977; Guza and Thornton, 1982; Wright et al., 1982).

An alternative macro-scale approach to forecasting beach profile evolution derives from the heuristic model based on the relative fall velocity parameter,  $\Omega = H/w_f T$ , developed by Gourlay (1968) and Dean (1973).  $\Omega < 2$  characterizes reflective beaches, whereas  $\Omega > 5$  defines dissipative ones and  $2 < \Omega < 5$  characterizes intermediate beach states. Essentially,  $\Omega$  is a measure of the ability of the prevalent wave energy to erode sand (Jiménez et al., 2008). This bulk-response approach has since been adopted in more complex form through equilibrium state or relaxation models. These models have been used to describe the types of beach states, evolution of beach states, shoreline movement and sand bar behaviour by numerous authors, using either  $\Omega$  or other measures of wave energy (Sunamara, 1984; Wright et al., 1985; Larson and Kraus, 1989; Dalrymple, 1992; Plant et al., 1999, Miller and Dean, 2004; Yates et al., 2009). While the success of these bulk-response models for delineating short and long term periods of erosion or accretion in field conditions has been mixed, there is a strong inheritance from antecedent conditions which influences the correlation between the observed parameter and instantaneous  $\Omega$ , as does the response time of the system (Wright et al., 1985). Very recently, Yates et al. (2009) have shown that, for the same beach, i.e. constant  $w_s$ , either wave energy or  $\Omega$  discriminate well between erosive and accretive events if the antecedent beach with is accounted for. This form of model appears to be a more robust predictor of beach response for laboratory conditions (Hattori and Kawamata, 1980; Sunamara, 1984; Dalrymple, 1992). In part, this is probably because of the reduced complexity of the forcing, “steady” wave and water level conditions and measurement accuracy. However, in such experiments, the initial beach profiles are usually the same or very similar for all wave conditions. Therefore, the absence of the influence of antecedent beach conditions is very likely to be the key reason why such models perform better for laboratory conditions. Further, since the laboratory tests typically commence with an initially planar profile, the evolution of the profile to either a bar (erosion) or berm (accretion) profile is a clear indicator of the direction of the total net sediment transport (e.g. figure 4 of Dalrymple, 1992). Hence, if  $\Omega$  describes the profile response from plane conditions, it will also provide a good estimate of the transport direction and whether erosive or accretive conditions dominate (Baldock et al., 2011).

Another, but equivalent, method to predict which type of incident-wave conditions, uses the Guza and Inman surf scaling parameter  $\varepsilon_b$  (Guza and Inman, 1975)

$$\varepsilon_b = \frac{4\pi^2 H_b}{2gT^2 \tan^2 \beta} \quad [1.5]$$

where  $H_b$  is the breaker height,  $g$  is gravity,  $T$  is the incident-wave period and  $\tan \beta$  is the beach gradient. Values of  $\varepsilon_b > 20$  indicate dissipative conditions (swash characterized by standing longwave motion), whereas  $\varepsilon_b < 2.5$  indicate reflective conditions (swash dominated by incident-wave bores) (Wright and Short, 1984; see also Carter, 1988). In summary, swash driven principally by low frequency infragravity waves which frequently have a cross-shore standing wave structure (Huntley et al., 1977; Guza and Thornton, 1982; Holland et al., 1995; Raubenheimer et al., 1995) or edge waves (Bowen and Inman, 1971; Guza and Thornton, 1985) is clearly identified on mild slope dissipative beaches (low  $\xi$ ) because the short-wave energy is dissipated in a saturated surf zone where the short waves are depth limited. Conversely, swash due to bores which collapse at the shoreline and then propagate up the beachface (Shen and Meyer, 1963; Hibberd and Peregrine, 1979; Yeh et al., 1989; Hughes, 1992) appears on steep beaches. Nevertheless, the morphodynamic taxonomy with its reflective and dissipative end members provides a useful first order framework for discussing swash processes. However it disregards the transfers of energy from high to low frequencies that commonly occur on natural beaches (Mase, 1988). This is well summarised by Brocchini and Baldock (2008): “On reflective beaches (higher  $\xi$ ), LFWs may still dominate the shoreline motion, but in addition to the standing LFWs, there is a significant contribution from frequency downshifting in the surf zone, wave grouping remaining in the unsaturated inner surf zone and swash-swash interactions”. For example, Karunarathna et al (2005) found that the swash magnitude increases with increasing incident wave height even though the surf zone is fully saturated. Data on a steep beach of 1:10 collected by Baldock et al. (1997) show that, unless the surf zone is totally saturated, a significant proportion of the low frequency swash motion may be directly due to incident wave grouping and not standing long waves. Indeed, spectral analysis of both wave group and random waves shows that the low frequency motion of the shoreline may be an order of magnitude greater than that measured in the inner surf zone, inconsistent with cross-shore standing long waves. An explanation for this could be given by observation of Watson and Peregrine, (1992) which found the low frequency motion in the surf zone to be in phase with the incident wave grouping and may therefore be regarded as a time varying setup. As demonstrated by Baldock and Holmes (1999) through numerical

simulation of swash oscillations on a steep beach, the low frequency components of the runup can be modelled directly using a sequence of incident short wave bores, with no direct long wave input to the numerical simulations. That is, the low frequency motion of the shoreline provides an excellent approximation to the runup of individual bores and therefore describes the runup envelope. This suggests that wave groupiness must be accounted for when modelling shoreline oscillations. In addition, numerical experiments performed by Karunarathna et al., (2005) show that the swash magnitude increases with increasing incident wave height even though the surf zone is fully saturated. It seems that energy carried by low frequency waves still depends on the height of primary waves while saturation only influences energy carried by primary waves.

Many researchers discuss the suitability of employing the parameters  $\zeta$ ,  $\varepsilon_b$  or  $\Omega$  to identify morphological patterns. Although morphodynamic classification of beaches has achieved widespread acceptance in both geological and geomorphological literature some studies have shown that these parameters are not accurate predictors of morphodynamic beach states in beach environments (e.g. Anthony, 1998; Levoy et al., 2000; Masselink and Pattiaratchi, 2001; Jackson et al., 2005, Jiménez et al., 2008). Two reasons were found. First, these parameters take into account only part of the real hydrodynamic forcing, while beach morphology depends on several additional variables. Particularly when used in extremely large tidal ranges and low wave energy situations, the parameters involved in its construction are of relatively low importance in determining beach dynamics compared to factors such as tidal and winddriven currents (e.g. Anthony, 1998; Levoy et al., 2000; Masselink and Pattiaratchi, 2001). For low energetic marine environment, such as Mediterranean, it has been observed that  $\Omega$ -values alone do not provide a realistic prediction of beach states statistics (Gómez-Pujol et al., 2007). Indeed,  $\Omega$ -values fail in summer predictions while are in agreement for winter predictions, when waves have large peak periods and bigger significant wave height. Thus, Jiménez et al., (2008) suggest that the intensity of the forcing, represented by the wave energy level and the duration of the events, must also be taken into account. Secondly, it is widely acknowledged that the pioneering Write and Short's scheme (Write and Short, 1983; 1984) for classifying/differentiating beach states is also inaccurate (e.g. Ranasinghe et al., 2004). For example, Wright et al. (1987) found only a 36% agreement between observed and predicted intermediate beach states. Consequently, Bauer and Greenwood (1988) concluded that these parameters are useful in discriminating between reflective and dissipative extreme beach states, but do not adequately characterise

intermediate situations. Therefore, Anthony (1998) suggested that for full validation these parameters must be tested against a wide range of natural environments, and not only in the Australian coastal areas.

Therefore, more detailed considerations of the different frequency components in the surf and swash zones is reviewed in the following Section 1.3.1.

## 1.3 Superficial SZ Hydrodynamics

### 1.3.1 High- and low frequency swash motion

Consistent with the forcing at the seaward swash boundary, two broadly different types of swash oscillations have been identified: (1) swash motion resulting from the collapse of high-frequency bores on the beachface; and (2) swash motion characterized by non-breaking standing, low frequency waves (leaky or edge waves) (see Butt et al., 2005, for time series displaying these differences). Swash oscillations due to incident bores which collapse at the shoreline and propagate up the beach are typically observed at higher frequency ( $f > 0.05$  Hz) short waves (Shen and Meyer, 1963; Waddell, 1976; Hibberd and Peregrine, 1979; Bradshaw, 1980; Packwood, 1983; Mase, 1988; Yeh et al., 1989; Hughes, 1992, 1995; Brocchini and Peregrine, 1996; Madsen et al., 1997; Baldock and Holmes, 1999). Conversely, cross-shore standing long wave swash oscillations are usually forced by infragravity frequencies ( $f < 0.05$  Hz) waves (Suhayda, 1974; Huntley et al., 1977; Guza and Thornton, 1982; Holland et al., 1995; Raubenheimer and Guza, 1996; Baldock and Holmes, 1999), as are shoreline oscillations due to edge waves (Bowen and Inman, 1971; Huntley et al., 1981; Guza and Thornton, 1985; Oltman-Shay and Guza, 1987; Holland and Holman, 1999). Although wind-waves or short-waves (typical period of about 10 seconds) are the major forcing for the SZ dynamics, it has been recognized the importance of the SZ for the generation/transformation of long-period motions (Watson et al., 1992; Mase, 1995; Baldock et al., 1997; Brocchini, 1998). In the SZ, in fact, while the final dissipation of short-wave (wind and swell) energy occurs, the low frequency wave energy (typical wave periods between 30 and 300 s) is, generally, reflected back seaward. In addition, intense interaction between short waves and between short waves and long waves at the surf-swash boundary can lead to the generation and reflection of further low frequency waves (LFWs) (Watson et al., 1994; Mase, 1995). Both nonlinearity and groupiness of short waves are the major

mechanisms responsible for the generation of LFWs. These waves can be either “bound” or “free”. Bound LFW are generated with the short waves group (i.e., propagating at the group velocity) and these grow as they propagate shoreward (Longuet-Higgins and Stewart, 1962, 1964; Agnon, 1993). The bound waves are released to propagate freely when the short wave lose their energy by breaking, or when they propagate over depth changes such as bars (c.f. Watson and Peregrine, 1992). On the other hand, free long waves may be categorized as follow:

- 1) bound waves freed from the group structure by wave breaking which dissipates the short-waves,
- 2) free long waves formed by short waves interacting in the SZ (Watson et al., 1994),
- 3) breakpoint-forced long waves (see, e.g., Baldock, 2006, and references therein).

The first type is particularly significant in the case of a “saturated surf-zone”, where the low frequency motion of the shoreline is dominated by the runup of low frequency cross-shore standing waves (Brocchini, 2002). The second mechanism of LFW generation, by which frequency downshift occurs (Mase, 1995), is more important in the case of an “unsaturated surf-zone” because waves are not so strongly depth limited. In fact, since in shallow waters the wave velocity is proportional to the square root of the total water depth, large waves travel faster than small waves and catch them up hence producing a single wave. Using numerical and analytical models based on the higher-order nonlinear Schrödinger equation, Uchiyama and Kawahara (1994) have shown that the down-shift is caused by a dissipative correction term representing the damping of mean flow (or a low frequency wave component). Effects of the damping term are a drastic change in the characteristic of the sideband instability, i.e., a uniform wave train becomes unstable for any wave number of disturbance. The process of the frequency downshift for a narrow-band wave train, finite-band width waves and wind waves were seen to be “*local, abrupt, and discrete*” (Huang et al. 1996). The mechanism responsible for the frequency downshift in nonlinear wave evolution in general could be the “*wave fusion*”, an event described as two waves merging to form one wave, or  $n$  waves merging to form  $n-1$  waves. The wave fusion is also the same phenomena of the “lost crest” observed by Lake and Yuen (1978), and the “crest pairing” observed by Ramamonjiarisoa and Mollo-Christensen (1979). Specifically, the frequency downshift is an accumulation of wave fusion events. Other than the fusion process, the local frequency can have small variations due to the amplitude modulations. Hence, it has long been recognized that the frequency downshift in the wave field evolution is a consequence of nonlinear wave-wave interactions (Huang et al,

1996). The latter free LFWs are forced by time-varying radiation stress gradients. This, in fact, is negative to shoreward of the breaking point and positive seaward. LFWs are generated as the wave breaking point oscillates onshore and offshore during the passage of groups of low and high waves (Symonds et al., 1982; Watson and Peregrine, 1992; Shaffer, 1993, Brocchini, 2002).

As seen in the previous Section 1.1.2, swash motion may be due to both infragravity standing waves and short wave bores, with the dominance of one form of motion over the other controlled by the conditions in the surf zone, which may at least be distinguished qualitatively by  $\zeta$ , i.e. the parameter used to determine whether the surf is saturated or unsaturated. However infragravity wave amplitudes (both in the swash and further offshore) are not necessarily related to  $\zeta$ , but are generally linearly related to the offshore wave height (Goda, 1975; Guza and Thornton, 1982; Herbers et al., 1995a). This implies that the swash does not saturate at similar values of  $\zeta$  (Elfrink and Baldock, 2002). Consequently, the relationship between the magnitude of infragravity swash oscillations and  $\zeta$  may be site-specific (Raubenheimer and Guza, 1996; Ruessink et al., 1998) since infragravity energy is dependent on location (mild or steep beaches, broad or narrow continental shelves) (Herbers et al., 1995b). Therefore, how LFWs dominate swash flows depend not only on the Iribarren number, but also on the relative beach slope in the SZ, characterized by Miche parameter:

$$\varepsilon = \frac{a_s \omega^2}{g\beta^2} \quad [1.6]$$

where  $a_s$  is the vertical amplitude of the shoreline motion,  $\omega$  is the angular wave frequency ( $2\pi/T$ , where  $f$  is the wave frequency). The Miche parameter is a measure of the ratio of the shoreline acceleration to the downslope gravitational acceleration and can also be regarded as a swash similarity parameter (Brocchini and Baldock, 2008). Miche (1951), in fact, proposed that the swash would be saturated (i.e., overlap of following swashes) when the incident wave amplitude increased above the limiting amplitude for non-breaking standing waves on a slope, with additional incident wave energy completely dissipated by wave breaking. Saturation is expected to occur when the non-dimensional parameter  $\varepsilon$  reaches some critical value (Iribarren and Nogales, 1949; Miche, 1951; Huntley et al., 1977). In particular, Baldock and Holmes (1999) derived a theoretical value for  $\varepsilon \approx 2.5$ , in closer agreement with most of the experimental values, for both monochromatic and random wave bore runup. In this instance, swash saturation occurs due to the duration (and hence magnitude) of swash oscillations being

controlled by the amplitude and frequency of the incident bores, rather than surf zone saturation.

On natural beaches, the swash motion at both low and high frequencies is also dependent on the interaction between successive swash events and the interaction between standing waves and incident bores. Swash-swash interaction occurs between incident waves (with period  $T$ ) and the runup or backwash of preceding waves (Brocchini and Baldock, 2008). Three principal types of wave-swash interaction can be distinguished (Hughes and Moseley, 2007):

- 1) wave capture, in which a wave travelling over an existing swash lens is overtaken by a following wave;
- 2) wave-uprush interaction, in which an incoming wave crosses the front of a swash lens while it is advancing up the beach;
- 3) wave-backwash interaction, in which an incoming wave advances across the front of an existing swash lens as it is receding down the beach as backwash, leading to a merging of swash cycles and a progressive increase in swash period with decreasing Iribarren number (Holman, 1986; Mase, 1988) (Fig. 1.3). In particular, if the backwash from a large uprush event prevent the uprush of later smaller waves (Kubota et al., 1993), a weak interaction occurs. In contrast, when the interaction is strong (i.e. the incoming uprush is of the same magnitude of the receding backwash), it results in a stationary hydraulic jump near the seaward edge of the swash zone.

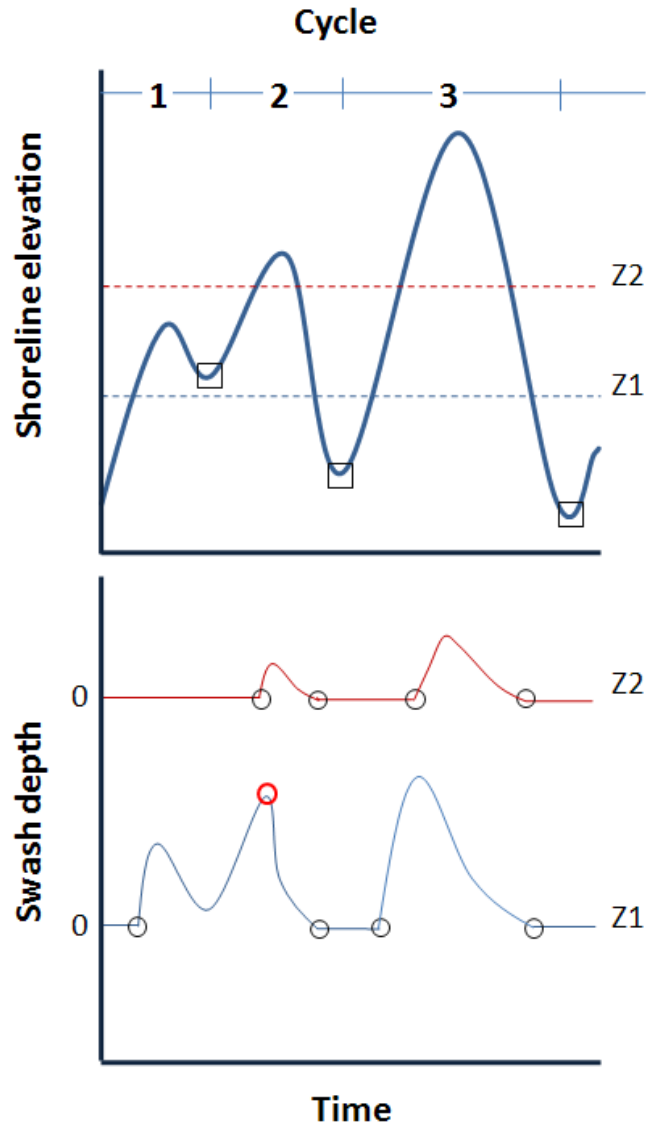


Figure 1.3. Schematic diagram defining a wave-swash interaction. Upper panel: shoreline elevation time series. Lower panel: water depth time series from two elevations Z1 and Z2 in upper panel. Note that Z2 is landward of Z1. Scales are arbitrary. Rundown used to delimit swash cycles are indicated by circles. Local swash events, defined by periods of bed immersion, are delimited by squares. Overrunning waves defined by secondary peaks within a local swash event are indicated by red circles. Wave-backwash interaction involves at the first square (adapted from Hughes and Moseley, 2007).

The wave-swash interaction generates a range of scales of new motion, from mean flows (swash setup) to LFWs, backwash bores and hydraulic jumps, and turbulence. This process of swash-swash interaction leads to further difficulties in determining how the swash forcing mechanism varies with the Iribarren number. For example, both Mase (1988) and

Baldock and Holmes (1999) showed that, due to wave grouping remaining in the inner surf zone, short wave bores could directly induce low frequency oscillations of the shoreline, even in the absence of low frequency waves in the surf zone (Elfrink and Baldock, 2002).

Theoretically, swash interaction occurs if the runup,  $R$ , exceeds the saturated runup height,  $R_s$ , given by Baldock and Holmes (1999):

$$R_s \leq \frac{g\beta^2}{8f_{sw}^2} \quad [1.7]$$

where  $f_{sw}$  is the frequency of the incident bores or swash frequency.

The degree of swash-swash interaction, in the frictionless case, is quantified through the natural swash period ( $T_s$ ) to wave period ( $T$ ) ratio:

$$\hat{T} = T_s/T \quad [1.8]$$

Small values of  $\hat{T}$  correspond to no interaction and values of  $\hat{T}$  greater than or equal to 1 correspond to strong interaction. The “natural swash period” is defined as the time for a runup/rundown cycle of a wave of given amplitude. For swash forced by non-interacting collapsing bores, and neglecting friction, Baldock and Holmes (1999) have shown how  $T_s$  appears to be a function of the bore height and speed at the mean water level shoreline, the beach slope, and gravitational acceleration. The initial speed of the shoreline,  $U_0$ , may be to some extent dependent on the nature of the bore collapse mechanism and hence the incident waves (e.g., uniform bores, undular bores or waves breaking onto the beach as shore breaks).  $U_0$  may therefore be written generally as:

$$U_0 = C\sqrt{gH_B} \quad [1.9]$$

where  $H_B$  is the height of the incident bore at the point of collapse,  $C$  is a coefficient which effectively describes the efficiency of the bore collapse and is expected to take a value in the range of 1 to 2 (see Baldock and Holmes, 1999). The duration or natural period of the swash,  $T_s$ , from the start of the uprush to the end of the backwash is then given by:

$$T_s = \frac{2U_0}{g \sin\beta} \quad [1.10]$$

$\hat{T}$  is usually greater than 1 except for long period swell on fairly steep beaches (Brocchini and Baldock, 2008). Swash-swash interactions is a complex matter but very important because they may also govern broader scale variations in the beach planform via morphodynamic/hydrodynamic feedback, in particular, the formation of beach cusps and

shore-connected bars (Masselink et al., 1997; Coco et al., 2000). However, the impact of these features on beach erosion and accretion remains to be determined. The interaction between the short-wave runup and standing long waves in the SZ, in fact, may be “constructive” or “destructive” in terms of both the hydrodynamics and beachface morphology. constructive interference occur when swash amplitudes and flow velocities increase due to the coincidence between short-wave runup (or backwash) and the runup (or drawdown) of the standing wave. In this case, the long waves move the short-wave runup zone across the beachface in a similar manner to the tide, significantly increasing the active SZ width. Destructive interference occurs if runup and backwashes oppose each other.

The presence of standing long waves in the SZ and inner surf zone from incident and reflected LFWs makes it difficult to determine if further LFWs are generated within the SZ itself (Brocchini and Baldock, 2008). Several observations (Baldock and Huntley, 2002; Battjes et al., 2004) show that the radiated LFWs are closely correlated reflections of the incident wave in the inner surf zone. This could suggest that LFW generation in the swash is not intense. The phenomenon of LFW generation in the SZ is strongly governed by an important time scale,  $T_G$ , sum of the periods of the waves in the group. To examine the correlation between wave group and LFW, in fact, Watson et al., (1994) introduces a group-based surf-similarity parameter,

$$G = T_G/T_B \quad [1.11]$$

where  $T_B$  is the time it takes the largest wave to reach the shore after breaking. A likely destructive interference should occur when  $G$  is small, which represents the condition where several groups may simultaneously be generating LFW. If  $G$  is large, there will only one or two waves in the surf zone at once, leading to little interaction and LFW generation is expected to be minimal. The strongest LFW generation is expected to occur when  $G$  is close to unity. Brocchini and Baldock (2008) suggest a parameter of swash-LFW interaction through a parameter of the form

$$\hat{T}_G = T_s/T_G = \hat{T}/N \quad [1.12]$$

where  $N$  is the number of short waves in the group. Analogously to  $G$ , significant LFW generation seem likely when  $\hat{T}_G$  is of order one. The values of  $\hat{T}$  vary between 1-3 for a wide range of wave condition and beach slope. Hence, in the SZ, significant LFW generation through shortwave interactions seems likely only for very short wave groups.

### 1.3.2 Internal flow kinematics

Three distinct timescales of scales and types of fluid motion may be present in the inner surf zone, which will subsequently govern shoreline oscillations and swash hydrodynamics (Battjes, 1988; Hamm et al., 1993; Svendsen and Putrevu, 1996; Bellotti et al., 2003; Brocchini and Baldock, 2008):

- 1) turbulent motions characterized by a timescale of about  $10^2$ - $10^1$  s;
- 2) wave motions (also known as short gravity waves) evolving on timescales of about  $10^0$ - $10^2$  s;
- 3) low frequency motions (low frequency waves, littoral currents, rip currents, and vertical motions) with periods ranging from about  $10^3$  to  $10^5$  s.

Recent studies of flow kinematics and sediment transport have identified clear differences in the nature of the outer and inner SZ. The outer swash included wave-swash interactions and the inner swash included only pure swash motion (i.e., free from interaction with subsequent waves) (Hughes and Moseley, 2007). Hence, particularly for the outer SZ, the advection of bore turbulence from inner surf hydrodynamic factors represents a fundamental feature of the inner surf kinematics which must be accounted for, without which no complete explanation of swash hydrodynamics and sediment transport could be realized. Turbulence is responsible of the highest frequency motions in the SZ, and are characterized by irregularity, diffusivity, rotation and dissipation (Bakhtyar et al., 2009). If turbulence impinges on the bed, can supply high shear stresses, representing an efficient sediment suspending mechanism that has been likened to a bulldozer (Nelson and Miller, 1974). This notion has been corroborated from studies that obtained suspended sediment concentrations on a natural beach and showed that the concentration was highest and nearly depth-uniform at the bore and leading edge of the swash where the turbulence is generated (Osborne and Rooker, 1999; Puleo et al., 2000; Voulgaris and Collins, 2000; Butt et al., 2004). The landward propagation of bores and their collapse at the beachface, the bed friction, backwash-generated bores and swash-swash interactions represent potential sources for turbulence. It is generally accepted that the turbulence may be classified into two main categories: free turbulence and wall turbulence. Although such a classification may appear reductive, it is necessary as makes it easier to study new phenomena by comparison with known phenomena (Petti and Longo, 2001).

Laboratory measurement of SZ hydrodynamics carried out by Petti and Longo, (2001) and Cowen et al., (2003) have suggested that breaking-wave induced (bore) turbulence dominates during the uprush. In fact, during runup, the Kolmogorov length scale increases

towards the bed indicating that dissipation is less important near the bottom than near the surface (Cowen et al., 2003; Petti and Longo, 2001). Furthermore, since the turbulent energy flux is essentially directed shore-ward and turbulent energy is much higher during uprush than during backrush (Petti and Longo, 2001), a lot of turbulence is expected to be advected in the SZ from combination of incoming highly turbulent flow (Battjes, 1975; Stive, 1980; Svendsen and Madsen, 1984; Svendsen, 1987; Svendsen and Putrevu, 1994; Ting and Kirby, 1996) and initial collapse generated turbulence (Yeh and Ghazali, 1988; Hughes et al., 1997a; Puleo et al., 2000), spreading downward toward the bed (Madsen and Svendsen, 1983; Svendsen and Madsen, 1984). Conversely, backwash turbulence is dominated by the growing boundary layer, and the wall turbulence appears to be the main source of turbulence generation (Petti and Longo, 2001), comparing well to the classic flat plate boundary theory near the bed. The formation of backwash bores (Shen and Meyer, 1963; Hughes, 1992) and hydraulic jumps due to swash-swash interactions (e.g. Osborne and Rooker, 1999) towards the end of the backwash/next runup, potentially enhance the backwash turbulence. In fact, Butt et al. (2004) found that the level of turbulence associated with the bore front were largest during the backwash/uprush transition and that the highest values of turbulent kinetic energy estimates occurred while the near-bed velocity was still offshore-directed. This confirms the idea of the surface-generated turbulence penetrating towards the bed (Longo et al., 2002) and of a increasing vorticity generation related to the surface shear waves due to flow separation from the bed towards the end of the backwash (Peregrine, 1974).

#### 1.4 Beach groundwater hydrodynamics

The beach groundwater (BG hereinafter) system is an unconfined aquifer (one in which the watertable forms the upper boundary) in which the responsible of flows are principally the hydrodynamics seaward, resulting from inner surf-swash interaction as tides, waves and swash itself. In fact in this process, in which flows are driven through saturated and unsaturated sediments, the atmospheric exchanges, such as evaporation and rainfall, and exchanges with deeper aquifers, loses importance with respect to an inland groundwater system. The key concepts are illustrated in Fig.1.4.

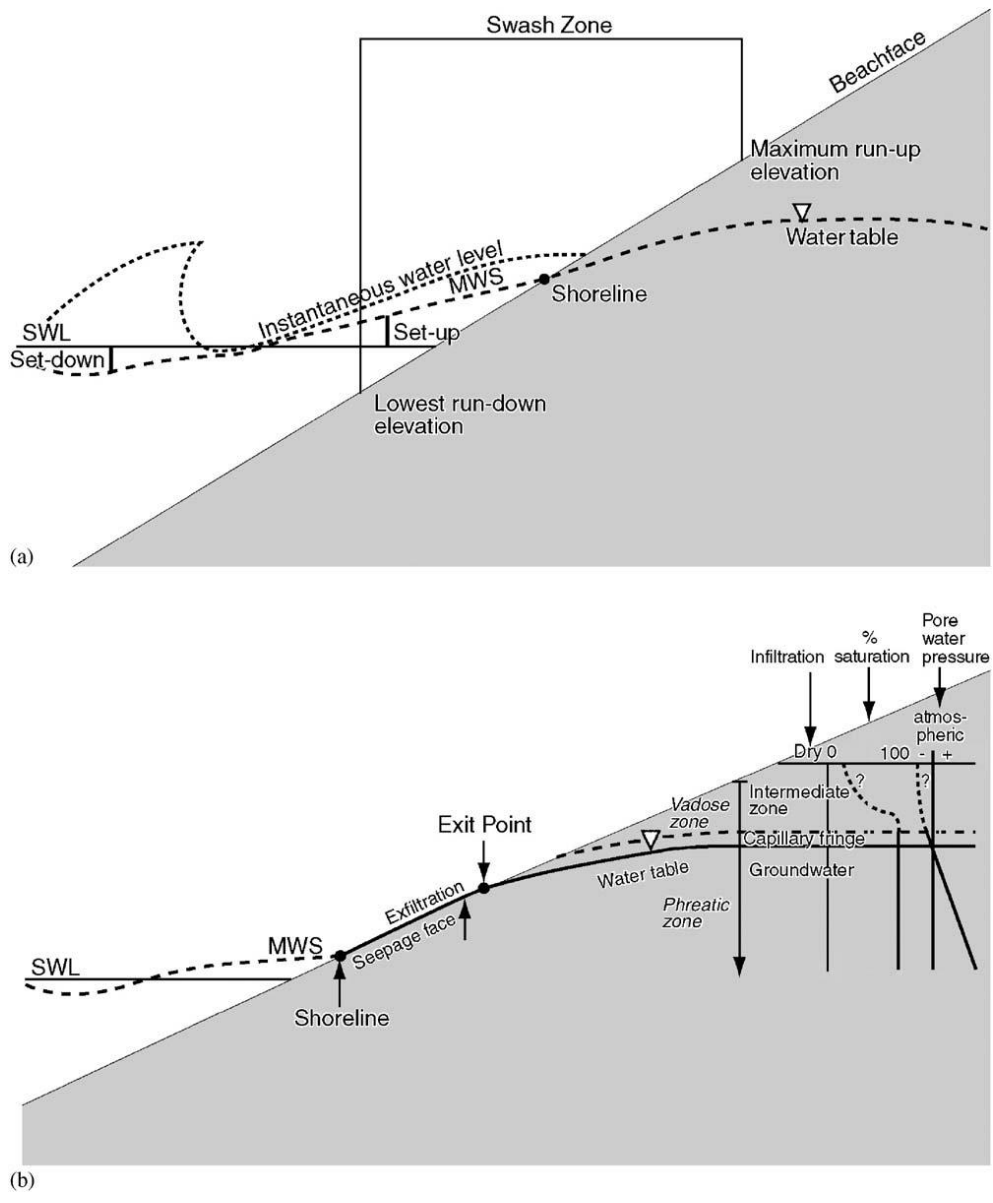


Figure. 1.4. a) Definition sketch of surface and subsurface water levels in the SZ. b) Definition sketch of beach ground water zones when the water table is decoupled from the tide (after Horn, 2006).

The mean water surface (MWS in Figure 1.4b) in the surf and swash zones generally has a gradient which balances the change in the radiation stress (Longuet-Higgins and Stewart, 1962, 1964). Changes in radiation stress are balanced by changes in hydrostatic pressure, i.e. by changes in water level. This difference is known as setup or set-down. The shoreline is the line of zero water depth at which the position where the MWS intersects the beachface. The beach watertable is generally considered to be the continuation of the MWS inside the beach (Horn, 2002) and therefore to have the same elevation as the tide. However, the tidal elevation generally drops more rapidly than the watertable elevation and decoupling occurs, with the

watertable elevation higher than the tidal elevation. The watertable is also referred to as the phreatic surface, which represents the permanently saturated zone. A definition physically correct of watertable is an equilibrium surface at which pore water pressure is equal to the atmospheric pressure. Below the watertable, therefore, a permanently saturated zone, where pore water pressure is greater than atmospheric pressure, is identified. Conversely, in the region of a beach sand body extending from the watertable to the sand surface, pore water pressure is less than atmospheric pressure. This region is not completely unsaturated. In fact, immediately above the watertable, the force of mutual attraction between water molecules and the molecular attraction between water and the surrounding sand matrix (suction) lead to developing of a capillary fringe (Price, 1985). In the capillary fringe, pore spaces are fully saturated, but the capillary fringe is distinguished from the watertable by the fact that pore water pressures are negative. For this reason, BG zones are better defined by pore water pressure distribution than by saturation levels. Finally, above the capillarity fringe, an unsaturated zone (also called vadose zone or zone of aeration) is identified. The thickness of the capillary fringe in sand beaches may vary between a few millimeters to nearly a meter, and it may extend to the sand surface. Some workers (e.g., Turner, 1993b) also refer to an intermediate zone which may occur above the capillary zone where the degree of saturation may vary, but remains less than 100%.

The presence of a capillary fringe has an important influences, especially when it lies just below the sand surface (Horn, 2006). In fact its presence can have a significant effect on the exchange of water between the ocean and the coastal aquifer, particularly in terms of the storage capacity of the aquifer. Many studies have demonstrated, in fact, that due to hysteretic water retention, capillarity affects watertable dynamics also at tidal frequencies (e.g. Nielsen and Perrochet, 2000a, b; Werner and Lockington, 2003). However, it is possible to neglect this influence (e.g. Barry et al., 1996; Li et al., 1997a). But the really important effect of a capillary fringe is the dispersion of watertable waves which occurs at higher frequencies. Field and laboratory observations (e.g. Nielsen and Turner, 2000; Cartwright et al., 2003, 2004b) have also shown that natural groundwater waves usually propagate faster and decay more slowly in aquifers with a capillary fringe. This effect, as it has been reported in some observations, could be due to the horizontal flows which also occur in the capillary zone.

BG can be considered at a range of scales: as a system in itself (subsurface flows), as a system that interacts with the swash (interaction between surface and subsurface flows), and as the interface between the land and the sea (interaction between the coastal aquifer and the

ocean) (Horn, 2006). In any case, the primary key characteristic of BG hydrodynamics is the hydraulic conductivity. As seen in Section 1.2.1, sediment characteristics play a fundamental role in BG, because entirely define the characteristics of the porous medium.

BG hydrodynamics are a result of combination between inner-surf hydrodynamics forcing and the terrestrial watertable (both already defined as boundary conditions) and the beach response correlated to the swash motion. As aforementioned, when the terrestrial watertable is referred to an appropriate extinction distance, it can be considered as a boundary condition for BG hydrodynamics. In the internal transition zone a time-varying water level occurs as a function of tide and waves at a range of frequencies. Swash-groundwater interactions allude to the presence of two distinct types of exchanges:

1. in/exfiltration across the saturated beachface below the location of the intersection between the water table and the beachface (i.e. the exit point; Turner, 1993);
2. infiltration of water into the unsaturated beach above the exit point.

This means that the inferior limit of the swash is not clearly determined, because also the flux under the exit point must be considered. In fact, watertable oscillations occur both for horizontal mass transport resulting from boundary condition changes at the beachface (tide-driven or change in terrestrial groundwater) and a local mass transfer across the watertable (wave-driven) (Li et al., 1997a). It is now well understood that these oscillations are related to how the beachface act as a frequency filter (Waddell (1976), Lewandowski and Zeidler (1978) and Hegge and Masselink (1991)). Investigations conducted on sandy beaches have demonstrated their faculty to selectively transmit lower frequencies, filtering higher frequencies (low-pass filter), causing a red-shifting of the spectra in the onshore direction. On the other hand, Blewett et al. (2001) and Horn et al. (2003) have clearly shown that by increasing the sediment size, an increasing presence of high-frequency watertable fluctuations may be registered. Waddell (1976), in particular, suggested that high frequency groundwater oscillations were forced by pressure transmission through the beachface induced by nearshore standing waves and also by the infiltration of swash-water through the beachface around the exit point. As suggested by Hegge and Masselink (1991), the pressure forces dominate seawards, where a mass pressure flux through saturated sands stabilizes a falling groundwater level. Conversely, landwards of the exit point, large swashes cause a rise in the groundwater table via vertical infiltration (or percolation).

Grant (1946, 1948) was among the first to suggest a link between beach groundwater behavior and SZ sediment transport. He noted the potential of beach groundwater fluctuations

to cause bed failure due to instantaneous and strong upward-acting force. However, implication of BG–swash dynamics on SZ sediment transport have been substantiated by researchers for many years (e.g., Bagnold, 1940; Shepard and LaFond, 1940; Emery and Foster, 1948; Longuet-Higgins and Parkin, 1962; Duncan, 1964; Otvos, 1965; Strahler, 1966; Schwartz, 1967; Harrison, 1969, 1972; Waddell, 1976; Chappell et al., 1979; Kirk, 1980; Clarke et al., 1984; Eliot and Clarke, 1986, 1988; Nordstrom and Jackson, 1990; Turner, 1990; Ogden and Weisman, 1991; Turner, 1993c, 1995a; Oh and Dean, 1994; Weisman et al., 1995). Most of these studies suggest that beaches with a low watertable tend to accrete and beaches with a high watertable tend to erode. Relative elevations of the beach watertable and swash induces cyclic erosion and accretion of the beachface, affecting the morphology of the beach by controlling the potential for offshore transport or onshore sediment transport and deposition above the still water level. The effect of swash infiltration on flow asymmetry was indirectly confirmed by Quick (1991), which found that the beachface gradient increases with the amount of swash infiltration. Indeed, infiltration loss in the swash is often given as the reason why gravel beaches are steeper than sand beaches (Horn 2007). Experimental observations from numerical modelling carried out by Masselink and Li (2001) confirm that the volume of infiltration into the beach during swash motion is directly related to the hydraulic conductivity. The lowering of the downrush limit due to infiltration is limited for less permeable sediments whereas the runup limit becomes significantly lower due to infiltration during wave uprush for more permeable sediments. Thus for both low and high  $K$ -values,  $R/H$  ( $R$  is runup elevation,  $H$  is wave height) is relatively small (Fig. 1.5a).

Because the swash lens is relatively shallow, a small change in water volume due to infiltration (or addition of water due to exfiltration) could influence uprush/backwash flow asymmetry and therefore the energy available for sediment transport (e.g. Bagnold, 1940; Grant, 1946; Grant, 1948; Duncan, 1964). Indeed, the difference in hydraulic head between the front and back faces of the grain defines a force (termed seepage force) acting on each individual grain (Freeze and Cherry, 1979). The seepage force,  $F$ , is exerted in the direction of flow and is given by:

$$F = \rho g \frac{\partial h}{\partial z} \quad [1.13]$$

where  $\rho$  is the density of the fluid and the hydraulic gradient  $\partial h/\partial x$  is the change in hydraulic head ( $h$ ) over distance. At the mid-swash position the swash flows velocity asymmetry  $u_u/u_b$  (where  $u_u$  and  $u_b$  are respectively the mean uprush and backwash velocity) progressively

increase from 1 to 1.8 with increasing hydraulic conductivity (Fig. 1.5b). The exit point on the beachface of this seepage force lags the rundown on all but the coarsest grained sandy beaches (Cartwright et al., 2006). Masselink and Li (2001) have shown that for  $K < 10 \text{ cm/s}$ , the asymmetry of the uprush/backwash period ( $T_u$  and  $T_b$ ) is smaller than one, indicating that the backwash is of longer duration than the uprush (Fig. 1.5c). On the other hand, for  $K > 10 \text{ cm/s}$   $T_u/T_b$  is larger than one, indicating that the uprush takes longer than the backwash. In summary, for small  $K$ -values, only a fraction of the swash volume (expressed as a percentage  $\%inf$ ) infiltrates (e.g. for  $K = 1 \text{ cm/s}$ ,  $\%inf < 2\%$ ), but for large  $K$ -values, a significant position of the swash volume is lost through infiltration (e.g. for  $K = 10 \text{ cm/s}$ ,  $\%inf = 15\%$ ) (Fig. 1.5d). A number of other studies also indicate that infiltration in the SZ may only be important for profile evolution on coarse-grained beaches (Bagnold 1940; Packwood 1983; Quick 1991).

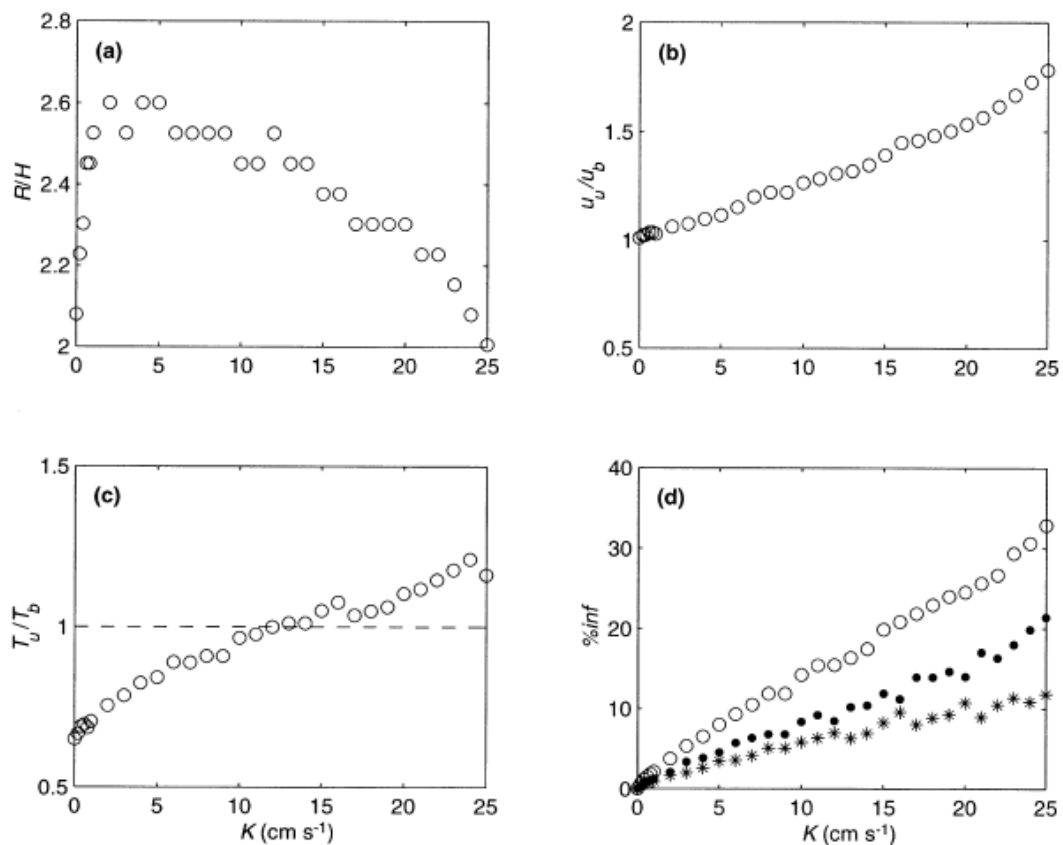


Figure 1.5. Relationship between hydraulic conductivity  $K$  and (a) normalized runup height  $R/H$ ; (b) velocity asymmetry  $u_u/u_b$ ; (c) time asymmetry  $T_u/T_b$ ; and (d) the percentage of uprush volume that infiltrates into the beach during swash motion  $\%inf$ . Symbols in (d): ( $\circ$ )  $\%inf$  over the complete swash cycle (uprush and backwash); ( $\bullet$ )  $\%inf$  during uprush; ( $*$ )  $\%inf$

during backwash. The asymmetry values in (b) and (c) relate to the mid-swash zone position. (after Masselink and Li, 2001).

## 1.5 Asymmetries in SZ hydro- sediment dynamics

Sediment transport mechanisms in the swash zone have traditionally received less attention than those in the surf zone. However, the study of the evolutionary trend of the shoreline requires a detailed knowledge of interaction mechanisms between the SZ hydro-morphodynamic and related sediment transport. The insufficient understanding of these issues and, in general, the complexity of the swash hydrodynamics modelling, currently leads to neglect almost completely the influence of the swash dynamics in the numerical computation of coastal dynamics. This means that the results of numerical models commonly used in coastal engineering focus on hydro-morphodynamics of the surf zone. Hence, a sort of bias remains on the phenomenology of the SZ. As a consequence, the confidence on the available transport models decreases drastically. Brocchini (2006), for example, evidences that if SZ transport is neglected the overestimates of available transport formulae (e.g. CERC formula) increase by 50–250%. This represents a significant shortcoming of predictive models of shoreline change (Masselink and Hughes, 1998), also in the perspective to consider the nearshore zone as a mutually interacting and coevolving system comprising SZ and surf zone.

Considerable efforts have been made to improve the state of knowledge of SZ transport processes. The main finding is that the intrinsic asymmetry between uprush and backwash velocities have far-reaching implications for sediment dynamics. It is now very evident, in fact, that there are some fundamental differences between the runup and rundown phases of the swash flow. Thus, it seems logical that the sediment transport processes during these phases of the swash flow would also be different. All the parameters and processes which form the different thematic groups we previously summarised in Fig. 1 (i.e. inner surf advectons, swash morphodynamics, swash and groundwater hydrodynamics) affect the swash flows asymmetry. In other words, SZ hydrodynamics contains a number of asymmetries which define which direction (offshore or onshore) of net sediment transport dominates. The key characteristics of swash flow motion can be summarised as follows: (1) the peak of uprush velocities are either comparable to (e.g., Puleo et al., 2003) or slightly stronger than (e.g., Hughes and Baldock, 2004) the peak backwash velocities; (2) flow durations are typically unequal, with uprush significantly shorter than the backwash (Larson

and Sunamura, 1993; Baldock and Holmes, 1997; Masselink and Hughes, 1998); as a result, (3) the horizontal asymmetry, also termed skewness (which is a measure of the difference between onshore and offshore velocity magnitudes) in the SZ is predominantly negative, i.e. offshore directed (Masselink and Russell, 2006).

Following these considerations, a first conclusion may be that the intrinsic asymmetry between uprush and backwash velocities tends to encourage sediment export from the SZ. This would mean that beaches could not exist due to the prevalence of offshore backwash flow. Even in the theoretical case of flow symmetry, i.e. uprush perfectly equal to backwash, the pickup and deposition of sediment is different during runup and rundown, due to gravity. In reality, measured SZ hydrodynamics contains a number of asymmetries which tend to favour offshore over onshore sediment transport but these asymmetries are balanced by other mechanisms.

Indeed, it is observed that the uprush is a more efficient transporter of sediment than the backwash. Possible balancing mechanism that promote uprush sediment transport and thereby compensate for the offshore-directed velocity skewness may be in/exfiltration effects, flow acceleration, bore turbulence and settling/scour lag. All these mechanisms are generated within the SZ itself and, thus, must be addressed by the swash hydrodynamics. The relative importance of each of these processes has not been completely established yet (since net sediment transport in the SZ is the difference between two very large numbers, neither of which can be quantified very well) but it is likely to depend on the type of SZ. Another important factor controlling net transport is the onshore advection of pre-suspended sediment by the collapse of the initial bore from the inner surf zone (e.g. Jackson et al., 2004). Neglecting it may lead to underestimation of suspended sediment transport within the SZ. For this reason, the inner surf advection of sediment is discussed in more detail in the following Section.

### 1.5.1 Sediment advection as a boundary condition for SZ

The role of sediment advection from the inner surf zone in controlling the sediment transport asymmetry in the SZ, and therefore the morphological development, has largely been ignored. However, it appears that in order to determine whether the SZ imports or exports sediment, it is crucial to determine accurately how much sediment is suspended by the incoming bore and advected into the SZ by the flow following the bore collapse. Hence, both

the total amount of this “pre-suspended” sediment and its phasing relative to the swash inflow are important if net deposition patterns are to be predicted accurately (Pitchard, 2009).

Sediment advection is the result of the hydrodynamic process known as “advection of turbulence”, due to the landward propagation of bores and the associated collapse at the beachface. Sediment, and to a lesser extent, turbulence, can also be advected from the SZ back into the inner surf zone, for example, in relation to hydraulic jumps that may develop at the bottom of the SZ (Masselink and Puleo, 2006). In that case, the advection could occur in both the offshore and onshore directions simultaneously depending on elevation in water column (Butt et al., 2004). Butt and Russell (1999) and Osborne and Rooker (1999) measured suspended sediment fluxes in the SZ of a high-energy dissipative beach and emphasised the occurrence of hydraulic jumps at the end of the backwash, when super-critical flow conditions prevail, resulting in sharp increases in the suspended sediment concentration. These elevated sediment concentrations may lead to advection of suspended sediment into the inner surf zone and may also enhance sediment concentrations during subsequent uprush events (c.f. Masselink and Puleo, 2006).

Sediment advection may provide an explanation of the failure of the energetic based models to predict the direction of SZ sediment transport correctly (Masselink and Russell, 2006). The energetic approach rely on the assumption that the sediment transport rate  $q$  is related to the instantaneous bed shear stress  $\tau$  according to  $q \propto \tau^n$ , where  $n = 1.5$  for bedload transport (Nielsen, 1992), implicitly considering the sediment load during the uprush is not locally entrained (i.e. sediment advection is neglected). Hence, the sediment advection role is expected to be particularly significant on steep beaches dominated by incident swash, in particular for fine sediment sizes and short uprush durations (Masselink and Puleo, 2006). On the other hand, field measurements on suspended sediment carried out by Masselink et al., (2005) showed how the influence of bore turbulence by suspending sediments is unlikely to have importance on dissipative beaches. Due to the larger SZ width, in fact, the distance between the region of bore collapse and the mid-SZ would have enabled the bore-collapse-entrained sediment to have settled to the bed prior to arriving at the mid-swash position.

Indeed, especially for gently sloping beaches, some additional mechanisms, known as, affecting advection of suspended sediment should be considered. Settling lag refers to the time required for suspended particles to settle to the bottom through slowly flowing water. Scour lag is a result of the higher flow velocities needed to re-suspend a deposited particle than to keep it in suspension (where it results in settling lag).

The region of the inner surf zone from which sediments are directly advected into the SZ during a single uprush is not easy to predict. For this reason, this distance is usually correlated to the maximum distance seaward of the swash boundary and below the bore-collapse point from which a fluid particle can enter the SZ (i.e. to cross the SZ seaward boundary) (Baldock et al., 2008). Following this definition, thus, the region defined by the advection length represents the potential effective pickup zone for pre-suspended sediment. Hence a further question is how the time-dependence of sediment supply during the fluid particle advection might affect net pre-suspension patterns. This time-dependence was found to be strongly dependent on the turbulent dynamics of the initial bore. For example, it is shown (Baldock et al., 2008) that the potential location of deposition of presuspended sediment is sensitive to the initial pickup location, as a result of the strongly diverging flow. Using the swash solution of Shen and Meyer (Shen and Meyer, 1963; SM63 hereinafter), Pritchard and Hogg (2005) suggested that sediment is advected into the SZ from a very narrow region of the inner surf zone, extending 1/16th of the runup length seaward of the location of bore collapse (the start of the runup). However, Guard and Baldock (2007) showed that the SM63 analytical swash solution is unrealistic, since the boundary conditions for the solution are not representative of real swashes. In fact, in the SM63 the pre-suspended sediment was represented by a fixed concentration imposed at  $x=0$  during the runup. Further, experimental results (Baldock et al., 2005) suggest that the SM63 solution seriously underestimates depths during the uprush. In fact, measurements in both the field and laboratory propose a greater potential length for the advection region Baldock et al., (2007a). In particular, Baldock et al. (2008) examined swash flow from a Lagrangian perspective, investigating both experimentally and under the model proposed by Guard and Baldock (2007). The advection lengths were normalised by the runup lengths to give an advection ratio,  $A_L$ . For each wave conditions, they found that the measured advection ratio is much greater than that predicted by Pritchard and Hogg (2005). In particular, for monochromatic breaking waves,  $A_L$  is about 0.25, four times greater than that predicted by the SM63 solution. For solitary fully developed bores, solitary surging breakers and solitary non-breaking long waves, the mean advection ratio may be still greater. This demonstrates that fine sediments that are suspended for long periods in turbulent flow may be advected into the SZ from within a region of the inner surf zone that extends up to one half of the runup length seaward of the bore collapse location. The extent of this region is about eight times that predicted by the SM63 swash solution. This suggests that surf beat also has the potential to transport large

quantities of sediment into the SZ during the uprush phase. No large significant differences are observed among breaker types. Finally, field observations shown the mean advection ratio again equal to about 0.3. Data show that the advection ratio is relatively insensitive to Iribarren number and wave type, i.e. non-breaking or breaking wave, consistent with self-similarity in typical swash flows. However, at low Iribarren numbers, there is considerable data scatter, which reflects experimental inaccuracy for small advection lengths and also the relatively unstable inner surf zone conditions that occur with laboratory waves. In fact, swash-swash interactions and swash-surf interactions in random sea states are likely to lead to greater variation in the advection ratio, which is consistent with the greater scatter observed in the field data. Note that models in a Lagrangian reference enable the inclusion of advected sediment and solutions of the advection-diffusion equation in sediment dynamics models (Alsina et al., 2005) and, therefore, further work is required using this approach.

### 1.5.2 Uprush hydro-sediment dynamics

As the bore height approaches the local instantaneous shoreline (zero depth), the bore front and the water behind the bore front rapidly accelerate (Whitham, 1958), and the bore collapses taking a small but finite time, during which the shoreline velocity increases to a maximum that corresponds to the initial uprush velocity. This positive flow acceleration occurs at the very beginning of uprush when the flow quickly changes from offshore to onshore. The short burst of acceleration may induce a horizontal pressure gradient enhancing sediment transport (Drake and Calantoni, 2001). Turbulence from the collapsing bore, then, is advected into the SZ (Yeh et al., 1989), such that presuspended sediment from the surf zone is added to the local sediment entrained within the SZ. The sediment is suspended relatively high into the water column so that a rather uniform distribution of sediment is found over the entire water column. Flow velocities, suspended sediment concentrations and suspended fluxes are maximum at the start of the uprush when the flow is most turbulent. The bore potential energy is suddenly transformed into the kinetic energy of a thin wedge of water that is very shallow in comparison to the horizontal length scale of the flow (shallow depth). Approximating the flow as tangential to the beach surface, make possible the using of the nonlinear shallow water equations (NSWE) with good confidence (Peregrine, 1972). Following the bore collapse, the water surface dips seaward, and the local and total flow acceleration are directed offshore for nearly the whole swash event. Indeed, an exception

occurs as the bore collapses (Baldock and Hughes, 2006). The boundary layer is therefore subject to an adverse (but weak) pressure gradient during the runup. The water pressure propagates rapidly into the upper layers of the sediment. The water infiltration into the bed contributes both to removing water available for the subsequent rundown phase (Turner and Masselink, 1998) and increasing the effective weight of sediment (i.e. bed stabilization), thereby decreasing the potential for sediment transport (Hughes et al., 1998; Nielsen, 1998). However, simultaneously, downwards-directed pressure gradients on the uprush act to alter the thickness of the bottom boundary layer. Laboratory investigations carried out by Conley and Inman (1994), confirmed that the thickness of the boundary layer is reduced by infiltration, making the near-bed velocity relatively greater. The turbulent vortices during infiltration are maintained closer to the bed, thereby increasing the potential for sediment transport (Butt et al., 2001). This mechanism combined with the intense flow velocity characterizing the uprush result in a relatively large shear stress on the seabed.

Hence, sediment transport during wave uprush may be envisioned as a two-phase process (Puleo et al., 2000; Jackson et al., 2004), where sediment entrainment and suspension can occur due to:

- 1) sediment entrainment during bore collapse seaward of the base of the SZ and subsequent advection of this bore-entrained sediment up the beach by wave uprush;
- 2) in-situ sediment entrainment and transport induced by local shear stresses during wave uprush.

Uprush turbulence is dominated by bore-generated and bore-advected turbulence which evolves analogous to grid turbulence (Petti and Longo, 2001a, b; Cowen et al., 2003). The turbulence associated with the collapsing bore, aided perhaps by the short phase of flow acceleration immediately following bore collapse, is likely to be responsible for much of the suspended sediment that is observed in the SZ at the start of the uprush (Butt and Russell, 1999; Puleo et al., 2000). Backwash/uprush collision is an additional factor responsible for enhanced bed shear stress which can mobilise and suspend sediment due to violent mixing (e.g., Puleo et al., 2000; Butt et al., 2004). Much of the sediment that is transported during uprush, in fact, occurs as suspended load, loosely defined as mobilized sediment that is supported by turbulent fluctuations, rather than grain-to-grain interactions (bedload) (Osborne and Rooker, 1999; Puleo et al., 2000; Voulgaris and Collins, 2000; Butt et al., 2004). The

quantity of presuspended sediment appears very important in controlling the net sediment transport over the swash cycle (Pritchard and Hogg, 2005).

Both mechanisms of uprush sediment transport are considered important but the first mechanism is considered most significant during the early stages of wave uprush when sediment is transported mainly in suspension, while the second mechanism is likely to dominate the mid- to later stages of wave uprush when sediment is transported mainly by sheet flow. The relative importance of the two mechanisms will vary between different beaches with the morphodynamic state of the beach (reflective versus dissipative) expected to play a major role.

The cross-shore distributions in sediment load for each of the two sediment entrainment mechanisms (bore collapse and local shear stress) were evaluated hypothetically by Jackson et al., (2004) using the process-based, numerical model of Li and Barry (2000 a,b) and Li et al. (2001). This model uses non-linear shallow water equations (Peregrine, 1972) to predict water depths and flow velocities in the SZ and has been used to investigate the effect of swash infiltration on swash zone hydrodynamics and beachface development (Masselink and Li, 2001). Fig. 1.6 shows the sediment load curves generated from the numerical models and the field data collected for an intermediate beach. The sediment load curves are normalized by the maximum load and the  $x$  cross-shore co-ordinate is normalized by  $S$  which is the horizontal swash excursion or swash length (hence  $x/S=0$  at the runup limit;  $x/S= 1$  at the bottom of the SZ).

The curve indicated by the dotted line has been obtained under the assumption that the sediment transport rate is proportional to  $u^3$  (Bagnold, 1963, 1966; Masselink and Hughes, 1998). The normalized sediment load is maximum at  $x/S = 0.8$  coinciding with the location of maximum uprush velocity, and progressively decreases in the landward direction. The shape of the onshore decrease in sediment load is convex-concave. The dotted line represents the cross-shore variation of the normalized sediment load assuming that all sediment is entrained at the start of the uprush ( $x/S = 1$ ) by bore collapse and that the sediment settles out over the remainder of the uprush.

The field data (solid line) reveal a profile similar to the profile generated by the shear model for conditions when the sediment transport rate is proportional to  $u^3$ . A portion of the sediment trapped at the base of the swash uprush may have been advected from the zone of bore propagation. Data collected by sediment trap located at  $x/S = 1.2-1.3$  and  $x/S \approx 0.8$  reveal that the amount of sediment in the zone of bore propagation is on average 22.6% of the

amount of sediment trapped in the area of maximum load. Sediment analysis of the trap and surface samples suggests that the sediment in transport in the upper swash uprush is locally entrained by instantaneous shear stresses.

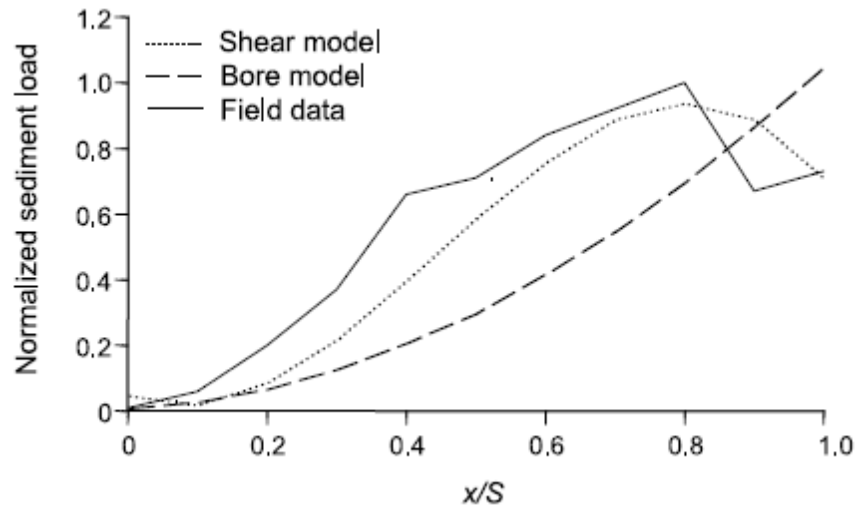


Figure 1.6. Schematic Comparison of field data on normalized sediment load with results from model of Li et al. (2001) (after Jackson et al., 2004).

Swash flow energetics decrease rapidly following the arrival of the swash front. At the time of flow reversal, the water is generally clear, indicating that the suspended sediment has settled to the bed prior to the start of the backwash (Puleo et al., 2000; Masselink et al., 2005). Settling velocity distributions of trap samples during individual uprush events are similar to distributions found on the beach surface, with the lowest settling velocities (finest sediments) near the base of the SZ and maximum settling velocities (coarsest sediments) around the mid-swash position (Jackson et al., 2004).

A general description of the hydro-sediment dynamics during runup phase is presented in Figure 1.7.

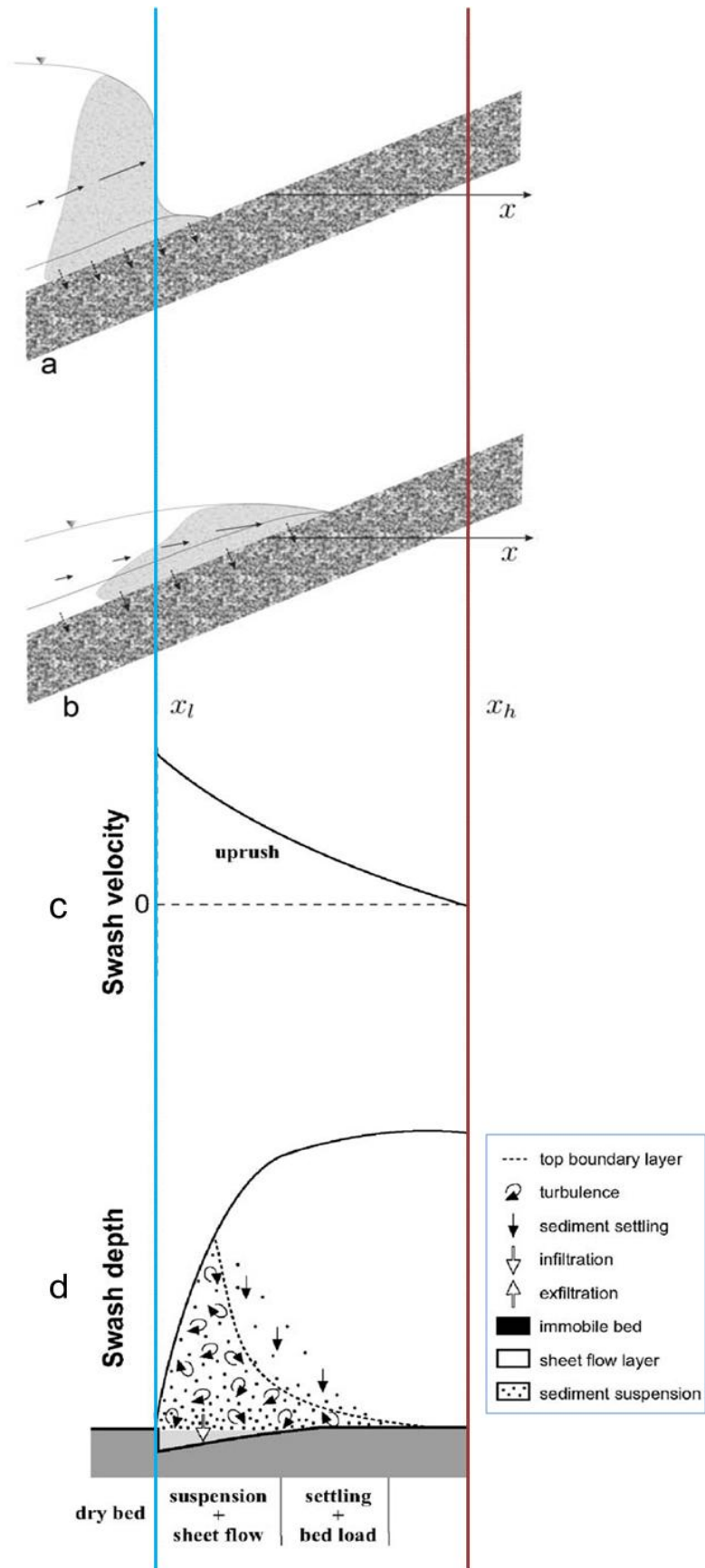


Figure 1.7. Schematic of sediment transport processes during runup phase of a swash event. a) Bore collapse at  $t = 0$ . (b) Runup at  $t \approx 2T_S/10$ . The solid arrows at mid water depth indicate

the intensity of the depth-averaged velocity, the dashed arrows at the bed indicate the direction of the water flow in the bed (infiltration), the solid line near the bed indicates the top of the bottom boundary layer, while the shaded area in the wave body indicates the region of highest sediment concentration and greatest shear stress. Here  $x_l$  and  $x_h$  are the lowest rundown and the highest runup, respectively, during a cycle. c) Horizontal mean velocity time series. d) Swash depth time series and schematic of sediment transport processes. (Adapted from Brocchini and Baldock, 2008 and Masselink and Puleo, 2006).

### 1.5.3 Backwash hydro-sediment dynamics

When the uprush is in its terminal phase, flow reversal (backwash) commences first at the seaward end. For instance, the backwash motion across the lower SZ may start before the uprush reaches its maximum landward extent (Raubenheimer et al., 1995; Raubenheimer and Guza, 1996; Hughes et al., 1997a; Puleo and Holland, 2001). The divergence of the flow field that takes place around flow reversal reduces the swash further, resulting in a thinning of the swash lens. This has implications when trying to ascertain the importance of uprush vs backwash flow durations, as well as net sediment transport, since these estimates will depend heavily on foreshore location. Around flow reversal, the flow velocity is so weak that much of the suspended sediment settles, so that during rundown most of the sediment transport occurs as a sheet flow (Brocchini and Baldock, 2008). At this time, the flow gradually accelerates until it reaches a maximum in the final stage of the rundown (Conley and Inman, 1994; Masselink and Hughes, 1998) and fluid may still be infiltrating the beach. Backwash flows accelerate under the forces of gravity, frictional processes and cross-shore pressure gradients, but they do not develop their full downslope gravitational potential (Puleo et al., 2003). Like the beginning of the uprush, the end of the backwash is a fuzzy concept and depends on the definition used and how the motions are recorded (Masselink and Puleo, 2006). Indeed, the seaward portion of the backwash may interact/collide with the next bore, causing the seaward swash flow to decelerate.

From an hydraulic point of view, the backwash flow rapidly becomes supercritical; consequently, at any given location is not influenced by the next incident wave or bore until the next wave arrives at that position. Moreover, if no new incident waves arrive, a backwash bore may form toward the end of the backwash (e.g., Peregrine, 1974). The influence of the

backwash flow may extend offshore of the rundown position through the formation of a wall jet or backwash vortex (Matsunaga and Honji, 1980, 1983).

Meanwhile, further shoreward, fluid may be exfiltrating. Clearly, the direction and magnitude of through-bed flow is dependent on permeability and groundwater levels. Grant (1946, 1948) noted that groundwater outcropping at the beach surface can cause dilation or fluidisation of the sand grains, allowing them to be entrained more easily by backwash flows. Fluidisation of sediment occurs when the upward-acting seepage force exceeds the downward-acting immersed particle weight (i.e. when the effective stress becomes zero) (Horn 2002). Indeed, during uprush, the sediment is saturated and movement of water into the beach is extremely limited since changes in porosity due to expansion and contraction of the mineral 'skeleton' is minimal. However, water pressures propagate rapidly through the sediment. But as the swash retreats, there is a release of porewater pressure on the beachface, potentially giving large hydraulic gradients acting vertically upwards just below the surface (Baird et al. 1996, 1998). However, if the resultant seepage force associated with these upward-acting hydraulic gradients is sufficient to induce fluidisation of the sand grains at the surface is not clear. Baird et al., (1996), concluded that fluidization may occur especially in the latter stages of the backwash. Nevertheless, even if the upwards-directed pressure gradients are too small to produce fluidisation, they may still increase sediment transport on the backwash by reducing the effective weight of the sediment (i.e 'destabilise' the bed). The understanding of the role of water fluidisation in the SZ and sediment transport processes is one of the main questions that current research on coastal processes has to answer (Ciavola et al., 2010). Another mechanism due to upwards-directed vertical flow, which may have the opposite effect, is the altering of the thickness of the boundary layer. During exfiltration, in fact, the turbulent vortices are elevated further from the bed, effectively thickening the boundary layer and decreasing the potential for sediment transport. This process would tend to decrease backwash transport.

Backwash turbulence is dominated by the growing boundary layer and compares well to the classic flat plate boundary theory near the bed (Petti and Longo, 2001a, b; Cowen et al., 2003), suggesting that backwash motion is dominated by shear derived at the bed. A general description of the hydro-sediment dynamics during rundown phase is presented in Figure 1.8.

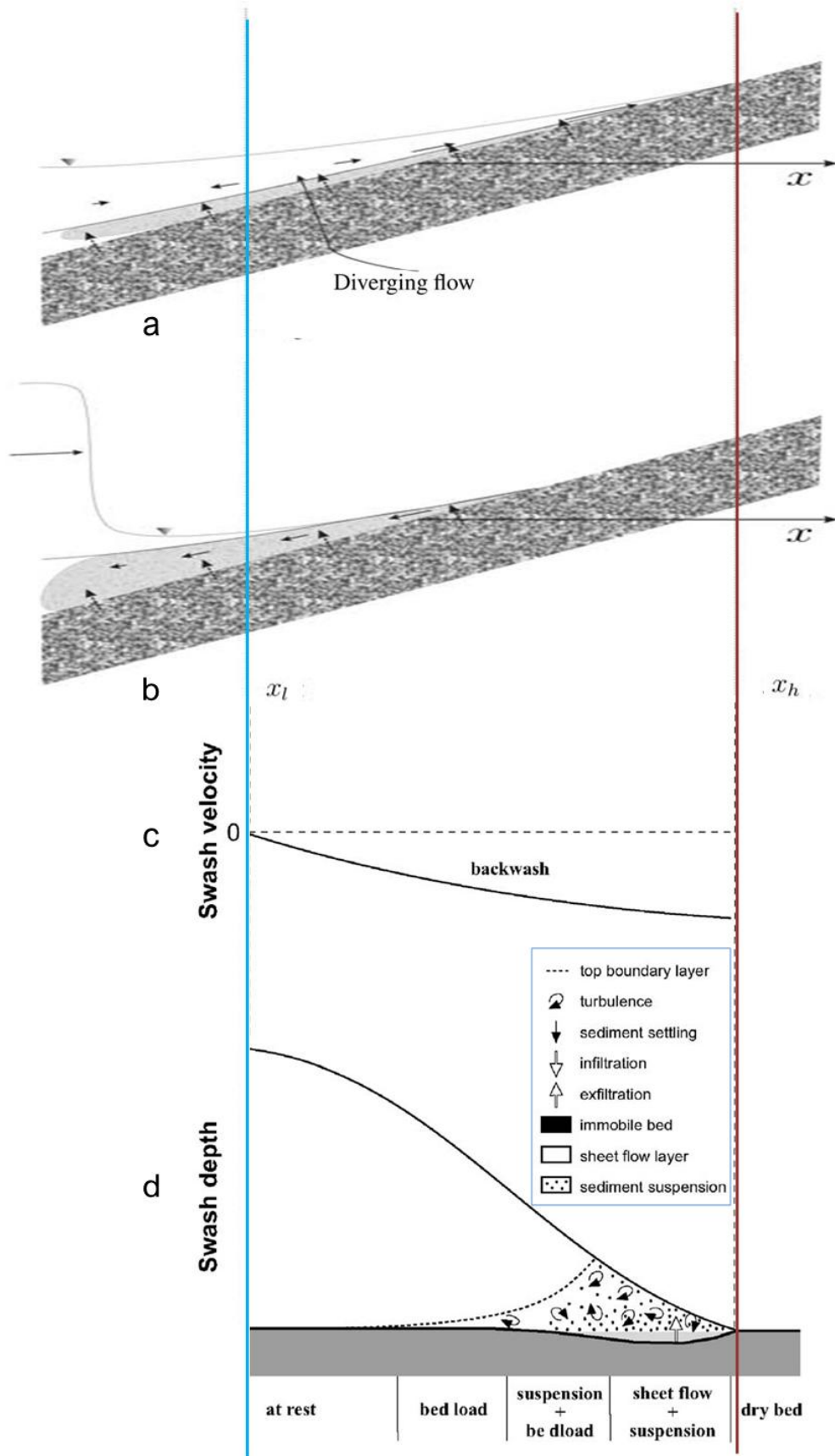


Figure 1.8. Schematic of sediment transport processes during rundown phase of a swash event. a) End of the runup and beginning of rundown at  $t \approx 4T_s/10$ . b) Rundown and

subsequent incoming wave at  $t \approx 8T_S/10$ . The solid arrows at mid water depth indicate the intensity of the depth-averaged velocity, the dashed arrows at the bed indicate the direction of the water flow in the bed (exfiltration), the solid line near the bed indicates the top of the bottom boundary layer, while the shaded area in the wave body indicates the region of highest sediment concentration and greatest shear stress. Here  $x_l$  and  $x_h$  are the lowest rundown and the highest runup, respectively, during a cycle. c) Horizontal mean velocity time series. d) Swash depth time series and schematic of sediment transport processes. (Adapted from Brocchini and Baldock, 2008 and Masselink and Puleo, 2006).

## 1.6 Beachface morphodynamics

### 1.6.1 Beachface morphology

The beachface is the sloping section of the beach profile normally exposed to the action of swash (Hughes and Turner, 1999). The shape of the beachface ranges from planar to concave, although under conditions of profile adjustment, usually accretion, the beachface may have a convex shape (Sonu and van Beek, 1971; Sonu and James, 1973; Makaske and Augustinus, 1998). The most characteristic feature of the beachface is its slope gradient. The beachface is in dynamic equilibrium with swash motion when the amount of sediment transported onshore by the uprush is equal to that transported seaward by the backwash, and the associated equilibrium gradient represents the balance between onshore swash asymmetry and the downslope component of gravity (Hardisty, 1986).

The equilibrium beachface gradient decreases with wave height, and increases with wave period and sediment size (Bascom, 1951; Kemp and Plinston, 1968; Dalrymple and Thompson, 1976; Sunamura, 1984). Bagnold (1940) contends that the only factor of significance in controlling the gradient of the beachface is the sediment size. Since the steepness of the beachface has been ascribed to the pronounced onshore asymmetry in the swash flow, it is obvious that hydrodynamic forcing play a fundamental role. Therefore, the only way to give an reasonable interpretation to the conclusions of Bagnold (1940) follows a different approach in considering the beachface controlling factors.

Reis and Gama (2010) developed a model of wave runup and rundown along the beachface, based on the Kozeny–Carmán equation. Then, they use the Constructal Law (Bejan, 1997) as the principle that governs flow processes in relation to beachface

morphodynamics. The Constructal Law has proven to be an important principle for flow architectures that evolve in time in systems out of equilibrium (see Bejan, 1997, ch.13) in that: “Flow systems morph in time in order to provide easier and easier flow access to the currents that flow through it, under the system constraints”. Following this principle, they found that the beachface slope will change in time such as to maximize the global currents (swash flows) that flow over and inside it. Said in another way, the beachface slope and the dominant sand grain size will adjust together so as to minimize the time needed to complete a swash cycle. Thus, according to their model, it should be noted how vertical swash flows are related to beachface slope. Since in/exfiltration are proportional to permeability, which in turn increases with grain diameter (see Section 1.2.1), for constant wave height they found that:

$$\beta \propto k^{\frac{2}{3}} \quad [1.14]$$

In this context, we can understand the conclusions of Bagnold (1940) (but also Quick (1991), Komar (1998) and Masselink and Li (2001)), since sediment size is the key factor in controlling the swash infiltration and, in turn, the slope gradient of the beachface.

However, recalling that swash infiltration is very important for profile evolution only on coarse grained beaches ( $D_{50} > 1\text{mm}$ ), Komar (1998) found another explanation for the dependence of beachface gradient on sediment size for beaches consisting of relatively fine sediments ( $D_{50} < 1\text{mm}$ ). Since the particle suspension is the main sediment transport, the beachface gradient is expected to increase with the ability of the sediments to resist transport (Dean, 1973) and will increase with the sediment fall velocity (a function of the size and density of sediment particles).

The response of the beachface to changing hydrodynamic conditions is traditionally perceived in terms of changes in equilibrium conditions on the beachface (too gentle or too steep), resulting in net onshore or offshore sediment transport (Masselink and Puleo, 2006).

If the beachface is too steep compared to the equilibrium gradient, the backwash moves more sediment than the uprush, inducing net offshore sediment transport. Sediment is eroded from the upper part of the beach and is deposited on the lower part, resulting in a flatter beachface. Maximum bed level changes are likely to occur around the mid-to lower swash position, leading the development of concave profile (Fig. 1.9a). If the beachface is flatter than the equilibrium gradient, the uprush moves more sediment than the backwash, inducing net onshore sediment transport and a convex profile (Fig. 1.9b). In both cases, morphological change (beachface steepening and flattening) as a result of mutual adjustment between

beachface morphology and swash asymmetry, will continue until a new equilibrium is attained.

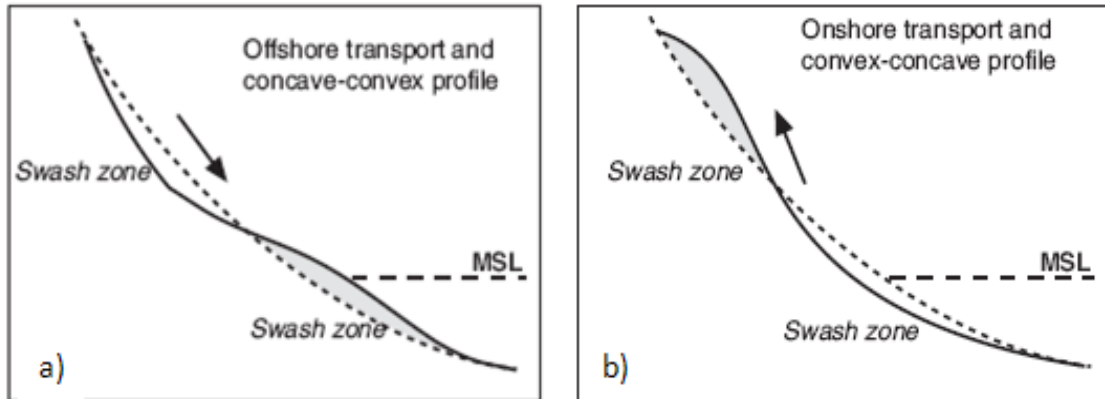


Figure 1.9 (a,b). Beachface response to changing wave conditions. (adapted from Masselink and Puleo, 2006).

The broad question of whether a beach is going to accrete or erode when exposed to a certain set of wave conditions may be answered with a certain amount of confidence according to Kraus et al., (1991). Based on a comprehensive review of field and laboratory data they suggested the criterion:

$$\text{Beach erode if } \frac{\bar{H}_0}{L_0} < 0.0007 \left( \frac{\bar{H}_0}{w_f T} \right)^3 \quad [1.15a]$$

$$\text{Beach accrete if } \frac{\bar{H}_0}{L_0} > 0.0007 \left( \frac{\bar{H}_0}{w_f T} \right)^3 \quad [1.15b]$$

where  $H_0$  and  $L_0$  are the deep water height and wave length respectively, and  $w_f$  is the fall velocity. They found the best correlation by using the mean offshore wave height  $\bar{H}_0$ . For a Rayleigh distribution, the mean wave height is related to the root mean square and significant heights by

$$\bar{H}_0 = 0.886 H_{rms} = 0.625 H_s \quad [1.16]$$

Another approach to predict as to whether the beach will likely erode or accrete by cross-shore transport processes, and used in this work, is the Dean's relationships (1973):

$$s_p \begin{cases} > 1.7 \frac{\pi w_f}{g T_m} & \text{offshore motion} & [1.17a] \\ < 1.7 \frac{\pi w_f}{g T_m} & \text{onshore motion} & [1.17b] \end{cases}$$

Finally, there is an additional way by which the surf zone wave can play a primary role in the SZ morphology. The beachface erosion during storm conditions is rarely accomplished by swash processes. During storms, the water level in the surf zone is elevated due to wave setup. As a result, the upper part of the beach (i.e., the beachface) becomes too steep in relation to this new water level, so swash flow processes start eroding the beachface. This results in a flattening of the beachface, not because the backwash is stronger than the uprush, but because surf zone waves are operating on a part of the beach shaped by swash processes. In fact, during major storms, swash processes are more likely to operate on the backshore than on the beachface.

### 1.6.2 Morphing feedback processes

Feedback processes between morphology and hydrodynamics are essential component of the SZ. As summarized by Masselink and Puleo (2006) feedback can be considered at two main spatial scales:

- 1) interactions between the morphodynamic systems of the beachface and the surf zone (“global” feedback);
- 2) interactions within the beachface morphodynamic system (“local” feedback).

The main features of the global feedback are related to dissipation and reflection mechanisms of the incident wave energy. Onshore sediment transport from the surf zone to the beachface, may cause an increase in the water depth at the base of the beachface. Wave energy dissipation will shift from the surf zone to the beachface, exposing the beachface to higher waves and more energetic swash dynamics. Conversely, beachface erosion by offshore sediment transport generally results in sediment deposition in the surf zone, possibly in the form of nearshore bar morphology (e.g., Wijnberg and Kroon, 2002). There will be a shift in the location of wave energy dissipation from the lower beachface to the surf zone, resulting in reduced amounts of wave energy reaching the base of the beachface and less energetic swash dynamics. Onshore sediment transport from the surf zone to the beachface, on the other hand, may cause an increase in the water depth at the base of the beachface. Wave energy dissipation will shift from the surf zone to the beachface, exposing the beachface to higher waves and more energetic swash dynamics. A change in the beachface gradient also modifies

the reflectivity of the beach and may increase (in case of steeper beachface) or decrease (in case of flatter beachface) the amount of reflected wave energy in the surf zone.

Many previous studies suggest that the local wave height in the surf zone is independent of the offshore wave height, i.e. the wave height is depth limited in the surf zone (Southgate, 1993). In fact, the beachface morphology leads to modify the local wave height ( $H$ ) to depth ( $d$ ) ratio  $\gamma = H/d$  (Raubenheimer et al., 1996). As result, on relatively gently sloping beaches, there is frequent interaction between the next incident short wave and the preceding swash. The time period between the beach emerging is then of the order of the period of any long waves present in the surf zone (e.g., Holland et al., 1995; Butt and Russell, 1999; Raubenheimer, 2002). Conversely, on relatively steeply sloping beaches, the swash period is equal to or shorter than the wave period. This is due to waves which often arrive at the exposed beachface at about the same location, and the ensuing swash sequence is largely or fully complete before the subsequent wave arrives (e.g., Shen and Meyer, 1963; Waddell, 1976; Yeh et al., 1989; Hughes et al., 1997; Baldock and Holmes, 1997; Peregrine and Williams, 2001; Puleo et al., 2003).

In order to provide a clear identification of the influence of beach gradient on shoreline motion, Figure 1.10 summarises and compares vertical swash oscillations on the 1:10, 1:30 and 1:60 slopes subjected to the same incident waves (Karunaratna et al., 2005). The low frequency energy at the incident wave group frequency plays a significant role in the shoreline excursion for all three cases but as the beach slope becomes steeper, individual swash events riding on the low frequency swash dominate the shoreline motion thereby increasing the width of the swash zone. Maximum swash oscillation occurred on 1:30 slope. This is due to the existence of partially saturated surf zone on moderate beach slopes which allows individual bores riding on large low frequency waves.

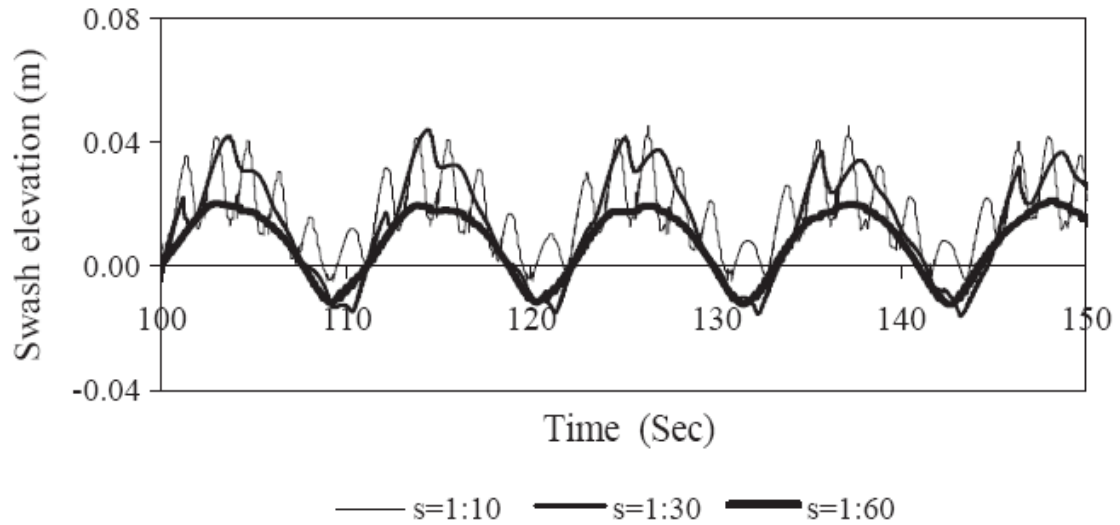


Figure 1.10. Vertical swash displacement on different beach slopes for same incident wave energy for  $f_m = 0.6$  Hz and  $H_0 = 0.1$  m (after Karunarathna et al., 2005).

In the contest of local feedback, the role of the beachface gradient is appealing, because it constitutes the main factor to balance the onshore swash asymmetry. The effect of beach gradient may be *direct* and *indirect*. To take in account direct effect, Fredsøe and Deigaard (1992) formulated a correction factor to consider the effect of a sloping bed on sediment transport. The steeper the beach, the more upslope transport is inhibited and the more downslope transport is enhanced. On a steepening and accreting beachface it therefore becomes increasingly difficult to move sediment upslope and at some stage an equilibrium will be reached. Similarly, on a flattening and eroding beachface the slope contribution to offshore transport progressively decreases and equilibrium will also be attained (Masselink and Puleo, 2006). Indirect effect, on the other hand, can be ascribed to the role of beach gradient in determining the amount of turbulence and suspended sediment advected into the SZ, by controlling the type of breaker or bore, previously investigated in the preceding Sections.

## 1.7 Modelling sediment processes in the SZ

The aim of this Section is to provide a selection of the simple models that are usually used as building blocks in comprehensive sediment transport models.

### 1.7.1 Water flow through a porous medium

Groundwater hydrologists generally model water flow using Darcy's Law in combination with an equation of continuity that describes the conservation of fluid mass during flow through a porous medium. Darcy's Law is valid as long as the flow is laminar, which is a reasonable assumption for sandy beaches. This may not be the case for gravel beaches (Packwood and Peregrine, 1980). Darcy's Law shows that the rate of groundwater flow (or specific discharge),  $u$ , is proportional to the hydraulic gradient, or slope of the watertable:

$$u = -K \frac{\partial h}{\partial x} \quad [1.18]$$

For modelling purposes, an important parameter is a dimensionless parameter known as specific yield, denoted by  $s_y$ . The specific yield, which is also known as the drainable porosity, is defined as the volume of water that an unconfined aquifer releases from storage per unit surface area of aquifer per unit decline in watertable (Freeze and Cherry, 1979). Of fundamental importance is, then, the hydraulic head,  $h$ , given as the sum of the elevation head,  $z$ , and the pressure head,  $\psi$ , and is measured in length units above a datum. There is no standard datum used in beach hydrology, but many researchers use the elevation of an impermeable layer below the beach sediment, so that the vertical coordinate  $z$  is measured from the impermeable base. Some workers have considered the hydraulic head in a beach groundwater system to be the elevation of the free water surface, or watertable elevation. However, this is only true when there is no vertical component to the flow; in other words, when Dupuit–Forchheimer conditions apply. Dupuit–Forchheimer theory states that in a system of shallow gravity flow to a sink when the flow is approximately horizontal, the lines of equal hydraulic head or potential are vertical and the gradient of hydraulic head is given by the slope of the watertable (Kirkham, 1967). Practically, the theory neglects the vertical flow components. A common approach to modelling beach groundwater flow in response to tidal forcing in sandy beaches uses the Boussinesq equation with the Dupuit–Forchheimer theory, for which two-dimensional flow to a sink can be approximated as one-dimensional flow, and the resulting differential equation is relatively easily solved. This one-dimensional form of Boussinesq equation is:

$$\frac{\partial h}{\partial t} = \frac{K}{s_y} \frac{\partial}{\partial x} \left( h \frac{\partial h}{\partial x} \right) \quad [1.19]$$

where  $h$  corresponds to the elevation of the watertable,  $t$  is time,  $K$  is hydraulic conductivity,  $s_y$  is the specific yield, and  $x$  is horizontal distance.

Where Dupuit–Forchheimer assumptions do not apply, such as in artificially drained beaches (e.g., Li et al., 1996), the beach aquifer should be considered as a two-dimensional flow system in which is assumed that the watertable is a free surface or flow line so that:

$$\frac{\partial h}{\partial t} = \frac{K}{s_y} \left( \frac{\partial H_h}{\partial z} - \frac{\partial h}{\partial x} \frac{\partial H_h}{\partial x} \right) \quad [1.20]$$

where  $H_h$  is the total hydraulic head and  $z$  is vertical distance.

To model watertable fluctuations in the zone of runup infiltration, Nielsen et al. (1988) and Kang and Nielsen (1996) proposed the use of a linearised version of the 1-D Boussinesq equation with an additional term:

$$\frac{\partial h}{\partial t} = \frac{K d_a}{s_y} \frac{\partial^2 h}{\partial x^2} + U_1(x, t) \quad [1.21]$$

where  $d_a$  is the aquifer depth and  $U_1(x, t)$  is the infiltration/exfiltration velocity per unit area. Other models of beach watertable fluctuations that incorporate wave effects have been developed by Li et al., (1997b) and Li and Barry, (2000), but none of these models have yet been tested against field or laboratory data.

### 1.7.2 Forces on sediment particles

For the purpose of sediment transport modeling, it is necessary to consider three type of forces which govern the behaviour of cohesion-less sediment particles whether they resting at the bed or moving around in a slurry or a thin suspension. These are:

- 1) the gravity force,  $F_g = M g$ ;
- 2) intergranular force related to collisions or continuous contact;
- 3) fluid forces which may be due to surface drag or fluid pressure.

The intergranular forces are well understood as far as resting (non shearing) grains are concerned. When a horizontal sand bed is exposed to a fast, steady flow, a finite top layer of sand will start to move with the flow, partly as bed load and partly in suspension. The fact that the moving layer is of finite thickness is significant although seemingly trivial, because it shows that the moving sand has increased the strength of the sand below. Since the shear stress is not decreasing downward, the top layer of immobile sand is able to withstand the

shear stress which eroded the top layer when the flow was started. This is due to the fact that the moving sand is transferring at least part of its weight to the bed as effective stress (generally referred as the dispersive stress) and thereby increasing the effective normal stress in the bed. Bagnold (1954, 1956) considered two different regimes in which different types of interactions dominate the behavior of the fluid-grain-mixture. For small, light grains in a very viscous fluid the interactions are dominated by viscosity and Bagnold termed this “the macro-viscous regime”. For large, dense particles at high shear rates the interactions are dominated by particles collision and this is called “the inertial regime”. The dimensionless parameter which separates the two regimes is:

$$B = \frac{sD_{50}^2\sqrt{\lambda}\partial u/\partial z}{\nu} \quad [1.22]$$

where  $s$  is the relative density of the sediment,  $\lambda$  is the linear sediment concentration and  $\nu$  is the kinematic viscosity.

The fluid forces on sediment particles are of two kinds, namely pressure forces and surface drag forces. The total pressure force which is determined as the surface integral of the pressure is by Green’s theorem equal to minus the volume integral of the pressure gradient,  $\nabla p = \left(\frac{\partial p}{\partial x}, \frac{\partial p}{\partial z}\right)$ . For example, if the pressure along the vertical is hydrostatic and there is a constant horizontal pressure gradient, the total pressure force on the body is

$$F_p = \begin{pmatrix} -V\frac{\partial p}{\partial x} \\ -V\frac{\partial p}{\partial z} \end{pmatrix} = \begin{pmatrix} -V\frac{\partial p}{\partial x} \\ \rho gV \end{pmatrix} \quad [1.23]$$

where  $V$  is the particle volume.

For a fixed body in a horizontally accelerated fluid, the pressure force is given by:

$$F_{p,x} = \rho(1 + C_M)V\frac{du}{dt} \quad [1.24]$$

where the term  $\rho C_M$  represents an extra mass due to the volume of surrounding fluid which the body keeps from accelerating.

For a particle of volume  $V$  which is fixed in a wave motion with homogeneous velocity field  $u=A\omega\sin\omega t$  the equation above gives:

$$F_p = \rho(1 + C_M)VA\omega^2\cos\omega t \quad [1.25]$$

The drag force is normally given in the form:

$$F_D = \frac{1}{2} \rho A_s C_D |u|u \quad [1.26]$$

where  $A_s$  is the cross sectional area facing the flow, and  $C_D$  is the drag coefficient which depend on the sediment shape and on the Reynolds number.

Drag forces (or total bed shear stress,  $\tau$ ) occur in two varieties: skin friction and form drag. The significance of each of these for sediment transport is quite different as described by Engelund and Hansen (1972). The form drag is generated by the difference in pressure between the upstream and the downstream sides of bedforms, and it does not directly affect the stability of individual surface sediment particles. The main disturbing influence to the surface grains is generally considered to come from the skin friction. In the SZ the bed can be considered flat (i.e. no bedforms are present) so the skin friction is referred as the effective stress,  $\tau$ .

Seepage or infiltration, may have a stabilizing or destabilizing effect on the sand because the vertical fluid drag changes the effective normal stress.

This mechanism should cause the formation of quicksand (or fluidization). Darcy' Law describes the water flow through porous medium:

$$\begin{pmatrix} u \\ w \end{pmatrix} = -K \begin{pmatrix} \frac{1}{\rho g} \frac{\partial p}{\partial x} \\ \frac{1}{\rho g} \frac{\partial p}{\partial z} + 1 \end{pmatrix} \quad [1.27]$$

where  $K$  is the permeability.

For vertical seepage rate with an outflow velocity  $w$ , the porewater pressure gradient is:

$$\frac{\partial p}{\partial z} = -\rho g \left( 1 + \frac{w}{K} \right) \quad [1.28]$$

corresponding to a to a buoyancy force per unit of volume of:

$$F_L = \rho g \frac{w}{K} \quad [1.29]$$

This means that, in order to lift a sediment particle with density  $s\rho$ , a vertical outflow velocity of magnitude  $(s-1)K$  is required.

A particle on the bed will also experience a lift force which is due to the curvature of the stream lines in the flow over the top of it. The force on the sediment particle with volume of the order  $D_{50}^3$  then is:

$$F_L = \rho C_L u^2 D^2 \quad [1.30]$$

$$F_L = \rho C_L u^2 D^2$$

By comparing the expression of pressure force and drag force on a spherical particle ( $D_{50}=D$ ), the ratio

$$\frac{F_{p,max}}{F_{D,max}} \propto \frac{D}{A_e} \quad [1.31]$$

is proportional to  $D/A_e$ , which is called the Keulegan Carpenter number.

For sand (of size  $D_{50} \approx 0.2$  mm) under waves with typical semi-excursions  $A_e$  of the order 0.1-2m, the Keulegan Carpenter number  $D_{50}/A_e$  is very small and, hence, the drag force tend to dominate over pressure force.

### 1.7.3 The flow-bed interaction

The water in streams and under waves interacts with the bed sediment mainly through the bed shear stress  $\tau(\theta, t)$ . Hence its determination is a crucial step in sediment dynamic. Jonsson (1966) developed a semi-empirical formula based on its early flow model, which describe  $\tau$  as function of the wave friction factor,  $f_w$ , as follow:

$$\tau = \frac{1}{2} \rho f_w (A_e \omega)^2 \quad [1.32]$$

where  $A_e$  is the water particle semi-excursion and  $\omega$  is the radian frequency. Jonsson, in fact, suggested that the structure of oscillatory boundary layers depend mainly on the relative roughness  $r/A$  and on the Reynolds number, written in the form  $A^2 \omega / \nu$ . Using laboratory data from Kamphuis (1975), Fredsøe (1984) found that wave friction factors in smooth turbulent flow fit the empirical expression

$$f_w = 0.065 Re^{-0.2} \quad [1.33]$$

Several investigators (Hughes, 1992; Puleo et al., 2000) have suggested that swash flow has more in common with steady flow than with oscillatory wave flow. In a review of all available studies, Dean (1978) suggested the following relation for friction factors in 2D duct flow:

$$f_w = 0.044Re^{-0.227} \quad [1.34]$$

these back-calculated estimates of friction factors were found to be an order of magnitude smaller than for the field measurement of Conley and Griffin, (2004). This discrepancy has yet to be resolved but may be due to different instrumental calibration. Often, the wave friction factor  $f_w$  is generally approximated following Swart (1974) as

$$f_w = \exp \left[ 5.5 \left( \frac{2.5D_{50}}{A} \right)^2 - 6.3 \right] \quad [1.35]$$

Considering that the roughness is closely related to the rate of momentum at the bed and hence to the friction factor, Guy et al., (1966) derived the steady flow friction factor through the definition:

$$\tau = \frac{1}{2} \rho f_r \langle \bar{u} \rangle^2 \quad [1.36]$$

where  $\bar{u}$  is the time averaged horizontal velocity and  $f_r$  is an empirical friction factor. The use of this equation presents two difficulties in terms of the appropriate value for  $\bar{u}$  and  $f_r$ . Indeed knowledge of the boundary layer is often unknown, so a single-point current metre measurement is often used in place of  $\bar{u}$ . On the other hand, at a point, the local Reynolds number varies rapidly with time, and simultaneously, the friction factor. Hence, for modelling purposes, the shear stress over the whole swash cycle is calculated as:

$$\tau = \frac{1}{2} \rho C_f U^2 \quad [1.37]$$

where  $C_f$  is a constant friction factor and  $U$  is a representative stream velocity.

It is now well established that the shear stress is very asymmetric (Hughes, 1995; Cox et al., 2000; Puleo and Holland, 2001; Archetti and Brocchini, 2002; Cowen et al., 2003; Conley and Griffin, 2004; Raubenheimer et al., 2004), with the maximum uprush bed shear stress more than twice that in the backwash (e.g. Masselink et al., 2005). The overall ensemble-averaged shear stress time series being skewed onshore (Conley and Griffin, 2004). This means that the usual assumption in sediment transport models of a constant friction factor over the whole swash cycle is not appropriate (Brocchini and Baldock, 2008), so using a constant friction factor,  $C_f$ , both during runup and for rundown to calculate the shear stress provides a poor fit to the measured stress data (Cowen et al., 2003). There is no generally accepted

explanation for the larger friction coefficients during uprush. However, Fredsøe et al.,(2003), examining the role played by externally generated turbulence found that:

- 1) externally generated turbulence penetrates the bed boundary layer, giving rise to an increase in both the mean and root mean square values of the bed shear stress when compared to the undisturbed case;
- 2) the phase lead of the shear stress over the flow velocity decreases and the friction coefficient increases with increasing turbulence intensity.

The turbulence stirring produced during the uprush by collapsing bores is absent during the backwash phase (Puleo et al., 2000). Thus, if these effects are applicable within the SZ, are likely to contribute to some of the asymmetry between uprush and backwash friction factors (Brocchini and Baldock, 2008). Hence, much effort has gone into estimation of friction factor. The wave orbital semi-excursion  $A_e$  (in m) for irregular waves with a peak wave period of  $T_p$  (in s) can be computed as

$$A_e = \frac{\sqrt{2}T_p}{2\pi} \sigma_u \quad [1.38]$$

where  $\sigma_u$  is the standard deviation of the cross-shore current velocity.

A simple, yet useful, dimensionless measure of the balance of the fluid forces on a sediment particle under waves is the sediment mobility number,  $\Psi$  (Nielsen, 1992) and can be written as:

$$\Psi = \frac{(A_e \omega)^2}{(s - 1)gD_{50}} \quad [1.39]$$

Some Authors (e.g. Conley et al., 2008), to provides a measure of the balance of forces on sediment in intense flows, use the mobility number in the form:

$$\Psi = \frac{u_m^2}{(s - 1)gD_{50}} \quad [1.40]$$

where  $u_m$  is the peak velocity under the wave.

A different measure of the balance between disturbing and stabilising forces on sand grains at the bed was suggested by Shields (1936) in a study of the incipient sediment motion in steady flow, and known as the Shields parameter:

$$\theta = \frac{\tau(o)}{\rho(s - 1)gD_{50}} = \frac{u_*^2}{(s - 1)gD_{50}} \quad [1.41]$$

This parameter found wide application, because it is particularly convenient to use in connection with steady flow. Indeed, the steady bed shear stress,  $\tau(o)$  and the friction velocity  $u_*$  are quantities easily measured:

$$\bar{\tau}(o) = \rho g D_z I \quad [1.42]$$

where  $D_z$  is the flow depth and  $I$  is the hydraulic gradient.

In connection with wave motion, the Shields parameter is generally defined in terms of peak bed shear stress

$$\theta = \frac{\hat{\tau}(o)}{\rho(s-1)gD_{50}} = \frac{1/2 f_w (A_e \omega)^2}{(s-1)gD_{50}} = \frac{1}{2} f_w \Psi \quad [1.43]$$

where  $f_w$  is the wave friction factor previously defined.

It was found that the critical value of  $\theta$ , e.g. the value where the motion of sediment particles is initiated, is a weak function of the Reynolds number and is in the order of 0.05.

The Shields parameter is usually calculated for a horizontal bed gradient and as such it may not be very suitable to predict sediment transport across sloping beds. However, an effective Shields parameter can be formulated to account for the effect of a the bed slope,  $\beta$ . according to Fredsøe and Deigaard (1992):

- for upslope flow

$$\theta_s = \theta \left( 1 - \frac{\tan\beta}{\tan\varphi} \right) \cos\beta \quad [1.44a]$$

- for downslope flow

$$\theta_s = \theta \left( 1 + \frac{\tan\beta}{\tan\varphi} \right) \cos\beta \quad [1.44b]$$

where  $\varphi$  is the friction angle.

Further modifications to Shields parameter have been proposed by several Author to provide change in transport rate due to infiltration/exfiltration effects.

Nielsen, (1997, 1998) designed the extra term in the numerator of Shields parameter's formula to represent the increase in shear stress due to the thinning of the boundary layer and the extra term in the denominator represents the effect of the downward seepage drag on the effective weight of the grains (Nielsen et al., 2001). Turner and Masselink (1998) also followed this approach, but included the effects of the seepage flow on the bed shear stress (e.g., Turcotte, 1960; Conley and Inman, 1994). They showed that the critical Shields

parameter may vary significantly due to the altered effective weight. Their modified Shields parameter incorporated an additional through-bed term, by which to calculate the swash zone transport rate in the presence of infiltration/exfiltration relative to the case of no vertical flow through the bed. Their modelling showed that altered bed stresses dominated during uprush, indicating enhanced sediment mobility relative to the case of an impermeable bed. They found that altered bed stress effects were also dominant during backwash. However, they found that the net effect of the enhanced bed shear stress was more important than the altered effective weight (seepage force) was less pronounced during backwash than during uprush, suggesting that infiltration/exfiltration processes support onshore sediment transport in the swash zone. Karambas (2003) also developed a numerical model to investigate effects of infiltration/exfiltration on sediment transport via a modified Shields parameter. He obtained similar results to Butt et al. (2001), with the numerical results indicating that for fine sediments, the time-averaged onshore transport was decreased, while the offshore transport was increased. For coarser sediments the time-averaged onshore transport was increased, while the offshore transport was decreased. He suggested that the critical grain size determining the transport direction was between 0.4 and 0.6 mm, but also noted that relatively small changes in the estimation of the friction factor could change the direction of the apparent influence of infiltration/exfiltration.

A Shields-type transport formula does not account for inertial forces, which may become significant for coarse grain sizes due to the high fluid accelerations during swash runup (Hardisty, 1990; Baldock and Holmes, 1997). Nielsen (2002, 2004) has proposed a modified Shields parameter for unsteady turbulent flow, which includes acceleration effects. This gives much higher shoreward-directed bed shear stresses during the uprush phase of the swash cycle than during the backwash.

#### 1.7.4 Sediment transport models

Sediment transport models are, essentially, of two kinds, namely discrete particle modeling and integral models (Nielsen, 1992). Discrete particle modeling (also termed particle trajectory models) is a promising approach because analyses at microscales interaction between the granular moving layer (sheet flow) and the fluid, which is crucial for more realistic prediction of the bed shear stresses (Calantoni and Puleo, 2006). However,

since it requires a two-phase flow analysis, it is beyond present computing power for practical applications (Brocchini and Baldock, 2008).

The majority of the existing sediment transport models are based on the integral approach. The main integrated properties are the sediment concentration and the velocity.

The sediment transport rate  $Q(t)$ , through a unit width of a vertical plane perpendicular to the x-u direction, can be calculated as:

$$Q(t) = \int_{z=0}^{D_z} c(z,t)u_s(z,t)dt \quad [1.45]$$

where  $D_z$  is the flow depth,  $c(z,t)$  is the local instantaneous sediment concentration and  $u_s(z,t)$  is the instantaneous, horizontal sediment velocity.

All the transport models were developed for the case of an exponential distribution of the time-averaged suspended sediment concentrations. Also in the SZ, the suspended sediment profile in the SZ can be described reasonably well by an exponential shape of the form:

$$c_z = C_0 e^{-z/l_s} \quad [1.46]$$

where  $c_z$  is the sediment concentration at a distance  $z$  from the bed,  $C_0$  is the reference sediment concentration at the bed ( $z=0$ ) and  $l_s$  is a mixing length scale. The latter represents the ratio between the eddy diffusivity of the sediment,  $\varepsilon_s$ , and the sediment fall velocity,  $w_f$ . Generally, it is assumed that  $\varepsilon_s$  is vertically invariant, i.e. independent of  $z$ . The mixing length scale suggested by Masselink et al., (2005) is of 0.02-0.03 m. In particular, they found that the reference concentration during the uprush ( $C_0=130 \text{ kg m}^{-3}$ ) is almost twice that during the backwash ( $C_0=71 \text{ kg m}^{-3}$ ). Moreover, the suspended sediment concentrations are not only higher during the uprush, but the sediment is also better mixed over the water column with the mixing length during the uprush ( $l_s=0.039 \text{ m}$ ) being almost twice that during the backwash ( $l_s=0.023 \text{ m}$ ).

The temporal variation in the average suspended sediment concentration and total suspended sediment flux is strongly related to the swash velocity.

Conley and Beach (2003) reported detailed measurements under storm conditions of the sediment load very near the bed. They observed that the vertical profile of net sediment transport could exhibit a reversal in cross-shore transport direction, with an offshore-directed transport high in the water column gradually weakening as the bed is approached and in the

bottom few centimetres a complete reversal in direction, with the bottom transport being directed onshore.

In addition, Conley et al. (2008) show that effect of flow stratification may be significant because it tends to increase sediment concentrations near the bottom and reduce concentration further from the bed and this effect is time varying and in-phase with the sediment concentration itself.

Sediment transport modelling typically relies on bed shear stress estimates indirectly derived from the near bed logarithmic velocity profile or the quadratic drag law. Close to the bed boundary, the current velocity  $U$  varies with the height  $z$  above the bed according to the logarithmic velocity profile

$$U(z) = \frac{u_*}{\kappa} \ln\left(\frac{z}{z_0}\right) + D_1 \quad [1.47]$$

where  $u^*$  is the friction velocity,  $z_0$  is the bed roughness length, and  $\kappa$  is von Karman's constant ( $\kappa \approx 0.41$ ). Schlichting (1979) defines the constant  $D_1$  as  $5.5U$  for smooth turbulent flow and  $8.5U$  for fully rough turbulent flow.

Empirical formulas based on numerous experiments on steady flow have been implemented to describe the amount of sediment transport in the SZ. Pioneering research on bed-load transport focused on unidirectional fluvial environments using a fluid energetic approach, where by the local sediment transport rate was related to the kinetic energy of the fluid (square of instantaneous velocity; Bagnold, 1966). Bagnold (1963, 1966) derived a stream-based sediment transport model. In that model, Bagnold assumes the sediment is transported in two modes, i.e., the bed load transport and the suspended transport. The bed load sediment is transported by the flow via grain to grain interactions, the suspended sediment transport is supported by fluid flow through turbulent diffusion. The total load sediment transport rate  $I_l$  reads (Bagnold, 1966):

$$I_l = \left[ \frac{\dot{\epsilon}_b}{\tan\phi - \tan\beta} + \frac{\dot{\epsilon}_s(1 - \dot{\epsilon}_b)}{w_f/u_b - \tan\beta} \right] P \quad [1.48]$$

where  $P$  is the available fluid power,  $w_f$  is the fall velocity of sediment.  $\dot{\epsilon}_b$  and  $\dot{\epsilon}_s$  are the bed load and suspended load efficiencies, respectively. The available fluid power is the work done by the bottom shear stress  $\tau_b$

$$P = \tau_b \cdot u_{bs} \quad [1.49]$$

where  $u_{bs}$  is the near bed free stream velocity.

Considering the bottom shear stress in the form of drag law (see the drag force previously seen) and also considering time averaging in the wave period  $T$ , Bailard and Inman (1981) relates the bed load to the third power of velocity and suspended load to the fourth power of velocity.

Concurrent field measurements of sediment transport and flow velocities in the swash zone have been obtained by Hardisty et al. (1984), Jago and Hardisty (1984). These studies investigate the applicability of the energetics-based sediment transport model of Bagnold (1963, 1966) to compute sediment transport rates in the SZ. Hardisty et al. (1984) proposed a modified energetics-based model of Bagnold (1966) for use in the SZ through the adding of a calibration coefficient for uprush/backwash phases. According to this model, the bed load transport for wave uprush and backwash can be written as

$$I_{wu} = \frac{k_u \bar{u}_u^3 T_u}{\tan\phi + \tan\beta} \quad [1.50a]$$

$$I_{wb} = \frac{k_b \bar{u}_b^3 T_b}{\tan\phi - \tan\beta} \quad [1.50b]$$

where the subscripts  $u$  and  $b$  denote uprush and backwash, respectively,  $I_w$  is the immersed weight sediment transport per unit meter beach width ( $\text{Nm}^{-1}$ ),  $k_u$  and  $k_b$  are calibration coefficients ( $\text{kgm}^{-3}$ ),  $\bar{u}$  is the mean flow velocity ( $\text{m s}^{-1}$ ),  $T_{(u,b)}$  is the uprush or backwash duration (s),  $\phi$  is the friction angle of the sediment and  $\beta$  is the beach angle.

The proposed modified energetics-based model is often used in modern process-based numerical model (e.g., Li et al.(2002)).

As seen this modification it seems adequately only for sediment transport by bed load, but Hughes et al. (1997) and Masselink and Hughes (1998) calibrated the Bagnold model for the SZ by relating the total sediment load carried up and down the beachface to uprush and backwash flow characteristics. Masselink and Hughes (1998) found that the value of this coefficient for upwash sediment transport is nearly twice as large as that for backwash sediment transport. If friction factors and/or transport coefficients are held constant for uprush and backwash, this invariably results in biasing predictions of net offshore transport (e.g. Masselink and Hughes, 1998; Puleo et al., 2000, 2001).

Energetics models (e.g. Bagnold 1963; Bowen, 1980; Bailard, 1981) do not work as well in the SZ as they do in the surf zone due to the influence of processes such as bore turbulence, in-exfiltration and sediment advection from the inner surf (Butt et al., 2007). Recent studies on sediment transport in accelerating flows (Drake and Calantoni, 2001; Nielsen, 2002; Hoefel and Elgar, 2003) have suggested that pressure gradients have a significant effect on sediment transport, a fact which would tend to favour transport under steep faced asymmetrical flows such as those occurring under swash bores or shoaling wave faces. These processes, in fact, may be just as important for sediment transport in the SZ, while their influence is either weak or non-existent further seaward, such as in the surf zone. Puleo et al. (2000) concluded that “Bagnold-type sediment transport equations are not adequate for describing sediment transport in the swash zone where complex fluid motions occur. This lack of success implies that not all the fluid physics are adequately described...”.

Anyway, to date, most swash sediment transport models are based on derivatives of the energetics approach, describing the bed load, suspended load or total load transport as a simple function of velocity, i.e.,  $u^n$  or equilibrium models (Pritchard and Hogg, 2005).

The energetics-based models are unable to account for the phase difference between the sediment transport rate and hydrodynamic forcing parameters (Bakhtyar et al., 2009). Hsu and Raubenheimer (2006) indicated that sediment transport in the SZ might not correlate to the instantaneous forcing computed in a specific location, so such equations might not be valid in the swash.

In this instance, an useful alternative to Bagnold’s energetics approach may be the Shield-type formulation, which relate the sediment transport rate to the Shields parameter. Most data on sheet flow sediment transport rates support formulas of the form:

$$A \propto (\theta - \theta_c)\sqrt{\theta} \quad [1.51]$$

where  $\theta_c$  is the threshold (critical) value for the Shields parameter below which no sediment movement occurs (for natural sand typical value is  $\theta_c \approx 0.05$ ) and  $A$  is the dimensionless sediment flux (cf. Dyer, 1986, p. 178). Nielsen (1992) slightly modified Eq. (1.51) and found:

$$A_{T/2} = 3(\theta - \theta_c)^{1.5} \quad [1.52]$$

where  $A_{T/2}$  is the dimensionless average transport over a half cycle and  $\theta$  is computed using the peak flow velocity attained during the half cycle.

Summarising the previous, none of the above models can resolve all potentially important details of the flow and sediment transport in the SZ, such as the wave boundary layer, percolation, flow separation at the beach step and the 2D or 3D distribution of suspended sediments. There is a need to obtain a predictive capability for sediment transport in the swash zone and two theoretical frameworks are available to be validated. Since physically the uprush and backwash flows are different, it seems logical that the associated sediment transport processes can also be different. This difference is likely to result in negatively (offshore) skewed velocity moments towards the seaward limit of the SZ (Elfrink and Baldock, 2002). As a result, steady flow energetics (Bagnold, 1963, 1966) and Shields-type (see Nielsen, 1992) sediment transport models based on the free stream velocities in the SZ may be inherently biased towards offshore transport. Consequently, the inclusion of turbulence in a description of the SZ kinematics appears necessary (Hughes et al., 1997a), together with a more detailed description of the bed boundary layer. Modelling turbulence generation by swash–swash interactions presents a major challenge, but appears critical to describing the total turbulent kinetic energy levels at the seaward swash boundary.

## 2. Literature review

As seen in the previous chapter, the SZ is a very special boundary layer in which not only must small scales be properly resolved and their influence fed into the larger-scale dynamics, but the connection between small and large scales must be performed (Brocchini and Baldock, 2008). Recent research has significantly increased both process knowledge and modelling ability (Elfrink and Baldock, 2002).

In the context of the micro-scale processes, despite good conceptual models of the influence of infiltration/exfiltration and beach groundwater on the boundary layer and swash hydrodynamics, quantitative measurements were prime requirement for future work, as prospected by some authors (Elfrink and Baldock, 2006). In this perspective, the tests carried out at GWK experiment explored the beach response induced by various groundwater regimes, where groundwater regimes were modified by a dewatering system. The beach dewatering can be treated as a local hydrodynamic process and considered as a swash zone boundary condition.

On the other hands, the scope of the tests carried out in the large wave flume of the Maritime Engineering Laboratory (LIM) at the Catalonia University of Technology (UPC), was to derive information in the changes in the beach response as a direct result of the wave groupiness. Wave grouping can be addressed to the global hydrodynamic processes and considered as a surf zone boundary condition.

### 2.1 The Beach Drainage System

The Beach Drainage Systems (hereinafter BDS) working principle is based on the concept that keeping the groundwater level low, back-swash is inhibited by increased grain friction in a non-saturated medium (Figure 2.1).

BDS enabling a decreased sediment transport from the swash area to the submerged beach have been considered as a soft-engineering solution by coastal managers for a number of reasons. Firstly, their installation is not so costly like building traditional breakwaters. Secondly, there is no visual impact. Thirdly, there is a perception that this is an environmentally sustainable solution to coastal erosion. However, the amount of published work on the performance of these systems is limited and often only grey literature (e.g.

unpublished technical reports) is available for most sites. The scientific background to the technology can be found by essentially looking at the research on the role of beach groundwater dynamics in controlling the erosion/accretion.

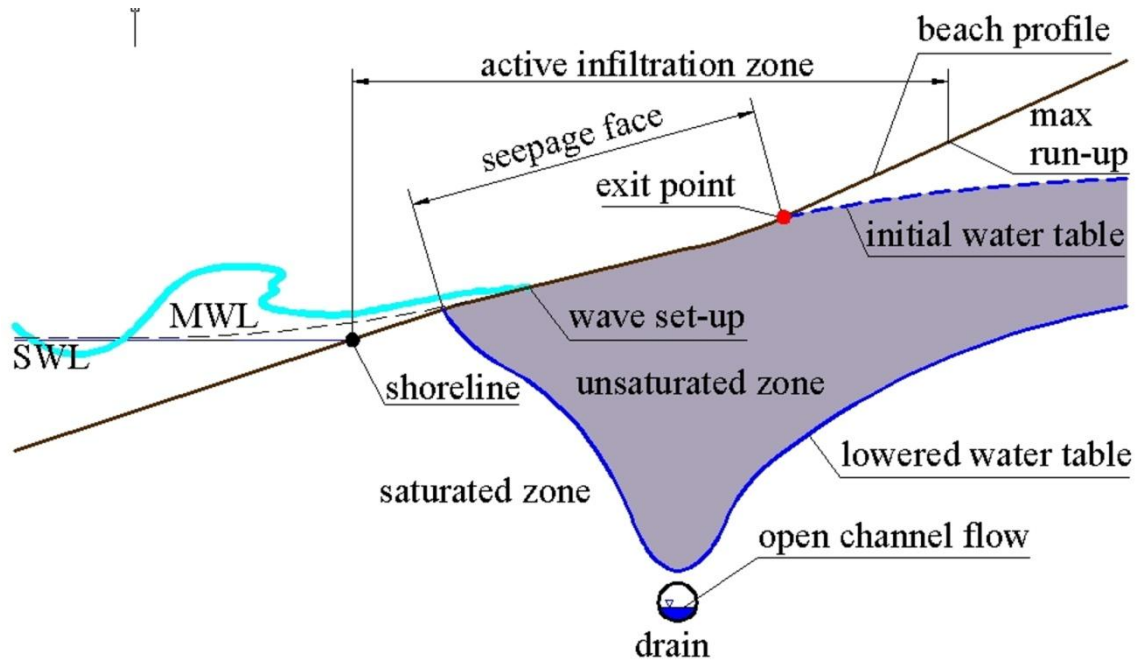


Figure 2.1: Role of a Beach Drainage System in controlling water table and nearshore hydrodynamic processes.

As seen in the previous chapter, the permeability, involved in the process of infiltration and exfiltration, more or less directly affects the beach profile evolution in the SZ. However, how the vertical flows over a porous seabed affect the swash hydrodynamics is not well known as yet (Horn, 2007). Many authors suggested that infiltration losses during swash uprush provide the main mechanism for beach accretion above the still water level. Because the swash lens is relatively shallow, a small change in water volume due to infiltration (or addition of water due to exfiltration) could influence uprush/backwash flow asymmetry and therefore the energy available for sediment transport (e.g. Bagnold, 1940; Grant, 1946; Grant, 1948; Duncan, 1964). However, others studies gave to infiltration/exfiltration minimal influence due to the small volume involved (e.g. Packwood, 1983). Researchers such as Martin (1970), Nielsen (1972, 1992, 1997), Turner and Nielsen (1997), Turner and Masselink (1998), Hughes and Turner (1999) and Baldock et al., (2001) consider the potential modifications of normal and shear stresses provided by vertical flows. An alteration in the effective weight of the surface sediment due to fluid loading/unloading acts to stabilise the

bed under infiltration or destabilises it under exfiltration. On the other hand, the vertical fluid drag leads to modified shear stresses exerted on the bed (Conley and Inman, 1992; Turner, 1995). Conley and Inman (1992) suggested that the sediment-mobilising properties of the flow would be diminished under exfiltration conditions due to decreased bed stress with turbulent kinetic energy removed from the bed, which would be characterized by thinner and less dense granular-fluid layers. Flow experiencing infiltration would be characterized by a more rapid and therefore distinct boundary layer, enhancing sediment mobilisation. They also suggested that different friction factors would be required for flow influenced by infiltration and exfiltration. Later Conley and Inman (1994) investigated the effect of seepage flows on oscillatory boundary layers in more detail, and suggested that infiltration tended to stabilise the flow while exfiltration tended to destabilise flow. Their experiments demonstrated that during infiltration, mean horizontal velocities throughout the boundary layer were uniformly greater.

Laboratory studies as early as the 1970s (Machemehl et al., 1975) have observed that by artificially lowering the groundwater level it is possible to enhance the sediment stability. The first field test was conducted by Chappell et al. (1979) in Australia, reporting qualitative evidence that the accretion of beach material on the foreshore of the profile was induced by lowering the groundwater elevation. Because of a highly dynamic shoreline, the investigators were unable to quantify the influence of the wells on the morphologic response of the beach. In 1985, the Danish Geotechnical Institute registered the first patent of a commercial drainage system (Vesterby, 1991, 1994), commonly called Beach Management System (BMS) or Beach Drainage System (BDS). However, it was only 4 years later that the first drainage prototype installation was finalized. The selected location was Hirtshals, on the north-eastern coast of Denmark.

The first scientific review to shed light on the topic was that of Turner and Leatherman (1997). After examining installations in USA, Denmark and UK, the authors concluded that there was too little evidence for being convinced that the systems had a positive effect. Nowadays, 14 years after the review, the number of published papers on the efficiency of beach dewatering remains limited, with a notable exception of a recent review paper related to Italian installations (Ciavola et al., 2008). The data published so far on Italian BDS refer to the sites of Lido di Ostia near Rome (Damiani et al., 2003), Alassio in Liguria (Bowman et al., 2007), Procida Island near Naples (Vicinanze et al., 2010) and Lido Adriano near Ravenna (Ciavola et al., 2009; Vicinanze et al., 2009). None of the cited case studies provide full

scientific evidence of undisputable positive results regarding beach stabilisation, although in some cases an overall reasonable performance was reported. In many cases no adequate long-term monitoring was undertaken at a frequency high enough to discriminate the response to high energy erosive events.

The spatial influence of the BDS has not previously been defined, as well as how the system performs under different wave conditions. Obviously a crucial point is where to locate the drain and at which depth, as this must influence the performance of the system. Another aspect which is unclear is also the possible benefit of using parallel drains. All these uncertainties can only be resolved through laboratory experiments under controlled conditions.

At present, the only studies present in the literature on laboratory experiments of BDS performance are that of Ranieri (2005), Horn et al. (2007) and Damiani et al. (2009), all likely to have suffered from scale effects. Of the three papers cited above, the most comprehensive piece of work is that of Horn et al. (2007). The experiments were carried out on fine and coarse sand beaches under raised and lowered back beach groundwater levels, concluding that the groundwater level had less effect on beach profile evolution under high energy storm conditions. The authors suggested that artificially lowered groundwater levels would not help much in the control of storm erosion, but could promote post-storm accretion.

## 2.2 Influence of free long waves, bichromatic wave groups and random waves

Swash motion is driven by both low frequency infra-gravity motions and short-period bores which collapse at the shoreline and then propagate up the beachface. The two mechanisms do not appear to be exclusive depending on the incident waves (Elfrink and Baldock, 2002) and foreshore slope (Hsiao et al., 2009). There have also been several observations and attempts to describe the interactions between subsequent swash waves within the SZ. Holland and Puleo (2001) showed that the presence or lack of swash collisions might describe whether foreshores accrete or erode (this was also suggested by Kemp, 1975). Recently, Alsina and Cáceres (2010) have shown the influence of the long wave component associated with wave groups on beachface erosion, notably the effects of long wave

backwash, the incidence of bores during the trough of the long wave water level oscillations and incident-backwash interactions.

Long waves have been proposed to be important for coastal zone sediment transport for many years (Carter et al., 1973; Short, 1975; Bowen, 1980; Holman and Bowen, 1982; Roelvink and Stive, 1989; O'Hare and Huntley, 1994). Although most gross sediment transport is induced by short-scale wind and swell waves, the morphological evolution depends on the gradients in the sediment transport, and these can be subtly changed over the time-scales of long waves and wave groups. In addition, the groups introduce further unsteadiness and intermittency into the short wave sediment transport processes, with the potential to change relationships between sediment pick-up, suspension and settling and hence net sediment transport rates and direction. Recent work has suggested that long time-scale beach evolution is deterministic (Ruessink et al., 2008), and that improved parameterisation of larger scale sediment transport processes is required, since the time-averaging in broad-scale models necessarily excludes long waves and wave groups. However, direct experimental investigation of the role of long waves and wave groups has been limited and, in the field, relies on correlating morphological and long wave length scales (e.g. Aagaard, 1990; Aagaard et al., 1994). However, because of hydrodynamic feedback between the morphology and long waves, the long-wave structure may be determined by the morphology, as proposed by Symonds and Bowen (1984) and as observed by Michallet et al. (2007), rather than the other way around. Therefore, it is difficult to identify the influence of the long wave on the morphology without a direct comparison between conditions with and without long waves. Over broader time and space scales, this morphological-hydrodynamic feedback becomes particularly important (Plant et al., 2004; Brocchini and Baldock, 2008).

The direct influence of long waves on sediment transport directions is complicated and varies across the nearshore zone. Offshore of the breakpoint, the expectation is that the bound long waves associated with wave groups will promote offshore transport (Shi and Larsen, 1984; Deigaard et al., 1999). Local suspended sediment transport measurements tend to support this model (Osborne and Greenwood, 1992; Aagaard and Greenwood 2008). Onshore of the bar, no clear model exists, but long wave transport tends to be predominantly landward. Aagaard and Greenwood (2008) proposed that long waves advect sediment away from maxima in the relative incident wave height ( $H/d$ ), which typically occurs near the crests of longshore bars, except very close to the shoreline where a monotonic increase in relative incident wave height is observed (Power et al., 2010). This implies divergence of infragravity

sediment transport at wave breakpoints (bars), which should cause destruction of the bar crest or the landward migration of the bar crest. This mechanism also offers an explanation for the very large range of observed magnitudes in long wave sediment transport, and also for the observed divergent transport directions. Offshore of the surf zone and in the outer surf zone, Ruessink et al. (1998) noted that long wave sediment transport was generally offshore, but an order of magnitude smaller than the transport by short waves and undertow, although these tend to cancel out near the breakpoint. Ruessink et al. (1998) also noted that the transport induced by free long waves did not appear to be significant around the outer breaker zone.

Wave groups also influence the short wave transport, as shown by Sato (1992). In this case, the inverse relationship between the direction of maximum flow velocity and the direction of suspended sediment transport over rippled beds can lead to onshore sediment transport at short wave frequencies, but offshore transport at long wave frequencies. Sato (1992) also noted that sediment concentrations were higher under grouped waves than for monochromatic waves with the same overall energy flux. The turbulence production and dissipation that is partially responsible for generating and maintaining sediment suspensions are also influenced by the mode of breaking, which varies for different wave steepness and for different waves within the wave groups (Ting and Kirby, 1995; Ting, 2002). This further complicates the influence of wave groups. Moreover, Goda (1975) suggested that this is an important phenomenon that leads to de-saturation of the surf zone at short wave frequencies due to the influence of long waves. In contrast, short waves may influence free long waves in several ways such as dissipation of long wave energy by short wave turbulence, phase changes due to variations in wave setup and changes in the reflectivity of the moving shoreline. Consequently, since long waves may strongly influence sediment transport, the influence of long wave-short wave interactions may be of significant importance for the modelling of coastal processes and the development of morphological features such as nearshore bars. The role of infragravity wave motion in influencing suspended sediment transport and morphology has been proved extensively in the field since the first studies almost 20 years ago (Roelvink and Stive, 1989; Beach and Sternberg, 1991).

It is now fairly well established that Low Frequency Wave motion (LFW) is able to affect the sediment transport as follows:

- the phase relationship between LFW and short waves undulation of the water surface will cause the short waves to vary in amplitude and, therefore, also to break at different positions over the beach profile;

- LFW velocities will advect sediment in suspension and will also alter the bed shear stress which entrains the sediment;
- LFW motion will include a second-order mass transport if a partial standing wave motion is set up by the reflected LFW (this will only be applicable if the motion is steady and has a narrow band spectrum);
- LFW are also powerful agents for removing sediment put in suspensions by breaking wind waves around Low Crested Structures, thus contributing significantly to their erosion and failure.

The importance of long waves, thus, is not only the additional wave induced velocity and the long wave influence on the short wave hydrodynamics (Goda, 1977; Baldock and O'Hare, 2004) but also the formation of standing waves, or a cross-shore and longshore nodal structure (e.g. Holman and Bowen, 1982). Dally (1987) investigated experimentally if the formation of longshore bars was consistent with the surf beat structure, yet very little evidence for surf beat contributing to the bar formation was observed, and undertow appeared the dominant bar forming mechanism. Numerical modeling (Roelvink and Stive, 1989; Roelvink, 1993) has been used to investigate the role of surf beat by including and excluding long wave terms from a numerical model and comparing the predicted morphology with a measured beach profile from random wave tests. Including long waves in the model smoothed the bar, reduced the bar height and moved the bar crest seaward, and also produced less erosion in the inner surf zone. Jannat and Asano (2007) adapted a numerical model from Kobayashi et al. (1987) to investigate sediment transport under long waves. The long waves induced small changes in the surf zone, and larger changes in the SZ, where long waves have maximum amplitude.

Both free and forced long waves occur in the nearshore zone and surf zone, but little previous work has considered the overall impact of free long waves on the beach evolution. Similarly, direct investigation of how long waves and wave groups modify sediment transport and the erosion or accretion of beaches is lacking. In fact, although there has been much investigations on the kinematics of extreme waves in deep water using focused wave groups in wave flumes and basins (Longuet-Higgins (1974), Rapp and Melville (1990), Baldock et al. (1996), Barnes (1996), and Johannessen and Swan (2001)) there has been little research on the wave grouping in the nearshore environment. For repeated wave groups, Borthwick et al., (2006) confirms the presence of a low frequency free wave, followed by higher frequency waves of the main group and trailing higher order harmonic waves.

Under random wave conditions in small-scale experiments, Dally (1991) observed that seiching influences the final equilibrium profile, smooths the bar-trough morphology and carries sediment higher in the swash zone.

Baldock et al. (1997) measured surface elevations in the inner surf zone and swash oscillations on a steep beach of 1:10 using regular waves, bichromatic wave groups and irregular waves. They found for bichromatic wave groups that much of the incident wave grouping remains both at the still-water shoreline (SWS) and within the swash and that the shoreline motion is modulated at the incident wave group frequency. They also found that the swash oscillation driven by the bichromatic wave groups on the 1:10 slope is largely dominated by low frequency motions.

Both bichromatic and random (JONSWAP) waves were used by Brocchini and Bellotti (2002) to evaluate and simplify a theoretical model of Shoreline Boundary Conditions to be used as SZ boundary in wave-averaged nearshore circulation models. Although there are insights about the effects of individual long-waves in hydrodynamic and shoreline motion terms, few direct experiments have investigated the influence of free long waves and wave groups on surf and swash zone morphodynamics. Their influence appears significant, as shown by Baldock et al. (2007) and Baldock et al. (2010), with free long waves tending to reduce offshore sediment transport or increase onshore sediment transport. On the other hand, bichromatic wave groups resulted in much greater erosion than equivalent monochromatic waves. However, those experiments did not consider random waves. Furthermore, the small-scale of the experiments (water depth 0.5m, wave height 0.05m-0.1m) meant that scale-effects could have been significant in influencing the results. The complexity of the problem suggested the need to obtain and operate on data acquired through high quality laboratory investigations at large scale.

### 3. Swash zone response induced by different groundwater regimes: large-scale experiments at GWK

#### 3.1 Experimental procedure and setup

##### 3.1.1 Wave flume and instrumentation

The 2D physical model was performed at the Coastal Research Centre (FZK) of University of Hannover and of Technical University of Brounischweig. In particular experimental tests were carried out at the "Grosser WellenKanal" (GWK), which represents an unique test facility to perform full scale laboratory experiments in coastal and offshore engineering researches (Fig. 3.1a).

The GWK is a 307 m long, 7 m deep and 5 m wide flume and represent the greatest laboratory of maritime hydraulic of the world. The facility is equipped with a piston type paddle of about 900 kW combined with an upper flap for generating regular and irregular waves (Fig. 3.1b).



Fig. 3.1. a) General view of GWK during a wave attack. b) View of the wave generator.

The gearwheel driven carrier gives a maximum stroke of  $\pm 2.10$  m to the wave paddle, which is 5 m wide and about 6.70 m high. Water waves up to a height of 2.00 m quasi-prototype conditions can be simulated. The stroke can be superimposed by upper flap movements of  $\pm 10$  degree in order to simulate natural water wave kinematics most accurately. A large cylinder integrated in the carrier compensates the water force in front of the paddle (rear is free of water). The wave generation is controlled by an online absorption system. This special system works with all kinds of regular and irregular wave trains. Thus, the tests are unaffected

by re-reflections at the wave generator and can be carried out over nearly unlimited duration (Fig. 3.2).

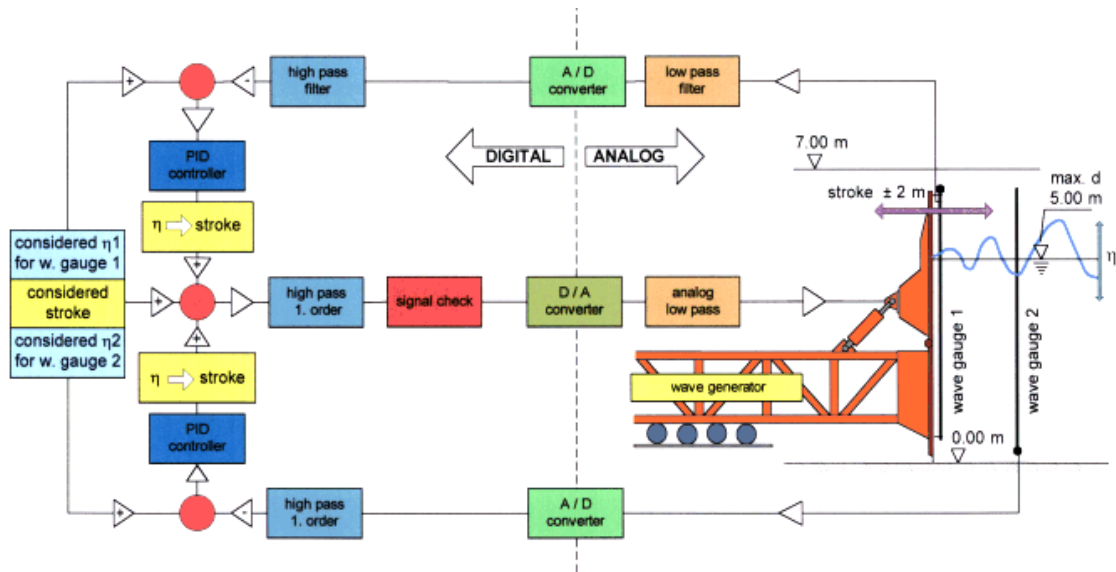


Figure 3.2. Online absorption control system for the wave generator of GWK.

The experimental strategy consisted of building a physical scale 1:1 model. The bed morphology was realized by placing the sand on the bottom of the flume, which in the final part has an asphalt permanent slope of 1:6 (Fig. 3.3).

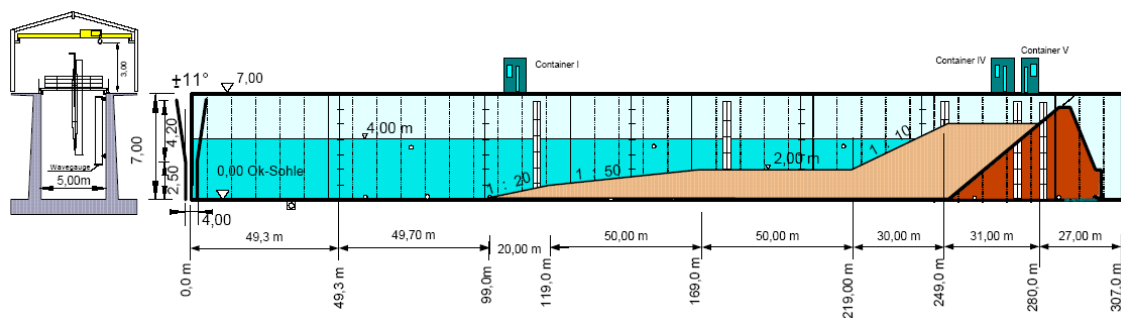


Figure 3.3. Scheme of the longitudinal profile of the wave channel with the principal characteristics of the movable bed.

Over 2000 tonnes of material were estimated to be used to cover a volume of approximately  $1300 \text{ m}^3$ . A non-erodible horizontal plane (the flume bottom) characterized the initial 99 m.

Then, it started the moulded sand beach with an initial slope of 1:20 ( $2.86^\circ$ ) for 20 m, changing to 1:50 ( $1.15^\circ$ ) in the next 50 m and in an horizontal part for the following 50 m. The last 30 m, corresponding to the surf and the swash zone, were reached with a slope 1:10 ( $5.71^\circ$ ) for static tests (Section 3.1.3) and for dynamic tests A1 (Section 3.3.2.1), of 1:8 ( $i = 8.00\%$ ) for dynamic tests A2 (Section 3.3.2.2), and of about 1:8 ( $i = 8.03\%$ ) during dynamic tests A3 (Section 3.3.2.3). The beach consisted of quartz sand, characterized by a reasonable well sorting with no mud fraction. Fine and very fine sand fractions characterized more than 20% of the sample. The characteristic diameter,  $D_{50}$ , was of 0.33 mm (medium sand in the Udden-Wentworth scale), with a permeability  $k = 3.2 \cdot 10^{-2}$  cm/s, and a vertical fall velocity  $w_f = 4.8$  cm/s. The grain size distribution of the sand used during the experiments is presented in Figure 3.4.

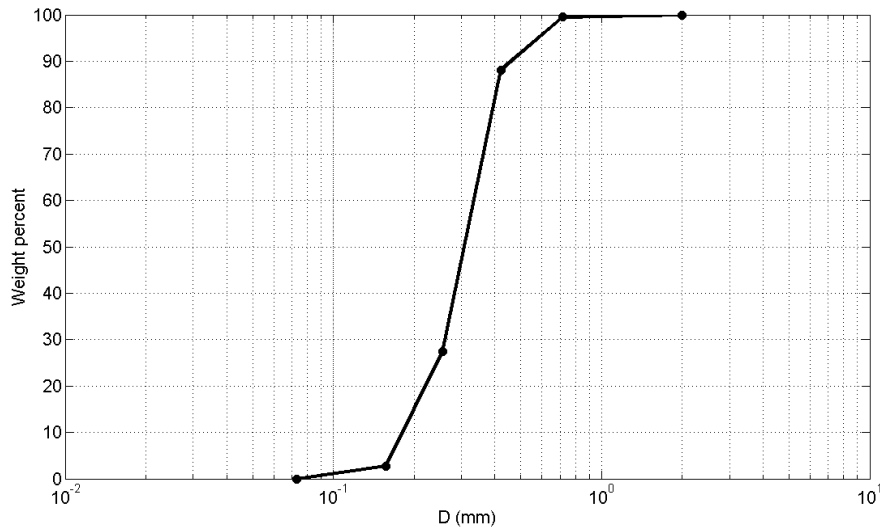


Figure 3.4. Grain size distribution of the sand used in the model.

The laboratory sand is analogous to that of the typical beaches of the Northern Adriatic Sea as showed, in particular, at Lido Adriano (Ravenna, Italy), where a prototype BDS installation was extensively studied by Ciavola et al. (2008, 2009).

The beach was equipped with a drainage system that consisted of four corrugated PVC drain pipes (hereinafter termed as D1, D2, D3 and D4) parallel to the shoreline, with a diameter of 0.2 m. To avoid blockage by sand during the infiltration processes, each drain was covered by a double layer geotextile drape. The pipes had a series of rectangular holes around their surface to drain the groundwater flow during the tests (Fig. 3.5).

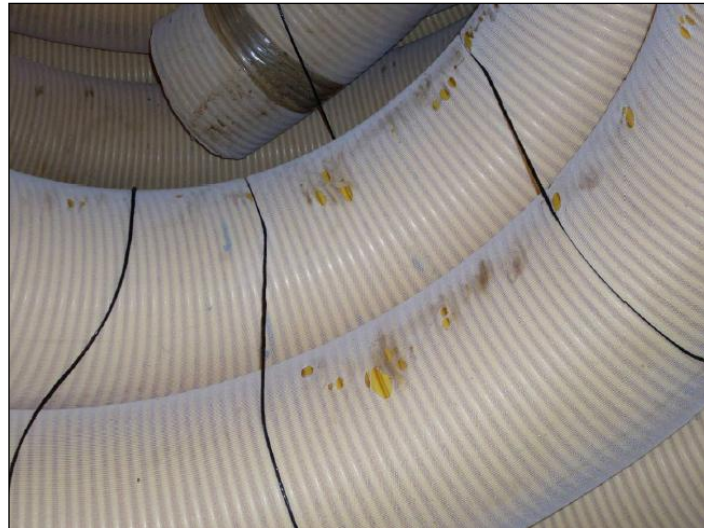


Fig. 3.5. Detail of the drains covered by geotextile.

The top of the drains was located below the emerged beach at 40 cm under the still water level. Starting from the wave paddle, the distance of each drain was 242.10 m, 242.40 m, 247.00 m and 252.00 m, i.e. at a distance from the shoreline ranging between about 1 and 12 m (Figure 3.6 and 3.7).

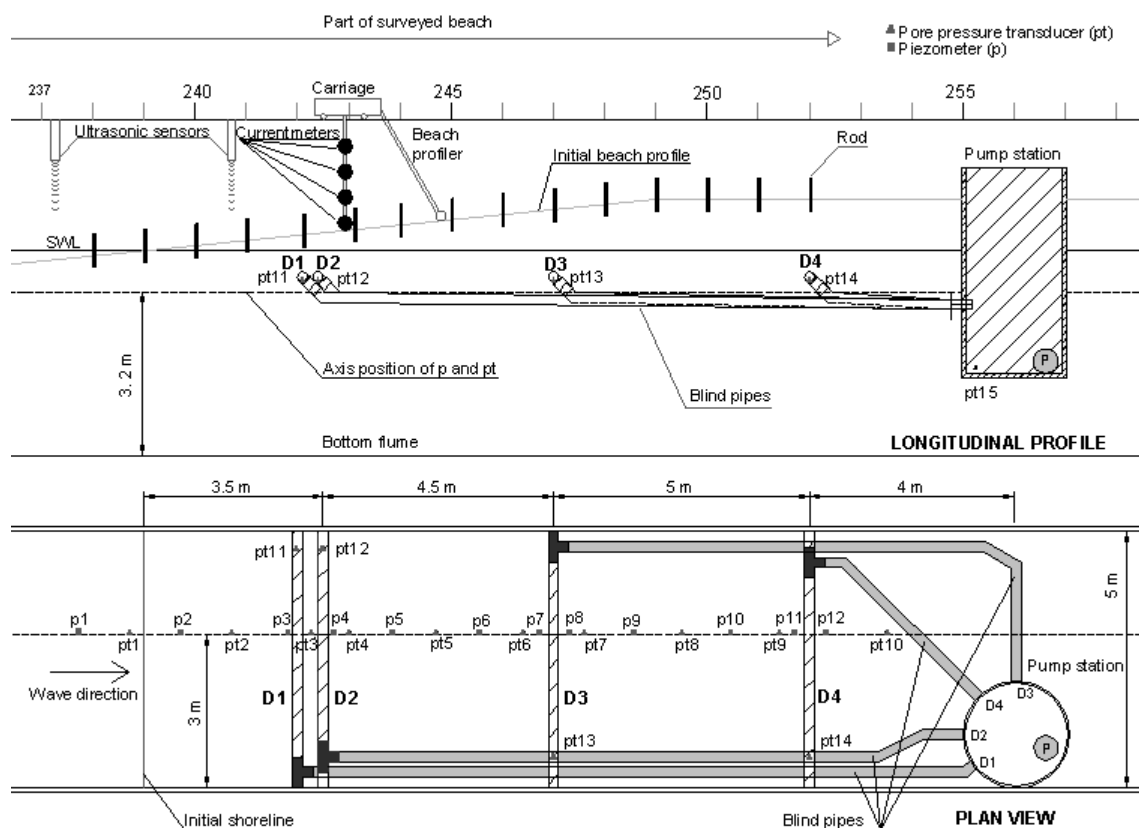


Figure 3.6. Longitudinal profile and plan view of nearshore experimental beach equipped with BDS.



Figure 3.7. Placement of the drains along the wave flume.

The installation of the drains with different spatial position was carried out to analyse their optimal distance from the shoreline in terms of morphodynamic and hydrodynamic efficacy of the system. Since the maximum run up resulted to be lower than expected and due to a reduction of the access time to the facility given to our research project, steps using D4 was never carried out. The drains had a small longitudinal slope which allowed their connection into rigid PVC blind pipes of the same diameter and a variable length ranging from 4 m to 13 m. The blind pipes were linked to a pumping station to collect the groundwater flow. A gate valve to allow the drains to be switched on/off. Its diameter was 2.08 m and it was made of 7 concrete elements of about 0.5 m height. The total height of the pumping station was 4.11 m and its distance from the bottom channel was equal to 1.61 m (Fig. 3.6 and 3.8). The level of the joints between blind pipes and the pumping station was at about 3 m from the bottom of the channel, to guarantee that the pump was submerged due to drainage by gravity. The automatic working of the pump was performed by two buoys placed at a relative vertical distance of 0.08 m which, simultaneously, measured the rate of drained flow. From the pump station the water was finally removed in the initial part of the flume by an iron pipe with a diameter equal to 0.2 m (Fig 3.9). A detailed profile of drains, blind pipes and pump station are shown in Figure 3.10.

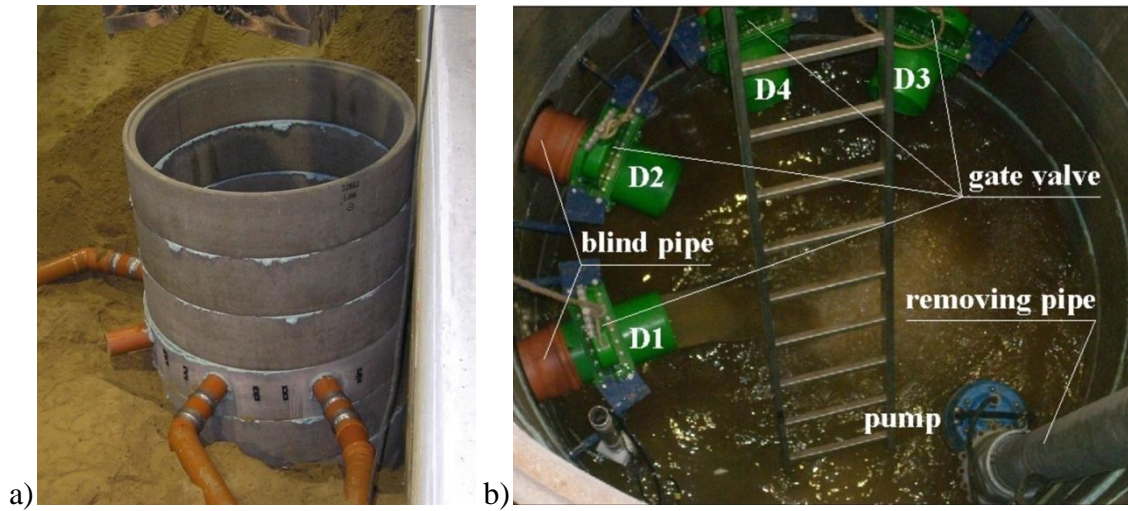


Figure 3.8. a) Blind pipes connected to the pump station. b) Valves and iron pipe inside the pump station at the end of blind pipes during a test.



Figure 3.9. a) Submerged pump. b) Iron pipe of the pump station.

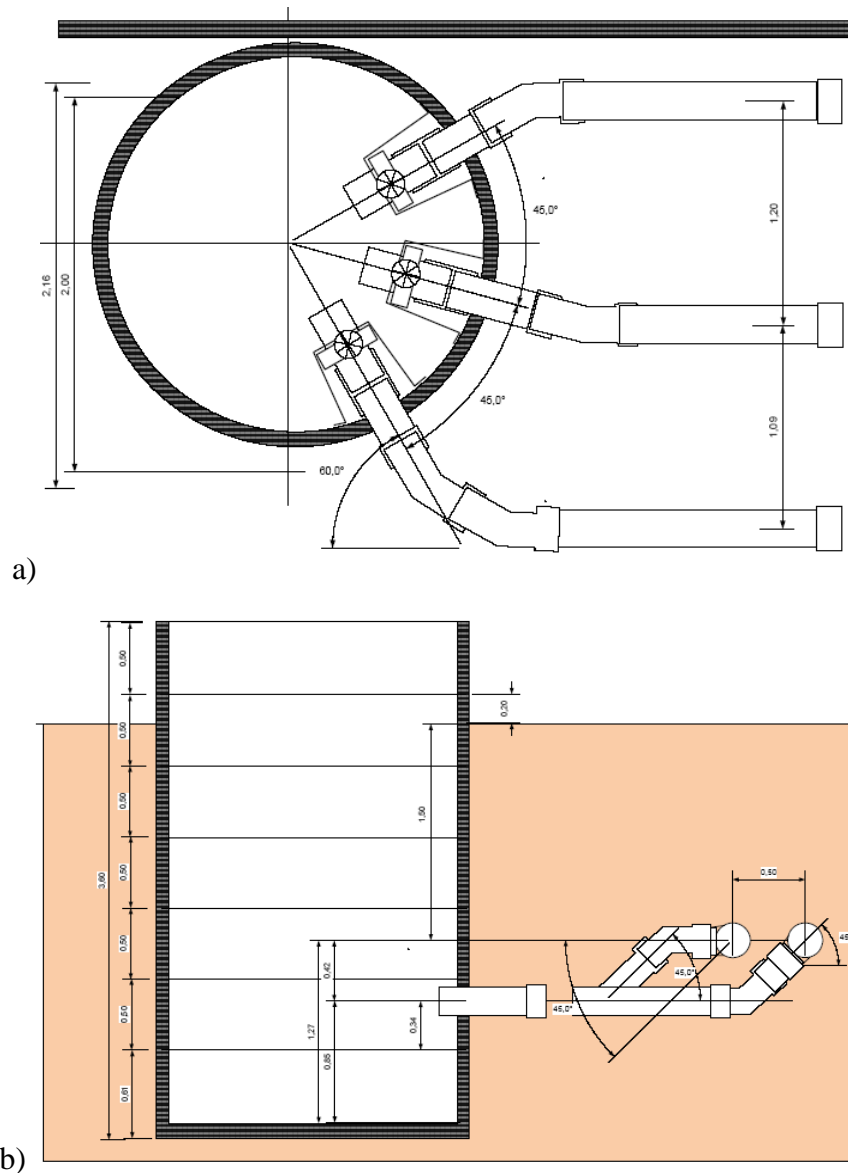


Figure 3.10. Pump station and terminal part of blind pipes: a) Plan view. b) Profile.

### 3.1.2 Measurement instruments

A large number of surface elevations, pressures, velocities, drainage flows and bottom beach experimental data were sampled to analyse BDS effects on the nearshore morphodynamics and hydrodynamics. During the experiments hydrodynamic measurements have been carried out inside the beach, by piezometers and pressure transducers, and along the channel, by wave gauges, electromagnetic currentmeters and ultrasonic sensors.

The instruments installed in the channel for both hydrodynamics and morphodynamics measurements were:

- 20 wave gauges;
- 12 piezometers;
- 16 pore pressure transducers;
- 1 flowmeter;
- 4 electromagnetic currentmeters;
- 2 camcorders;
- 1 propeller;
- 64 rods;
- 1 bottom profiler,
- 2 altimeters.

Wave characteristics were measured along the flume by 20 resistive gauges (wg). With reference to the wave paddle the x-positions of the gauges are illustrated in Table 3.1. Before the test starting, the wave gauges were subjected to the preliminary calibration on the basis of the water levels (Fig. 3.11).

	<b><i>x</i> (m)</b>		<b><i>x</i> (m)</b>
<b>WG1</b>	50.10	<b>WG11</b>	108.00
<b>WG2</b>	52.20	<b>WG12</b>	116.00
<b>WG3</b>	55.90	<b>WG13</b>	126.22
<b>WG4</b>	61.30	<b>WG14</b>	140.00
<b>WG5</b>	79.05	<b>WG15</b>	161.90
<b>WG6</b>	81.15	<b>WG16</b>	180.00
<b>WG7</b>	84.85	<b>WG17</b>	200.00
<b>WG8</b>	90.25	<b>WG18</b>	210.00
<b>WG9</b>	97.30	<b>WG19</b>	220.00
<b>WG10</b>	102.09	<b>WG20</b>	230.00

Table 3.1. Wave gauges positions with respect to the wave generator



Figure 3.11. Wave gauges along the channel

Water table measurements were carried out below the beach surface using a set of 12 piezometers (p) and using 10 pore pressure transducers (pt) as reported in Figure 3.12 and 3.13. The piezometer sensors were located at about 2 m from the left wall of the channel and connected by small plastic pipes to cells installed in the sand at about 0.1 m under the drains at a distance of 3.2 m from the bottom channel. They were respectively located at 237.80 m, 239.79 m, 241.79 m, 242.72 m, 243.89 m, 245.55 m, 246.68 m, 247.33 m, 248.59 m, 250.50 m, 251.70 m and 252.30 m from the wave generator.

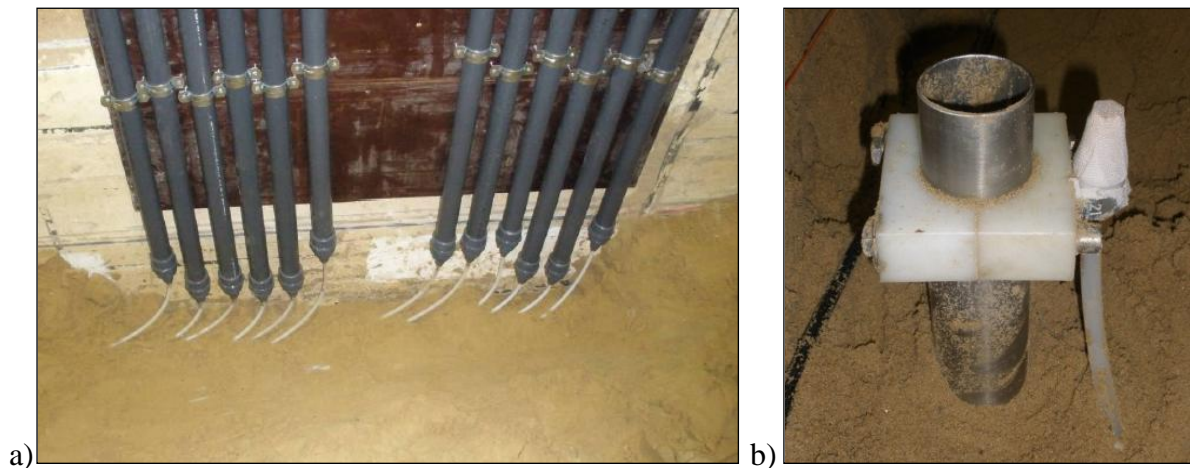


Figure 3.12. a) Detail of piezometers, b) Placement of a piezometer sensor.

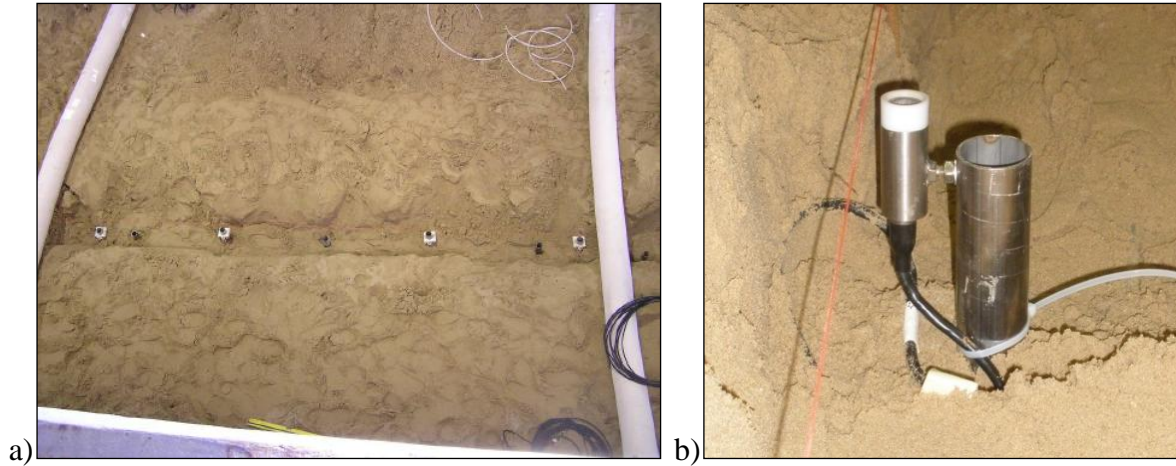


Figure 3.13. a) Placement of piezometer sensors and pressure transducers below the drains.  
 b) Detail of a pressure transducer.

In Tab. 3.2 the plano-altimetric measurements of the piezometers are explained. The y-values are referred at about 0.1 m under the drains.

	<b>x (m)</b>	<b>y (m)</b>
<b>P1</b>	237.8	3.2
<b>P2</b>	239.79	3.2
<b>P3</b>	241.79	3.2
<b>P4</b>	242.72	3.2
<b>P5</b>	243.89	3.2
<b>P6</b>	245.55	3.2
<b>P7</b>	246.68	3.2
<b>P8</b>	247.33	3.2
<b>P9</b>	248.59	3.2
<b>P10</b>	250.5	3.2
<b>P11</b>	251.7	3.2
<b>P12</b>	252.3	3.2

Table 3.2. Piezometers position with respect to the wave generator

The pore pressure transducers (pt), instead, were located at about the same level of the piezometers but at a different spatial distribution. Additional 4 pressure transducers (transducers pt11, pt12, pt13 and pt14) were located inside the lowest part of the drains in

order to analyse their hydraulic regime (Fig. 3.14a). As aforementioned, a last pressure pore transducer (pt15) has been placed in the pump station to evaluate the drained flow (Fig. 3.14b). In particular, this transducer was located at 0.08 m from bottom pump station and at 1.69 m from the bottom channel. Her distance from the wave paddle was 255.15 m. Tab. 3.3 shows the plano-altimetric position of all pressure transducers (Tab. 3.3).

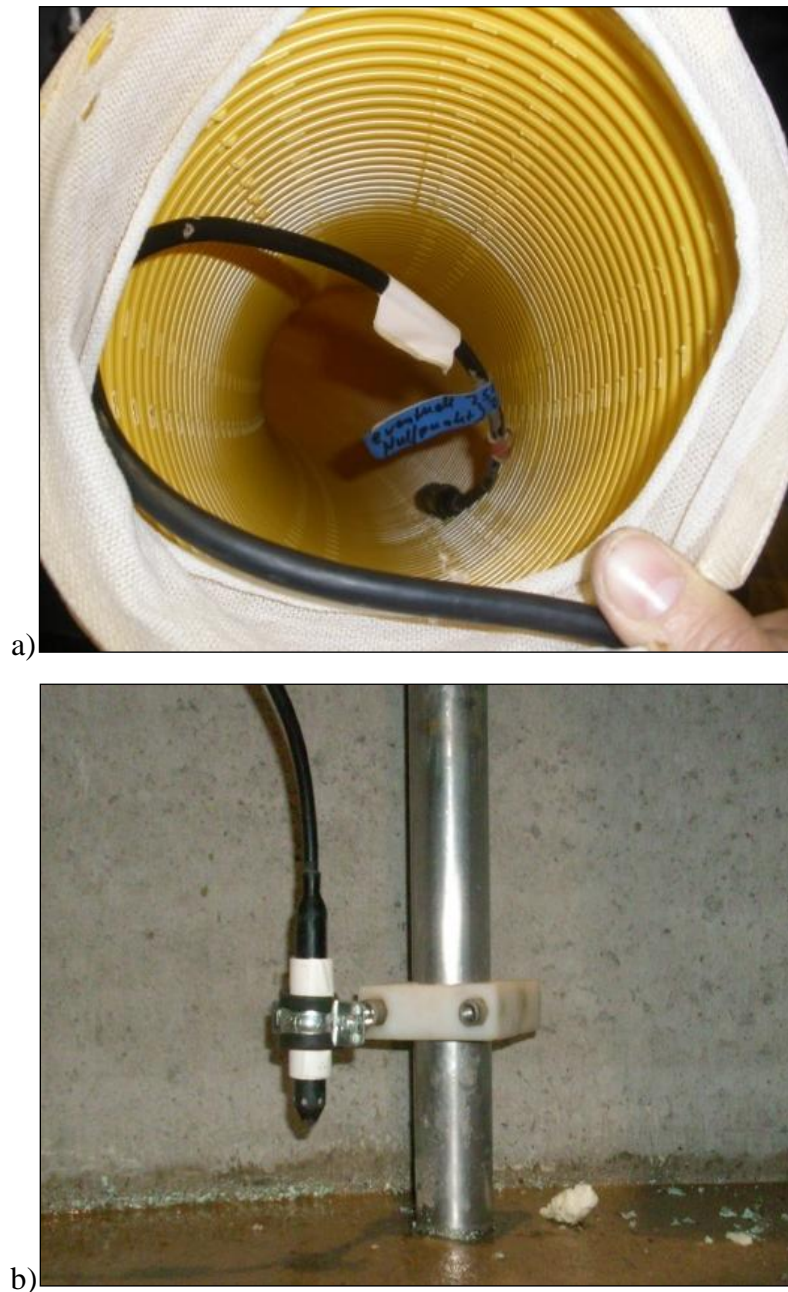


Figure 3.14. a) Transducer in the drain. b) Transducer in the pump station.

Pressure transducers	x (m)	y (m)
pt1	238.83	3.186
pt2	240.80	3.182
pt11	242.25	3.189
pt3	243.79	3.188
pt12	244.83	3.189
pt4	246.28	3.195
pt5	247.63	3.193
pt6	249.56	3.191
pt13	251.52	3.195
pt7	253.63	3.197
pt8	242.10	3.460
pt9	242.40	3.470
pt14	247.00	3.450
pt10	252.00	3.450
pt15	255.15	1.690

Table 3.3. Pore pressure transducers position with respect to the wave generator.

Moreover the measurements of the drainage discharges have been also performed using a flowmeter placed on the iron pipe (Fig. 3.15). This instrument was equipped by an internal digital oscilloscope and set using a sampling frequency  $f = 1$  Hz.



Figure 3.15. Flowmeter placed on the external iron pipe.

In order to analyse the nearshore flow field in presence or not of the drains, 4 two-dimensional electromagnetic currentmeters (ECM) have been used to measure the nearshore horizontal ( $u$ ) and vertical ( $v$ ) wave velocity. The instruments were installed on a vertical pier connected to the carriage of the channel. For each wave test the electromagnetics have been placed in different transversal sections inside the surf zone as function of the nearshore bed evolution. The electromagnetics were staggered (2 in right side and 2 in left side) with a distance one from other equal to 0.07 m for preventing possible mutual interferences. The lowest ECM was placed at 0.1 m from the flume bottom and the higher was frequently across the water surface during the dynamic tests (Fig. 3.16).



Figure 3.16. (a) Relative distances of the electromagnetic currentmeters.  
(b) Electromagnetics connected to carriage.

A propeller currentmeter was installed in the swash zone, near the shoreline and the right wall, at 230.7 m from the wave generator and at a distance from the bottom channel equal to 4.155 m. The instrument allowed to measure the positive horizontal velocity induced by the run up flow (Fig. 3.17).



Figure 3.17. Propeller in the swash zone

Two bed-level ultrasonic sensors (M-300/95 model by Massa), also called altimeters, were installed in the swash zone at 232.2 m and 240 m from the wave paddle (Fig. 3.18). They allowed the study of intermittent bed changes and the position of the water level during uprush and backwash cycles in the swash zone. These acoustic sensors were installed at 6.03 m and 5.04 m above the bottom of the channel. Following the calibration approach adopted by Turner et al. (2008) and the suggestions on the acoustic considerations and the optimization of sensor selection provided by Massa (1999a,b), the distance resolution of the sensors combined with the electronic noise resulted in an accuracy of  $\pm 1$  mm.

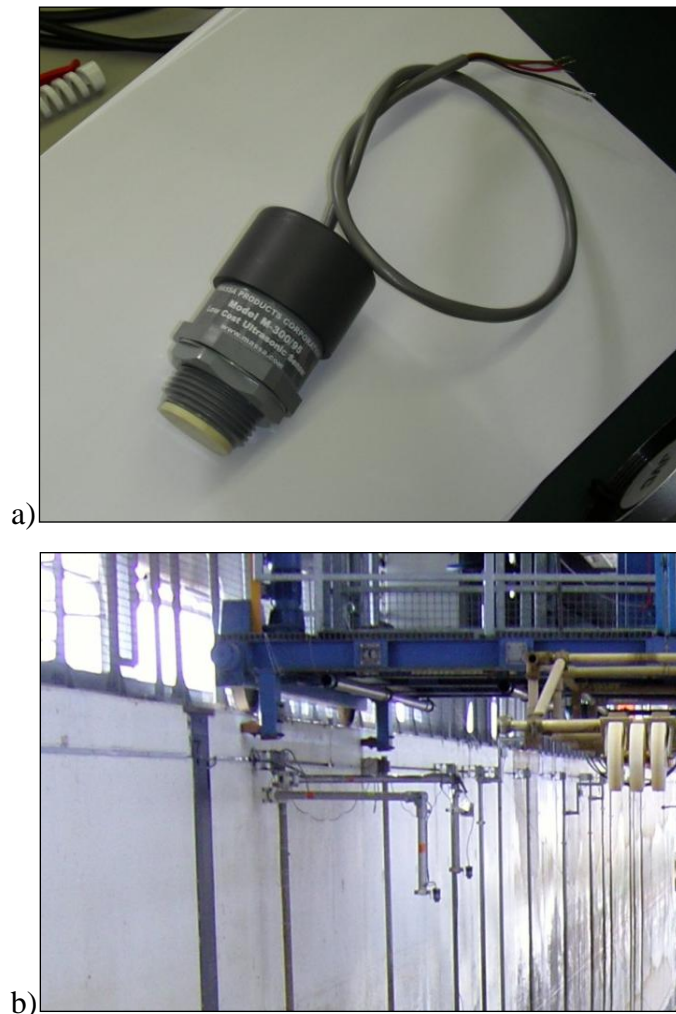


Figure 3.18. (a) Altimeter before the installation. (b) Altimeters placed along the flume.

The time series recorded by wave gauges, pressure transducers, electromagnetic currentmeters, propeller and altimeters have been sampled by 64 channels PRESTON acquisition system adopting a sampling frequency  $f = 20$  Hz.

Beach morphological measurements were performed using a beach profiler mounted on a carriage. (Fig. 3.19). The profiler consisted of a wheel, a metal jib and a PC-based acquisition

system (Fig. 3.20). A software converted the wheel rotations and the angle of the jib to distance and elevation above a reference level. As already mentioned, measurements were conducted after each cycle of wave attacks. The depth samplings of the profiler were horizontally spaced every 0.025 m at a distance between 206.375 m to 252.575 m from the wave paddle and performed within the closure depth and the maximum runup level for the adopted wave conditions.

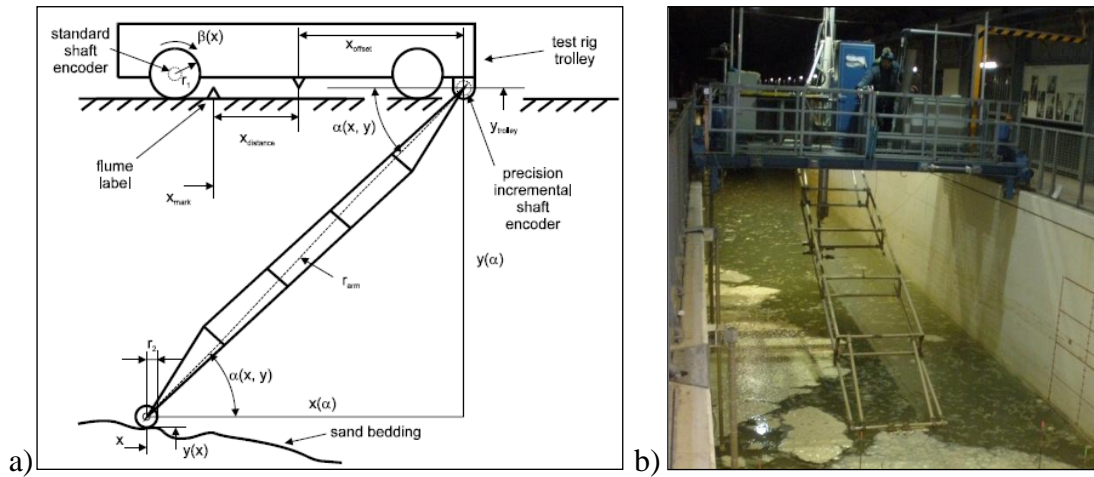


Figure 3.19. (a) Characteristics of adopted bottom profiler on the carriage.  
(b) Profiler mounted on the carriage.

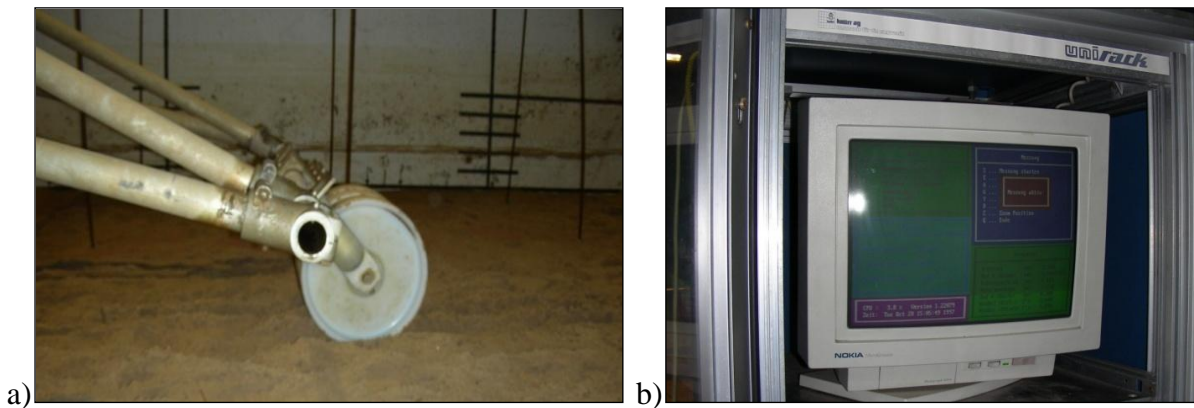
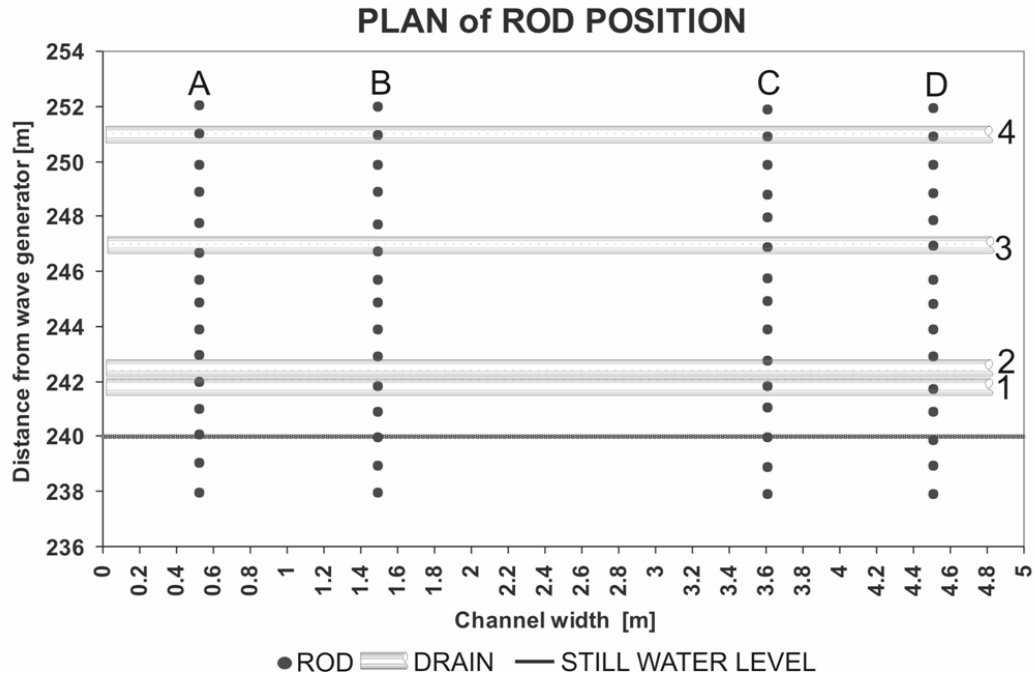


Figure 3.20. a) Metal jib with the wheel; b). Bottom profile acquisition system.

Disturbance was studied installing 60 metal rods with washers along four lines spacing from the lower swash zone to the berm (Figure 3.21a,b). Readings of the depth of the washer and bed elevation were undertaken at the end of each run of waves using a graduated pin with millimetre precision. While the bed elevation was always referred to the top of the rod, the depth of the washer was measured by inserting the pin into the sand, till it was felt that the washer had been hit. The definition of the measured DoD parameters can be seen in Fig. 3.22.



a)



b)

Figure 3.21. a) View of the area studied using rods. The drains are numbered 1-4; b) Rods along the channel.

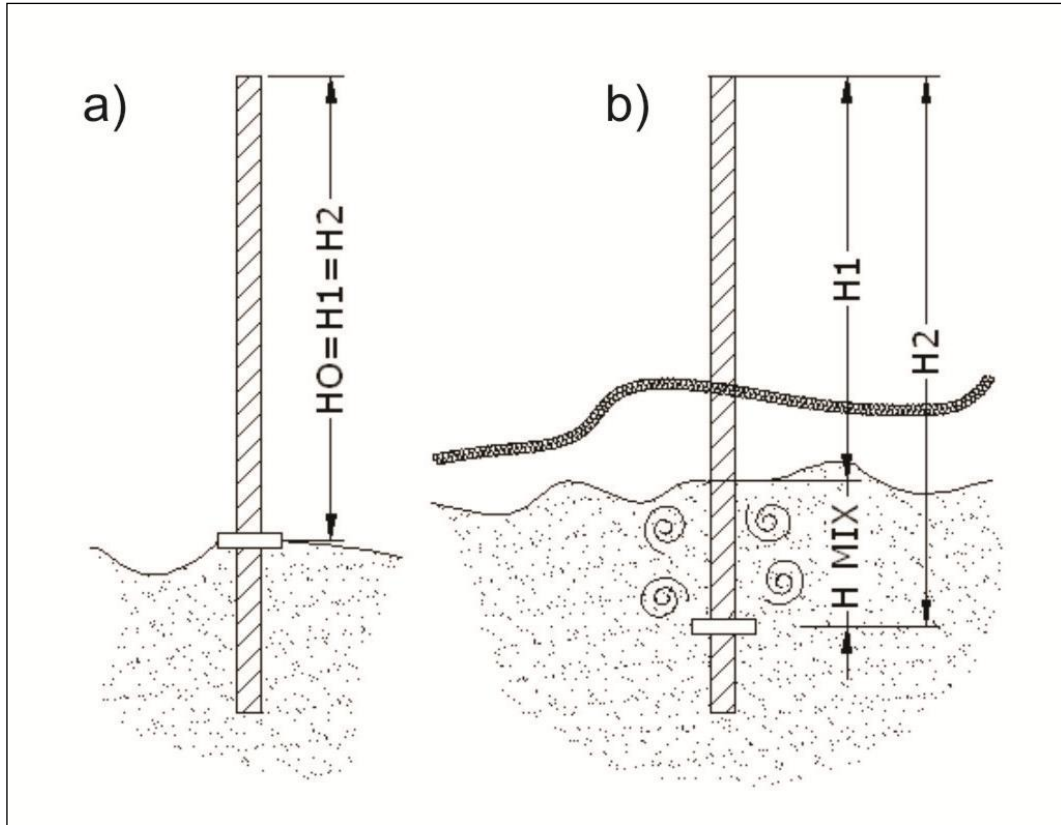


Figure 3.22. Definition of DoD parameters.

### 3.1.3 Test program

The experimental tests on the morphodynamic and hydrodynamic effects for a beach protected by a drain system have been carried out during February-March 2009 for a total period of 23 days. The experimental procedure consist of two kinds of test, termed “statics” (with undisturbed water levels) and “dynamics” characterized by different irregular wave attacks. The laboratory experiments have been characterized by different configurations with one or more drain opened or without.

#### 3.1.3.1 Static tests

The experimental program for the 15 “statics” tests has been made of two set by using two different static levels: 4.00 m (S1) and 4.20 m (S2) from the bottom of the channel.

The aim of these tests was to study the influence of the drains depth respect the still water level on the system in working. The static experiments, in fact, have been characterized by different drain configurations, evaluating the water table lowering and the drained flow induced by the drain opening and, finally, the changes of the water table when the drains have been closed. The assumption of an higher water level (S2) has been addressed to simulate set up phenomena and to compare the water table lowering with S1 tests. In this case, only the hydrodynamic aspects have been analyzed inside the beach induced by presence or not of the drains. The evaluation of the water table fluctuations have been performed using piezometer and transducer measurements. The measurements of the water column pressures in the sand has been started after about 1' from the opening of the valves ( connected to the activation of the drains) in order to minimize the initial depression phenomenon induced by the air entrance due to the fast opening of the gate valve (more details are discussed in Section 3.3.1.2).

The test duration was variable as function of the performances of the beach to reach a quasi-equilibrium regime of the water table. The characteristics of the static experiments with different configurations of drains are reported in Table 3.4, showing test name, water level, status of the drains, and test duration. The name of each test “0” indicated drains off, while “1” indicated drains on. Each test, except for the test 01\_S1\_1000, was defined by a first condition with drain/drains opened, followed by a successive condition without drains, having similar duration. This approach allowed to analyse the reaching of initial hydraulic conditions of the piezometric before the influence of a drain.

<b>Test name</b>	<b>Static level (m)</b>	<b>Drains on</b>	<b>Drains off</b>	<b>Test duration (min)</b>
01_S1_1000	4.00	1	2_3_4	60.00
02_S1_0100	4.00	2	1_3_4	68.60
02_S1_0100	4.00	-	1_2_3_4	51.40
03_S1_1100	4.00	1_2	3_4	45.28
03_S1_1100	4.00	-	1_2_3_4	48.95
04_S1_0010	4.00	1_2	3_4	48.87
04_S1_0010	4.00	-	1_2_3_4	42.78
05_S1_0001	4.00	4	1_2_3	49.37
05_S1_0001	4.00	-	1_2_3_4	52.32
06_S1_0011	4.00	3_4	1_2	49.38
06_S1_0011	4.00	-	1_2_3_4	70.62
07_S1_1110	4.00	1_2_3	4	48.02
07_S1_1110	4.00	-	1_2_3_4	44.53
08_S2_1000	4.20	1	2_3_4	47.65
08_S2_1000	4.20	-	1_2_3_4	48.90
09_S2_1100	4.20	1_2	3_4	48.61

09_S2_1100	4.20	-	1_2_3_4	46.81
10_S2_0001	4.20	4	1_2_3	48.51
10_S2_0001	4.20	-	1_2_3_4	59.41
11_S2_0010	4.20	3	1_2_4	58.28
11_S2_0010	4.20	-	1_2_3_4	47.40
12_S2_0011	4.20	3_4	1_2	47.93
12_S2_0011	4.20	-	1_2_3_4	49.08
13_S2_0100	4.20	2	1_3_4	48.17
13_S2_0100	4.20	-	1_2_3_4	49.82
14_S2_0001	4.20	4	1_2_3	48.24
14_S2_0001	4.20	-	1_2_3_4	48.93
15_S2_1110	4.20	1_2_3	4	49.28
15_S2_1110	4.20	-	1_2_3_4	49.78

Table 3.4. Characteristics of static tests for 4.00 m (S1) and for 4.20 m (S2)

### 3.1.3.2 Dynamic tests

The second set of experimental wave tests have been performed by three kinds of irregular wave attacks. These ones were characterized by JONSWAP spectrum in order to reproduce high (HE,  $H_s = 0.76 \div 0.83$  m,  $T_m = 5.15 \div 5.44$  s), medium (ME,  $H_s = 0.57 \div 0.61$  m,  $T_m = 6.16 \div 6.27$  s) and low (LE,  $H_s = 0.39 \div 0.42$  m,  $T_m = 6.24 \div 6.46$  s) wave energy conditions, where  $H_s$  is the significant wave height and  $T_m$  the mean wave period. For the JONSWAP spectrum was adopted a peak-enhancement factor  $\gamma_f = 3.3$ , an energy scale parameter,  $\alpha = 8.1 \cdot 10^{-3}$ , and a spectral width parameters,  $\sigma$ , equal to 0.07 (for  $f < f_p$ ) and 0.09 (for  $f > f_p$ ), where  $f$  is the frequency and  $f_p$  is the peak frequency. The adopted wave conditions were chosen in order to have probable accretion or erosion on the beach. In particular, on the basis of the experimental wave and beach conditions, a possible erosion was expected for HE and ME tests and a possible accretion for LE tests, in accordance with laboratory observations (Kraus, 1992). The tests were repeated one or more times in order to identify the temporal effect of the drains on the morphodynamic and hydrodynamic variations inside the zone of influence of the water table. However, in order to enable measurement of the morphodynamic response over time, each wave test was not run as a continuous time series but as a series of irregular wave batches. In this way, a set of 51 experimental wave steps was performed with different configurations, with one or more drains opened or closed. The duration of these steps were 60 minutes with a mean number of waves ranging approximately from 550 to 700. During all experimental tests the Still Water Level (SWL) was kept constant at 4.00 m, using different drain configurations characterized by single or coupled drains switched on/off. The

main characteristics of the experimental tests (HE, ME and LE) are reported respectively in Tables 3.5, 3.6 and 3.7, showing for each test the status of the drains, the wave parameters (significant wave height  $H_s$ , mean wave period  $T_m$ , peak period  $T_p$ , spectral wave energy  $m_0$ , and average wave steepness  $s_p$ ) and the beach-response predictions using the Dean (1973)'s relationships:

$$s_p \begin{cases} > 1.7 \frac{\pi W_f}{g T_m} & \text{offshore motion (erosion)} \\ < 1.7 \frac{\pi W_f}{g T_m} & \text{onshore motion (accretion)} \end{cases} \quad [3.1]$$

where  $g$  is the gravity acceleration and  $w_f$  is the fall velocity.

Test name and number	Drains on	$H_s$ (m)	$T_m$ (s)	$T_p$ (s)	$s_p$	$m_0$ (m <sup>2</sup> )	$\Delta x_s$ (m)	$N_0$	beach response
HE_1	-	0.80	5.29	6.40	0.012	0.040	-2.100	3.151	erosion
HE_2	-	0.79	5.24	6.40	0.012	0.039	-0.700	3.141	erosion
HE_3	-	0.80	5.25	6.40	0.012	0.040	-0.525	3.175	erosion
HE_4	1	0.78	5.26	6.40	0.012	0.038	-0.775	3.089	erosion
HE_5	1	0.76	5.20	6.40	0.012	0.036	-0.375	3.045	erosion
HE_6	1	0.81	5.44	6.40	0.013	0.041	-0.200	3.102	erosion
HE_7	-	0.83	5.27	6.40	0.013	0.043	-0.350	3.281	erosion
HE_8	-	0.82	5.26	6.40	0.013	0.042	-0.425	3.248	erosion
HE_9	-	0.81	5.26	6.40	0.013	0.041	-0.425	3.208	erosion
HE_10	1+2	0.79	5.24	6.40	0.012	0.039	-0.200	3.141	erosion
HE_11	1+2	0.82	5.25	6.40	0.013	0.042	-0.200	3.254	erosion
HE_12	1+2	0.83	5.24	6.40	0.013	0.043	-0.225	3.300	erosion
HE_13	1+2	0.79	5.22	6.40	0.012	0.039	-0.250	3.153	erosion
HE_14	3	0.79	5.26	6.40	0.012	0.039	-0.275	3.129	erosion
HE_15	3	0.80	5.25	6.40	0.012	0.040	-0.100	3.175	erosion
HE_16	3	0.80	5.24	6.40	0.012	0.040	-0.225	3.181	erosion

Table 3.5: Main characteristics of HE tests

Test name and number	Drains on	$H_s$ (m)	$T_m$ (s)	$T_p$ (s)	$s_p$	$m_0$ (m <sup>2</sup> )	$\Delta x_s$ (m)	$N_0$	beach response
ME_2	-	0.60	6.26	7.88	0.006	0.022	-0.025	1.997	erosion
ME_3	-	0.59	6.27	7.88	0.006	0.022	-0.100	1.960	erosion
ME_4	-	0.60	6.25	7.88	0.006	0.022	-0.250	2.000	erosion
ME_5	1	0.57	6.22	7.88	0.006	0.020	-0.025	1.909	erosion
ME_6	1	0.60	6.22	7.88	0.006	0.023	-0.175	2.010	erosion
ME_7	1	0.60	6.23	7.88	0.006	0.023	-0.350	2.006	erosion
ME_8	1+2	0.60	6.20	7.88	0.006	0.022	-0.075	2.016	erosion
ME_9	1+2	0.60	6.20	7.88	0.006	0.022	0.075	2.016	erosion
ME_10	1+2	0.60	6.16	7.88	0.006	0.023	0.025	2.029	erosion
ME_11	1+2+3	0.60	6.23	7.88	0.006	0.023	-0.250	2.006	erosion
ME_12	1+2+3	0.60	6.21	7.88	0.006	0.023	-0.275	2.013	erosion
ME_13	1+2+3	0.60	6.18	7.88	0.006	0.023	-0.025	2.023	erosion
ME_14	3	0.61	6.18	7.88	0.006	0.023	-0.275	2.056	erosion
ME_15	3	0.61	6.18	7.88	0.006	0.023	-0.125	2.056	erosion
ME_16	3	0.60	6.16	7.88	0.006	0.023	-0.025	2.029	erosion

Table 3.6: Main characteristics of ME tests

Test name and number	Drains on	$H_s$ (m)	$T_m$ (s)	$T_p$ (s)	$s_p$	$m_0$ (m <sup>2</sup> )	$\Delta x_s$ (m)	$N_0$	beach response
LE_1	-	0.39	6.46	7.88	0.004	0.010	-0.150	1.258	accretion
LE_2	-	0.39	6.41	7.88	0.004	0.010	-0.050	1.268	accretion
LE_3	-	0.41	6.36	7.88	0.004	0.011	-0.150	1.343	accretion
LE_4	-	0.41	6.40	7.88	0.004	0.010	0.000	1.335	accretion
LE_5	1	0.42	6.34	7.88	0.004	0.011	0.000	1.380	accretion
LE_6	1	0.40	6.35	7.88	0.004	0.010	0.025	1.312	accretion
LE_7	1	0.41	6.31	7.88	0.004	0.011	0.000	1.354	accretion
LE_8	1	0.41	6.29	7.88	0.004	0.011	0.050	1.358	accretion
LE_9	1	0.41	6.32	7.88	0.004	0.011	-0.050	1.352	accretion
LE_10	-	0.41	6.32	7.88	0.004	0.010	0.025	1.352	accretion
LE_11	-	0.41	6.28	7.88	0.004	0.011	-0.075	1.360	accretion
LE_12	-	0.41	6.25	7.88	0.004	0.010	-0.075	1.367	accretion
LE_13	-	0.40	6.27	7.88	0.004	0.010	0.100	1.329	accretion
LE_14	1+2	0.41	6.25	7.88	0.004	0.011	-0.050	1.367	accretion
LE_15	1+2	0.41	6.24	7.59	0.005	0.010	0.025	1.369	erosion
LE_16	1+2	0.41	6.33	7.88	0.004	0.010	0.025	1.349	accretion
LE_17	1+2	0.41	6.27	7.88	0.004	0.010	0.100	1.362	accretion
LE_18	1+2	0.41	6.25	7.88	0.004	0.010	-0.025	1.367	accretion
LE_19	1+2	0.42	6.29	7.88	0.004	0.011	0.025	1.391	accretion

Table 3.7: Main characteristics of LE tests

For all conditions, the variation of the significant wave height and the mean wave steepness is characterized by a general increase after the second slope break in the channel, followed by a nearshore decrease. The values of  $H_s$  and  $s_p$  evaluated by the last wave gauge prove to be higher than the next to last ones due to the wave reformation phenomenon after the first breaking. The spectral wave energy shows a general slight decrease trend from offshore to nearshore (Fig. 3.23). In particular, Figures 3.24 highlight, respectively for HE, ME and LE conditions, the shapes and the amplitudes of the wave spectra calculated by the first offshore gauge (WG1 at  $x=50.10$  m from wave paddle), an intermediate gauge (WG15 at  $x=161.90$  m) and the last one (WG20 at  $x=230.00$  m). A general energy reduction and a broader shape of the spectra associated to a frequency dispersion during the wave propagation can be observed. Moreover, the arising of a secondary relevant energetic component is noticed. For ME and LE tests, a greater spectral amplitude associated to a sharper shape is also observed for the intermediate gauge.

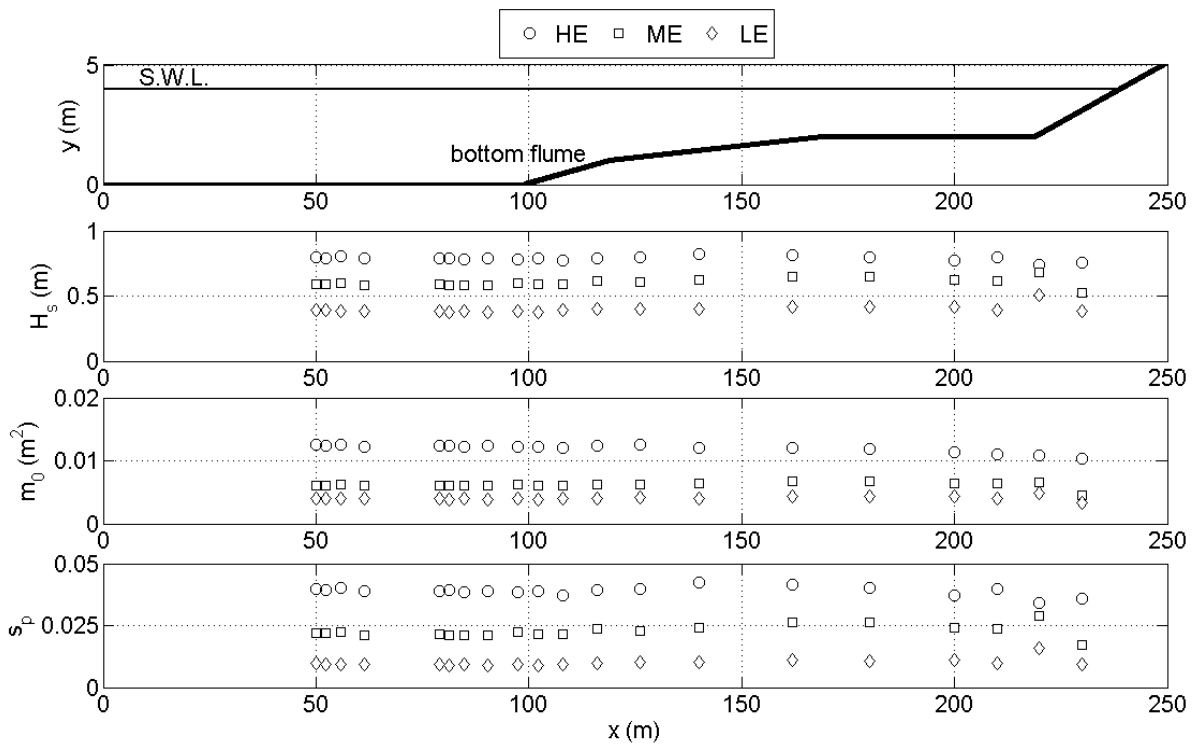


Figure 3.23. Spatial variation along the flume of significant wave height  $H_s$ , spectral wave energy  $m_0$ , and mean steepness  $s_p$  (HE, ME and LE tests).

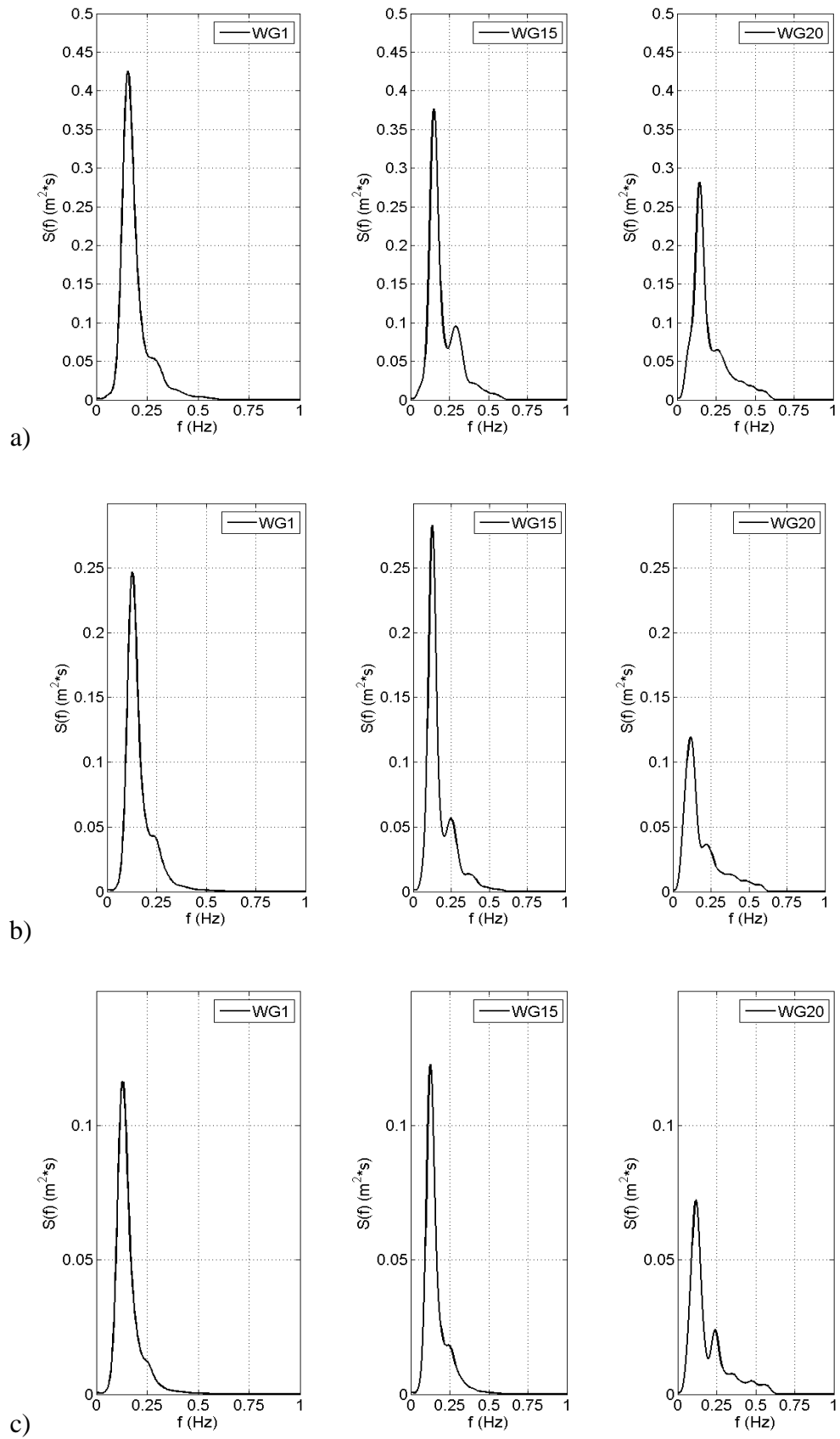


Figure 3.24 Energy density spectra of WG1, WG15 and WG20: a) HE tests; b) ME tests; C) LE tests.

Due to the impossibility to operate a reshaping procedure after each test case, the tests sequence was programmed considering the above mentioned predictions about overall morphodynamic behaviour. Reshaping the beach after each step in such a large facility is impracticable, because it would mean enormous time consuming. Albeit this procedure introduces some uncertainty, in large scale experiments it is commonly assumed acceptable the initial beach condition for each step. However, a remoulding was operated after the HE test recreate something similar to the initial experimental condition. Subsequently, it was decided to run the LE test, for which smaller bed variations were expected. In fact, reshaping was not needed before the next ME case. For representation purposes, the results are presented in order of decreasing wave energetic conditions. The wave conditions were calculated using the farthest offshore wave gauge, located at 50.1 m from the wave paddle. The switching sequence (on/off) for the drains was defined by using two criteria. First, to assume that a morphodynamic equilibrium was reached at the end of each test, the draining condition was changed if the variation of the beach slope was less than 5 % (which corresponded to an average vertical erosion of about 1 cm). Second, before changing the drainage conditions, the test should have run for at least three hours. Profile measurements were made at 1 hour steps. In Figure 3.25 the average slope, computed between the shoreline and the bar crest, and the slope variation between subsequent beach profiles are reported for all HE tests. Since for ME cases the slope variation was always smaller than 5 %, only the second criterion was used. The slope variation for LE cases was very limited (less than 0.06 %) and therefore the simulations were extended (4 h undrained, 5 h with drain D1, 4 h undrained, 6 h with drains D1 and D2).

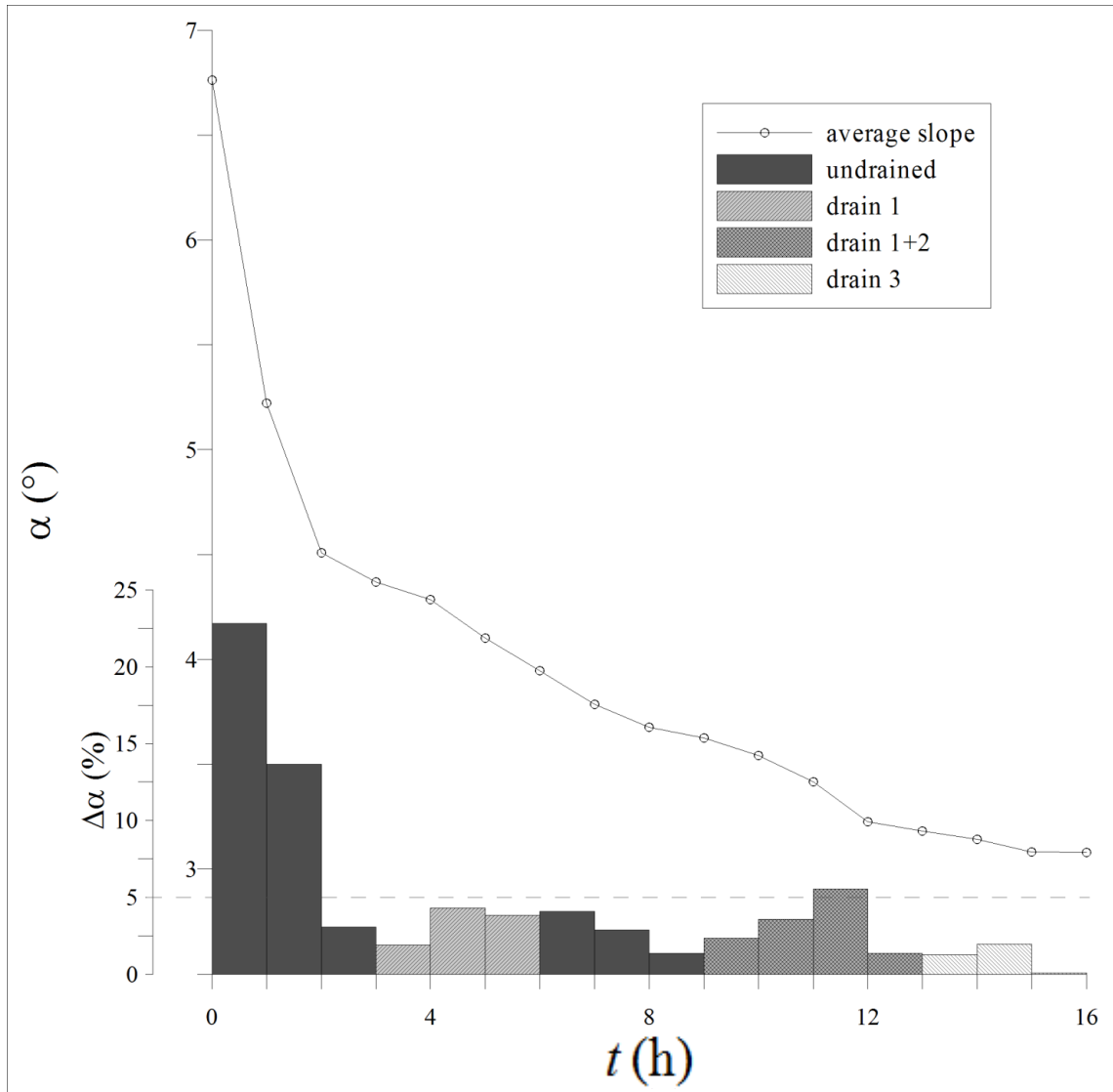


Figure 3.25. Average slope,  $\alpha$ , between the shoreline and the bar crest (solid line), and slope variation,  $\Delta\alpha$ , between successive beach profiles (histogram) for HE wave conditions. The dotted line represents the threshold value of  $\Delta\alpha = 5\%$  below which the draining condition was changed.

## 3.2 Pre-processing and data analysis

### 3.2.1 Signal processing

The recording signals of adopted instruments during the static tests (S1 and S2) and the dynamic tests (HE, ME and LE) have been subjected to a processing by filtering of raw data

and a successive evaluation of the principal morphodynamic and hydrodynamic characteristics.

The time series recorded by wave gauges, pressure transducers, electromagnetic currentmeters, propeller and altimeters have been sampled by 64 channels PRESTON acquisition system adopting a sampling frequency  $f = 20$  Hz. The adopted steps for signal processing and the analysis of all experimental data are illustrated as in the following.

On the basis of each recorder static or dynamic test by PRESTON system, having variable duration, the first and the last instants of raw registration have been cut because the recording were not significant. This preliminary analysis was not computerize because the triggering operations have been performed manually. The selection of these time instants has been carried out by the observations of real surface oscillations (for dynamic tests) and of dynamic pressures induced by drain opening (for static tests) in order to synchronize these values to the piezometer measurements.

Successively a detrending operation has been applied to surface elevation time series respect to the static water level, and to dynamic pressures respect to the corresponding mean values. The detrending has allowed to eliminate the water losses along the wave flume (about 1 cm/h). Detrending is the statistical or mathematical operation of removing trend (a slow, gradual change in some property of the series over the whole interval under investigation) from the series. This processing has been performed only for pressure time series having a defined increasing or decreasing trend. In particular, the Matlab function *detrend* has been adopted. This operation has been applied starting from the instants corresponding to the significant losses in the channel.

The raw time series recorded by all wave gauges (from WG1 to WG20) and electromagnetic currentmeters (ECM1, ECM2, ECM3 and ECM4) has been subjected to a band-pass filtering in order to eliminate spurious oscillations. The long period oscillations have been forced by seiching effects along the flume and the small period fluctuations have been induced by instrumental noise. For all dynamic tests the low-pass frequency has been set equal to 0.05 Hz, as a function of the seiching periods which could be generated along the channel (Dean and Darlymple, 2002). The high-pass frequency has been set equal to 0.6 Hz, on the basis of the noise levels of the adopted instruments and of the original power spectra transmitted to the stroke movement of the wave generator. The band-pass filtering has been performed using the Matlab function *filtfilt*. On the basis of a preliminary cut of erroneous frequencies, this

function allows to have a filtered time series of surface elevations (Fig. 3.26) and velocities from WG and ECM, respectively.

The raw times series deduced by pressure transducers and altimeters have been filtered in order to eliminate high-frequencies induces by the instrument noise. A least-square minimization method by Savitzky and Golay (1964), based on a 3<sup>rd</sup> order polynomial function and adopting a span = 201, has been applied. This value has been sometimes changed as a function of the noise level of each instrument. This filtering was different that those adopted for wave gauges and electromagnetics because the frequency answer of pressure transducers was linked to the characteristics of the sand beach (Figs. 3.27, 3.28, 3.29 and 3.30).

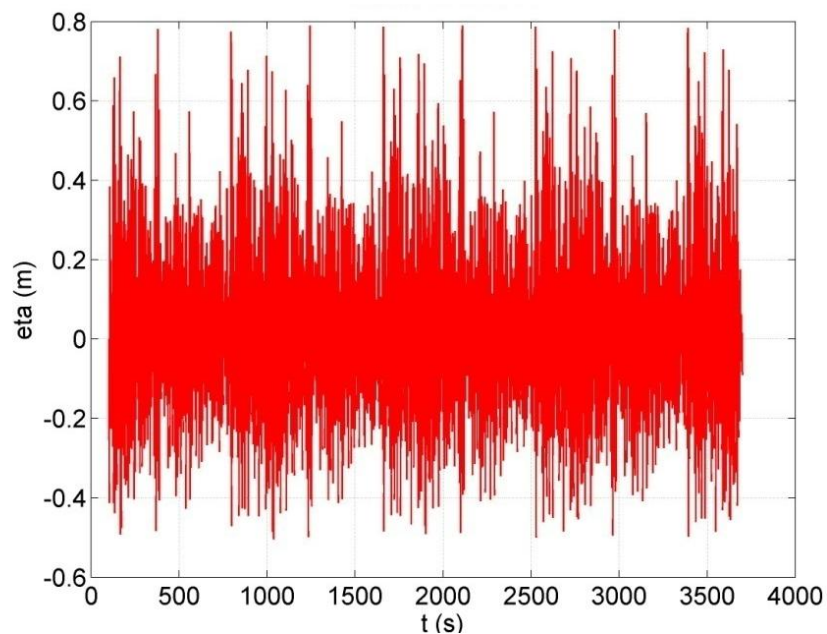


Figure 3.26. Filtered time variation of surface elevation - wave gauge WG1 (HE 1).

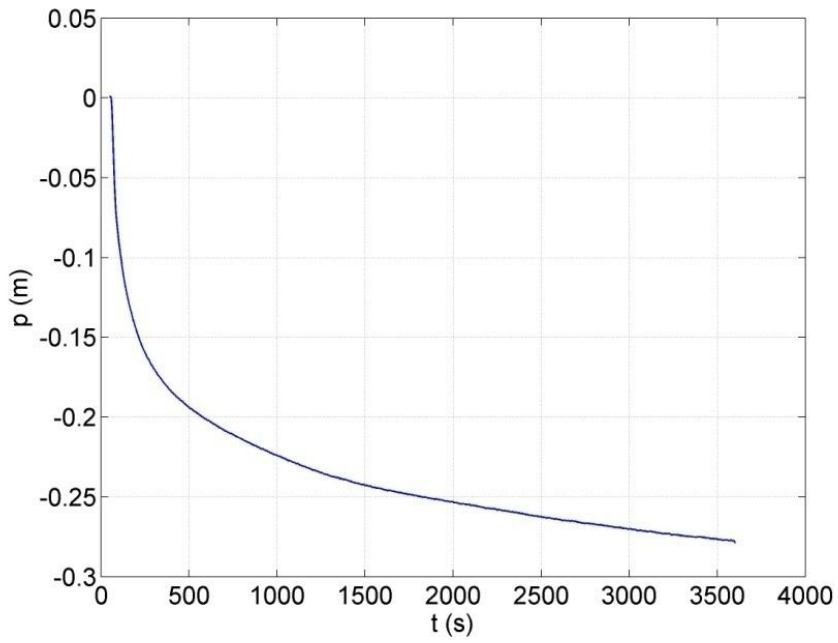


Figure 3.27. Filtered time variation of dynamic pressure for pressure transducer pt4 (test 01\_S1\_1000).

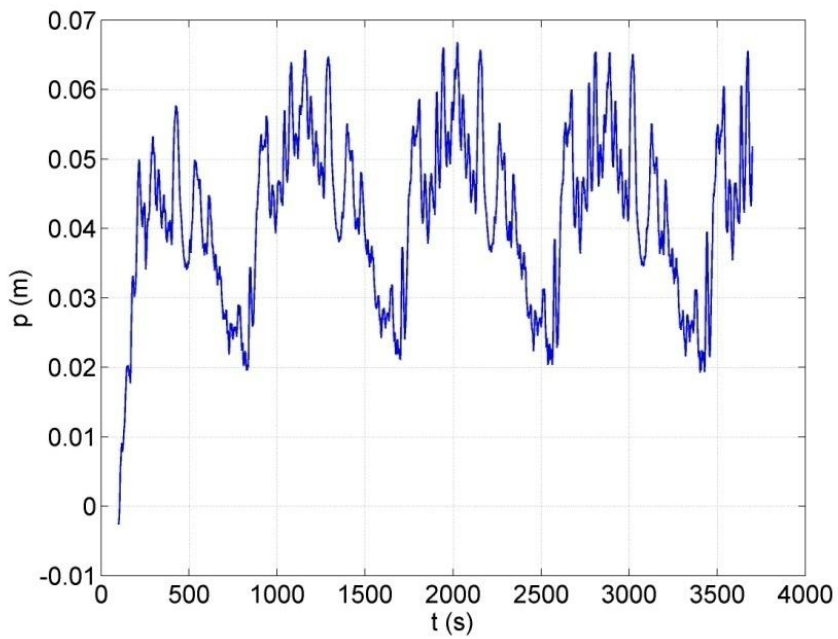


Figure 3.28. Filtered and detrended time variation of dynamic pressure for pressure transducer pt1 (HE 1).

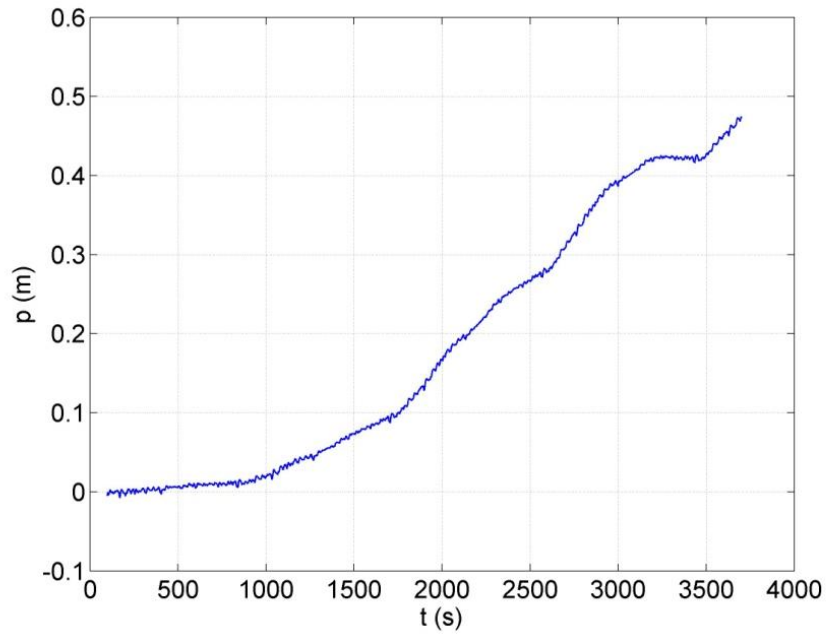


Figure 3.29. Filtered time variation of dynamic pressure for pressure transducer pt9 (HE 1).

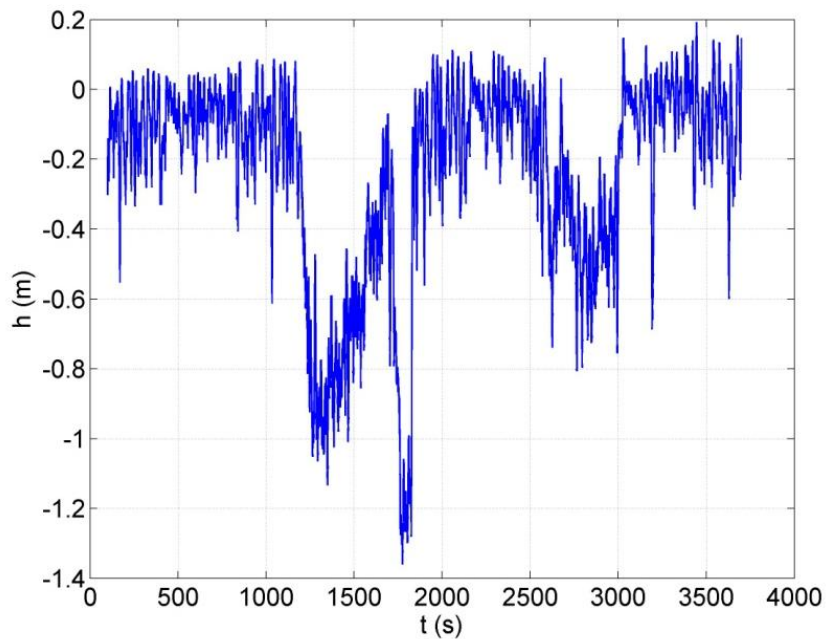


Figure 3.30. Filtered time variation of altimeter ALT1 (HE 1).

The mean values of dynamic pressure have been evaluated to compare these values to the manual piezometric measurements. These dynamic pressure values have been determined by the time series of filtered pressure transducer signals. For static tests the mean pressure values have been calculated every 5', performing an average over 1'. For dynamic tests the analysis

has been performed every 15', finding a mean pressure value over 2'. Figure 3.31 shows a time comparison between piezometer and transducer measurements. Figure 3.32 shows the spatial comparison between these two kind of measurements.

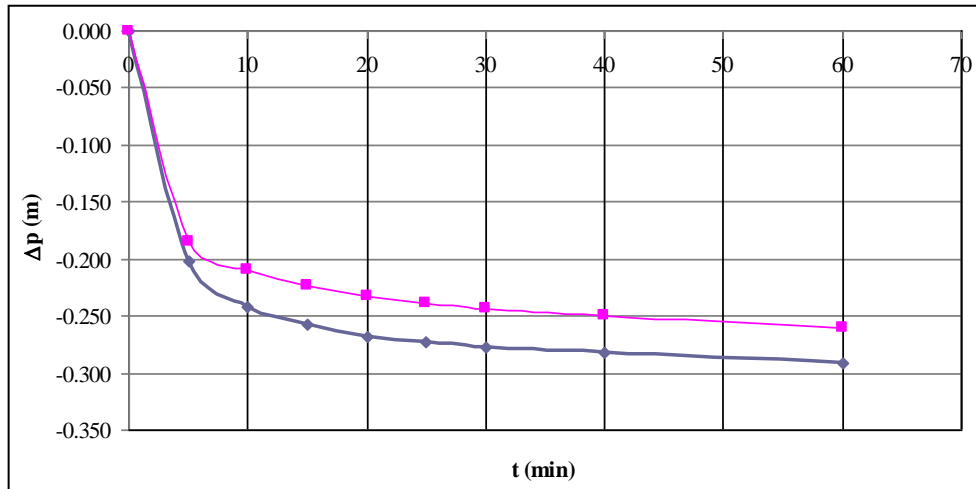


Figure 3.31. Time comparison between piezometer P4 (Blue) and pressure transducer pt4 (Violet) (test 02\_S1\_0100).

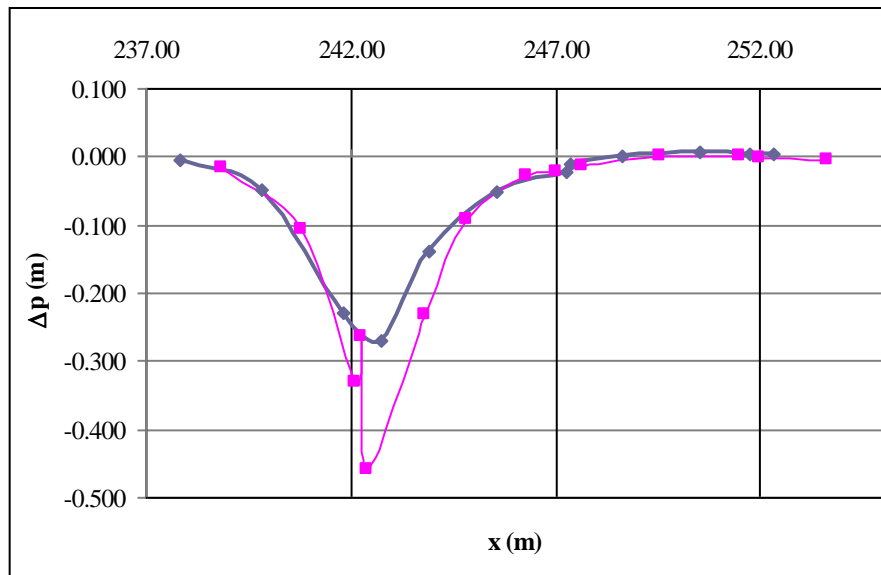


Figure 3.32. Spatial comparison between piezometers (Blue) and pressure transducer (Violet) after 20' (test 02\_S1\_0100).

On the basis of a filtered time series of surface elevations, horizontal and vertical component of the wave velocities, pressure transducers, the spectral analysis has been performed to evaluate the energy characteristics induced by wave motion. This analysis has allowed to calculate the spectral power density and the corresponding frequencies. The Matlab Wafo

function *dat2spec* has been used, using a window equal to 2049 values of frequency. This function is based on Welch's averaged periodogram method with no overlapping batches. The power spectra of some representative gauges are reported in Figure 3.33.

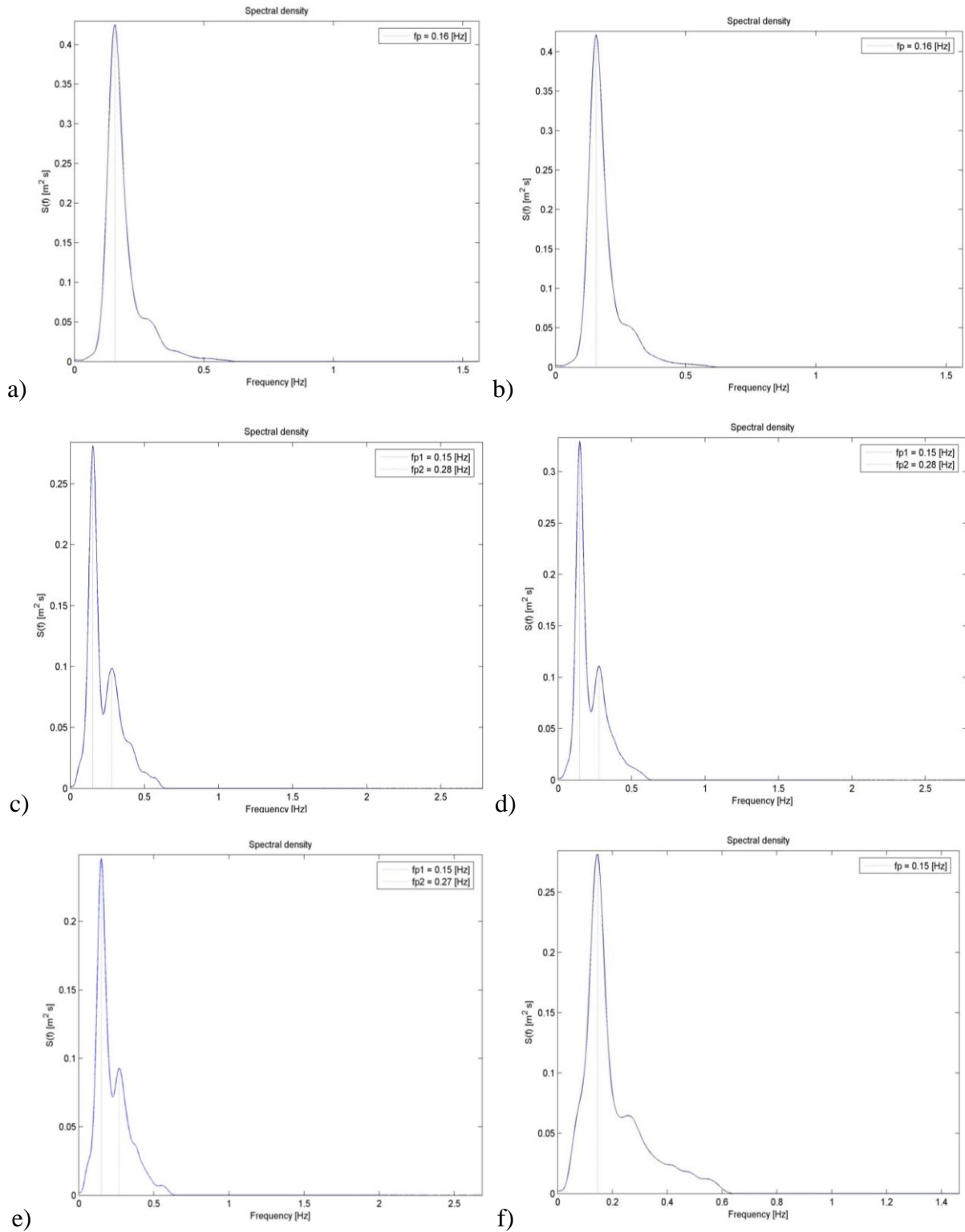


Figure 3.33. Power spectrum for test HE 1:  
a) WG1; b) WG2; c) WG17; d) WG18; e) WG19; f) WG20.

The electromagnetics ECM1, EMC2, ECM3 and ECM4 have been installed along the vertical of the same flume cross section. ECM1 was placed near the water surface, while ECM4 was installed near the flume bottom. Examples of power spectra of horizontal velocity components (ECM1- $x$ , ECM2- $x$ , ECM3- $x$  and ECM4- $x$ ) are shown in Figure 3.34.

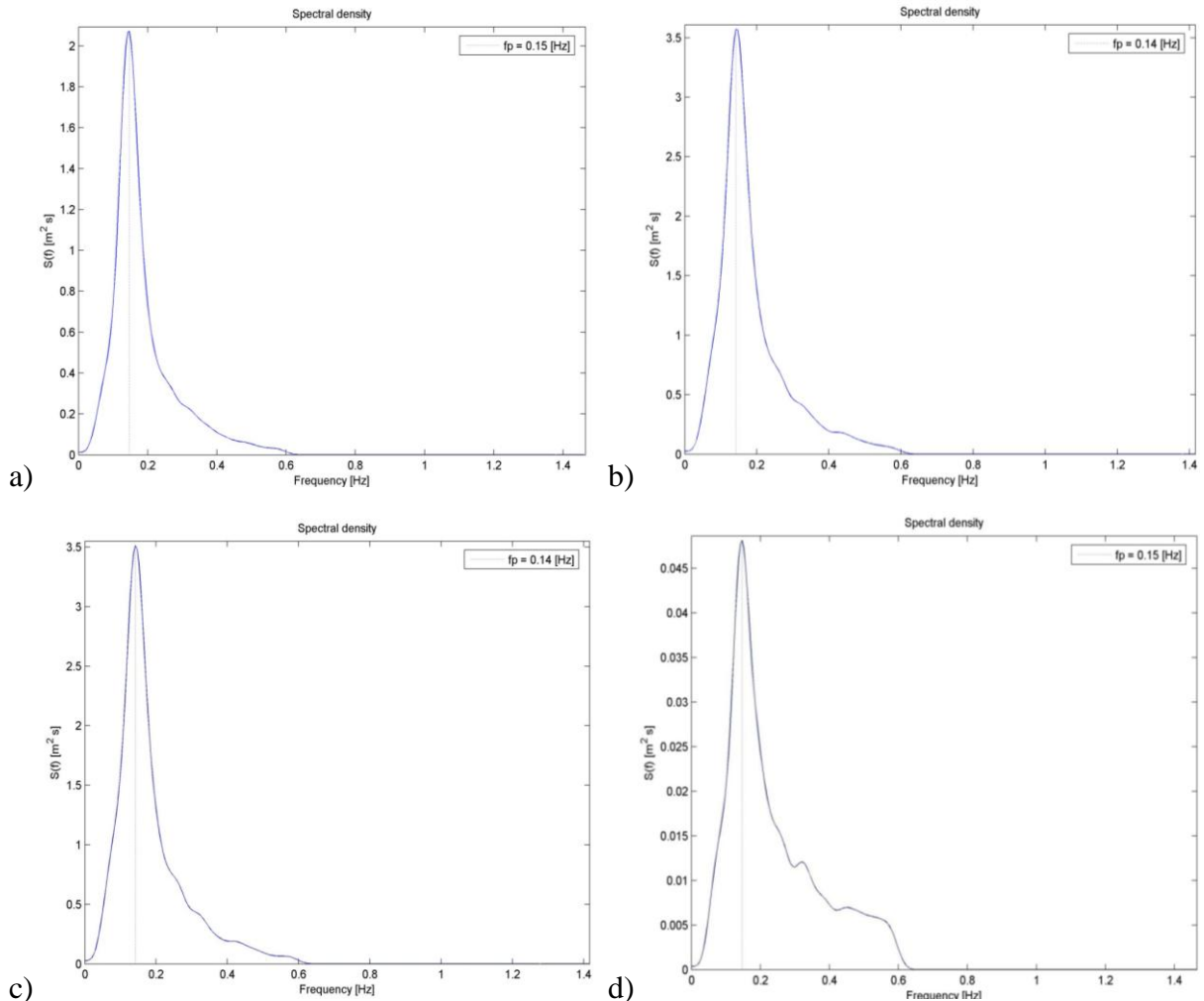


Figure 3.34. Power spectrum for test HE 1 from electromagnetic: a) ECM1 –  $x$ -direction; b) ECM2 –  $x$ -direction (HE 1); c) ECM3 –  $x$ -direction (HE 1); d) ECM4 –  $x$ -direction (HE 1).

Examples of power spectra of dynamic pressures placed in the sand (pt1 and pt4) are shown in Figures 3.35.

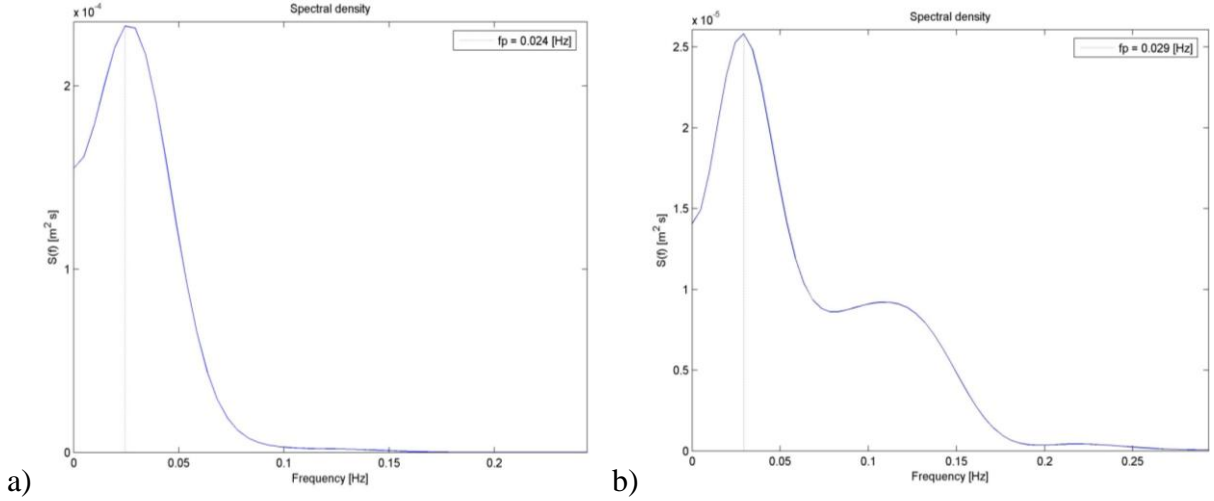


Figure 3.35. Power spectrum for test HE 1: a) pt1; b) pt4.

Referring to the surface elevation measurements, the Wafo Matlab function *spec2char* has been applied for the evaluation of the following spectral wave characteristics:

- Spectral (significant) wave height,

$$H_{m0} = 4\sqrt{m_0} \quad [3.2]$$

- Mean wave period,

$$T_m = 2\pi m_0 / m_1 \quad [3.3]$$

- Peak period,

$$T_p = \frac{2\pi}{f | \max(S(f))} \quad [3.4]$$

- Mean wave steepness,

$$s_p = \frac{2\pi H_{m0}}{g T_p^2} \quad [3.5]$$

The use of Wafo Matlab function *spec2mom* has allowed to calculate the spectral moments  $m_0$  (variance or spectrum energy),  $m_1$  (first-order moment) and  $m_2$  (second-order moment) for surface elevations, wave velocity components and dynamic pressures.

Successively the following statistical wave characteristics have been calculated:

- Mean surface elevation,

$$\bar{\eta}_w = \frac{\sum \eta_w}{N'} \quad [3.6]$$

where  $\eta_w$  is measured surface elevation and  $N'$  is sampling number between the first and the last zero-upcrossing points of the recording.

- Maximum surface elevation,  $\eta_{\max}$
- Minimum surface elevation,  $\eta_{\min}$
- Standard deviation of surface elevation,

$$\sigma_w = \sqrt{\frac{\sum (\eta_w - \bar{\eta}_w)^2}{N_T}} \quad [3.7]$$

where  $N$  is the total number of sampling values.

- Skewness of surface elevation,

$$\mu_3 = \frac{\sum (\eta_w - \bar{\eta}_w)^3}{N_T \sigma_w^3} \quad [3.8]$$

- Kurtosis of surface elevation,

$$\mu_4 = \frac{\sum (\eta_w - \bar{\eta}_w)^4}{N_T \sigma_w^4} \quad [3.9]$$

For the horizontal,  $u$ , and vertical,  $v$ , flow velocities, deduced from the time series of 4 electromagnetics, the following statistical characteristics have been calculated:

- Mean velocity:

$$\bar{u} = \frac{\sum u}{N_T} \quad [3.10a]$$

$$\bar{v} = \frac{\sum v}{N_T} \quad [3.10b]$$

- Standard deviation of velocity:

$$\sigma_u = \sqrt{\frac{\sum (u - U)^2}{N_T - 1}} \quad [3.11a]$$

$$\sigma_v = \sqrt{\frac{\sum (v-V)^2}{N-1}} \quad [3.11b]$$

Skewness of velocity:

$$\mu_{3,u} = \frac{\sum (u-U)^3}{(N-1)\sigma_u^3} \quad [3.12a]$$

$$\mu_{3,v} = \frac{\sum (v-V)^3}{(N-1)\sigma_v^3} \quad [3.12b]$$

- Kurtosis of velocity:

$$\mu_{4,u} = \frac{\sum (u-U)^4}{(N-1)\sigma_u^4} - 3 \quad [3.13a]$$

$$\mu_{4,v} = \frac{\sum (v-V)^4}{(N-1)\sigma_v^4} - 3 \quad [3.13b]$$

- Maximum velocity,  $u_{max}$  and  $v_{max}$
- Minimum velocity,  $u_{min}$  and  $v_{min}$

For the dynamic pressures, deduced from the time series of 14 transducers, the following statistical characteristics have been calculated:

- Mean dynamic pressure:

$$\bar{p}_w = \frac{\sum p_w}{N_T} \quad [3.14]$$

- Standard deviation of dynamic pressure:

$$\sigma_p = \sqrt{\frac{\sum (p_w - \bar{p}_w)^2}{N_T - 1}} \quad [3.15]$$

- Skewness of dynamic pressure:

$$\mu_{3,p} = \frac{\sum (p_w - \bar{p}_w)^3}{(N_T - 1)\sigma_p^3} \quad [3.16]$$

- Kurtosis of dynamic pressure:

$$\mu_{4,p} = \frac{\sum (p_w - \bar{p}_w)^4}{(N_T - 1) \sigma_p^4} - 3 \quad [3.17]$$

Note that various definitions of **skewness** and **kurtosis** can be found. The adopted definitions have been referred to the work of Kraus and Smith (1994), divided by  $N$ . From the filtered time records of surface elevations, wave velocities and pressure transducers, a variable number of wave packets has been extracted as a function of the repetition time,  $T_R$ . The number of wave packets, ranging from 2 to 5, was different for each wave condition. The Matlab Wafo function *dat2spec* has been used, using a window equal to 2049 values of frequency. This analysis has been useful to check the goodness of repeatability of the wave spectra generated in the channel during each dynamic step. For wave gauge WG1 the power spectra of wave packet 1, 2, 3 and 4 are reported in Figure 3.36.

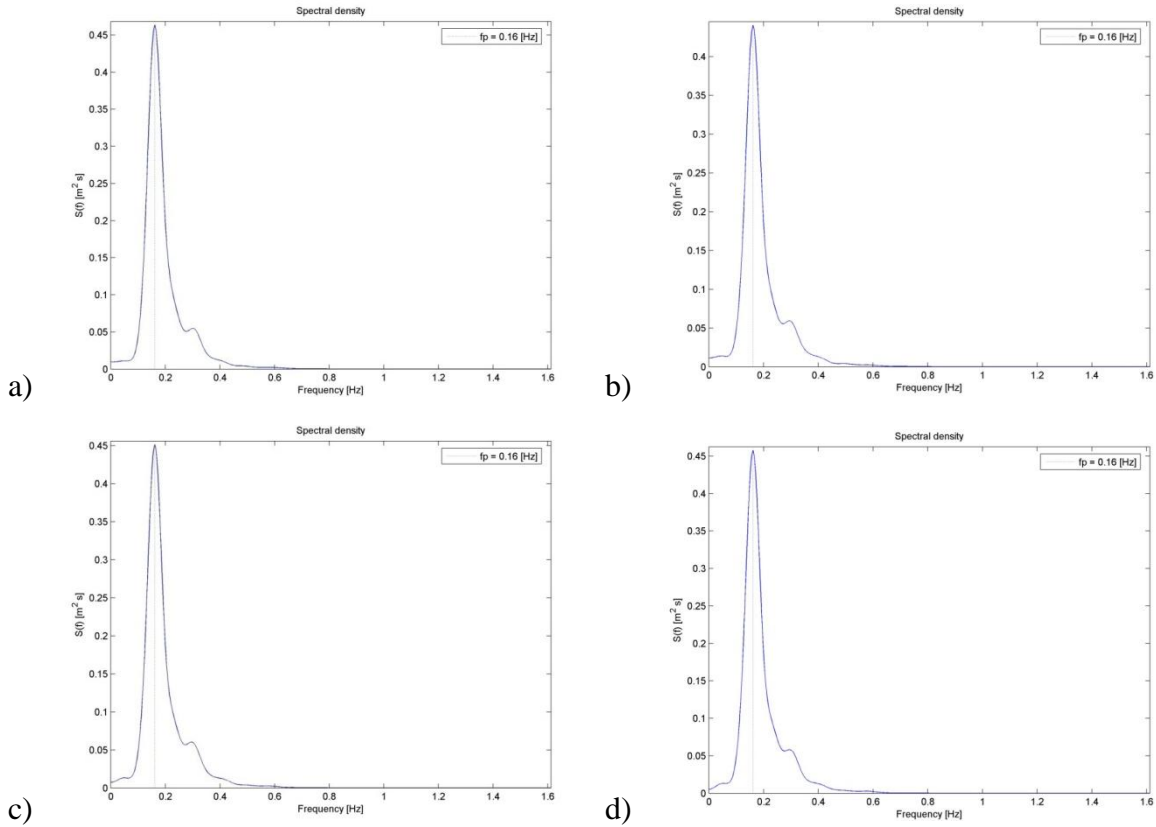


Figure 3.36. Power spectrum from wave gauge WG1 for the test HE 1:

a) 1<sup>st</sup> wave packet. b) 2<sup>nd</sup> wave packet. c) 3<sup>rd</sup> wave packet. d) 4<sup>th</sup> wave packet.

The wave packets extracted by the filtered time series of surface elevations and velocities has been processed in order to evaluate the spectral and statistic characteristics, as carried out for the total time series recorder by wave gauges and electromagnetics.

The wave reflection analysis, based on the separation of incident and reflected waves, resulted fundamental because the adopted sand beach shown a relevant capability of wave reflection (about 8% and dependent on the wave magnitude). In particular, Goda and Suzuki (1976), and Mansard and Funke (1980) methods have been applied for this analysis. The assumption of irregular wave attacks on the beach did not allowed to separate incident and reflected waves with the same amplitude and phase components because its application is possible only for regular waves. Starting from the filtered time series of surface elevations, the reflection coefficients, the incident and reflected values of significant wave heights have been calculated using two mentioned approaches (Goda, 2002). The application of Goda and Suzuki (1976)'s method has required the use of wave gauges WG18 and WG19 (third last and next to last wave gauges from the wave generator and placed at a mutual distance of 10 m). Instead Mansard and Funke (1980)'s method has required the values of surface elevations of WG17, WG18 and WG19. These three gauges has been installed at a water depth of about 2 m (flat bottom) and a mutual distance of 10 m. The last wave gauge (WG20) has not considered in determining the reflection coefficients and the separate significant wave heights because the waves were essentially broken in this position as deduced by the relevant broadness of the power wave spectrum.

Figure 3.37 shows an example of total, incident and reflected wave power spectra calculated by Goda and Suzuki (1976)'s method. Figure 3.38 reports a comparison among these power spectra using two mentioned wave reflection methods.

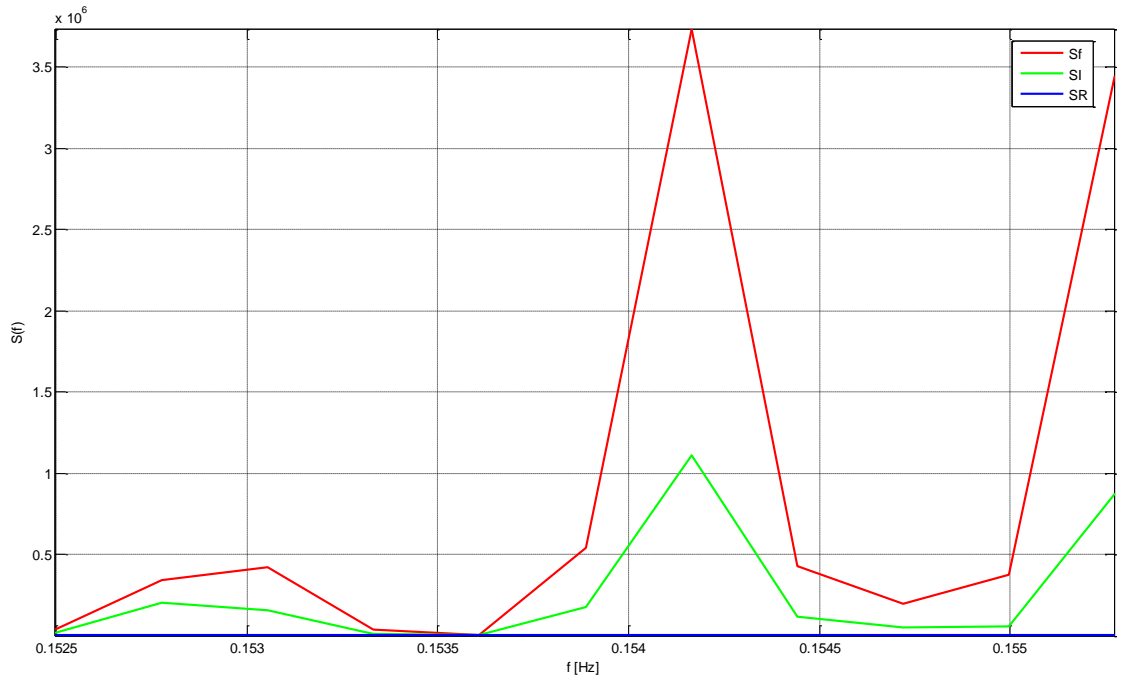


Figure 3.37. Total (Sf), incident (SI) and reflected (SR) power wave spectra by Goda and Suzuki's method (HE 1).

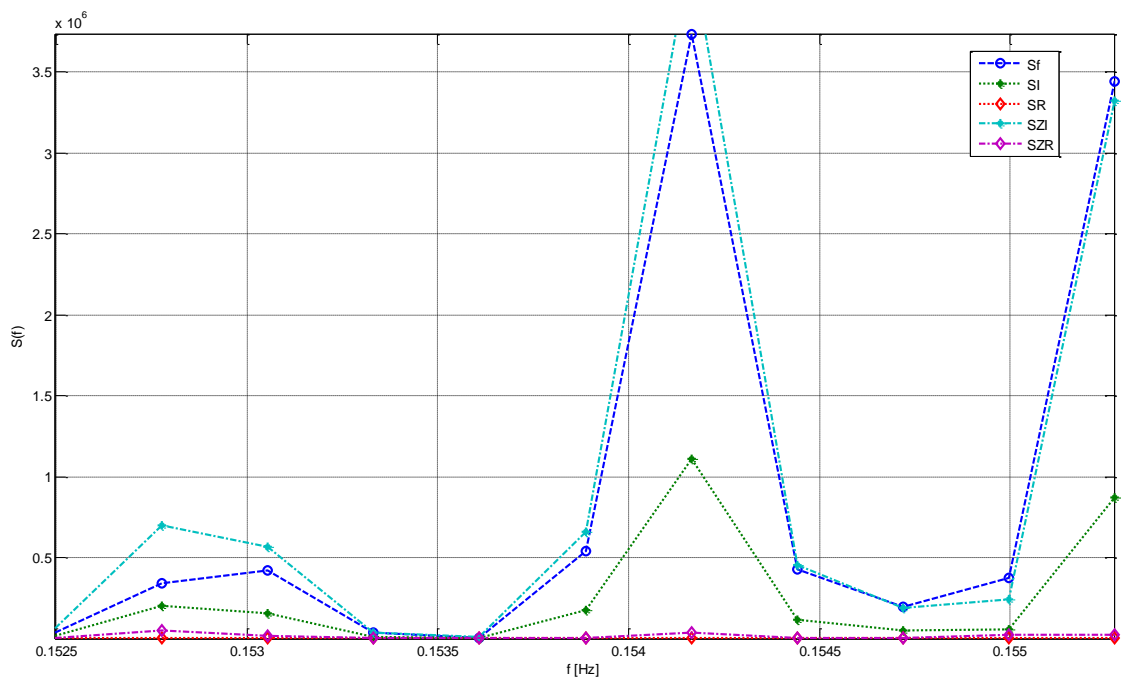


Figure 3.38. Total (Sf), incident (SI) and reflected (SR) power wave spectra by Goda and Suzuki's method, and incident (SZI) and reflected (SZR) power wave spectra by Mansard and Funke's method (HE 1).

### 3.2.2 Groundwater Hydrodynamics Measurement methods

In this section attention is paid to the comparison between different kind of instruments to be able to measure water table oscillations and drained flows. The analysis is addressed to check the performances of the adopted experimental setup (see Damiani et al., 2010).

Piezometers and pore pressure transducers have allowed to analyse the variation of the water table at different time steps for both static and dynamic tests, by the knowledge of the static level in the sand at the beginning of each test. Figure 3.39 shows an example of the spatial variation of the water table lowering,  $\Delta h$ , evaluated at the time  $t = 60'$  by piezometers and pore pressure transducers for static test S1 with drain D2 opened (the  $x$ -positions are referred to the wave generator section). Although piezometers and transducers give respectively static and dynamic measurements, the comparison highlights a good agreement between the two kind of measurement. Therefore, the following analyses will be carried out on the basis of the good performance obtained by comparing different measurements. This check allows the use of a single instrument to analyse a particular hydrodynamic aspect inside the equipped beach.

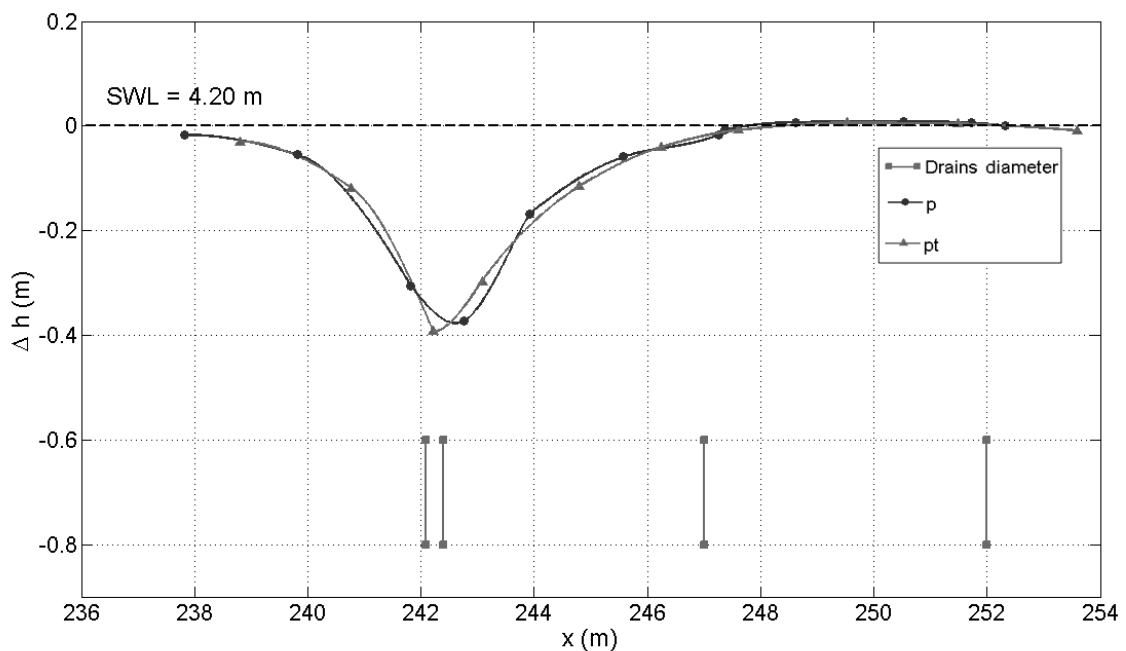


Figure 3.39 Spatial variation of the water table evaluated by piezometers and transducers at  $t = 60'$  (Static test S1, drain D2 on).

The duration of static and dynamic tests have been set in order to reach a quasi-stationary condition of the water table evolution on the beach. The optimal setting of the duration of the

tests proves to be evident by analysing the space-time variation of the water table lowering. Figure 3.40 reports the spatial variation of  $\Delta h$  evaluated by piezometers at different time step measurements ( $t = 5', 10', 15', 30', 50'$  and  $60'$ ) for S1 test with drain D1 opened.

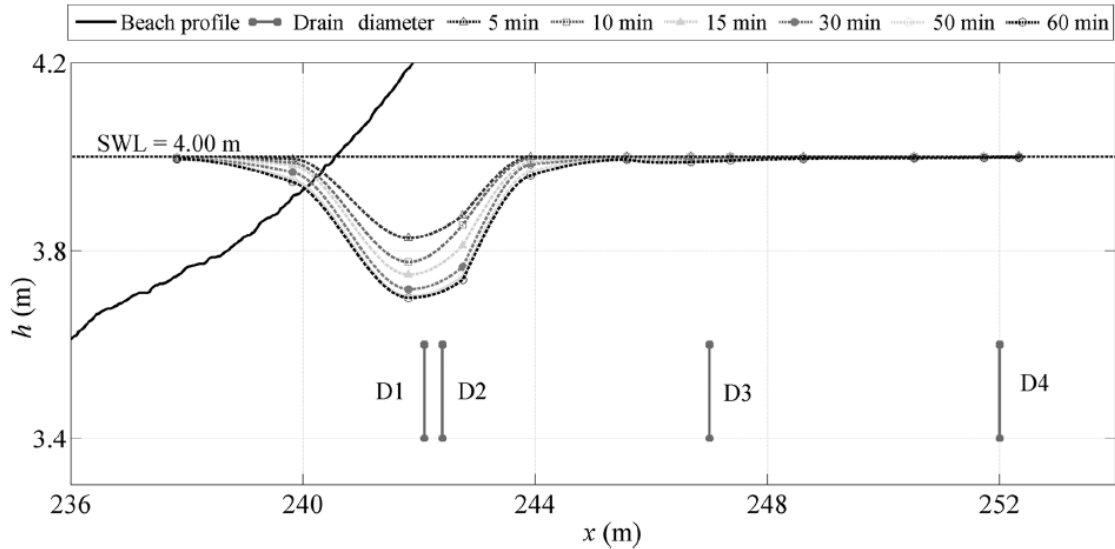


Figure 3.40. Spatial variation of water tables evaluated by piezometers at different time steps (Test S1, D1 on).

With reference to the phases of the automatic switch on/off of the pump inside the well during the tests, the drained flow has been calculated through the methods described in the following. By the measurements of the submerged pressure transducer, the water level in the pump station shows a so-called “sawtooth profile” and this feature is reported as example for HE test with drain 1 on (i.e. HE 4, in Fig. 3.41). During the filling up of the pump station, the time evolution of the water level is linear for a time interval corresponding to the water arising from the first to the second buoy of the pump (dotted line). Successively, during the filling down of the water inside the well induced by the pump, a decreasing trend has been observed. A cyclic phenomenon has been observed until the end of each test having one or more drains opened. The number of cycles was variable as function of the value of the incoming drained flow. The same behaviour has been observed during previous BDS experiments (Damiani et al., 2009). Starting from the evaluation of the mean time,  $t_m$ , of all pump cycles, and the mean water depth,  $h_m$ , deduced as difference between the maximum and the minimum levels of each cycle. The mean drained volume,  $V_m$ , is calculated as follows:

$$V_m = h_m A \quad [3.18]$$

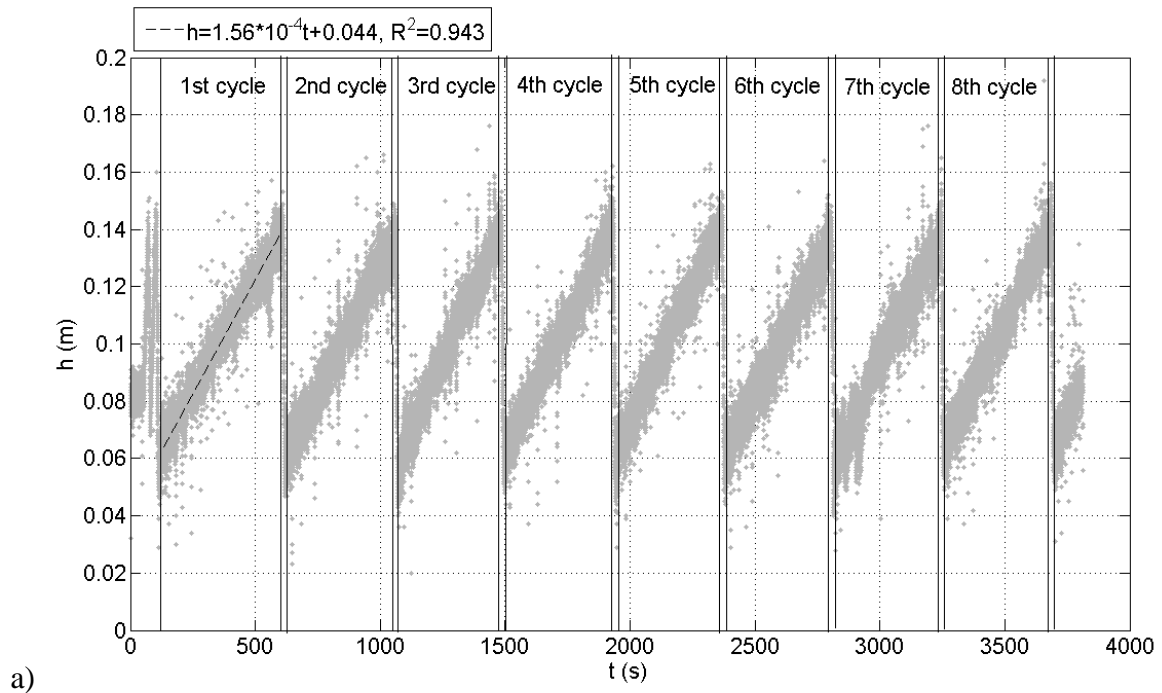
where  $A$  (pump station area) =  $3.4 \text{ m}^2$ .

The mean drained volume and the mean time of all pump cycle allow to determine the mean drained discharge,  $Q_m$ :

$$Q_m = \frac{V_m}{t_m} \quad [3.19]$$

The drained flows have been also calculated using a different method by the flowmeter recordings. Because the flowmeter was placed on the external pipe of the flume, this instrument has measured the passage of the water flow during the filling down of the pump station. The first step was the evaluation of the mean time between successive peak signals recorded by the flowmeter and the mean drained volume from the water level in the pump station. The evaluated mean time corresponded to the filling down time of the pump station. The values of  $Q_m$  have been calculated as in the case of the previous method deduced by the transducer measurements.

With reference to the same dynamic test, Figure 3.41 shows the time variation of the flowmeter signal, highlighting the different filling up cycles and the passages of the water flow in the external iron pipe.



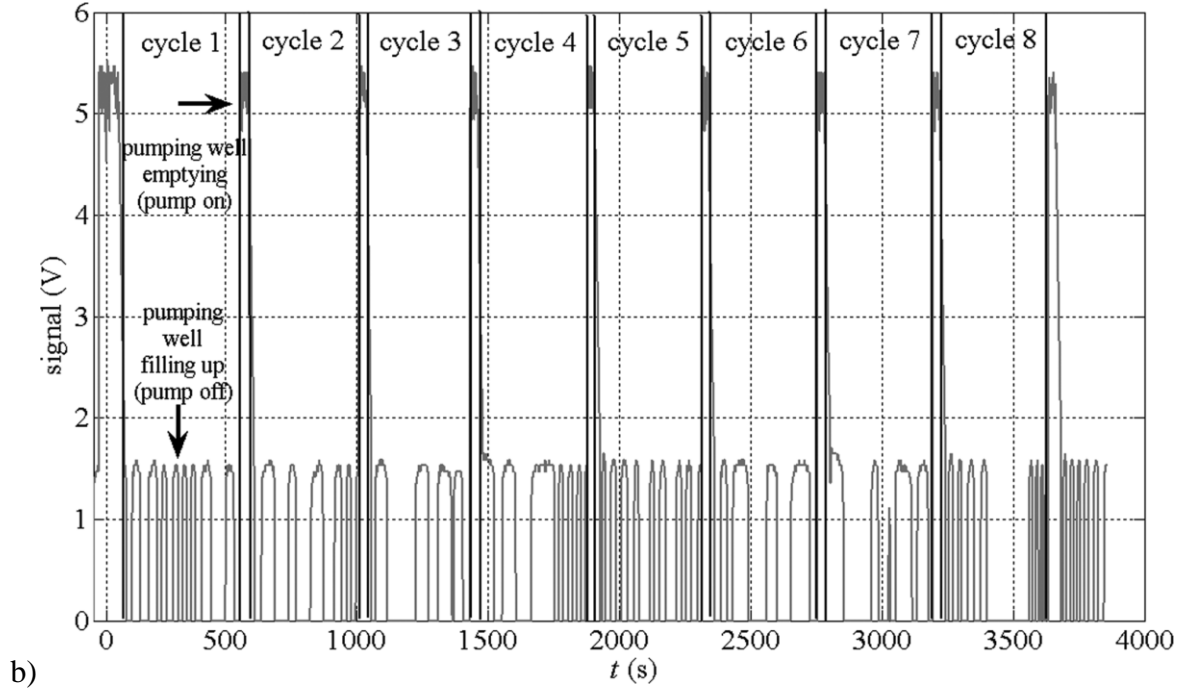


Figure 3.41. a) Time variation of water level,  $h$ , in the pump station by transducer pt15 (HE 4). b). Time variation of flowmeter signal (HE test, drain 1 on).

### 3.2.3 Morphodynamic Measurement methods

The net sediment volume variation,  $\Delta V$ , was computed, starting from  $x = 240$  m, by integrating the vertical area delimited between two profiles: The coordinate  $x = 240$  m represents the lower limit of influence of drain D1 (i.e. the seaward limit of depression in the aquifer's surface seen in Fig. 3.40). The computational procedure is shown in the follow:

$$z_i^{j-1} - z_i^j = \Delta z_i^j \quad [3.20]$$

$$\Delta z_i^j \frac{\Delta x}{2} = \Delta v_i^j \quad [3.21]$$

$$\sum_{i=1}^N \Delta v_i^j = \Delta V^j \quad [3.22]$$

where  $z$  is the vertical coordinate of each profile point, starting from the flume bed,  $j$  is the step index,  $i$  the measured point index,  $\Delta x$  the spatial resolution on the horizontal coordinate ( $x$ ),  $\Delta v_i^j$  is the sediment volume variation per meter of cross-shore section between points at  $j$  and  $j-1$ ,  $\Delta V^j$  is the sediment volume variation over  $x = 240$  m per meter of cross-shore section between steps  $j$  and  $j-1$  with positive values for accretion, and negative values for erosion.

The dimensionless relative volume variation,  $\Gamma$ , was calculated, starting from  $x = 240$  m, through the following procedure:

$$(z_i^j + z_{i+1}^j) \frac{\Delta x}{2} = w_i^j \quad [3.23]$$

$$\sum_{i=1}^N w_i^j = W^j \quad [3.24]$$

$$\frac{W^j - W^{\min}}{|W^{\max} - W^{\min}|} = \Gamma \quad [3.25]$$

where  $w_i^j$  is the sediment volume per meter of cross-shore section at step  $j$  between points  $i$  and  $i+1$ ,  $W^j$  is the sediment volume over  $x = 240$  m per meter of cross-shore section at step  $j$  using identical signs as for  $\Delta V^j$ , and  $W^{\min}$  ( $W^{\max}$ ) is the minimum (maximum) sediment volume  $W^j$  for each wave condition.

For HE and ME tests,  $W^{\max}$  is evaluated in correspondence of the initial profile (see also Section 3.3.2), whereas the initial sediment volume, for the LE test, corresponds to  $W^{\min}$ . In this way,  $\Gamma = 1$  is related to the profile with the largest volume and  $\Gamma = 0$  is related to the profile with the smallest volume for each wave condition.

### 3.3 Results

#### 3.3.1 Hydrodynamic response

##### 3.3.1.1 Water table

The water table trend highlights the system effectiveness in increasing the thickness of the unsaturated layer. This effect is induced by the activation of the drains for both static and dynamic conditions. To analyse the groundwater behaviour, a typical example is reported in Fig. 3.42, which shows the spatial variation of water tables, evaluated by the piezometers, for Test S2 with D1, D3 and D4 opened. The data refer to the test end when steady state was reached. In addition, Fig. 3.42 shows the water level inside the drains to highlight the different hydraulic regimes developed in the sand–drain system. For all configurations a lowering in the water table close to the drain is identified along with a rise in the unsaturated zone. The maximum water table lowering is 0.57 m for D3, corresponding to 95% of the upper drain part of the drain depth, whereas the opening of D1 and D4 produces a water table lowering of only 65%.

The best efficiency in water table lowering given by D3 is probably due to its plane placement, as also confirmed by dynamic tests. The drain D1 is the nearest to the shoreline and thus receives not only the vertical infiltration flux but also water directly into the unsaturated beach above the exit point. The position of D4 proves to be influenced by the higher degree of compaction degree due to the upper sand weight with respect to D1 and D3. The system was tested for various drain configurations, also opening more drains simultaneously. The spatial water table variations for Test S1 with drain D1, and the addition of D2 and D2+D3 are reported in Figure 3.43. The configuration D1+D2 leads to a small increase in the water table lowering with respect to D1 but a remarkable increase of the unsaturated area, emphasized by the addition of D3. When D1, D2 and D3 are opened simultaneously, the distance between D2 and D3 leads to the suppression of their mutual influence. The water table rises between D2 and D3, reaching about the same value induced when both D1 and D2 are activated. The maximum lowering occurs in correspondence to D1 and D2 because these drains simulate a single drain of double diameter. Relative maximum lowering with respect to the static levels appears in S2 for all drain configurations.

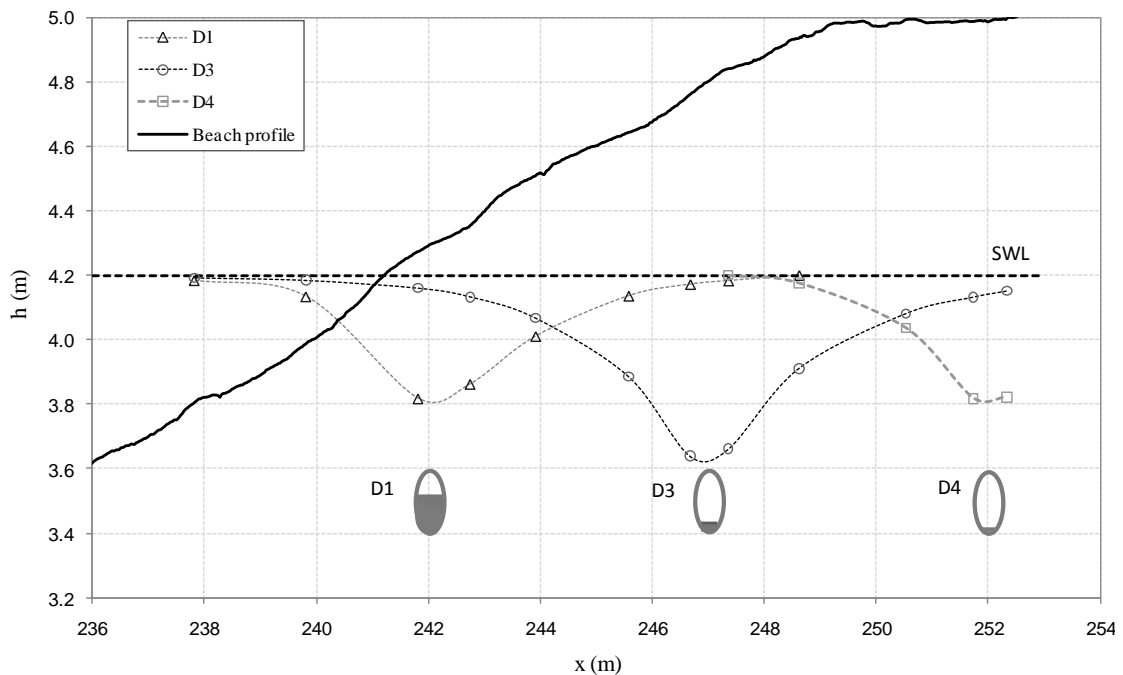


Figure 3.42. Spatial variation of water tables and water depths for Test S2, D1, D3 and D4 on (after Damiani et al., 2011).

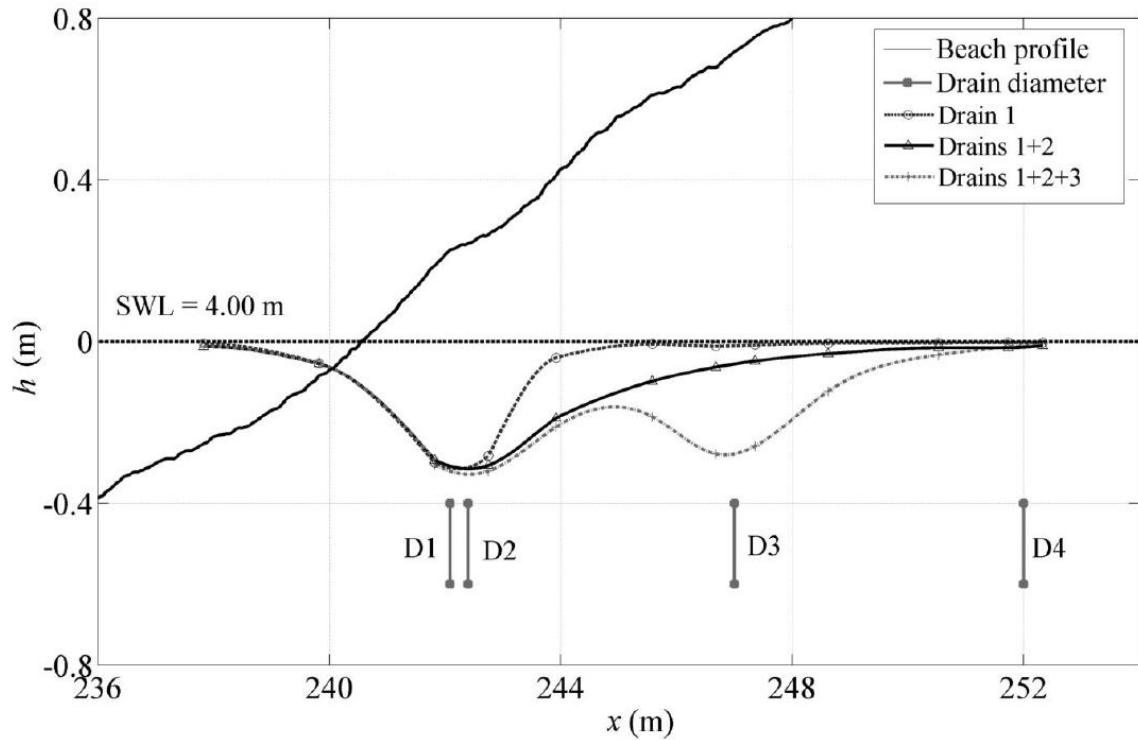


Figure 3.43. Spatial variation of water tables for Test S1, D1, D1 + D2 and D1 + D2 + D3 on (adapted from Damiani et al., 2011).

Dynamic tests are characterized by a smaller lowering of the water table with respect to the static conditions due to runup flow. Figure 3.44 shows the spatial variation of water tables for both undrained and drained conditions with D1 for Test HE. An “active infiltration zone” is defined as the beach area limited by shoreline position and maximum runup (Cartwright et al 2002). This zone is important because it involves infiltration and exfiltration processes during uprush and backwash phases influencing sediment transport patterns. An increase in the vertical flux motion produces a sediment drift which otherwise would be transported offshore during wave rundown. Note that the mean shoreline position in Figure 3.44 is evaluated at the end of the undrained test. Thus it is moved onshore with respect to previous spatial variation in the water tables, because of the beach profile changes due to the wave action during Test HE (Figs. 3.42 and 3.43). The wave motion produces a rise in the water table with respect to the static level and the maximum runup, evaluated by video recording, is located at the upper horizontal beach portion. This value is located offshore with respect to the maximum water table level inside the beach (see also Cartwright et al., 2002). The opening of D1 induces a water table depression along the beach which leads to a decrease in the saturated area inside the active infiltration zone of about 44% (shaded area of Fig. 3.44). This phenomenon was noted for all dynamic tests and drain configurations. In addition,

the drain is able to move the maximum water table value offshore with respect to the undrained condition. The spatial variation of water tables in both static and dynamic tests shows the influence on drain opening also on SWL (static tests) and MWL (dynamic tests), especially when D1 is on. This is the closest drain to the shoreline. After first tests, beach erosion caused a shoreline retreatment, drain D1 lying under the submerged beach and thus affecting the external wave motion in the shore zone.

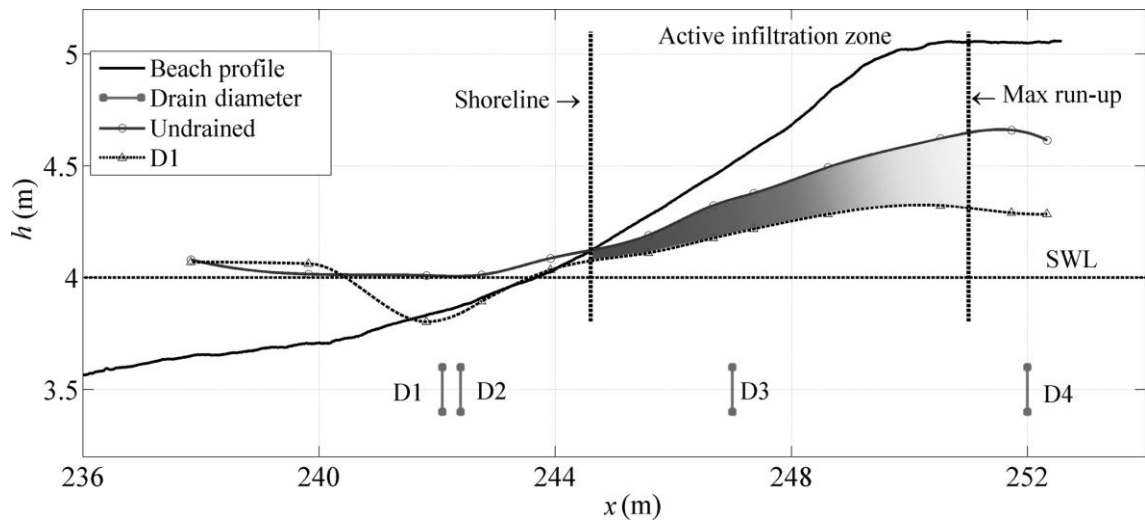


Figure 3.44. Spatial variation of water tables for undrained and drained conditions for Test HE, D1 on (after Damiani et al, 2011).

### 3.3.1.2 Hydraulic regime of drains

The efficiency of a beach drainage is strongly influenced by the pipe characteristics and their hydraulic regime. The head losses on the external surface of drains and their capability in collecting the drained discharge influence both the water table lowering and infiltration processes. Up to now the flow regime inside the drains has not yet been analyzed. Previous experimental (Damiani et al 2009) and numerical (Vesterby 2000, Li et al 2001, Karambas 2009) BDS modelling aimed to analyse only the dynamic fluctuations on the beach. These investigations, however, did not clarify the real drain flow regime, assuming identical hydraulic heads outside and inside the drains. Pressure measurements inside the drains showed that their internal regime occurs as an open-channel flow. This hydraulic discontinuity is mainly related to the non-linear effects of the groundwater field characterized

by strong streamline curvature near a cylindrical obstacle as the drains. The hydraulic regime inside the drains proves to be different from that developed in the sand. This behaviour is related to the energy losses induced by the water infiltration phenomena. The energy losses depend on the sand permeability and on the material and the covering system of the drains. With reference to the spatial variation in the water tables and the water depths inside the drains for Test S2 with all drains opened separately (Fig. 3.42), low filling degrees follow from transducer measurements. A general decrease of the drain water depths as a function of the shoreline distance is noted. When more drains are opened simultaneously, the lowest filling degrees occur for combinations of three drains. Conversely to above, the water depth has an increasing trend. Figure 3.45a shows the time variation of relative water depth  $\Delta h$  measured by the pressure transducer placed inside drain D2 (pt12) and the transducer located in the sand close to the drain for S1 (pt3 and pt4), including the opening phase of the drain and its successive closure phase. The time evolution of pt12 is characterised by an initial depression of  $\Delta h$  and a successive constant stabilization, followed by an increasing trend to reach the initial static conditions after the drain closure. The depression phenomenon is induced by the air entrance due to the fast opening of the gate valve, as shown in detail in Figure 3.45b. In this case, the interval between the maximum depression and the constant value of  $\Delta h$  is correspondent to the air propagation time occurred from the end of the pipe system to the transducer position in the drain. In particular, the duration of this transitory phase is less than 1' for all tests and related to the length of each blind pipe. The time evolution of pt3 and pt4 shows a decreasing trend during the entire phase of drain opening. The opening phase is therefore characterised by a fast reaching of a proper trend inside and outside the drain. Conversely, the closure phase proves to be slower respect to opening phase. In this phase the mentioned two flow regimes of the system came back to an unique groundwater condition. With reference to the initial time after the drain closure, Figure 3.46 reports the time variation of rising velocity,  $w_{\Delta h}$ , deduced by the time variation of  $\Delta h$  for pt3, pt4 and pt12. The initial rising velocity of pt12 proves to be higher of about 4 times respect to those deduced by pt3 and pt4 and shows a fast decreasing trend. The values of  $w_{\Delta h}$  by pt3 and pt4 show an initial arising phase, followed by a successive decay. This feature is due to the different resistance offered by the air inside the drain for pt12 and by the porous media for pt3 and pt4. After about 300 s, all velocities attain the same regime value. The reaching of this value is correspondent to the full ejection of the air from the drain.

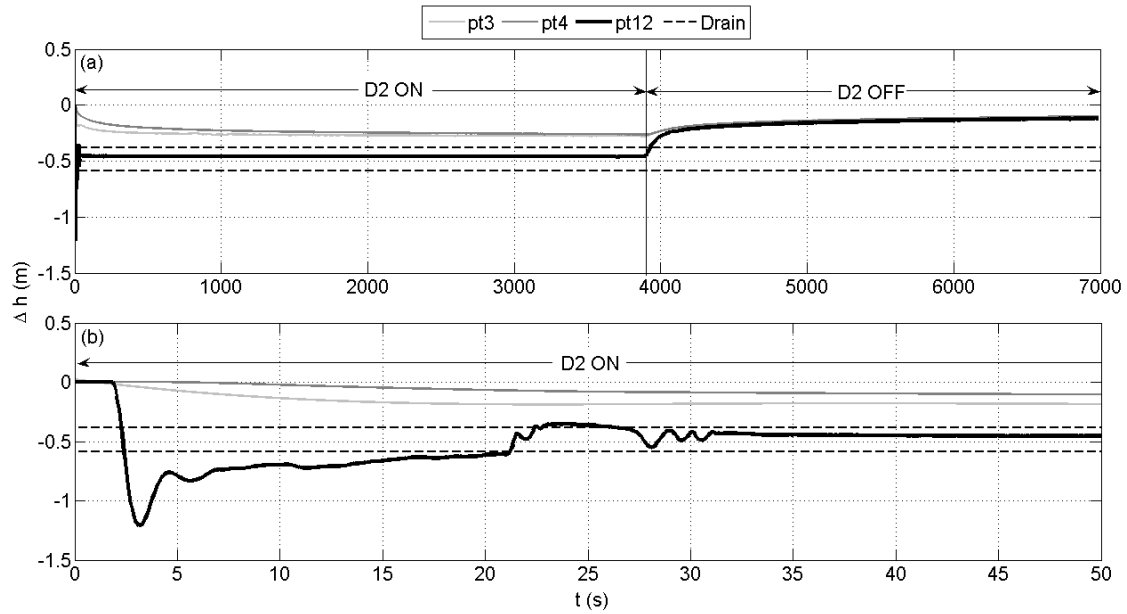


Figure 3.45. a) Time variation of dynamic pressure,  $\Delta h$ , by transducers pt3, pt4 and pt12; b) Initial instants of dynamic pressure,  $\Delta h$ , by transducers pt3, pt4 and pt12 (S1 test, D2 on and off) (Damiani et al., 2011)

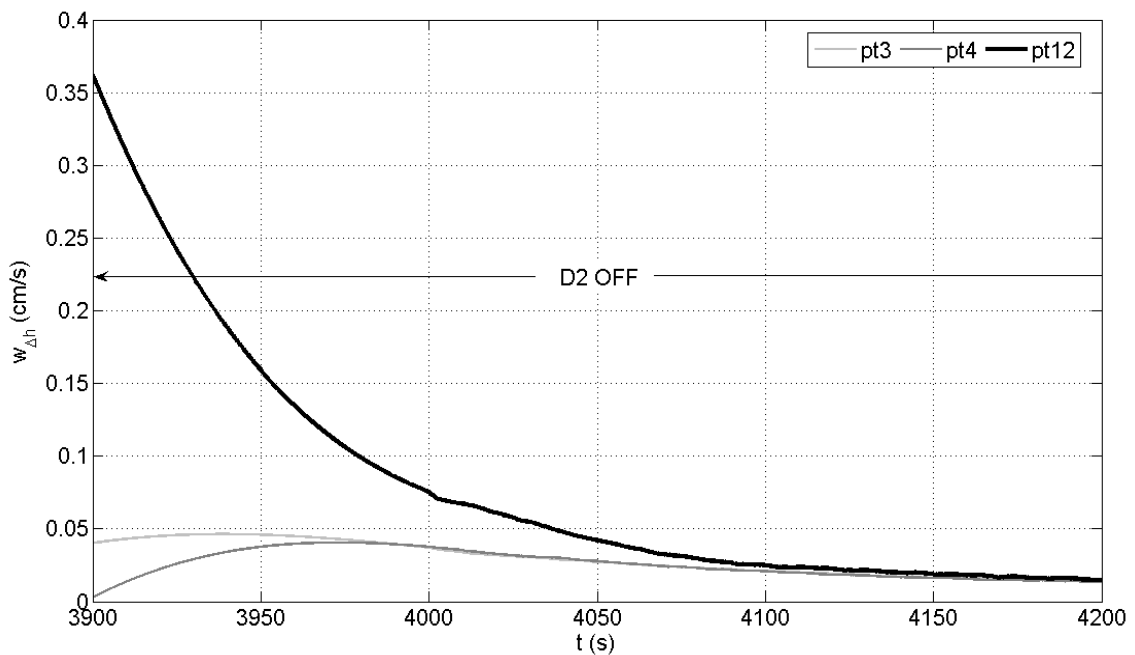


Figure 3.46 Time variation of rising velocity,  $w_{\Delta h}$ , deduced by the transducers pt3, pt4 and pt12 (S1 test, D2 off). (Damiani et al., 2011)

The energy losses along the drains and the blind pipes due to the water infiltration have led to low drainage discharge values for all static and dynamic conditions. For the static tests, the

drained discharges were higher for S2 than for S1, showing a poorly-defined trend during the activation of each drain and higher values when more drains were opened. The values of average drained water flux,  $Q_m$ , ranges from about 0.3 l/s to 1.3 l/s. For all dynamic tests the drainage flows are higher and more defined with respect to the static cases, ranging from 0.5 l/s to 1.9 l/s. The values of  $Q_m$  deduced by the transducer placed in the pumping well as a function of offshore wave parameters such as the zero-order moment of wave power spectrum  $m_0$ , mean wave celerity  $c_0$  and mean wave energy flux  $P_0$  are shown in Fig. 3.47 for static S1 and dynamic HE, ME and LE tests. These values were determined by the first offshore wave gauge. The increasing trend of  $Q_m$  is directly associated with  $m_0$  and  $P_0$ , showing higher values when more drains work. Note that the highest values of  $c_0$  are not associated with the maximum drainage discharges which therefore appear to be related to the maximum incident wave energy and wave steepness (Damiani et al, 2011).

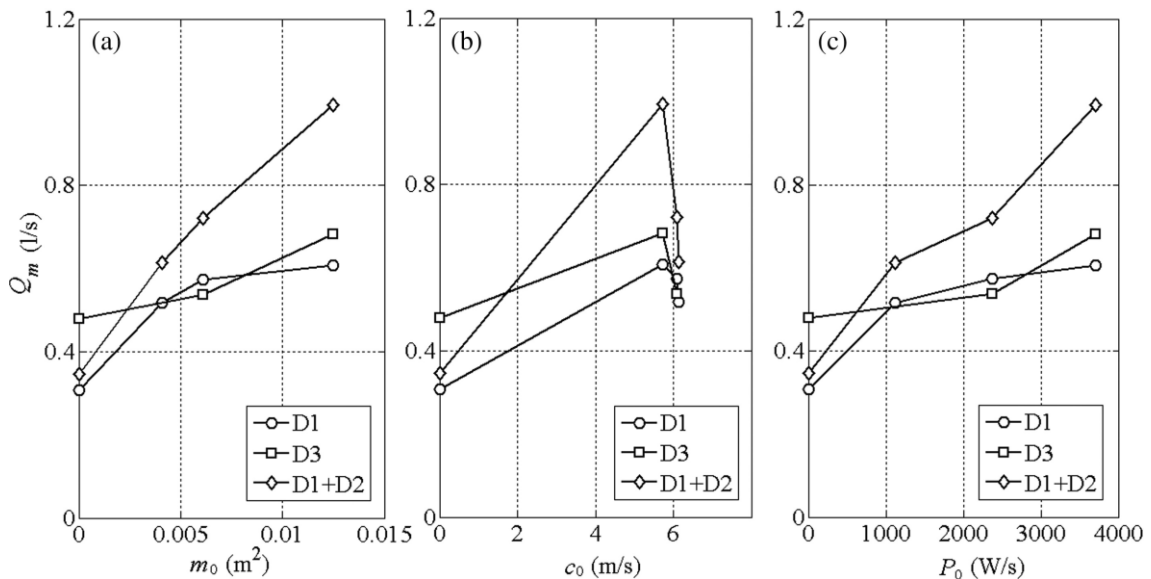


Figure 3.47. Mean drainage discharge versus (a) offshore zero-order moment of wave power spectrum, (b) offshore mean wave celerity, (c) offshore mean wave energy flux for Tests S1, HE, ME and LE, (Damiani et al, 2011).

### 3.3.1.3 Wave setup

Although drainage cannot change the saturation degree in the submerged beach located in the surf zone, it may influence the mean water level on the submerged beach.

In fact the water table lowering leads to a reduction in the wave set up on the beach. The piezometers also allow estimating the maximum wave setup in both undrained and drained

conditions, from the intersection between the beach profile and the water table at the end of each test. Overall, the reduction in the water table elevation leads to a lowering of wave set up on the beach. Figure 3.48 shows the maximum wave set up,  $\eta$ , on the beach as a function of the offshore zero-order moment of wave power spectrum,  $m_0$ , in undrained conditions and in all single and coupled drained configurations. The influence of the BDS on the reduction of wave set up can be observed for all drains activated for all HE, ME and LE wave tests. The reduction of the set up due to the drains opening is more remarkable when  $m_0$  increases. Note that, as seen previously, the drained flows increase is directly associated to the values of  $m_0$ , showing higher values when more drains work. This tendency corresponds to a decrease in maximum set up.

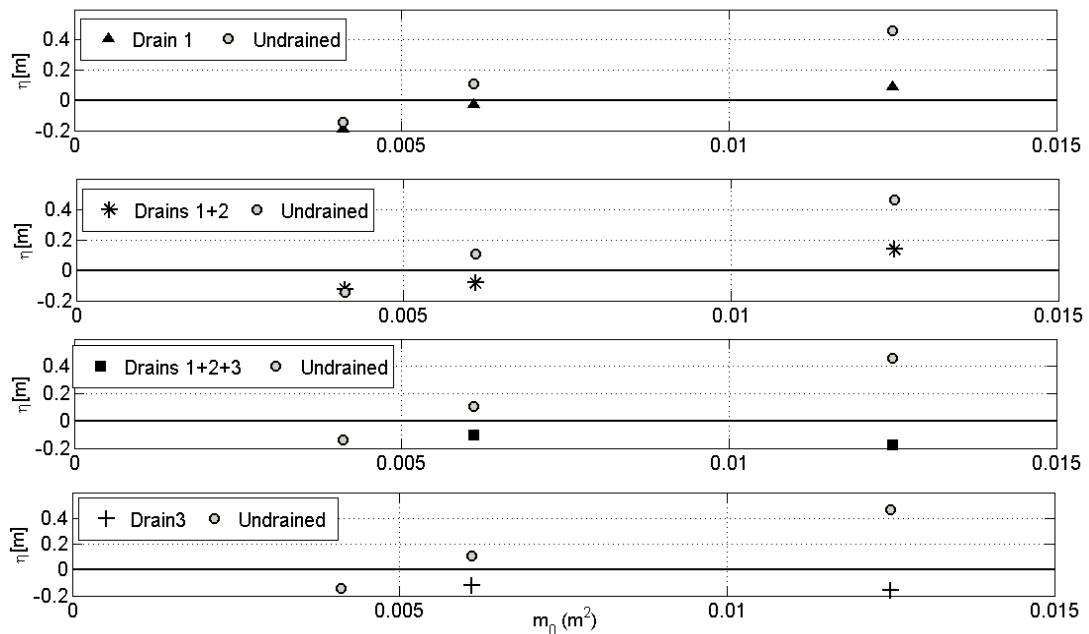


Figure 3.48. Maximum wave set up vs. offshore zero-order moment of wave power spectrum for the three energy level in undrained conditions and all drain configurations.

#### 3.3.1.4 Undertow current profiles

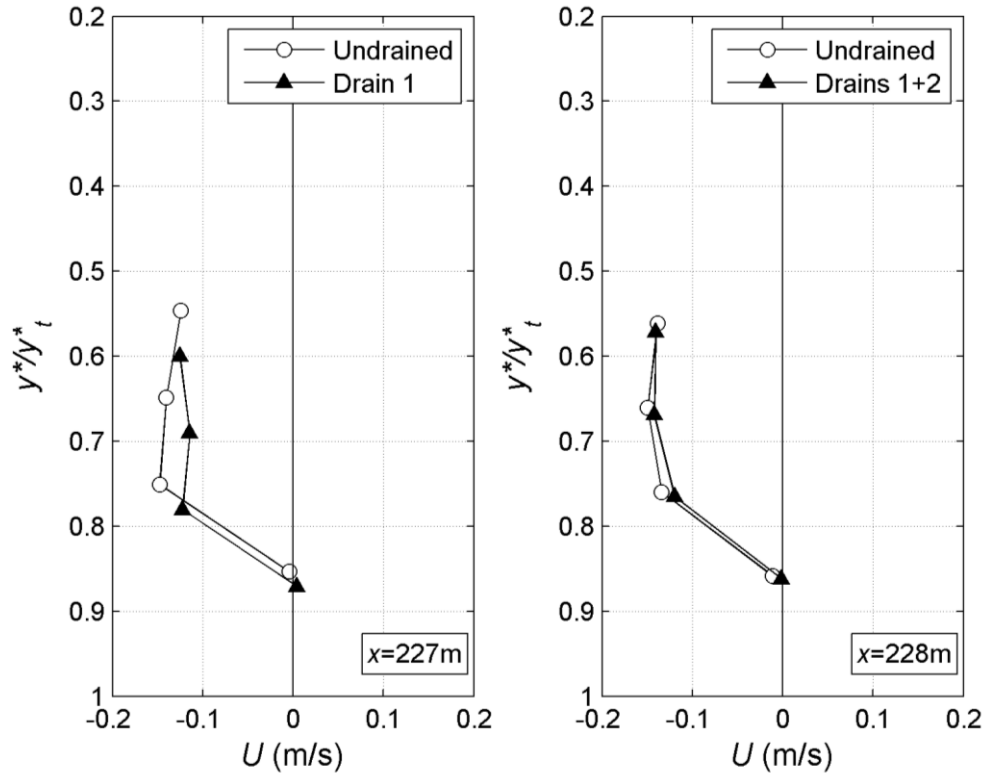
As seen, the presence of the BDS inside the beach leads a reduction of wave set up. This mean that the BDS may lead to significant changes in nearshore hydrodynamic processes, principally in the swash zone and secondly in the surf zone. Indeed, as is well known the set up constitutes a hydraulic head driving undertow currents. After wave breaking a seaward

flow near the bottom of the beach due to different vertical pressure profiles appears. The undertow represents a mass conservation response to the associated landward drift of water under the crests of the breaking incident waves (Greenwood and Osborne, 1990). These currents are a cause of cross-shore transport of sediments moved and suspended by turbulence due to breaking.

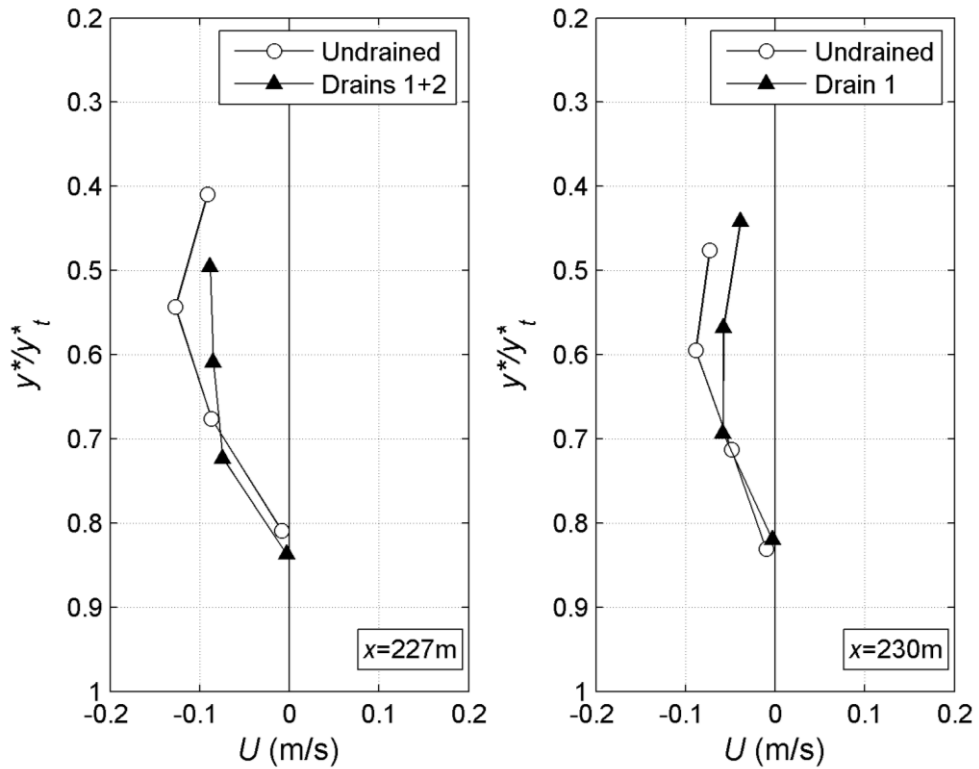
The evaluation of the undertow current profiles in the presence/absence of a BDS has been performed for all wave attacks by 4 electromagnetic currentmeters as a function of the bed evolution. In particular, to perform measuring the seaward currents (undertow currents), flowing in the lower portion of the water column under breaking waves, the instruments position was suitable.

Figures 3.49a and 3.49b show the undertow current,  $U$ , for undrained and drained conditions, respectively, for ME and LE wave attacks. The ordinate is dimensionless, pointing from the mean water level downward, and is defined by the ratio  $y^*/y_t^*$ , where  $y^*$  and  $y_t^*$  are, respectively, the instrument and the beach depths for the specific test. A larger modification of the beach depth occurs when a series of other tests was performed on the two tests under comparison. Therefore it is reasonable to expect that the velocity comparison between tests in which  $y_t^*$  changes significantly are less reliable.

In the following the analyses focus on comparing the undertow current for the sections where tests were performed in undrained and drained conditions. The cross-shore reference locations for the LE tests are  $x = 227$  m and 230 m. The drained conditions lead to a general reduction of the undertow current. When drains D1 and D2 are simultaneously opened a larger attenuation in the undertow current is not observed with respect to the case of activation of only D1 (Figure 3.49a). From the analysis of LE data a general attenuation in undertow currents for almost all tests has been observed. For ME wave attacks a smaller decrease in the seaward current in drained conditions with respect to LE tests can be observed, as reported in Figure 3.49b under the activation of D1, also coupled with D2 in two different sections ( $x = 227$  m and 228 m). This behaviour has only been observed in some tests. The smaller reduction in the undertow current observed in drained conditions for ME tests with respect to LE cases might depend not only on the larger wave energy attack but also on the more offshore position of the analyzed sections with respect to the position of the drains. For HE conditions the undertow current profiles do not show any sensible variation for undrained and drained conditions confirming that in storm cases the system is not working in stabilizing the beach (Ciavola *et al.*, 2010) and does not influence therefore the surf zone kinematics.



a)



b)

Figure 3.49. Comparison of the undertow current measured by currentmeters in undrained and drained conditions: a) for ME tests; b) for LE tests.

### 3.3.1.5 Analysis of surf beat

The analysis of the energy density spectra measured by the pressure transducers inside the beach shows significant influence of the BDS on the shape characteristics of surf beat oscillations (Aristodemo et al., 2011). Water energy level inside the nearshore beach is evaluated by pressure transducer measurements in terms of zero-order moment of pressure power spectrum,  $m_{0p}$ . The spectral evolutions of the wave characteristics are showed in Figure 3.49, which contrasts:

- a) Wave energy density spectrum of wg1, placed at 50.1 m from the wave paddle, over a water depth of about 2 m;
- b) Wave energy density spectrum of wg20, located at 230 m from the paddle, over a water depth of about 0.9 m;
- c) Pressure energy density spectrum of pt3 for undrained condition;
- d) Pressure energy density spectrum of pt3 with drain D1 open.

As expected the spectral wave evolution from wg1 to wg20 is subjected to the shoaling phenomena, leading to an energy reduction and a broader shape of the spectrum associated to the frequency dispersion (Figures 3.50a and b).

Within the infragravity wave frequency range (0.001-0.05 Hz), the magnitude of the pressure density spectrum is reduced by the drain activation. Modifications of the shape of surf beat spectra in comparison with the undrained cases are also observed. In particular the presence of the BDS tends to move the surf beat peak frequency ( $f_p \text{ beat} \approx 0.03$  Hz) towards lower frequencies with respect to the undrained condition (Figures 3.49c and d). For all HE, ME and LE tests, the effect of the drains on the surf beat frequencies is analyzed by the frequency peak ratio,  $f_p \text{ beat}/f_p \text{ wg20}$ , where  $f_p \text{ wg20}$  is the peak frequency deduced by wg20 (Figure 3.51) at pt3 (between D1 and D2) and pt6 (near D3).

The frequency peak ratios range about between 0.2 and 0.4 for undrained tests. The drains lead to lower values of this ratio due the frequency shift towards a lower infragravity range. This effect is particularly evident for the first drainage conditions in the LE case.

The presence of the BDS, thus, tends to back shift the wave frequencies towards the frequency range of long period infragravity waves. The presence of a larger infragravity energy induced by the drainage tend to enhance the onshore sediment flux.

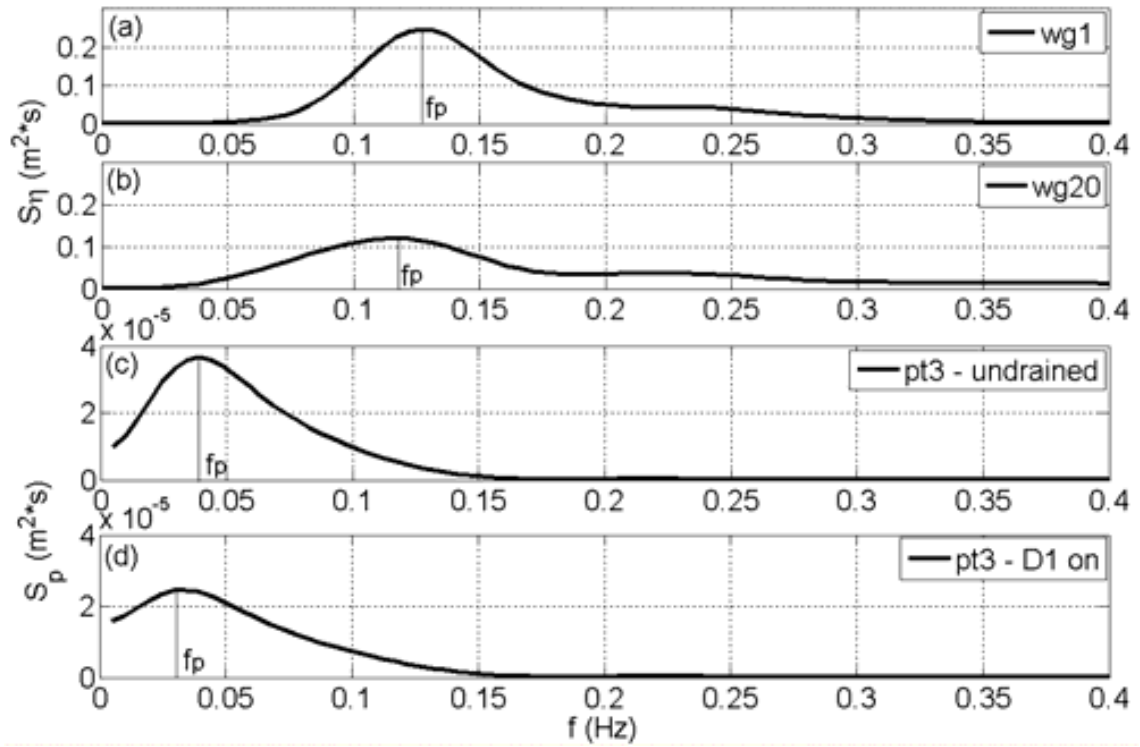


Figure 3.50. a) Wave energy density spectrum of  $wg1$ , b) Wave energy density spectrum of  $wg20$ , c) Pressure energy density spectrum of  $pt3$  for undrained condition, d) Pressure energy density spectrum of  $pt3$  with drain D1 on (ME test). (Aristodemo et al., 2011).

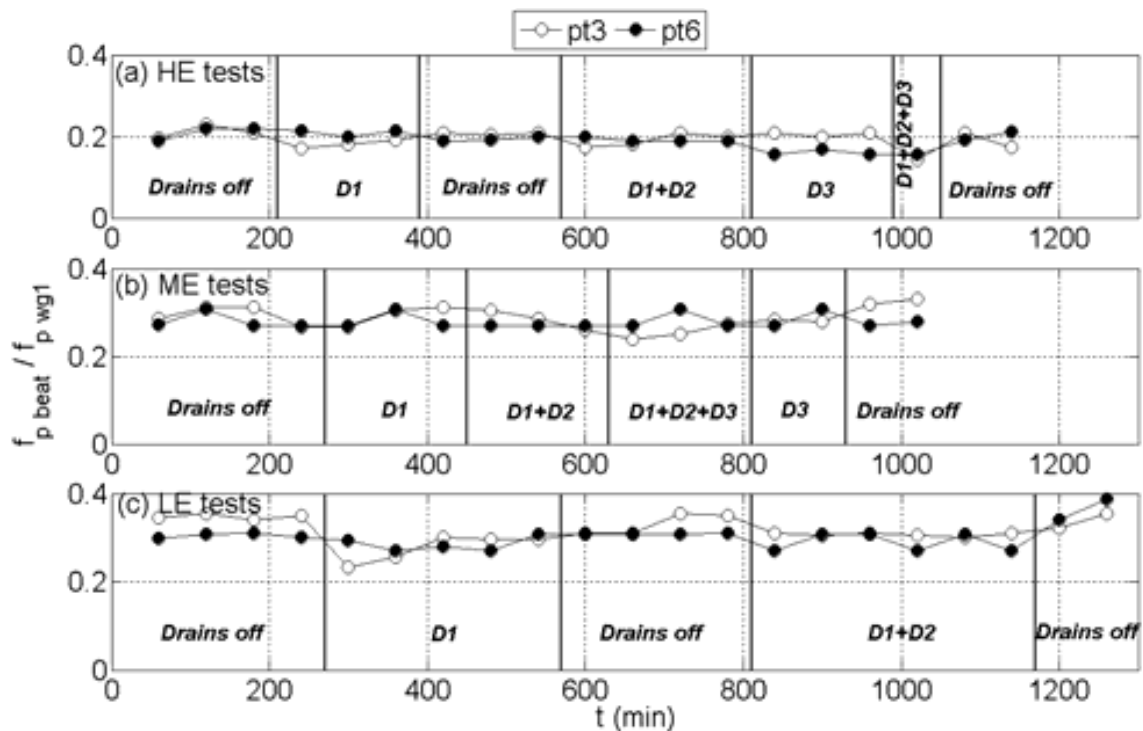


Figure 3.51. Time variation of frequency peak ratio,  $f_{p \text{ beat}} / f_{p \text{ wg1}}$ , for undrained and drained conditions. (a) HE tests, (b) ME tests, (c) LE tests (from Aristodemo et al., 2011).

### 3.3.2 Morphodynamic response

#### 3.3.2.1 Morphodynamic analysis under High Energy conditions

To immediately appreciate the morphological evolution of the beach, the results are graphically represented with subsequent profiles related to significant step batches assembled in Figure 3.52. A clear overall erosive trend of the beach is recognizable. The sand moved from the swash zone to the submerged beach generating a bar. The beach profiles seemed to move towards a proper equilibrium configuration characterized by an exponential shape with negligible overall effects induced by the drains. Consequently, the shoreline migration has a tendency to reach equilibrium configuration. The trend is also noticeable in Figure 3.53 through the time variations of dimensionless relative volume variation,  $I$ , and volume variation,  $\Delta V$ , in which positive values represent accretion and negative values represent erosion.

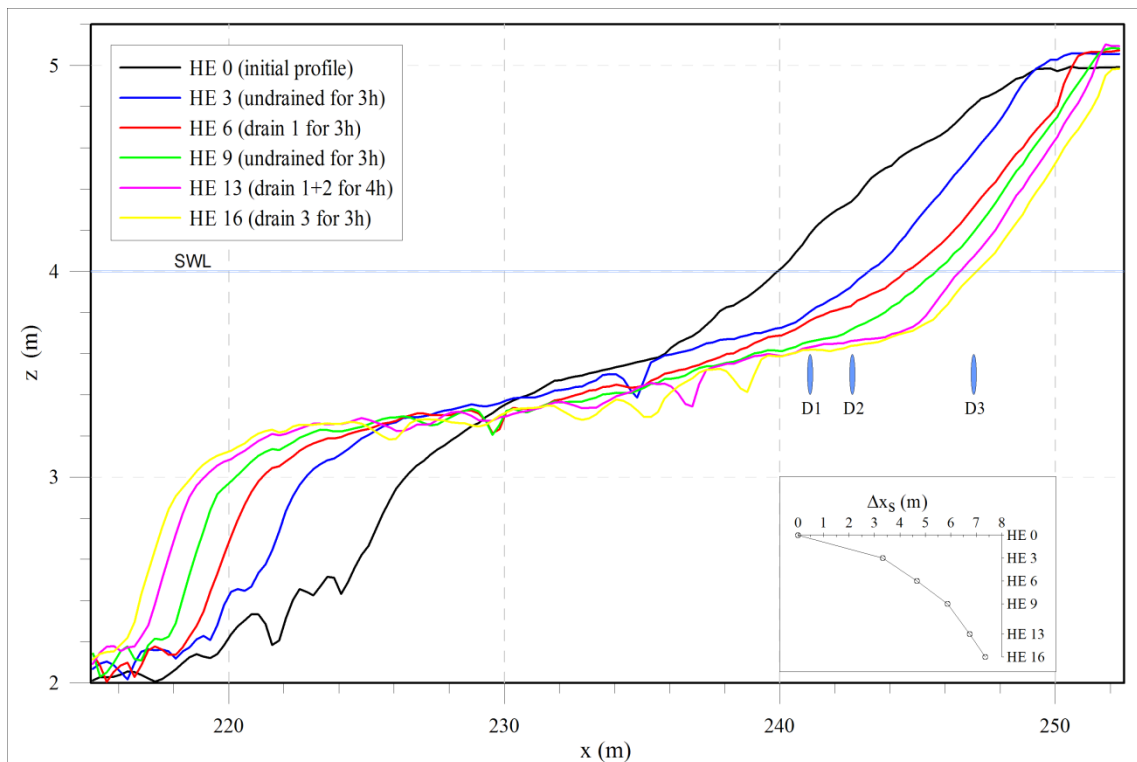


Figure 3.52. Significant beach profiles and relative shoreline migrations  $\Delta x_s$  under HE wave conditions.

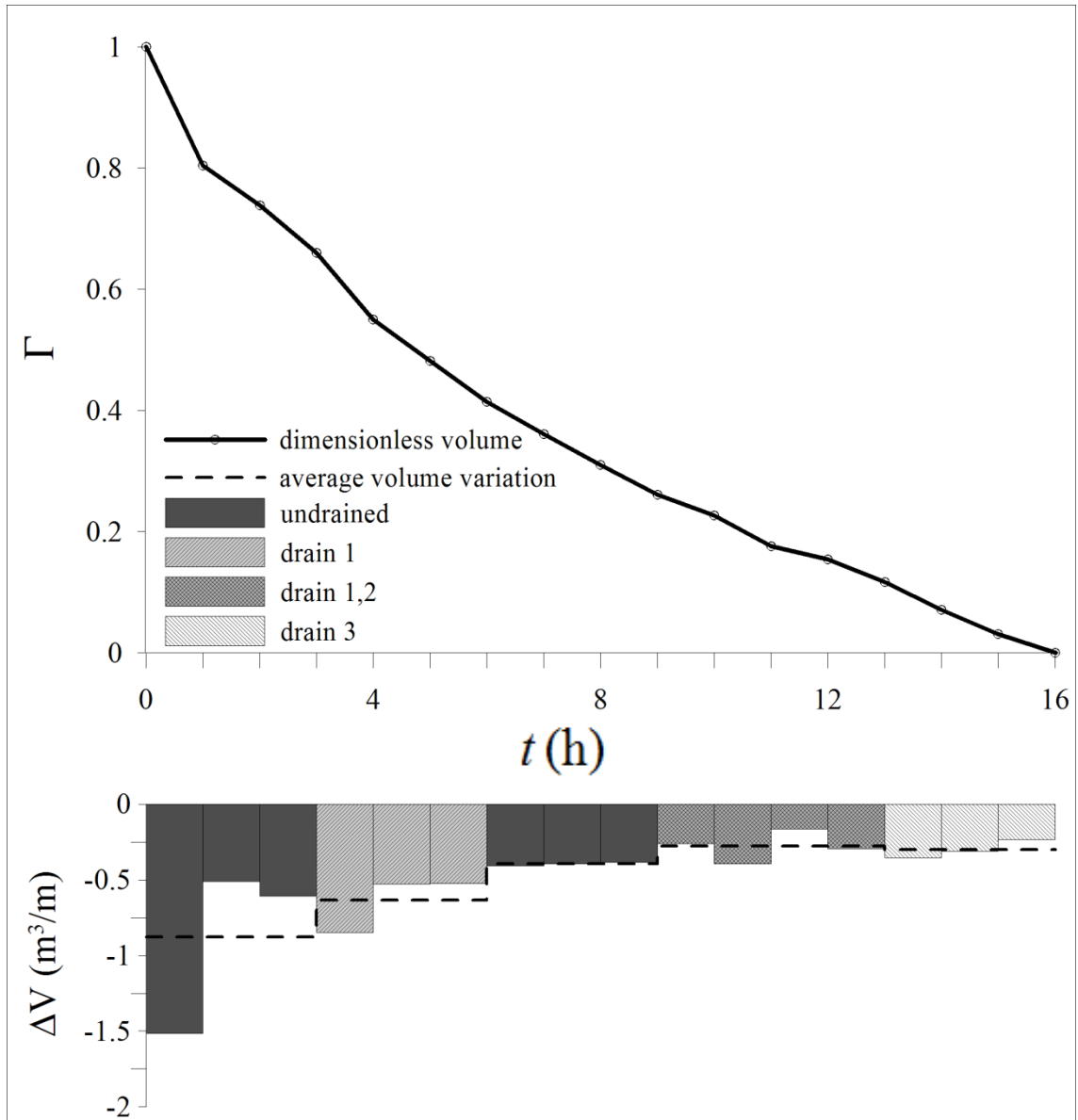


Figure 3.53. Time variation of dimensionless relative volume variation  $\Gamma$  and volume variation  $\Delta V$  above  $x = 240$  m for HE tests.

At the end of the first step under HE condition without drains, the observed erosive trend was the highest of the test ( $1.51 \text{ m}^3/\text{m}$ , see Figure 3.53). During the second and third step the eroded volume were respectively  $0.51$  and  $0.61 \text{ m}^3/\text{m}$ . At the end of three steps, an average of  $0.87 \text{ m}^3/\text{m}$  of lost volume was computed, while the shoreline had retreated  $3.32 \text{ m}$  (Figures 3.52 and 3.53). Switching D1 on, overall the erosive trend did not change. Indeed, the sand volume loss was about  $0.6 \text{ m}^3/\text{m}$  as in the previous steps without drainage. However, focussing on the area above the cone of depression of the groundwater table (from  $x = 240 \text{ m}$  to  $241.5 \text{ m}$ ), some positive localized effects were recognizable, as shown in detail in Figure

3.54a. In this area the relative vertical variation of bed level,  $\Delta z$ , after 2 hours of drainage was zero. Three subsequent steps in undrained condition, showing an upturn of erosion tendency, and further successive three steps with the drains operative, exhibiting local morphodynamic effects, confirm the observation of the stabilization. (Figure 3.54b and 3.55a).

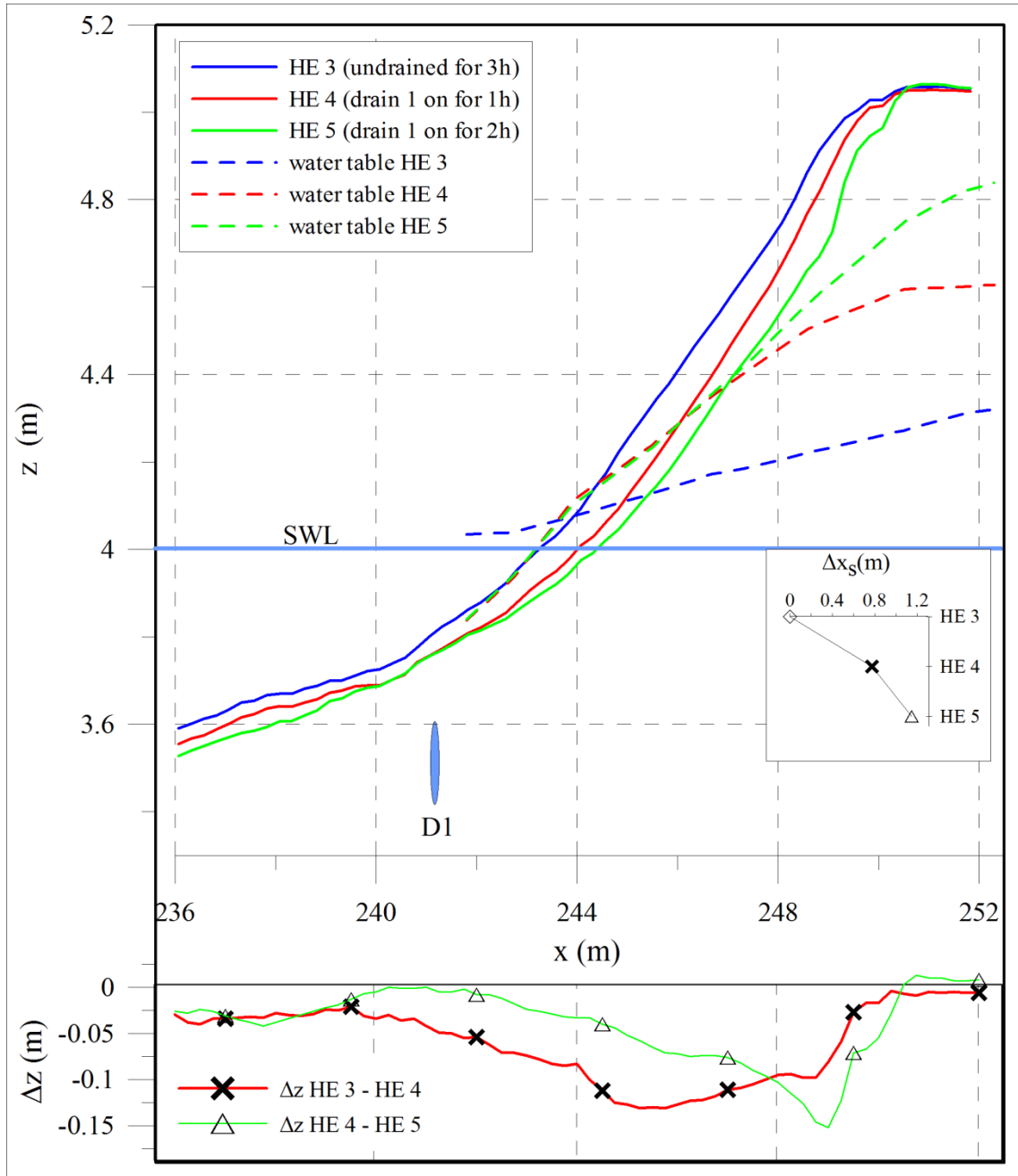


Figure 3.54a. Beach profiles, water tables and relative shoreline migrations  $\Delta x_s$ , under undrained HE 3, with D1 after one step (HE 4) and after two steps (HE 5).

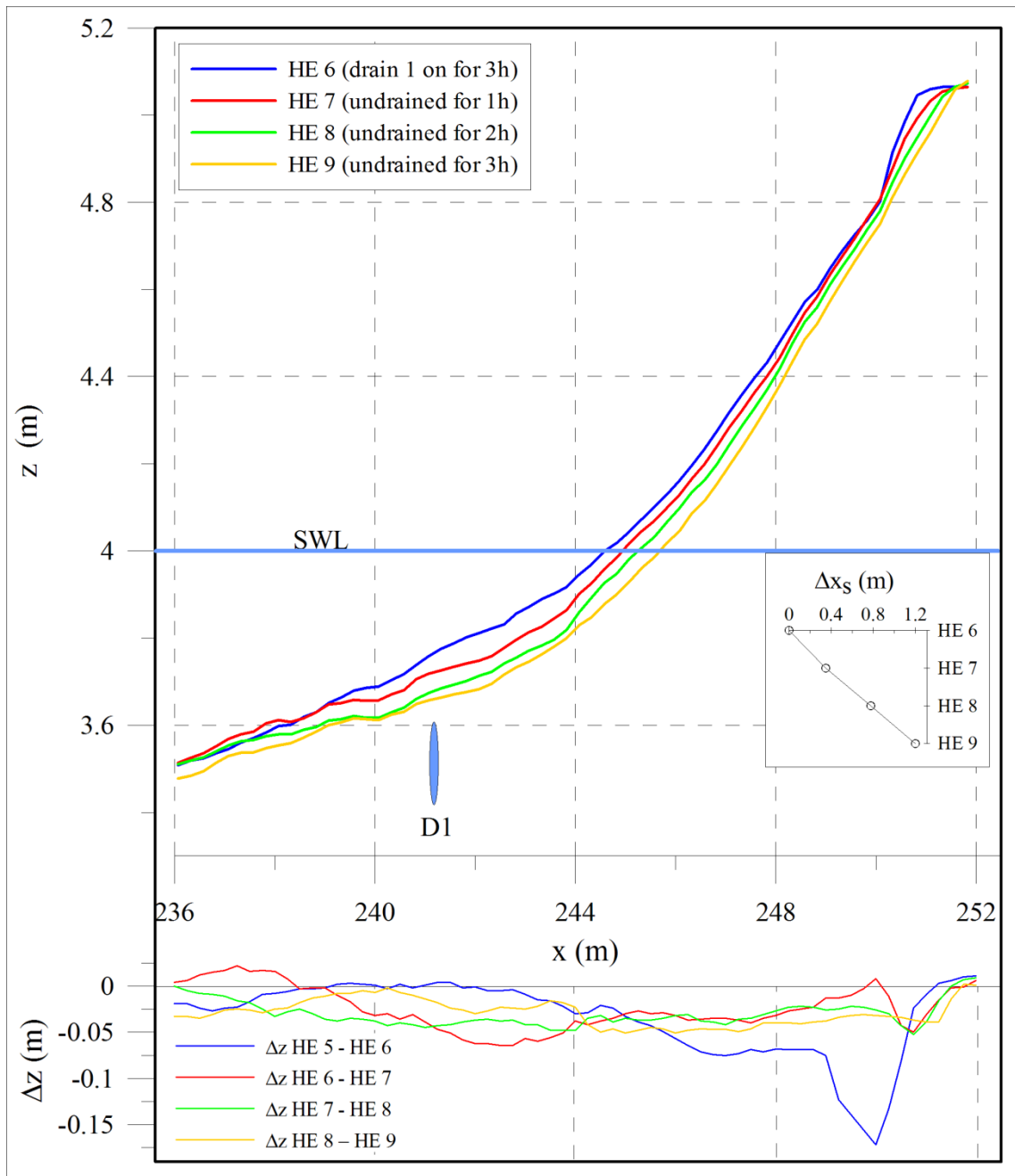


Figure 3.54b. Beach profiles and relative shoreline migrations  $\Delta x_s$  after three steps in undrained conditions (HE 7-8-9), following the test with D1 (HE 6).

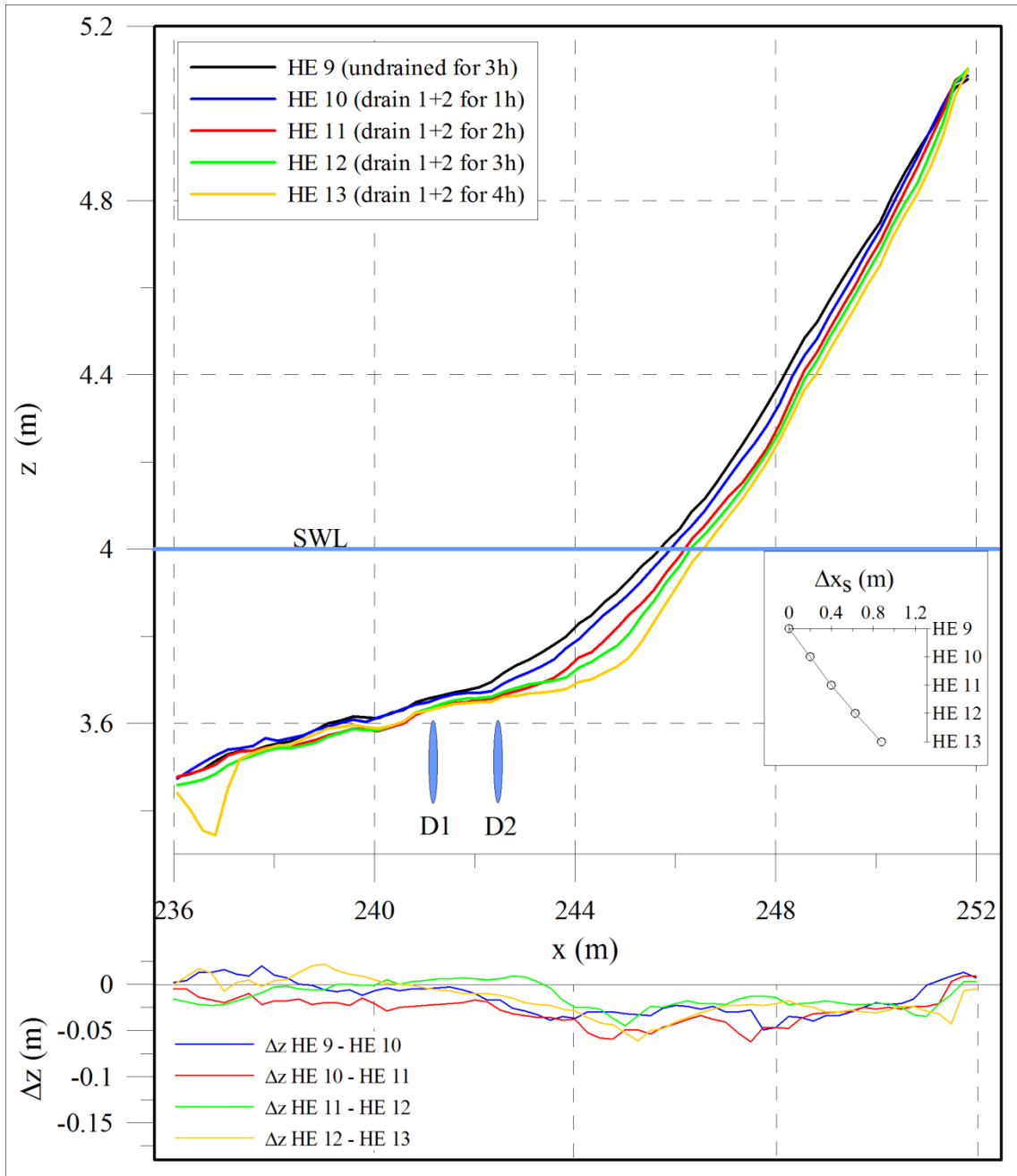


Figure 3.55a. Beach profiles and relative shoreline migrations  $\Delta x_s$  after four tests in drained conditions with D1+D2.

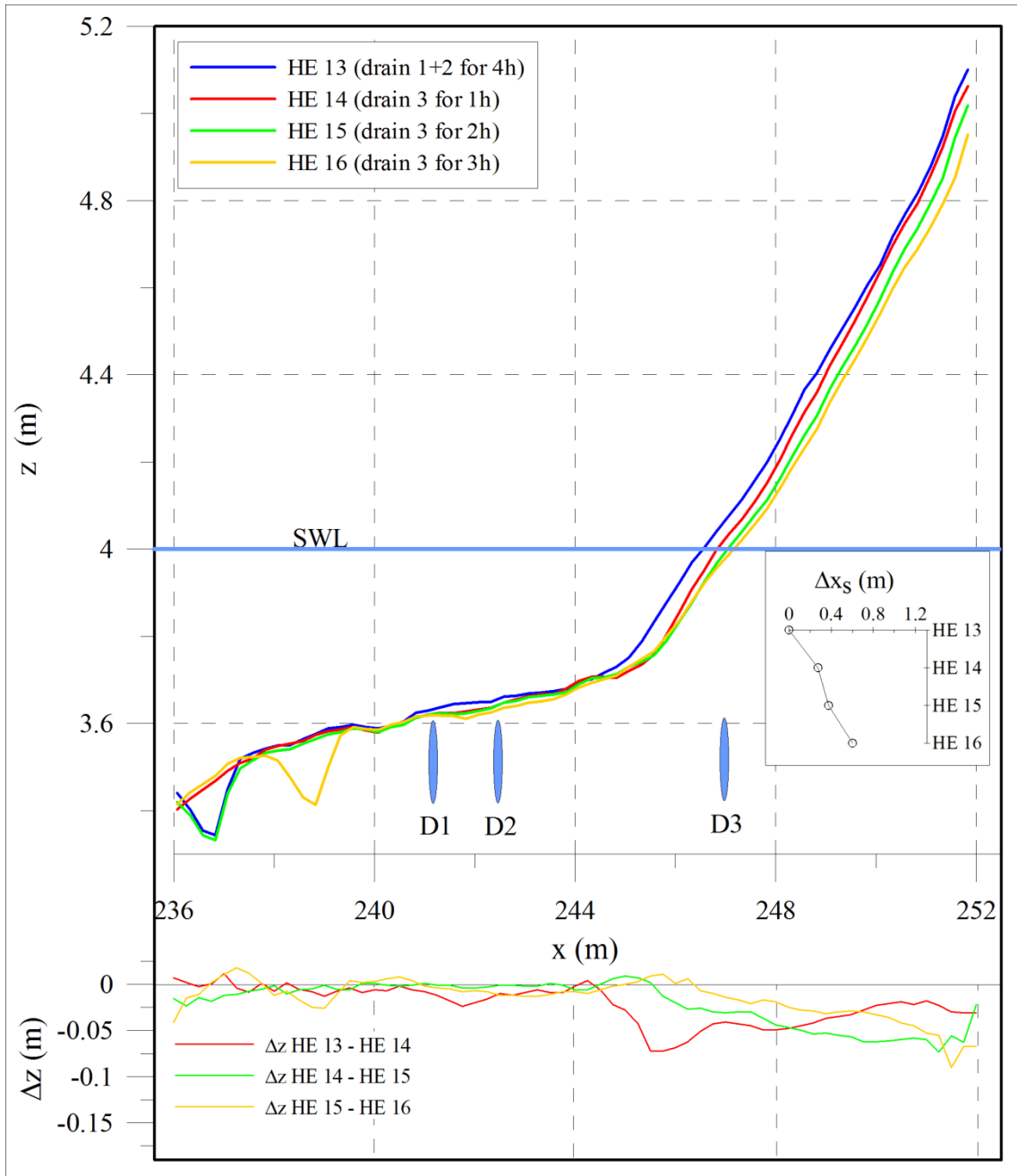


Figure 3.55b. Beach profiles and relative shoreline migrations  $\Delta x_s$  after three tests in drained conditions with D3.

In fact, in the proximity of D1 and D2, negligible or no bed variations were found, while moving away from the zone of the drain's hydraulic influence the erosion pattern still remained the same. The area influenced by the drain was identified between 240 m and 243 m, in correspondence of smaller  $\Delta z$  values. It is worth to notice that the length of this area was doubled than that related to D1 alone. However, to define a clear relationship between the size of the stabilized zone and the number of drain requires more detailed investigation (parametric study). If one looks at the position of the drains, under these conditions they were acting only under the submerged beach (Figure 3.52). Conversely, in the last three steps only the innermost drain (D3) was used, which operated under the emerged beach. In any case, no significative effects were highlighted. Indeed, its only role was to decelerate the erosion slightly (Figure 3.55b). The stabilized part moves on drain D3 (from  $x = 245$  m to 247m) with a deceleration of the shoreline migration. Comparing the values of  $\Delta z$  obtained with D1 and D3, it is possible to conclude that the drainage acting in the saturated zone (under the exit point) and in the unsaturated zone (above the exit point) have similar effects.

The relative bathymetric variation,  $Z_R$ , above each drain illustrates the stabilization effect of D1 and D2 (Figure 3.56).

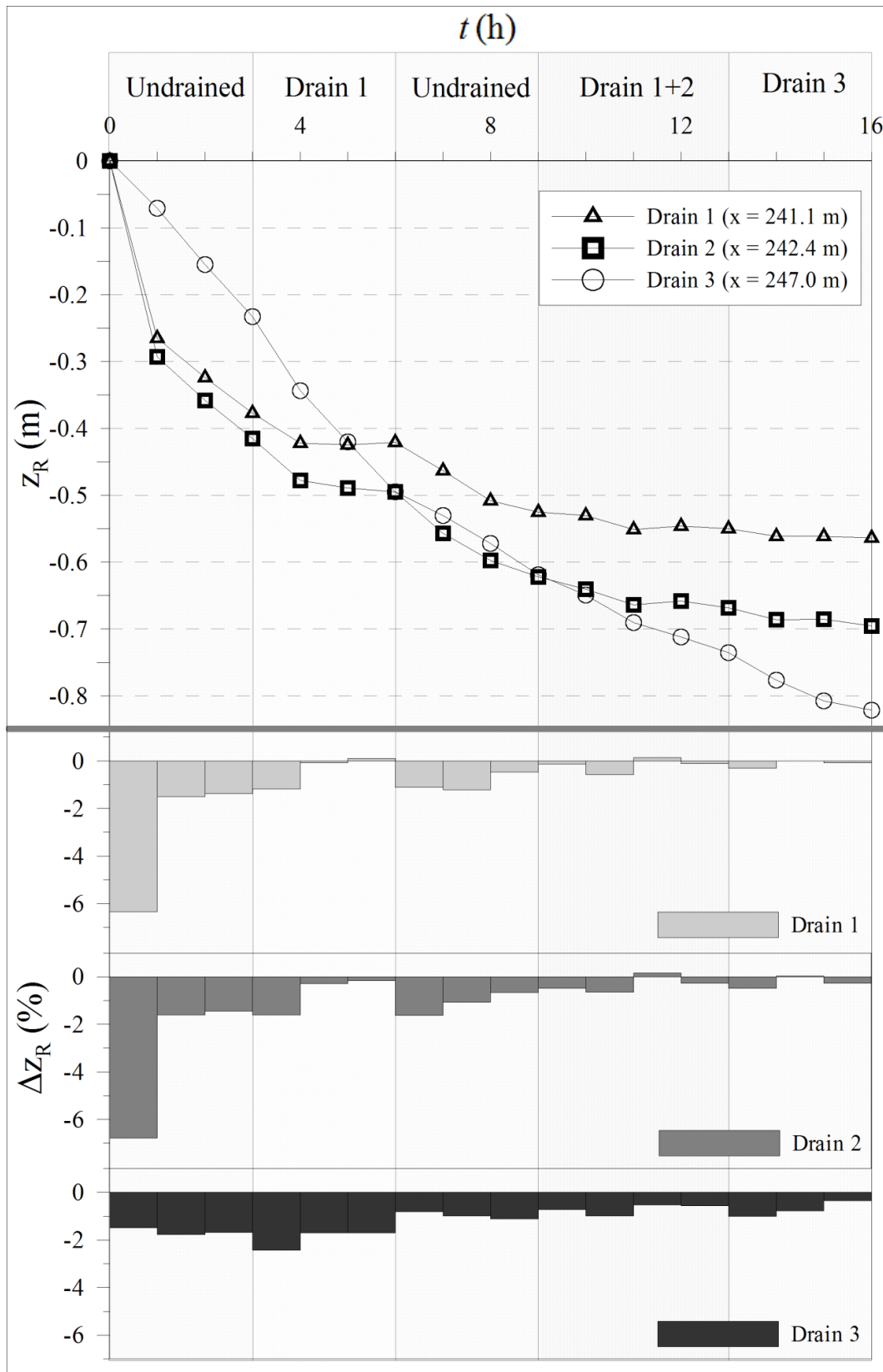


Figure 3.56. Relative bathymetric variation  $Z_R$  on the drains' axis and relative percent variation  $\Delta Z_R$  under HE tests. A local stabilization effect on D1 and D2 can be observed.

### 3.3.2.2 Morphodynamic analysis under Medium Energy conditions

Cross-shore profile modification during ME conditions are showed in Figure 3.57. Albeit less powerful wave condition than the HE tests were provided (see Tables 3.5 and 3.6), also the ME tests appear evidently affected by net offshore transport. Data exhibit a clear pattern, characterized by a rapid formation of a bar/trough system. In fact, at the dominant breaking point (at about a relative depth  $h/H_s \approx 0.5$ ), the greatest bed erosion was found. No change in this overall behaviour was observed activating D1 for three hours (ME 6 in Figure 3.57). In contrast, a completely different result was triggered during the simultaneous activation of D1 and D2 for three steps (ME 7÷ME 9). To make sense of this behaviour it is worth to note that the aforementioned profile M6 and M9 in Figure 3.57 were practically the same. Thus, it was obviously expected to reconfirm the beach stabilization when all three drain were operative. Surprisingly, the opening of D1, D2 and D3 not only did not lead to stabilization, but even re-triggered the original erosive trend. This erosive pattern persisted even using D3 alone (M 15) matching the magnitude of bed variation (Figure 3.57) with the eroded sand volume (Figure 3.58).

The same conclusions are confirmed from the analysis of relative bathymetric variations above the drains axes (Figure 3.59). An heuristic explanation of the efficacy of 2 drains and the inefficacy of 3 drains could be the combination of increasing/decreasing the normal and shear stresses due to infiltration/exfiltration effect. In fact, the infiltration effect induces an increasing in the effective weight of the sediment by a pressure gradient in the vertical lift force (Baird et al., 1996; Baldock et al., 2001), and leads to a thinning of the boundary layer and a greater shear stress (Conley and Inman, 1994; Turner, 1995) and vice versa for exfiltration. As shown by Turner and Masselink (1998), the boundary layer and shear stress changes appear to be dominant over the lift forces. Furthermore, when the drains D1 and D2 were operative, an increase of the swash length due to the lowering of down rush limit, it is likely to have occurred. Thus, the increase of the infiltration and the related decrease of exfiltration in the upper part of the beach, with D3 associated to D1 and D2 operating close to the shoreline, may have promoted an increase in shear stress during the backwash rather than during the uprush phase. Overall, this effect may be responsible for a net offshore sediment transport.

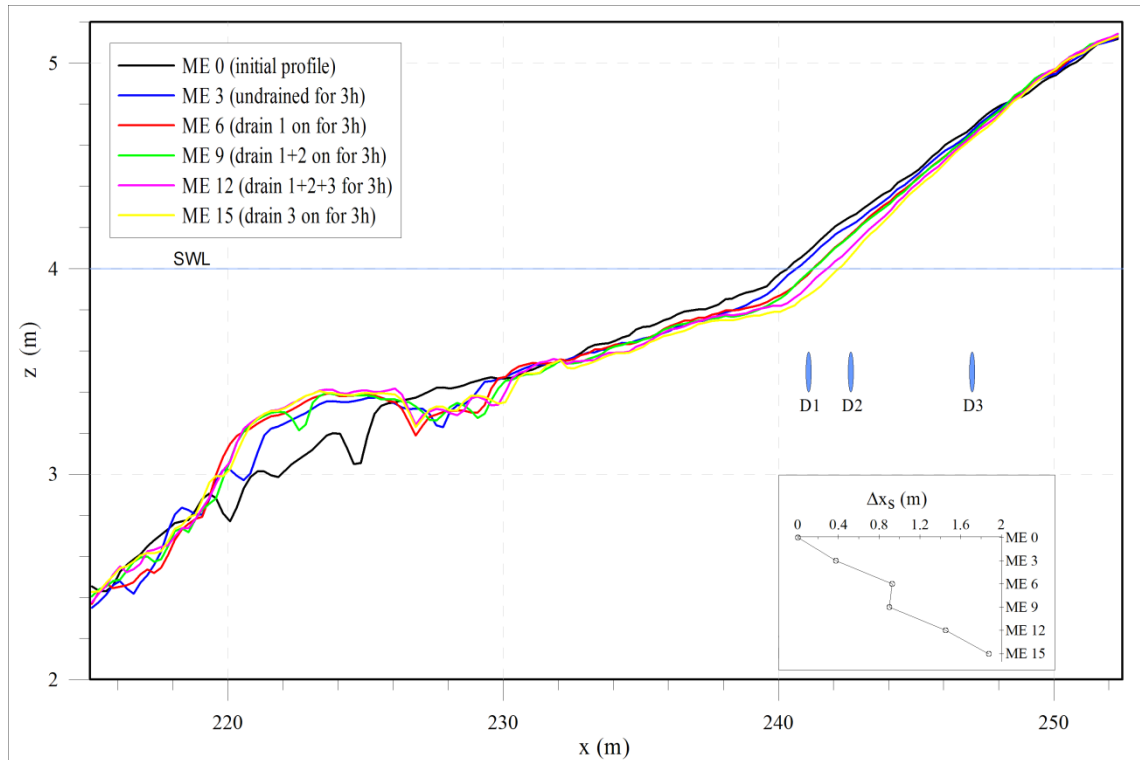


Figure 3.57. Significant beach profiles and relative shoreline migrations under ME conditions without drain (ME 3), with D1 (ME 6), D1+D2 (ME 9), D1+D2+D3 (ME 12), and with D3 (ME 15). It can be noticed the coincidence of profiles ME 6 and ME 9, highlighting that D1 and D2 operate with efficacy under ME conditions.

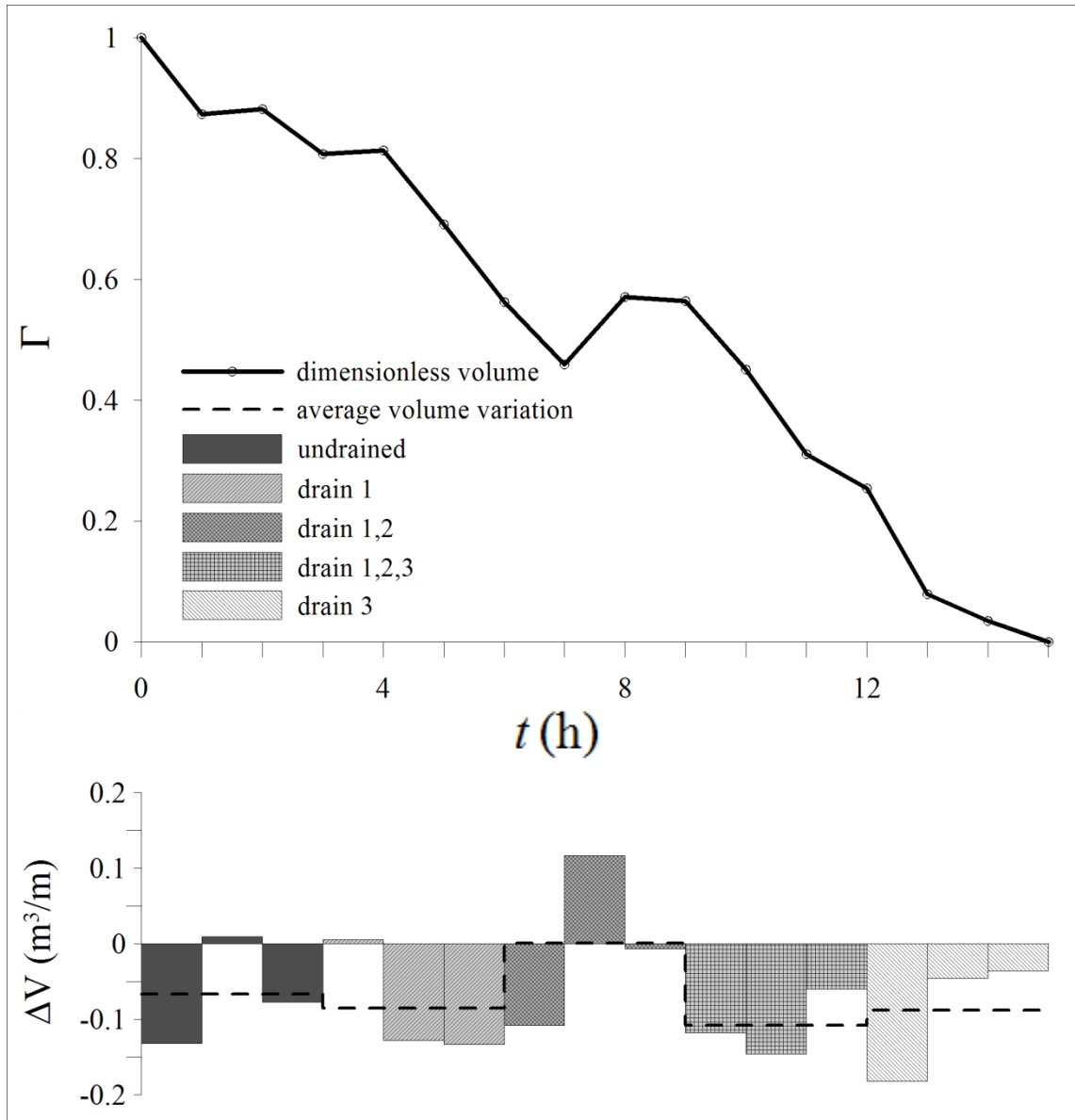


Figure 3.58. Time variation of dimensionless relative volume variation  $\Gamma$  and volume variation  $\Delta V$  above  $x = 240$  m for ME tests.

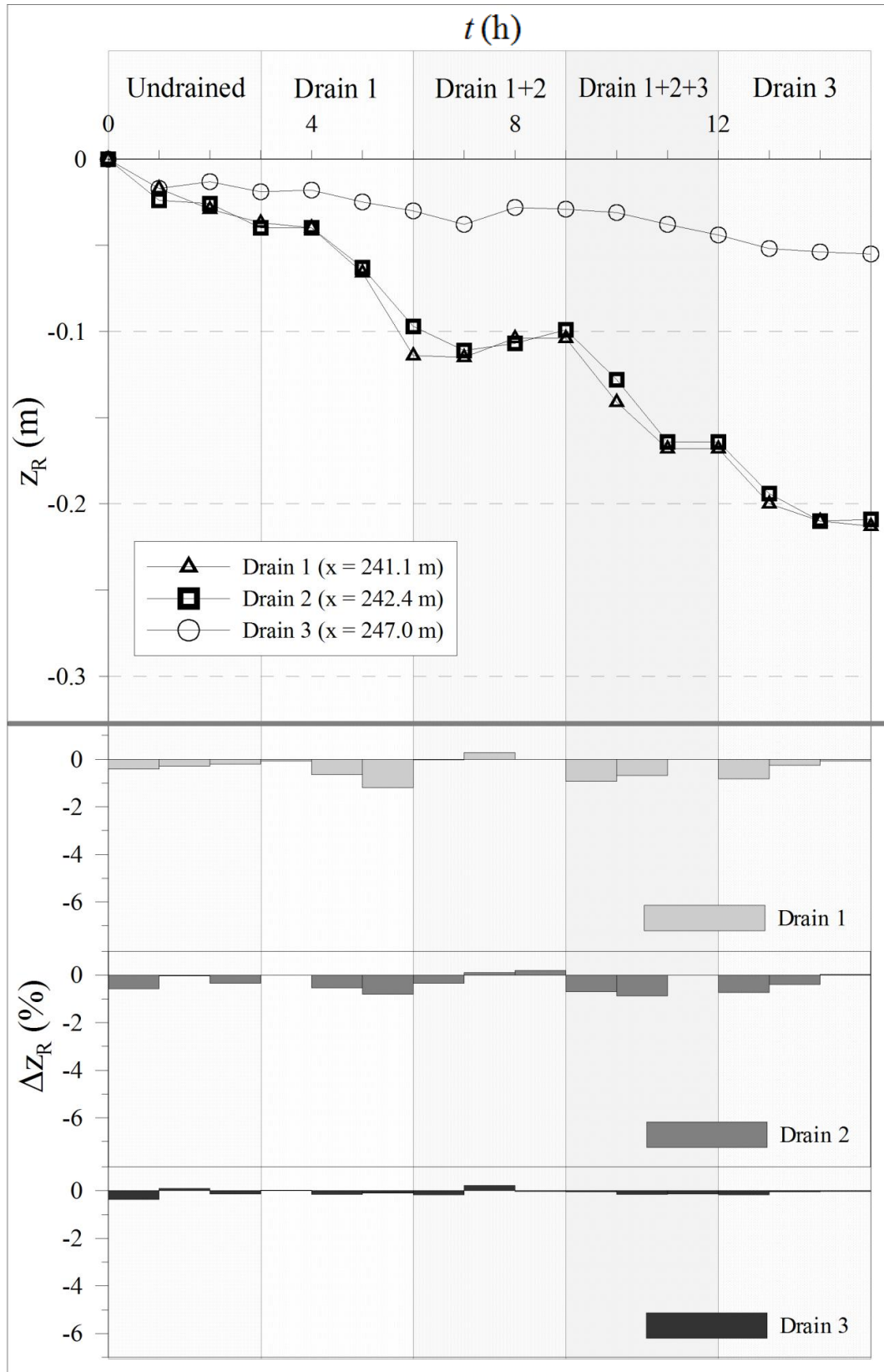


Figure 3.59. Relative bathymetric variation  $Z_R$  on drains axis and relative percent variation  $\Delta Z_R$  under ME tests. A local stabilization effect on the drains D1 and D2 under drained conditions with D1+D2 operative can be noticed.

### 3.3.2.3 Morphodynamic analysis under Low Energy conditions

The analysis of profile evolution under LE wave condition highlighted a well-delineated accretionary trend. Evidently, the smaller the wave energy, the greater the role of test duration. Hence, LE test should be run for larger time to appreciate bed variation of the same order of magnitude than those observed in higher energy conditions. However, our scope was to focus on the understanding of how a BDS affects the normal beach evolution under different wave conditions. In any case, while HE and ME tests were generally constituted by three step, under LE the duration was extended adding one or two steps. This test program was not much more time consuming as only D1 and D2 were used given that run up was much more limited than in the HE and ME tests.

A slight accumulation on the upper swash zone after four “undrained” steps was found (LE 4 in Figure 3.60). Passed just one hour step a clear net accretion took place ( $0.08 \text{ m}^3/\text{m}$  of increased volume). Afterwards, the accretion rate was smaller and an asymptotic trend in accretion could be recognizable. When D1 became operative, a new upsurge in accretion was observed. Under these conditions, the sand volume in the swash increased at an hourly average of  $0.04 \text{ m}^3/\text{m}/\text{h}$ . At the end of the fifth step (L 9), the gained net volume was about  $0.20 \text{ m}^3/\text{m}$ , corresponding to the highest in the test ( $\Gamma = 1$ , Figure 3.61). This “artificially induced” morphodynamic state was confirmed by the following four steps in undrained condition (L 10÷L 13), for which a slight erosion appeared again. In Figure 3.62 it can be noticed that when D1 was operative, the relative bathymetry  $Z_R$  on D1 decreased while on D2 increased. In other words, D1 promoted a steepening of the beach around the drain, while the undrained condition re-established the natural nourishing slope. The positive hourly average volume variation under undrained condition was comparable to the negative one obtained with D1 operative ( $0.038 \text{ m}^3/\text{m}$ ) (see also the theoretical accretion trend in undrained condition shown in Figure 3.61). Finally, switching on D1 and D2 triggered an initial stabilization, at first, and a successive accretive effect. The trend of  $Z_R$  at the location of D3 confirms the overall accretive trend under LE conditions (Figure 3.62).

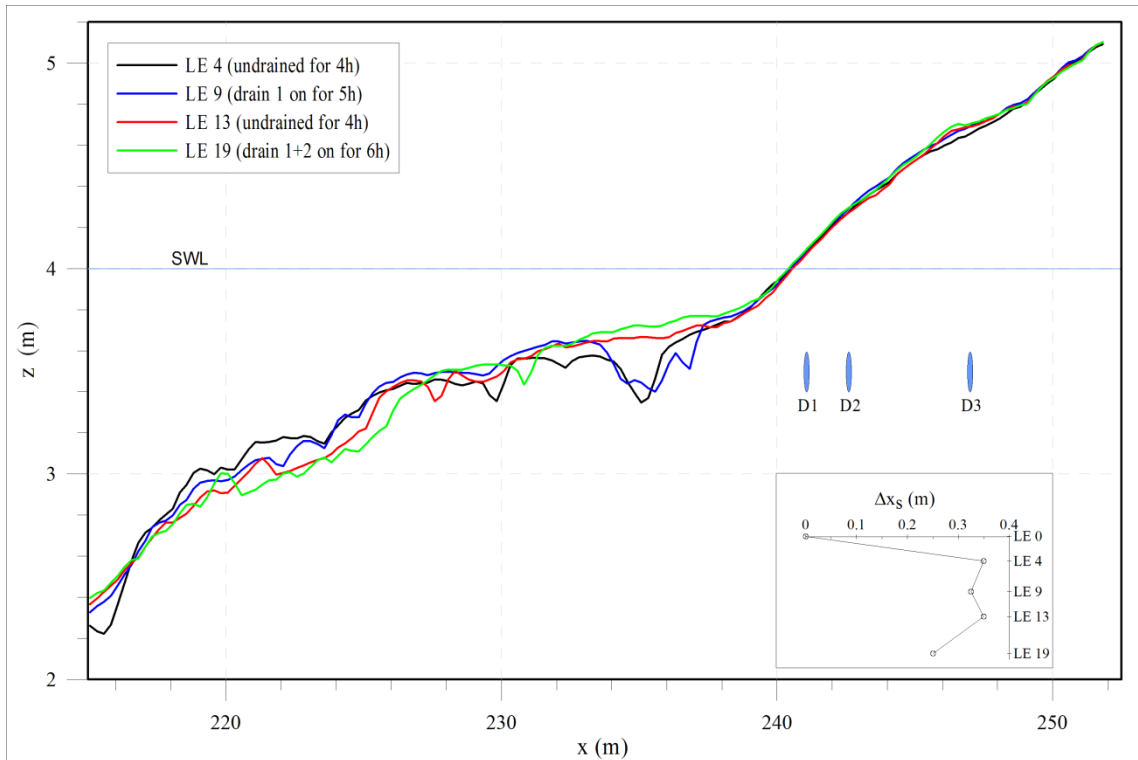


Figure 3.60. Significant beach profiles under LE conditions without drain (LE 4, LE 13), with D1 (LE 9) and with D1+D2 (LE 19). A slight accumulation in the emerged part of the beach can be observed.

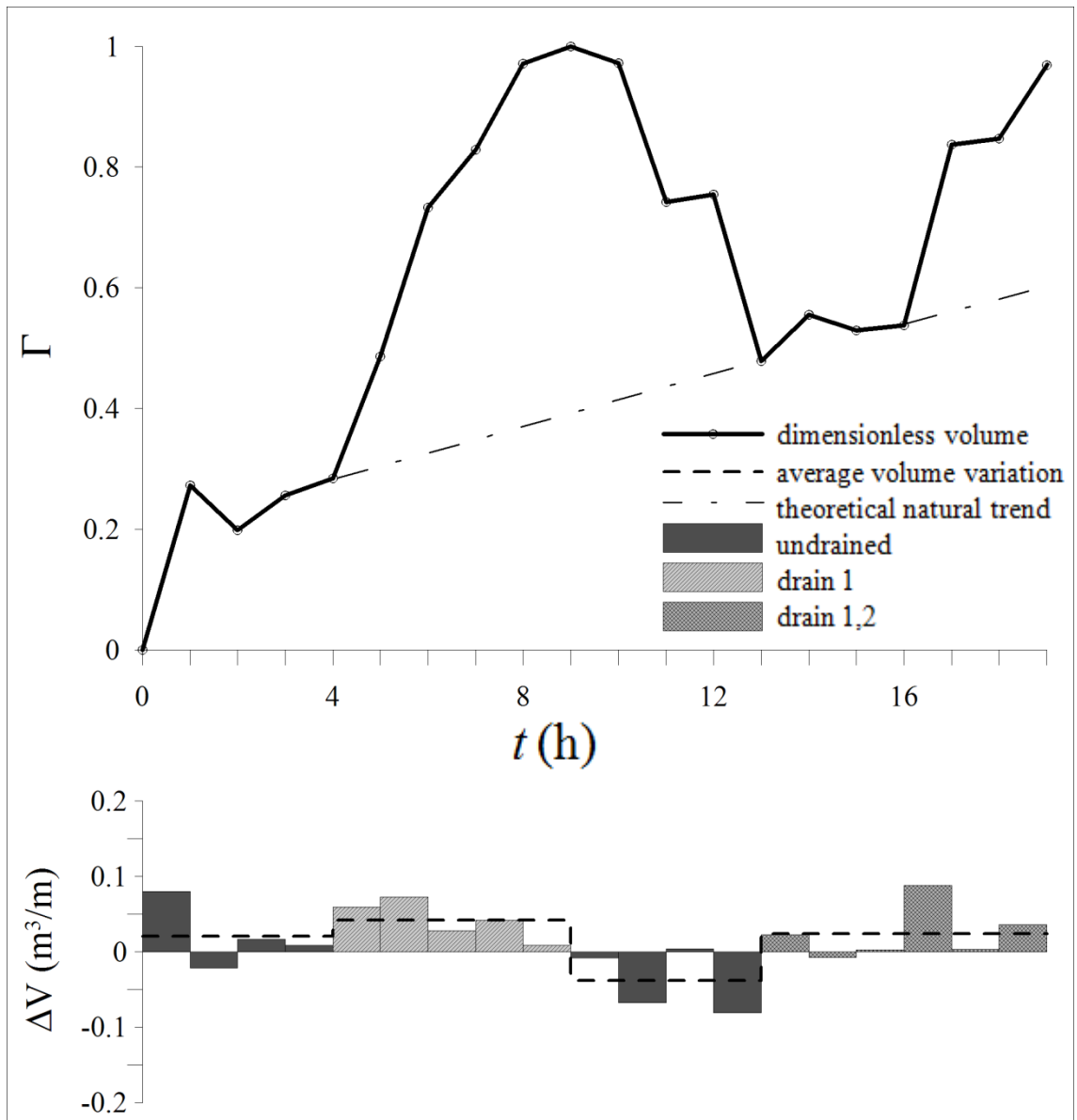


Figure 3.61. Time variation of dimensionless relative volume variation  $\Gamma$  and volume variation  $\Delta V$  above  $x = 240$  m for LE tests.

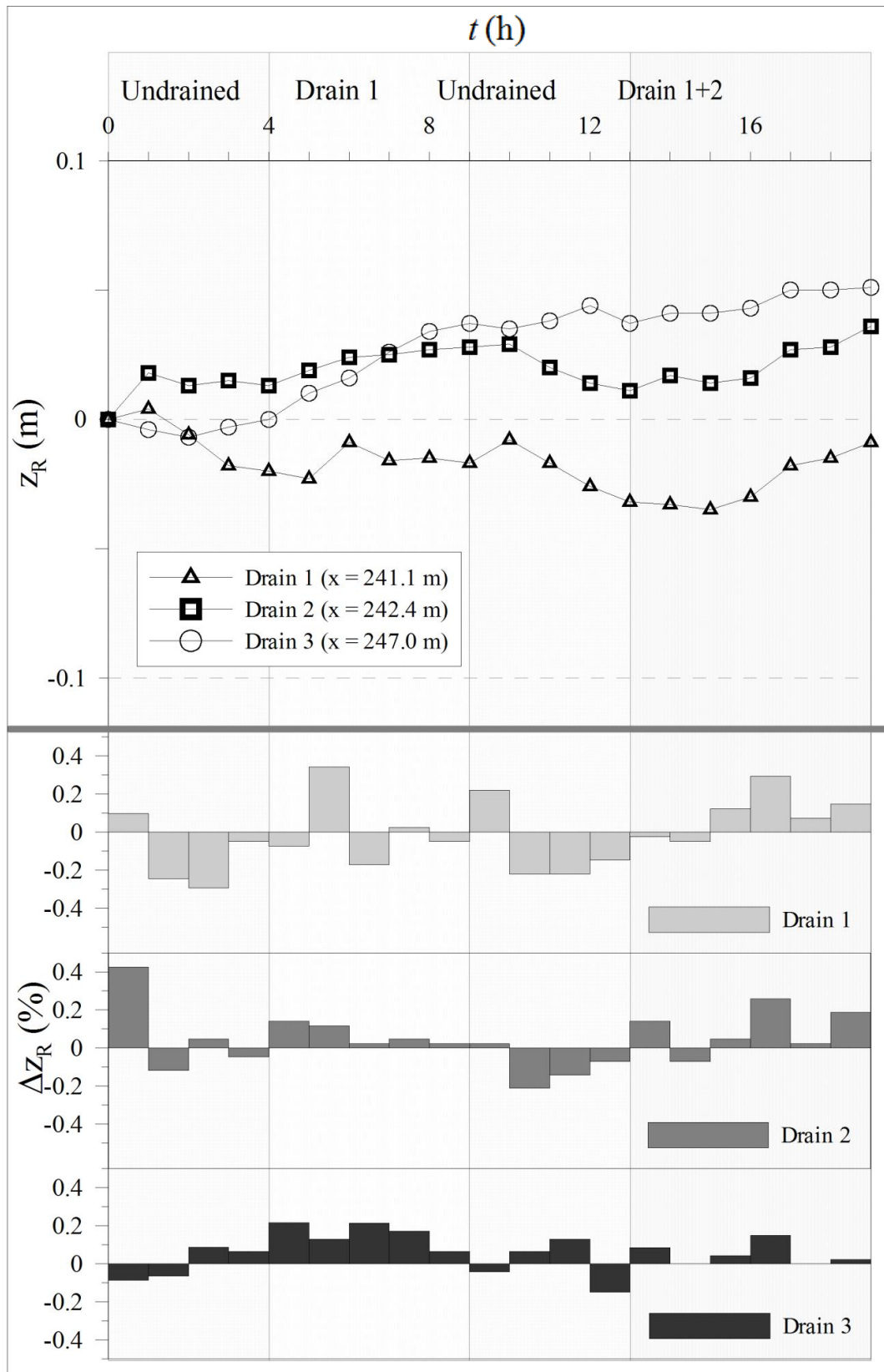


Figure 3.62. Relative bathymetry  $Z_R$  on drains axis and relative percent variation  $\Delta Z_R$  under LE tests. A local stabilization effect on D1 and D2 is highlighted. The trend of  $Z_R$  on D3 confirms the accretive trend of LE cases.

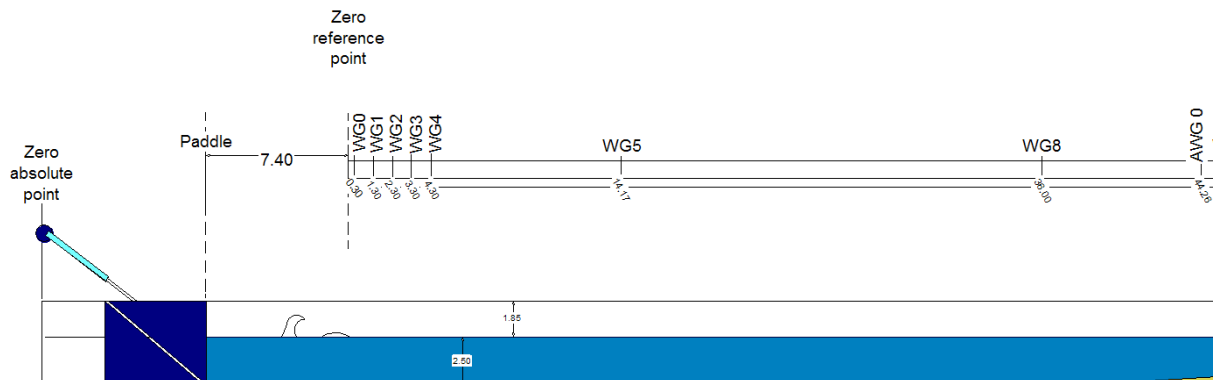
## 4. Swash Zone Response induced by long waves, wave groups and random waves: large-scale experiments at CIEM

### 4.1 Experimental procedure and setup

#### 4.1.1 Wave flume and instrumentation

The model tests were carried out in the large-scale CIEM wave flume at UPC. The large-scale wave flume has a length of 100 m, a width of 3 m and is 5 m deep (Fig. 4.1a,b). Controlled wave generation was achieved by a wedge-type wave paddle, particularly suited for intermediate-depth waves. The wave generation software used for controlling the wave paddles is AWASYS5 (<http://hydrosoft.civil.aau.dk/AwaSys/>). It accounts for reflection, but it was not utilised for this test as it was not connected for beach profile sediment transport tests. The paddle absorbing system developed by Aalborg University is functional when reflection is important (over 30%). For sandy slope profiles, there is certain degree of reflection that is noted from the data treatment, usually on frequencies of  $\approx 0.02$  Hz. Yet this amount of energy in that band is unimportant, and cannot be effectively absorbed due to stroke limitations by the paddle.

a)



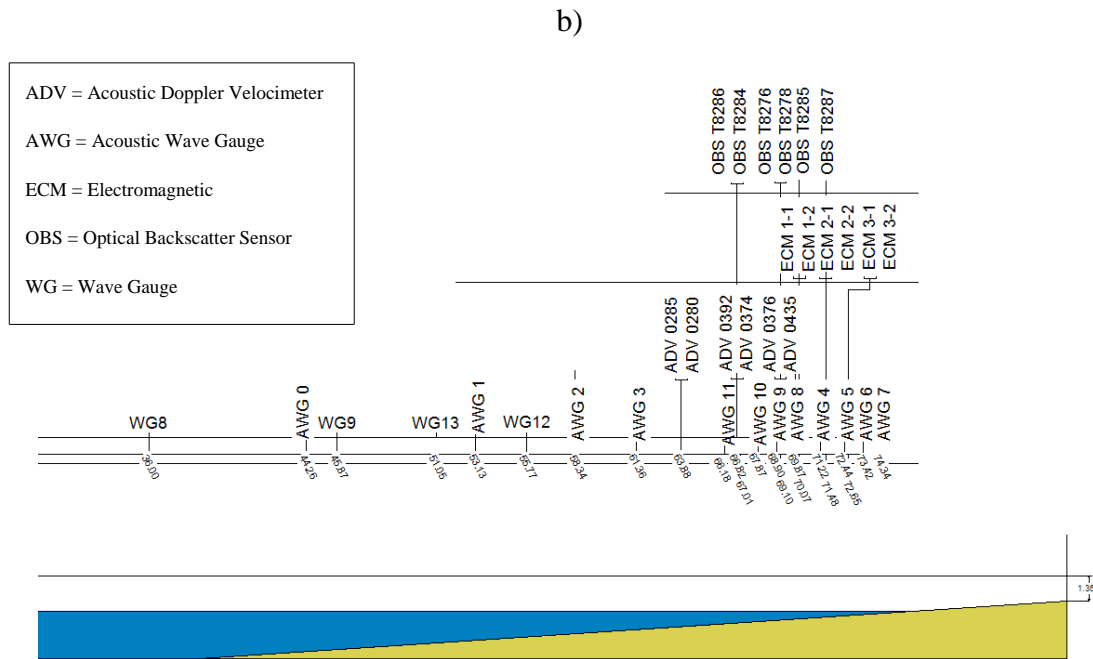


Figure 4.1 UPC flume, longitudinal cross-section, and detail of instrumentation location in most active beach part (lengths in m): a) zoom on the first part of wave flume; b) zoom on the final part of wave flume

The flume bathymetry was formed by moulding sand in the channel to form the required shape. The profile consisted, from the wave paddle toward the shoreline, of an initial section (1:20 slope from  $x = 31$  to  $37$  m) prior to a plane bed (from  $x = 37$  to  $42$  m), followed by a 1:15 slope plane beach. The beach consisted of commercial well-sorted sand of  $D_{50} = 0.25$  mm medium sediment size and measured sediment fall velocity of 34 mm/s. The grain size distribution of the sand used during the experiments is presented in Figure 4.1.1. Despite the sand was not mechanically compacted prior to this test, it had been in the flume for a year during previous experimentation so that natural wave compaction was assumed. The water depth at the toe of the paddle was fixed to 2.5 m.

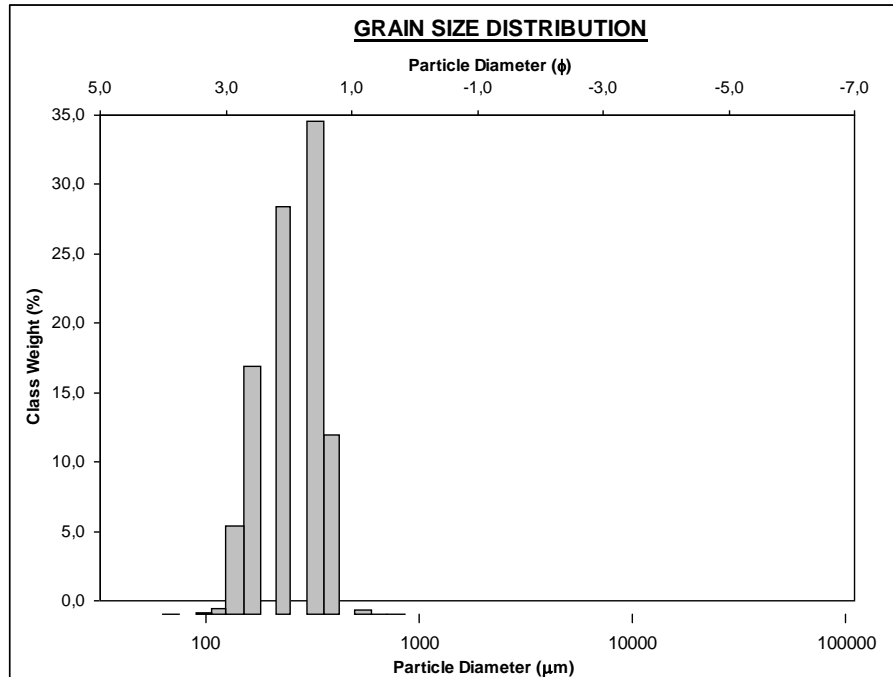


Figure 4.1.1. Grain size distribution of the sand used in the model.

A wide range of instrumentation was utilised in the SUSCO experiments, distributed in the surf and swash zone. Video images of selected portions of the surf and swash zones were also obtained. The instrument position along the flume is reported in Figure 4.1.

The water surface elevation was measured by means of 10 resistive wave gauges placed along the wave flume at different cross-shore locations (Fig. 4.1.2). The resistance-type wire wave gauges are 2m long, use a wire diameter of 1.5mm and were calibrated during changes of water level in the flume. They have an accuracy of  $\pm 2\text{mm}$ . The resistance type wave gauges used in the CIEM operate on the principle of measuring the current flowing in an immersed probe which consists of a pair of parallel stainless steel wires (the absence of other support reduces the interaction between the measuring device and the incoming/reflected waves). The current flowing between the probe wires is proportional to the depth of immersion and this current is converted into an output voltage proportional to the instantaneous depth of immersion. The output circuitry is suitable for driving both a chart recorder and a data logger.



Figure 4.1.2. Wave gauges along the channel.

Each wave probe needs a wave probe monitor with the energising and sensing circuits for the operation. Each monitor contains the circuits required to compensate for the resistance of the cable that is connected to the probe. Without this, the output of the wave probe monitor would be non-linear. In order to avoid polarisation effects at the probe surface, a high frequency square wave voltage is used to energise the probe. The oscillator that produces this square wave may be set to one of six different frequencies. This allows probes to be used close together without causing any interference. The current in each probe is detected by measuring the voltage drop across two resistors. Because the measured voltage is alternating, the signal is fed to a precision rectifier to produce a DC voltage proportional to the wave height. This signal feeds a small centre-zero balance indicator and a BNC socket on the front of the panel. The signal is also fed to a preset gain stage that may be set for a gain of between 0.5 and 10. Controls on the front of each wave probe module enable the output signal to be set to zero for any given initial depth of probe immersion. This, together with the gain adjustment, produces a full-scale output of  $\pm 10V$  for all waves.

4 Acoustic Wave Gauges (AWG) and 8 micro Acoustic Wave Gauges (mAWG) of limited range but great accuracy were placed mainly in the surf and swash zones to characterize the bores and the runup reaching the beachface (Fig. 4.1.3). The Acoustic wave gauges have a range of 0.2-3.5m depending on application and an accuracy of  $\pm 1mm$  under stable environmental conditions. The mAWG have a range of 0.2-1.7m but a resolution of 0.18mm.



Figure 4.1.3. Micro Acoustic Wave Gauge in the channel.

Water velocities were measured by 6 Electromagnetic Current Meters (ECM) with two instruments at each position at different elevations  $z = 0.03$  and  $0.13$  m,  $0.03$  and  $0.07$  m,  $0.03$  and  $0.055$  m from the sandy bottom at each position (Figure 4.1.4). The Electromagnetic Current Meters used in CIEM are the Model 802, supplied by Valeport Limited. The ECM is a sensor that uses the Faraday principle to measure the flow past the sensor in two orthogonal axes. The magnetic field is generated within the sensors by a coil, and the electronics detects the signal generated across two pairs of electrodes, one pair for each axis. Their accuracy is  $\pm 5$  mm/sec plus 1% of reading on each axis (average data).



Figure 4.1.4. Electromagnetic currentmeters in the swash zone.



Accuracy

Turbidity	0.25 NTU or 1% of reading
Concentration	Mud 0.5 mg/l or 1% of reading; Sand 0.25 g/l or 1% of reading



Figure 4.1.6. Optical Backscatter Sensors.

The  $z$  coordinates of the ADVs and OBSs were verified and adjusted to the reported elevation from the sandy bottom at the beginning and the end of each step to assure identical vertical distance from the bed during the various experimental tests. The sampling frequency for all equipment was fixed to 20 Hz. The ADVs, which use an external computer, had a sampling frequency of 100 Hz. The velocity information acquired with the ADVs was time-synchronised and de-spiked using the method of Goring and Nikora (2002). Low quality data, where signal to noise ratio or signal amplitude was low, were discarded and cubic interpolation was performed. Each deployed OBS was calibrated using the laboratory sand and the glycerol technique developed by Buut et al. (2002).

The beach evolution along the centre-line of the wave flume was measured with a semi-automatic mechanical bed profiler that measures both the sub-aerial and sub-aqueous beach elevation over a range of up to 3m (Figure 4.1.7). The profiler consists of a wheel 0.2m in diameter on a pivoting arm of length 3m, which is mounted on a platform that moves at constant velocity above the flume. A computer monitors the arm rotation, from which the beach elevation can be calculated from calibrated control points. The wheel is too large to follow individual ripple elevations and tends to cut through ripple crests, so the measured profile is approximately the elevation of the ripple troughs. The overall vertical profile accuracy is estimated to be  $\pm 10$ mm. The vertical datum for the profile data presented below is the SWL. The horizontal datum is that of the reference point in the flume, which is 7.4m from the wavemaker and approximately 42m seaward of the beach toe.

The detailed flume setup, instrumentation and complete test description is reported by Vicinanza *et al.* (2009, 2010).

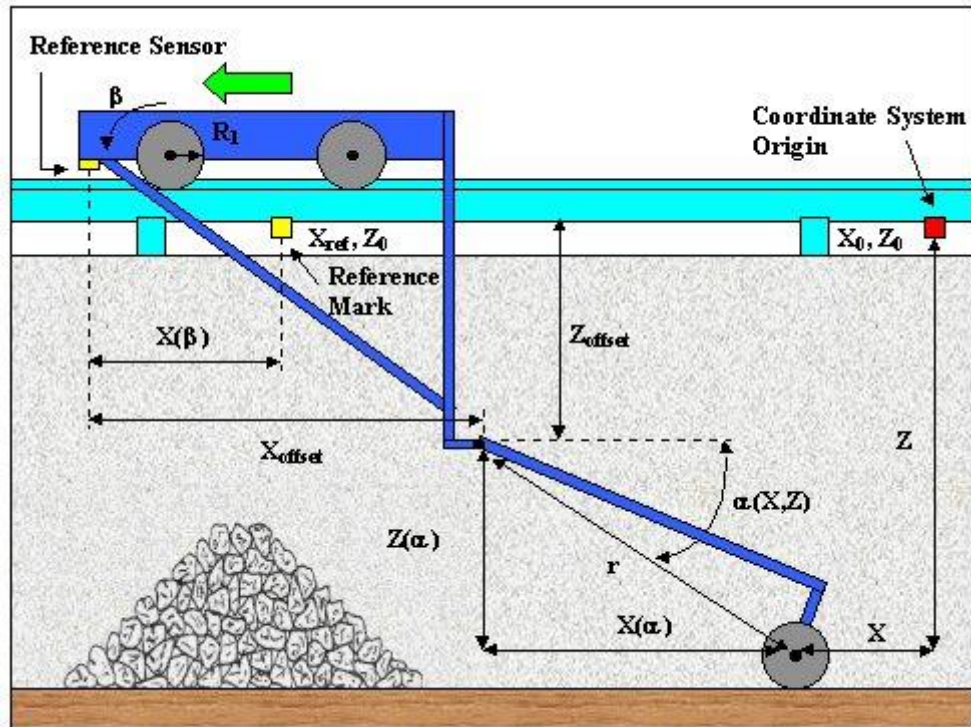


Figure 4.1.7. Characteristics of adopted bottom profiler on the carriage.

#### 4.1.2 Test program

The experimental program was divided in two test series (erosive and accretive). Within each series a number of different wave cases with identical energy level and energy flux were run, including regular monochromatic, combination of free long waves plus monochromatic short waves, bi-chromatic waves including bound long waves, and random waves of different groupiness factor (GF hereinafter) (Table 4.1). The tests were composed of four steps of different durations: step one and two of 23 minutes duration and steps three and four of 46 minutes duration. Wave conditions were chosen as likely to be erosive or accretive for the monochromatic conditions on the basis of previous experiments in the CIEM flume and typical erosion/accretion threshold criteria based on the relative fall velocity, and the final profiles and net sediment transport are consistent with these initial estimates. Case M\_E represents the monochromatic control conditions for the erosive test series, with  $H=0.4\text{m}$ ,  $T=3.7\text{s}$  at the wave paddle; the profile evolution for the other erosive wave cases are therefore compared to that for case M\_E. Case M\_A is the equivalent monochromatic control case for the accretive test series, with  $H=0.16\text{m}$  and  $T=4.8\text{s}$  at the wave paddle. To perturb the monochromatic conditions, small amplitude long waves were added to the control signal to

generate long-wave short-wave combinations, cases C\_E1, C\_E2, C\_A1, and C\_A2 representing the addition of free long waves to otherwise monochromatic wave conditions. Unfortunately, an error in wave generation resulted in a reduction of the intended wave height for case M\_A, such that it has a smaller wave height and mean energy flux than the corresponding long-wave short-wave combinations, bi-chromatic wave groups and random waves for the accretive tests. The wave period was also altered, with the result that the wave steepness remained similar to the target wave. This reduces the extent to which the data are useful and, accordingly, case M\_A cannot be directly compared with the others. Four fully modulated bichromatic wave trains were generated, with the intention that each case would have the same theoretical root mean square wave height (and mean energy flux) as its corresponding monochromatic wave. Cases B\_E1 and B\_E2 generate erosive conditions, and are paired with case M\_E. Cases B\_A1 and B\_A2 are paired with case M\_A and give accretive conditions. The bandwidth of each pair of bichromatic waves differs, and is set by the frequency difference between the two primary short waves within the group. The bichromatic wave groups force an associated bound long wave at the group frequency (e.g. Longuet-Higgins and Stewart 1962; 1964) and may also generate free long waves at the breakpoint (Symonds et al., 1982; Baldock et al., 2000). The usual assumption is that the bound wave is released at short-wave breaking, although this not supported by some recent data (see Baldock, 2009 for a discussion). Nevertheless, a partial standing wave structure is usually observed in the surf zone. The root mean square variance based bichromatic wave height  $H_{bi} = \sqrt{2}H_p = H_s$ , where  $H_{bi}$  is the variance based bichromatic wave height,  $H_p$  are the heights of the primary short waves,  $H_p=H_1=H_2$ , and  $H_s$  is the corresponding monochromatic short wave height. Since the mean primary short wave frequency of the groups is the same as that of the corresponding monochromatic waves, the mean energy flux is the same for the corresponding pairs of wave trains. Four random wave trains, R\_E1, R\_E2, R\_A1, R\_A2, were generated similarly, again with the same variance based wave height and the same peak frequency as their corresponding monochromatic pair, and where the groupiness was varied slightly between cases. Therefore, random waves of identical energy spectrum were obtained by choosing different phases. Hence, random waves with a certain GF result from correlating phases, as high correlations lead to high groupiness, and vice-versa. GF was calculated using the Hilbert transformation to obtain half the squared envelope curve  $E(t)$  and the variance of the surface elevation time series  $\sigma^2(\eta_w(t))$  with  $\eta_w$  as sea surface elevation and  $t$  as time (Hald 1995)

$$GF = \frac{\sigma[E(t)]}{\sigma^2[\eta_w(t)]} \quad [4.1]$$

For a monochromatic (sinusoidal) signal the envelope  $E(t)$  is constant leading to a groupiness factor  $GF = 0$  while the groupiness factor value of a completely Gaussian signal is expected to be equal to 1, independently of the spectrum shape. The standard approach of wave generation is to use random uncorrelated phases which in the average lead to  $GF = 1.0$  along with  $\sigma^2 \approx 0.13$  for 500 waves. By correlating the phases, higher  $GF$  values were obtained. Herein the wave phases  $\theta_w$  are correlated to the neighbouring frequency components at distance  $x$  from the paddle by prescribing the paddle surface elevations and the corresponding paddle motions using the Biesel transfer function

$$\eta_w(x=0, t) = \sum_{i=1}^N a_i \cdot \cos(\omega_i t - k_{w,i} x + \theta_i) \quad [4.2]$$

$$\theta_{wi} = (1 - p) \cdot 2\pi \cdot \varphi_{r,i} + p \cdot \theta_{i-1} \quad [4.3]$$

where  $a$  are the amplitudes,  $\omega$  is the cyclic frequency,  $k_w$  the wave number,  $\varphi_r$  a random variable from 0 to 1 and  $p > 0$  gives the correlated phases.  $GF$  varies along the flume and thus  $k_w x$  is important as the highest groupiness in the SZ. Herein  $k_w$  is approximated from that calculated with the linear dispersion equation using the water depth at the paddle.  $x = 50$  m was used for  $p = 0.0$  and  $0.2$  leading to the theoretical groupiness factors as given in Table 4.1. Due to variations of the sloping bed the actual obtained  $GF$  are different than predicted.

For comparison with the “offshore” wave condition shown in Table 4.1, Table 4.2 shows the measured wave heights at  $x = 53$  m, which is seaward of the depth of closure (negligible profile change or transport) for all tests. All the erosive cases have nearly identical short-wave height. However, as noted, case M\_A has a smaller incident wave height than intended. Nevertheless, the remaining accretive cases have very similar incident wave height, as intended.

<b>Erosive Conditions</b>					
Test	Long Wave				Wave type
case	Short Wave				
	H (m)	T(s)	H (m)	T(s)	
M_E	0.4	3.7			Monochromatic
C_E1	0.5	3.7	0.023	29.25	Combination
C_E2	0.41	3.7	0.011	15.1	Combination
B_E1	0.29	3.5	0.29	3.9	Bi-chromatic
B_E2	0.34	3.1	0.34	4.3	Bi-chromatic
R_E1	0.45	4.2	0.06	22.5	Random GF=1
R_E2	0.46	4.2	0.06	22.7	Random GF=1.1
<b>Accretive Conditions</b>					
Test	Long Wave				Wave type
case	Short Wave				
	H (m)	T (s)	H (m)	T(s)	
M_A	0.16	4.9			Monochromatic
C_A1	0.252	5.7	0.031	29.2	Combination
C_A2	0.254	5.7	0.15	15.2	Combination
B_A1	0.21	5.2	0.15	6.3	Bi-chromatic
B_A2	0.17	4.8	0.15	7.1	Bi-chromatic
R_A1	0.24	6.3	0.027	22.7	Random GF=0.96
R_A2	0.24	6	0.03	22.7	Random GF=1.08

Table 4.1. Spectral significant wave height  $H_{m0}$  and peak wave period  $T_p$ , computed by spectral techniques at wave sensor located 10 m from wave paddle. Short and long wave component are displayed.

<b>Erosive Conditions</b>							
Test case	Short Wave		Long Wave		Wave type	$H/w_s T$	Iribarren number
	H (m)	T(s)	H (m)	T(s)			
M1	0.43	3.7			Monochromatic	3.2	0.38
C2	0.48	3.7	0.034	29.25	Combination	3.9	0.34
C4	0.49	3.7	0.013	15.1	Combination	3.2	0.38
B3	0.34	3.9	0.31	3.5	Bi-chromatic	2.4	0.44
B5	0.43	4.3	0.31	3.1	Bi-chromatic	3.2	0.39
R1GF1	0.44	4.2	0.07	22.7	Random GF=1	3.1	0.37
R1GF2	0.45	4.2	0.07	22.7	Random GF=1.1	3.1	0.37
<b>Accretive Conditions</b>							
Test case	Short Wave		Long Wave		Wave type	$H/w_s T$	Iribarren number
	H (m)	T (s)	H (m)	T(s)			
M2	0.17	4.9			Monochromatic	0.9	0.64
C10	0.23	5.7	0.034	29.2	Combination	1.3	0.52
C12	0.23	5.7	0.016	15.2	Combination	1.3	0.52
B11	0.21	5.2	0.16	6.3	Bi-chromatic	1.2	0.56
B13	0.19	4.8	0.16	7.1	Bi-chromatic	1	0.62
R2GF1	0.24	6.3	0.03	22.7	Random GF=0.96	1.1	0.53
R2GF2	0.25	6	0.033	22.7	Random GF=1.08	1.1	0.53

Table 4.2. Summary of SUSCO wave conditions; wave height is obtained by spectral moment computed at sensor located at  $x = 53.22$ .

To enable consistent comparison of the beach evolution between wave cases, beach profile reshaping was performed prior to each different wave condition to start with a similar initial profile. The majority of the beach volume was well compacted from previous SANDS experiments (Cáceres et al., 2009) with the exception of the upper layers of the inner surf and swash zones. In fact, the flume had been drained for a period of several weeks, so the sand on the upper beach profile was initially dry. Hence, following the SANDS experiment, the upper part of the beach profile had to be reshaped to an approximately plane slope. Therefore, prior

to commencing the main experiments, the upper beach and SZ were compacted and smoothed by running each wave condition, which also enabled fine tuning of the wave generation signals. Following, the instrumentation was subsequently installed. The initial plan with the SUSCO experiments was to attempt to re-shape the beach back to an approximately similar initial condition by running a series of “reshaping” waves between each wave case. However, this was unsuccessful because the time taken to achieve significant profile “recovery” was too long. In addition, after cumulative tests, the breaker bar tended to develop cross-tank asymmetry, and morphodynamic–hydrodynamic feedback led to increasingly rapid development of profile asymmetry across the flume. Consequently, instrumentation on one side of the flume and adjacent to the bar was removed or repositioned, and testing times were reduced. Therefore, the approach was to manually reshape the upper beach portion prior to each test followed by a 10 minutes ‘smoothing’ wave condition. The smoothing test consisted of random waves with  $H_s = 0.2$  m and  $T_p = 6$  s. For the erosive tests, manual reshaping was performed over the part of the profile between the seaward flank of the breaker bar and the runup limit. For the accretive tests, part of the purpose of the experiments was to observe the influence of long waves and groups on the evolution of the breaker bar. Consequently, reshaping was performed from the landward edge of the bar trough to the runup limit. This approach successfully limited the development of cross-tank asymmetry and enabled each wave case within the two series (erosive or accretive) to commence with a very similar profile, particularly in the region between the bar and the runup limit (see figure 4.2). Unfortunately, the beach was not reshaped between cases R\_A1 and R\_A2, so the data from R\_A2 cannot be compared to that of the other accretive test conditions. In addition, case C\_E1 formed part of the tests that developed cross-flume asymmetry, and there was insufficient time to re-run this case again. Profile measurements were made prior to each test, and then after each constituting step, i.e.: 23 minutes, 46 minutes, 92 minutes and 138 minutes of wave generation. Wave generation was halted and restarted every 23 minutes, even if no profile was measured.

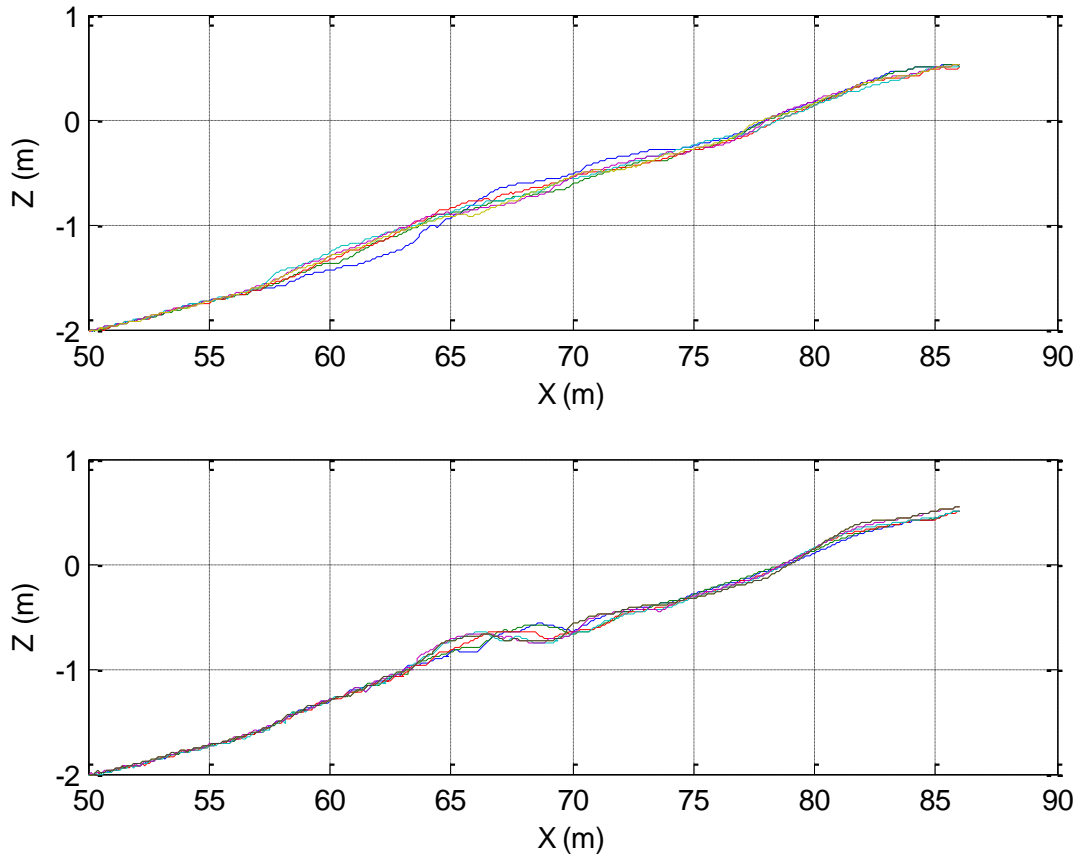


Figure 4.2. Reshaped initial profiles for cases M\_E, C\_E2, B\_E1, B\_E2, R\_E1, R\_E2 (upper panel) and cases M\_A, C\_A1, C\_A2, B\_A1, B\_A2, R\_A1 (lower panel). After Baldock et al., (2011).

## 4.2 Data analysis

The data presented here focuses on the differences in the beach profile evolution and cross-shore sediment transport rates between the different wave conditions. Net time-averaged sediment transport,  $Q_x$  along the flume was calculated using the sediment conservation law and a known boundary condition ( $Q(x) = 0$ ) at the landward or seaward end of the profile.  $Q(x)$  is given by:

$$Q(x_i) = Q(x_{i-1}) - \int_{x_{i-1}}^{x_i} M_s \frac{\Delta z_b}{\Delta t} \quad [4.4]$$

where  $Q(x_i)$  is the integral volume of sediment transport ( $\text{m}^2/\text{s}$ ) at position  $i$ ,  $\Delta z_b$  is difference in bed elevation between measurement intervals (m),  $\Delta t$  is the time difference between

measurement intervals ( $s$ ) and  $M_s$  is the solid fraction, approximately 0.4 for the laboratory sand.

The boundary conditions at each end of the beach are that there is no sand transport seaward of the beach toe, and no transport landward of the runup limit. Before and after a wave test the beach profile is measured from landward of the runup limit to the beach toe (concrete floor), and application of Eq. [4.4] should return a zero sediment flux at the beach toe. Alternatively, calculations can start at the seaward end and should return zero sediment flux at the runup limit. However, due to measurement errors and non-uniformity of the profile across the tank,  $Q(x)$  calculations do not return zero at the beach toe, and this is expected for most published beach profile tests but very rarely calculated. Errors in the calculated  $Q(x)$  were corrected by distributing the mismatch in sediment volume before and after the measurement time interval evenly across the profile, leading to a zero value of  $Q(x)$  at the closure points (Baldock et al., 2010). Generally, this does not significantly alter the estimated sediment transport rates and cross-shore pattern of  $Q(x)$  between the corresponding cases, unless the transport magnitude is very small, in which case the correction can cause a change of sign.

Since the profiler has a defined measuring accuracy, errors in the total measured sediment volume accumulate over the long section of the outer profile, seaward of  $x = 60\text{m}$ . In this zone, very little sediment motion occurs, and the profile changes very little over the duration of each test in comparison to the profile change over the active beach. Figure 4.3 contrasts the observed bed elevation changes offshore of the bar with those observed in the bar-trough region and around the still water shoreline. Consequently, the present analysis assumes a depth of closure for the sediment transport calculations at  $x = 60\text{m}$  (at a water depth of approximately 1m), and applies the sediment continuity correction over the active profile, i.e. landward of  $x = 60\text{m}$  or shallower than 1m. This enables greater resolution and improved accuracy in the  $Q(x)$  calculations shown below. Closure errors correspond to a mean error in vertical elevation across the profile that ranged from 2.5 mm to 15 mm, with an average of 7 mm over all tests, which is consistent with the estimated accuracy of the bed profiler. The mismatch was distributed evenly over the profile since it is not possible to determine where the errors occurred.

An alternative method of inferring differences in the total net sediment transport between tests is from the computation of suspended sediment transport from discrete measurements of velocity and sediment concentration. However, this is subject to a number of

difficulties. These include sparse instrumentation, differences in instrument location relative to the bed, the breakpoint and the SWL, plus the inability to measure over the whole of the water column and within the sheet flow layer at the bed. For example, Yu et al. (2010) suggested non-linear boundary layer processes due to wave shape are particularly important under wave groups, but detailed measurements of the sediment flux in the intense sheet flow region over an evolving beach are very difficult. Similarly, high SZ sediment transport during large backwash events (Nielsen, 2009) occurs in water depths that are too shallow for the instrumentation (see photographs in Baldock and Hughes, 2006), leading to bias in sediment flux estimates. Consequently, we use the morphology measurements to determine total sediment transport rates, which allows the whole beach profile to be considered as a complete system.

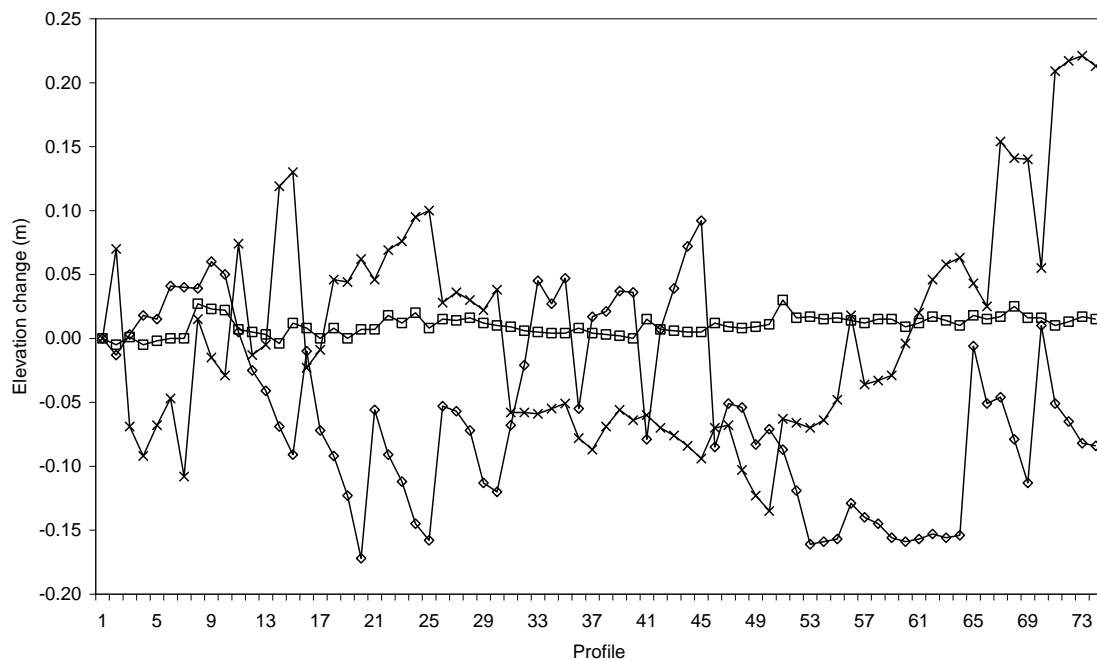


Figure 4.3. Bed elevation changes at assumed depth of closure ( $x=50\text{m}$ ), in the bar-trough region ( $x=70\text{m}$ ) and adjacent to the SWL ( $x=78\text{m}$ ). □,  $x=50\text{m}$ ; ×,  $x=70\text{m}$  ◇,  $x=78\text{m}$  (After Baldock et al., 2011).

## 4.3 Results

### 4.3.1 Hydrodynamic results

#### 4.3.1.1 Waves data

The wave conditions were designed to obtain a comparable energy flux of short wave energy for monochromatic, bichromatic, combination and random waves for two sets of wave conditions, erosive and accretive (Table 1). The similitude in wave energy for the corresponding cases is demonstrated in Figures 4.4 and 4.5, where the cross-shore distribution of significant wave height is displayed for the erosive and accretive series, respectively. Significant wave height is computed from the power spectrum at the initial test stages of each wave conditions, using

$$H_{m0} = 4\sqrt{m_0} \quad [4.5]$$

where the zero order moment is computed as the integral in the frequencies range between 0.1-0.6 Hz. Erosive conditions displayed in Figure 4.4 show a similar wave height in the shoaling area in terms of wave propagation and energy associated to wave conditions, cross-shore locations between  $x = 0-50$  m, with differences due to the presence of the standing long waves. Wave breaking occurs between  $x = 60-70$  m for all the cases. Wave height cross-shore distribution differences are also due to reflection and the long wave cross-shore structure (Baldock et al., 2000; Baldock and Huntley, 2002).

It is worth noting that the high wave height for the B\_E2 condition at  $x = 60-70$  m is due to a strong incident/reflected wave interaction with generation of high breaking waves. The cross-shore variation in wave height for the accretive conditions are displayed in Figure 4.5. Unfortunately, the target wave height for case M\_A was not met due to a communication error. Direct comparison of condition M\_A with the other accretive conditions is, therefore, not possible. For the remaining cases, the wave height distribution displays a similar pattern, with differences again due to cross-shore long-wave structure. The small waves for case M\_A break very close to the shoreline in the accretive tests, i.e. at a cross-shore location landward of  $x = 70$  m. For the B\_A2 condition a behaviour similar to the erosive corresponding condition is visible.

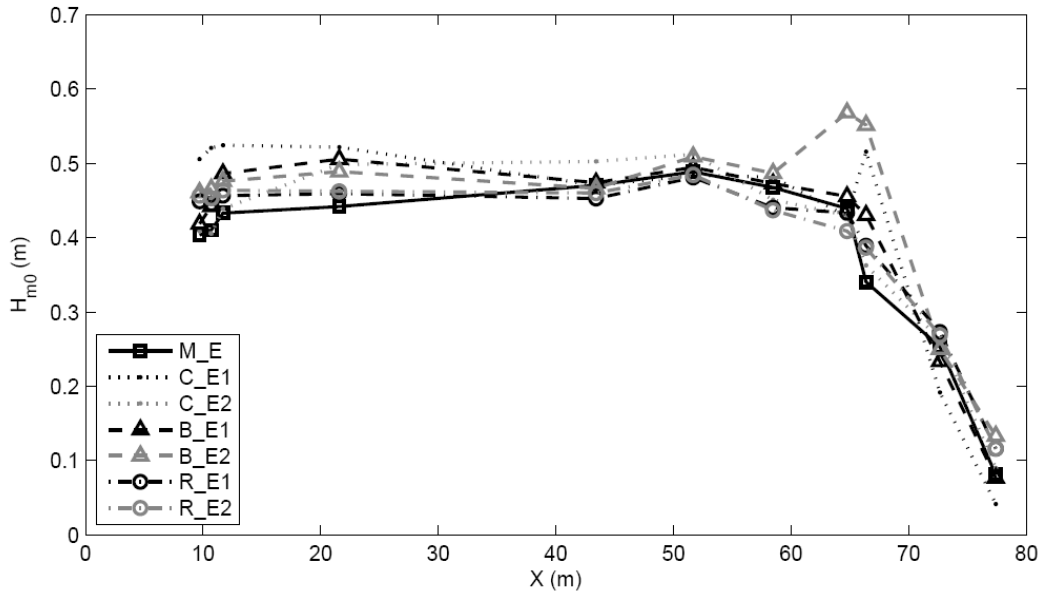


Figure 4.4. Cross-shore distribution of spectral significant wave height for erosive tests; M\_E (solid line with squares), C\_E1 (dotted black), C\_E2 (dotted grey), B\_E1 (dashed black with triangles), B\_E2 (dashed grey with triangles), R\_E1 (dash-dotted black with circles), R\_E2 (dash-dotted grey with circles) (from Vicinanza et al., 2011).

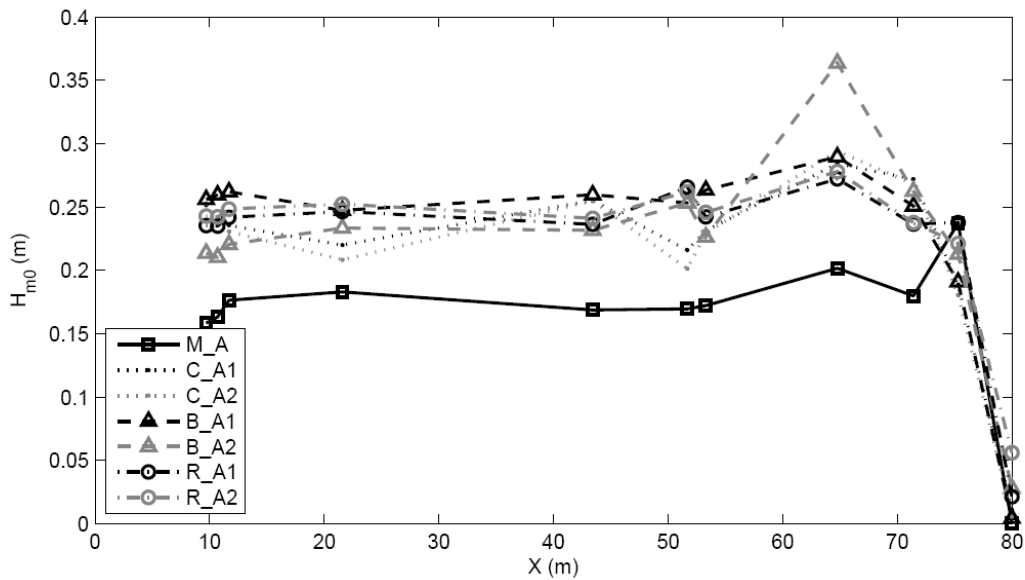


Figure 4.5. Cross-shore distribution of spectral significant wave height for accretive tests; M\_A (solid line with squares), C\_A1 (dotted black), C\_A2 (dotted grey), B\_A1 (dashed black with triangles), B\_A2 (dashed grey with triangles), R\_A1 (dash-dotted black with circles), R\_A2 (dash-dotted grey with circles) (from Vicinanza et al., 2011).

## 4.3.2 Morphodynamic results

### 4.3.2.1 Erosive conditions

During erosive condition overall transport is offshore directed and a classic bar profile forms at the breakpoint. Focussing on the monochromatic wave, M\_E, it should be noted that the sediment motion results in a substantial bar-trough at about  $x = 72$  m (short wave breakpoint), about 6 m from the shoreline.

The influence of free long waves on the morphological response under erosive conditions is illustrated by the comparison of case M\_E and case C\_E2 in Figure 4.6. Combining a free long wave with the monochromatic wave the bar crest and trough are shifted offshore and a small swash berm is built higher on the beach. However the pattern of the beach profile evolution does not change much. The analysis suggests that the free long wave effect is substantially the widening of the active part of the beach (i.e. the region where sediment transport takes place) since both an inner and outer breakpoint occur as a result of the modulation induced by the long wave. Moreover, the long wave-induced modulation affects the short wave runup. The growth of the small swash bar is consistent with the influence of seiching that was observed by Dally (1991). However, there is no significant evidence of the smoothing of the bar for this case. This behaviour differs in general from the small scale tests of Baldock et al. (2010), where the free long waves tended to move the bar landward in addition to the growth of the swash berm. However, one of the small scale tests did exhibit the same behaviour as observed in Figure 4.6, i.e. the bar moved offshore while a swash berm formed higher on the beachface compared to the monochromatic conditions. Unfortunately case C\_E1 developed cross-flume asymmetry, and there was insufficient time to re-run this case again, so only one erosive data set exists for the combination case, and therefore the results are a slight inconclusive. Nevertheless, in combination, the small-scale and large-scale tests show that the free long wave has a clear effect on the position of the bar compared to the position induced by monochromatic waves only. However, whether this effect is onshore or offshore in general and the detailed dependence on surf conditions requires further work.

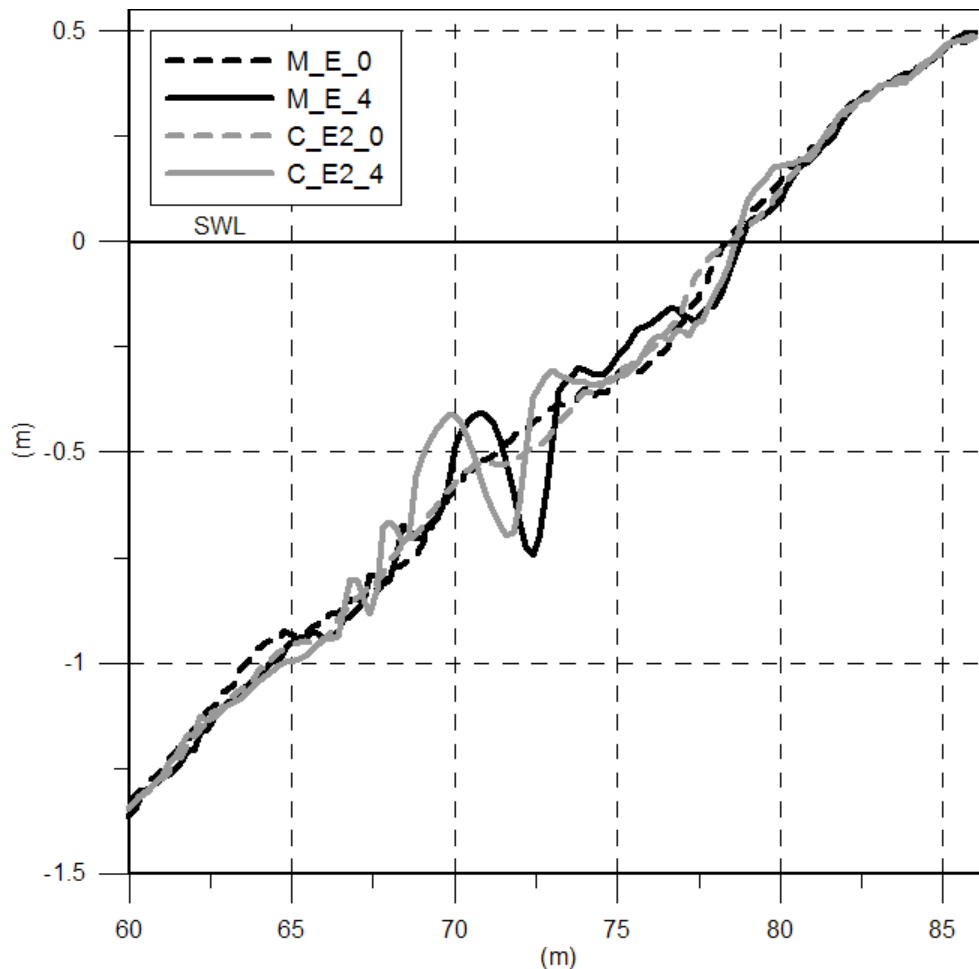


Figure 4.6. Beach profile comparison for tests M\_E and C\_E2 (adapted from Vicinanza et al., 2011).

The comparison between initial (B\_E1\_0, B\_E2\_0) and final profile (B\_E1\_4, B\_E2\_4) for the bichromatic waves shows that, although the mean energy flux is the same, the profile response is strikingly different (Fig. 4.7). Bichromatic waves with narrower bandwidth (B\_E1) give a little more offshore transport than the bichromatic waves with larger differences between the frequencies of the components (B\_E2). Furthermore, B\_E1 results in greatest erosion in the offshore portion of the domain (around the bar), whereas B\_E2 produces more erosion in the inner surf zone and also creates a swash berm and sand accumulation on the sub-aerial beach. The profile of B\_E2, in particular, above -0.5 m develops an exponential shape, resembling an equilibrium profile. Both the bichromatic waves give much greater offshore transport than the equivalent monochromatic erosive case (M\_E), which results in a much wider and higher bar further offshore than for the monochromatic conditions (Fig. 4.8). While the bar trough is still pronounced, it is smoothed in comparison to case M\_E, which is a

result of the varying breakpoint position, and this smoothing is greatest for the broader banded group (B\_E2). Indeed, for case B\_E2, no trough forms below the original/initial profile level.

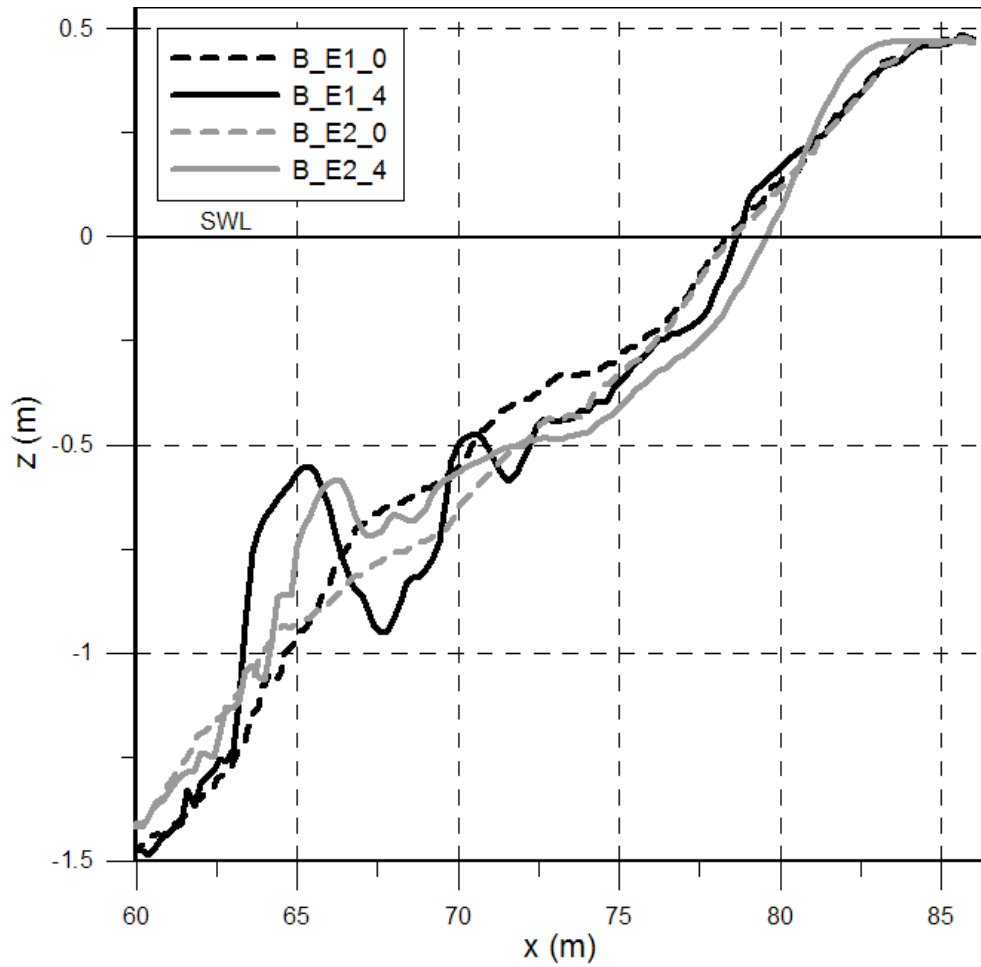


Figure 4.7. Beach profile comparison for tests B\_E1 and B\_E2 (adapted from Vicinanza et al., 2011).

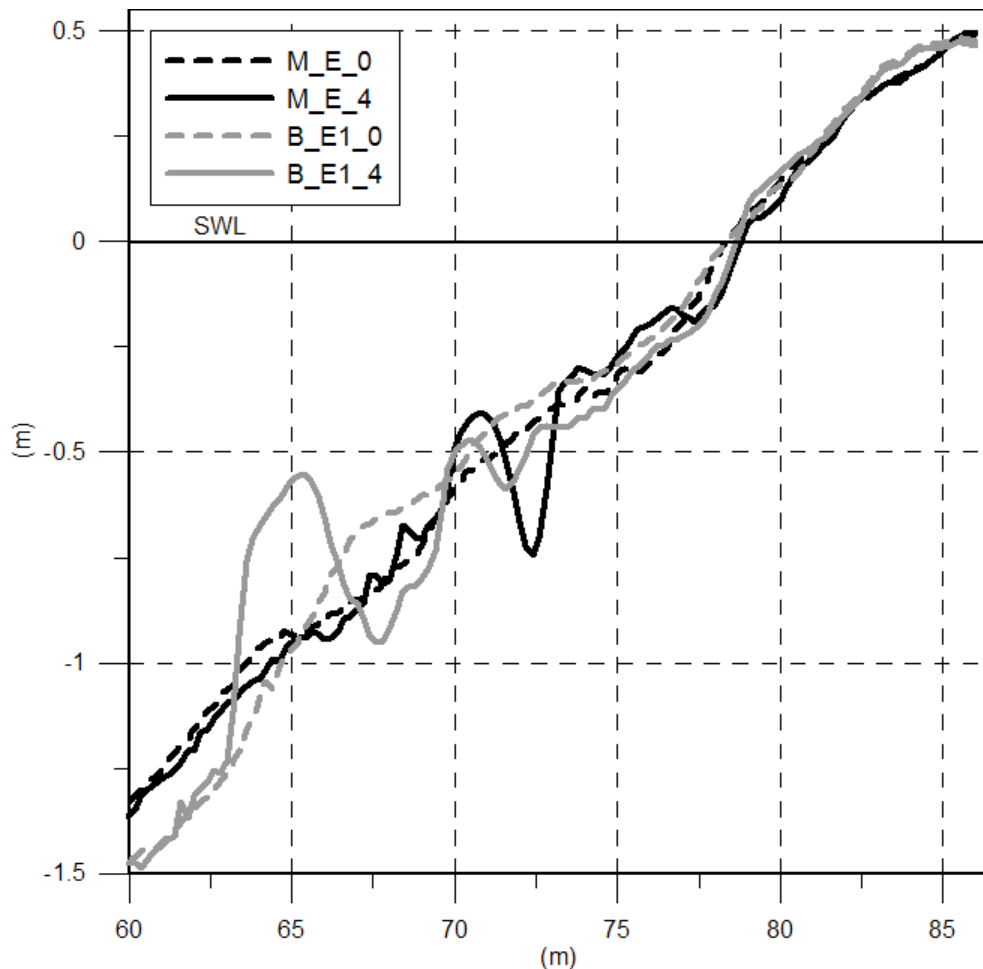


Figure 4.8. Beach profile comparison for tests M\_E and B\_E1 (adapted from Vicinanza et al., 2011).

Figures 4.9 compare the morphological response for the two random wave cases R\_E1 and R\_E2. Overall, the random waves produce the same type of response as the bichromatic wave groups, generating much greater offshore transport and much larger bars further offshore in comparison to the monochromatic case. In more detail, the morphological response of the random wave cases appears closer to that of the narrow-banded bichromatic wave group than to that of the broader-banded bichromatic wave group. Consistent with the observations for the bichromatic groups, the more broad-banded random waves (R\_E2) appear to generate a bar that is further landward than for the more narrow banded waves.

The good consistency in the profile response for the pairs of bichromatic experiments and the pairs of random wave experiments gives confidence in the data, i.e. similar wave conditions produce a very similar beach profile response, despite the

slightly different initial conditions. Hence, the morphological response is repeatable and not subject to systematic errors (Fig. 4.9b).

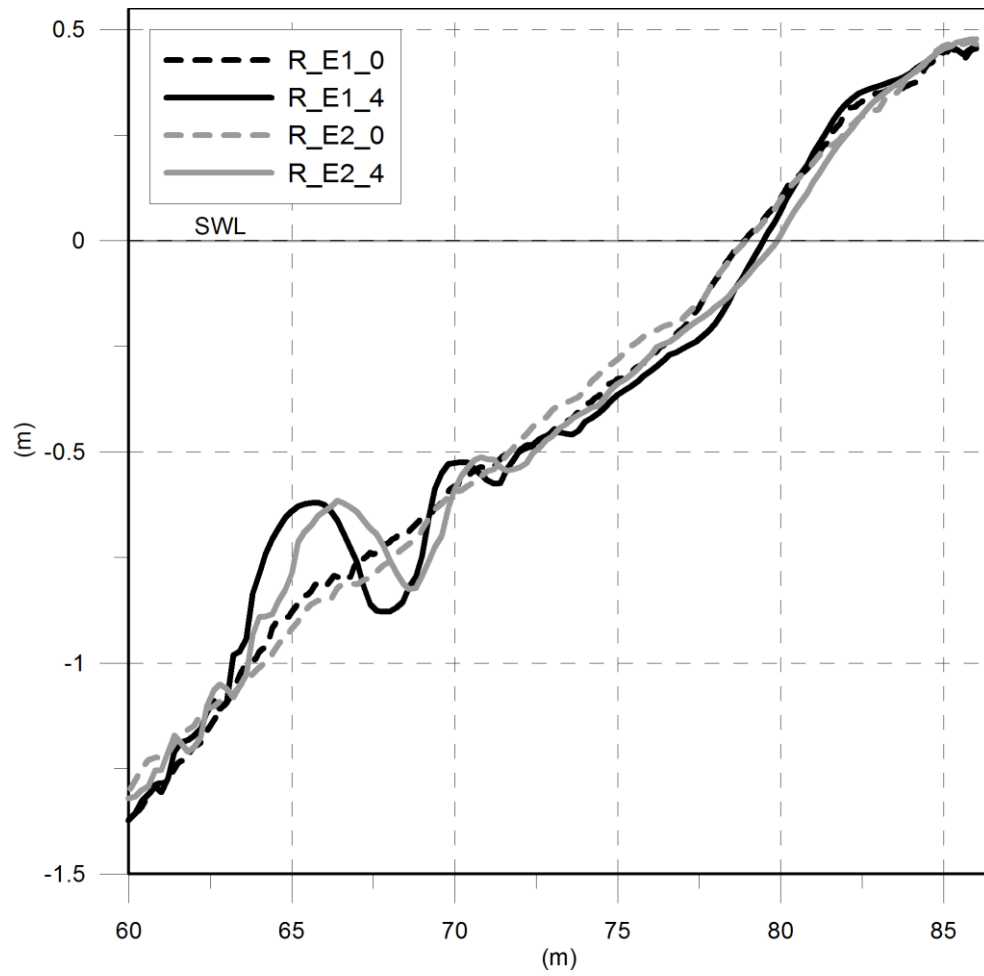


Figure 4.9a. Beach profile comparison for random tests R\_E1 and R\_E2.

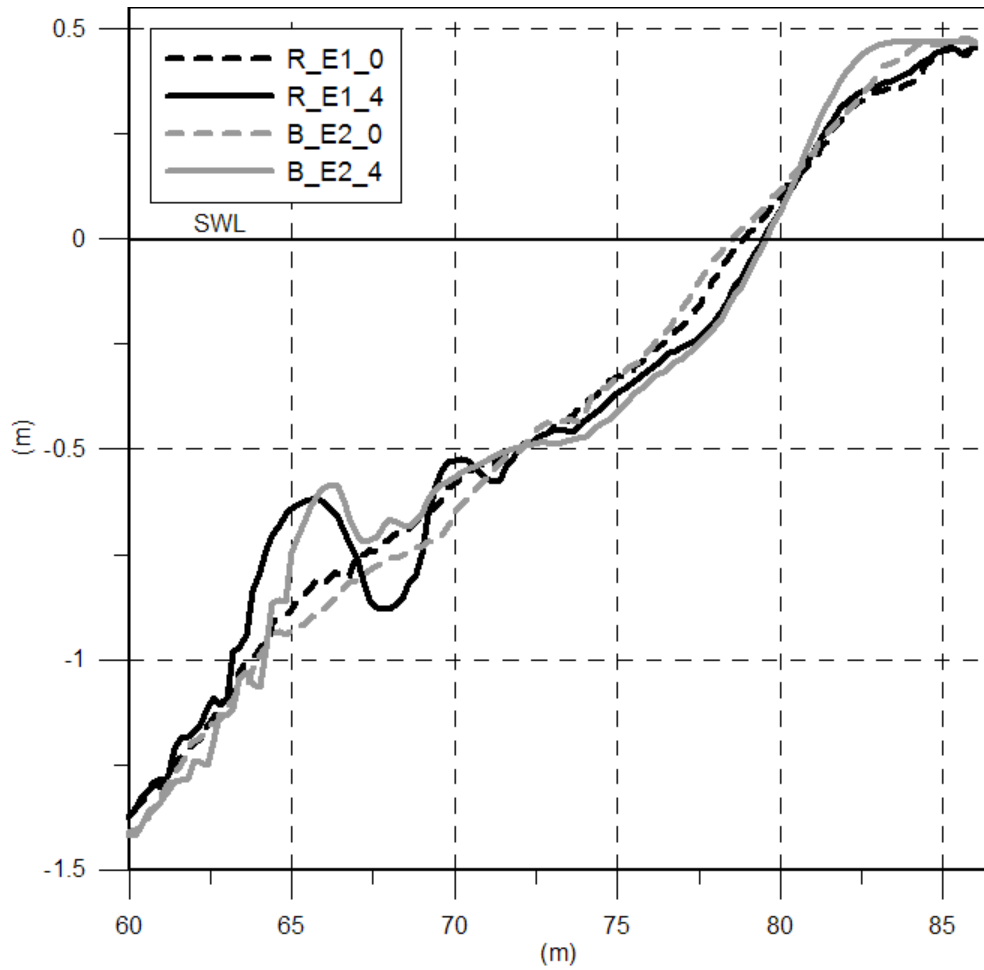


Figure 4.9b. Beach profile comparison forttests R\_E1 and B\_E2 (adapted from Vicinanza et al., 2011).

#### 4.3.2.2 Accretive conditions

The bichromatic condition B\_A1 and B\_A2 (Fig. 4.10) show the formation of a second and well-defined secondary bar with the crest located at -0.5 m ( $x = 74$  m), having a shape and size very similar to the first one, followed by a narrow trough. The effect of the different frequencies of the two components is the speed of beach evolution. When the two components are similar ( $f_1 \approx 0.19$  Hz and  $f_2 \approx 0.16$  Hz in test B\_A1), a quasi-steady equilibrium profile has been reached in about 23 minutes of testing. The profile, after an initial formation of a swash berm, remains totally stable for all duration of the test. On the other hand, in the case of the bichromatic condition with the two components having a larger frequency difference ( $f_1 \approx 0.21$  Hz and  $f_2 \approx 0.14$  Hz in test B\_A2), the secondary bar moves onshore with constant speed (about 25 cm/h). However, the shoreline remains spatially fixed while the SZ increase its slope due to the sediment supply coming from the inner surf zone within a region of 4 m from the shore. Since case M\_A has the incorrect wave height, cases B\_A1 and B\_A2 can be instead directly compared to case C\_A2, which has the same short wave height and only a weakly energetic long wave.

The combination cases are characterized by the generation of a berm on the backshore: the sand is directly taken from the erosion of the crest of the bar and from the upper part of the submerged beach (Fig. 4.11). In comparison to cases C\_A2, the bichromatic groups generate significantly less morphological modification in the upper part of the beach (Fig. 4.12). Observations during the course of the experiment show that swash overtopping is particularly important in this growth process, as observed in the field (Weir et al., 2006), and that overtopping of the growing berm is assisted and increased by the modulation of the short wave runup by the long wave. There is a strong feedback between the morphology and sediment transport rate under these conditions; the long waves promote overtopping, which changes the backwash flows and enhances the landward sediment transport seaward of the SZ (Baldock et al., 2005).

As for the erosive test series, the random wave case R\_A1 (Fig. 4.12) shows a similar trend to the bichromatic wave groups and, in comparison with case C\_A2, shows a clear reduction in the landward sediment transport rate in the surf zone, the formation of a small bar further offshore, and the growth of a higher swash berm.

Unfortunately, the profile was not reshaped prior to running case R\_A2, so the data from R\_A2 cannot be compared directly to that of the other accretive test conditions.

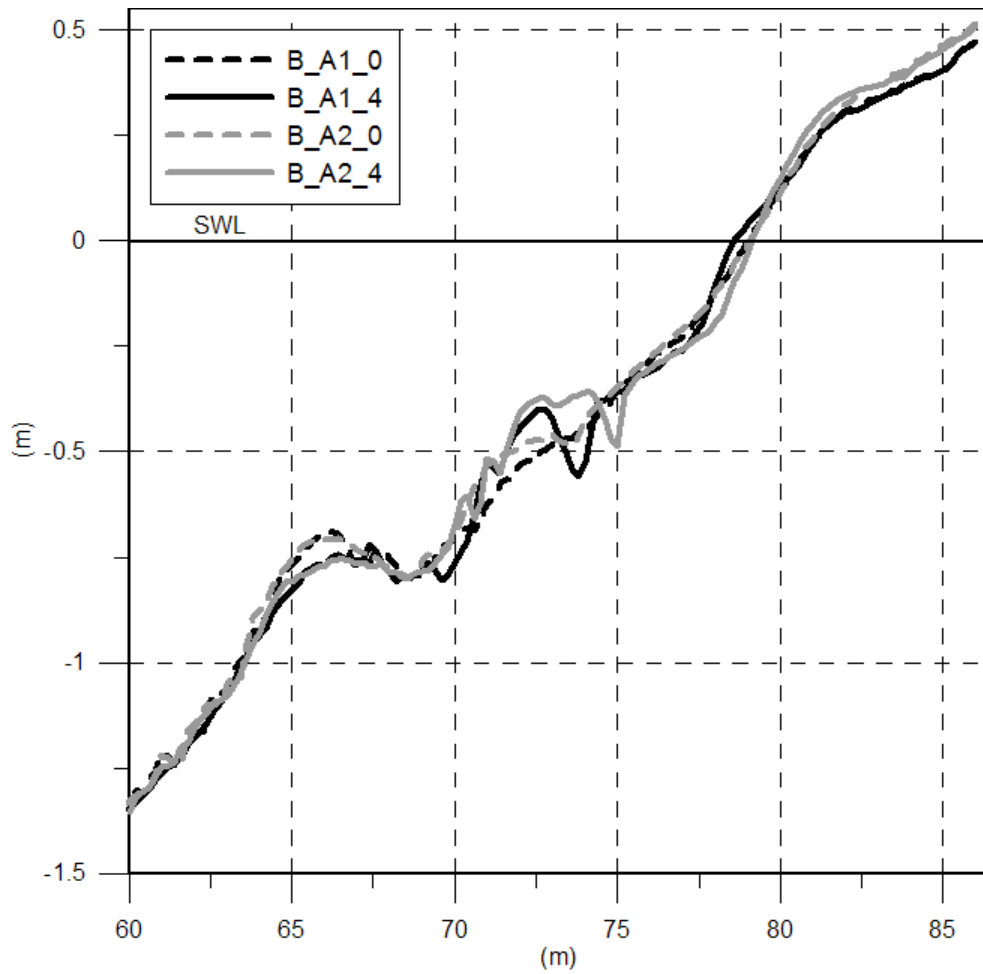


Figure 4.10. Beach profile comparison for tests B\_A1 and B\_A2.

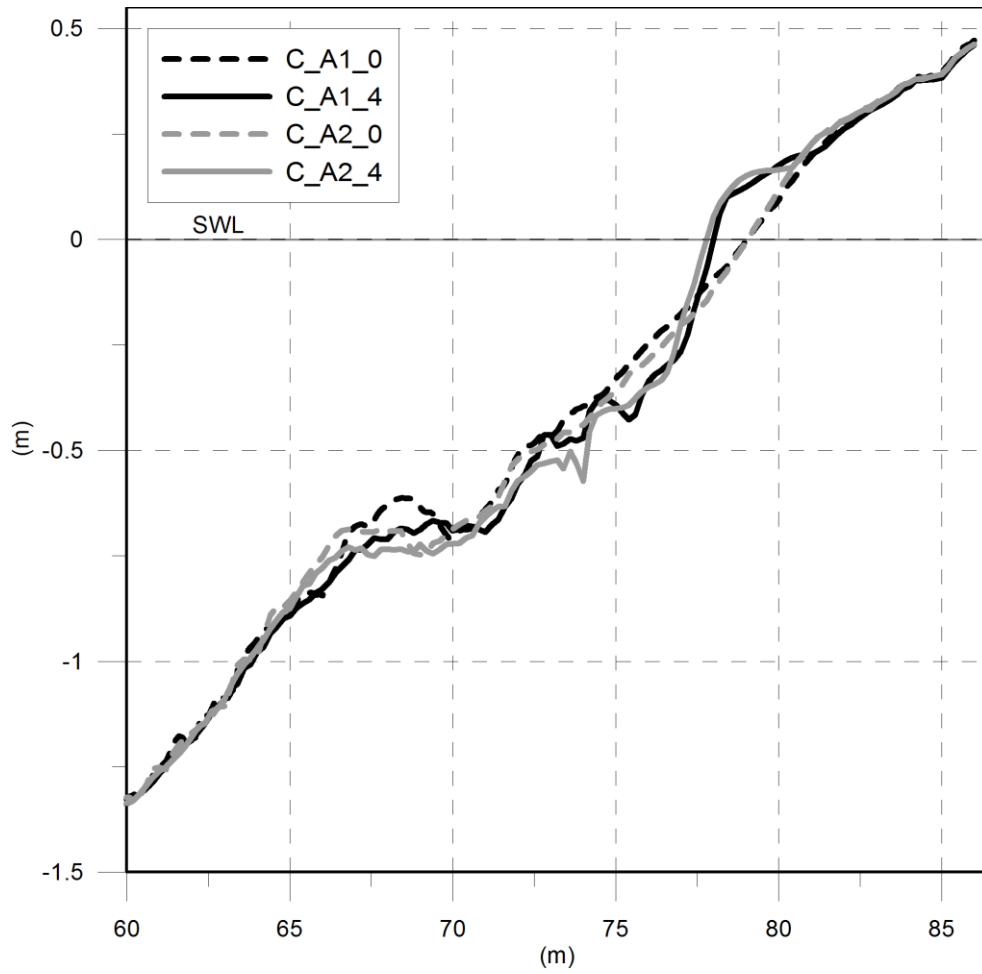


Figure 4.11. Beach profile comparison for tests C\_A1 and C\_A2

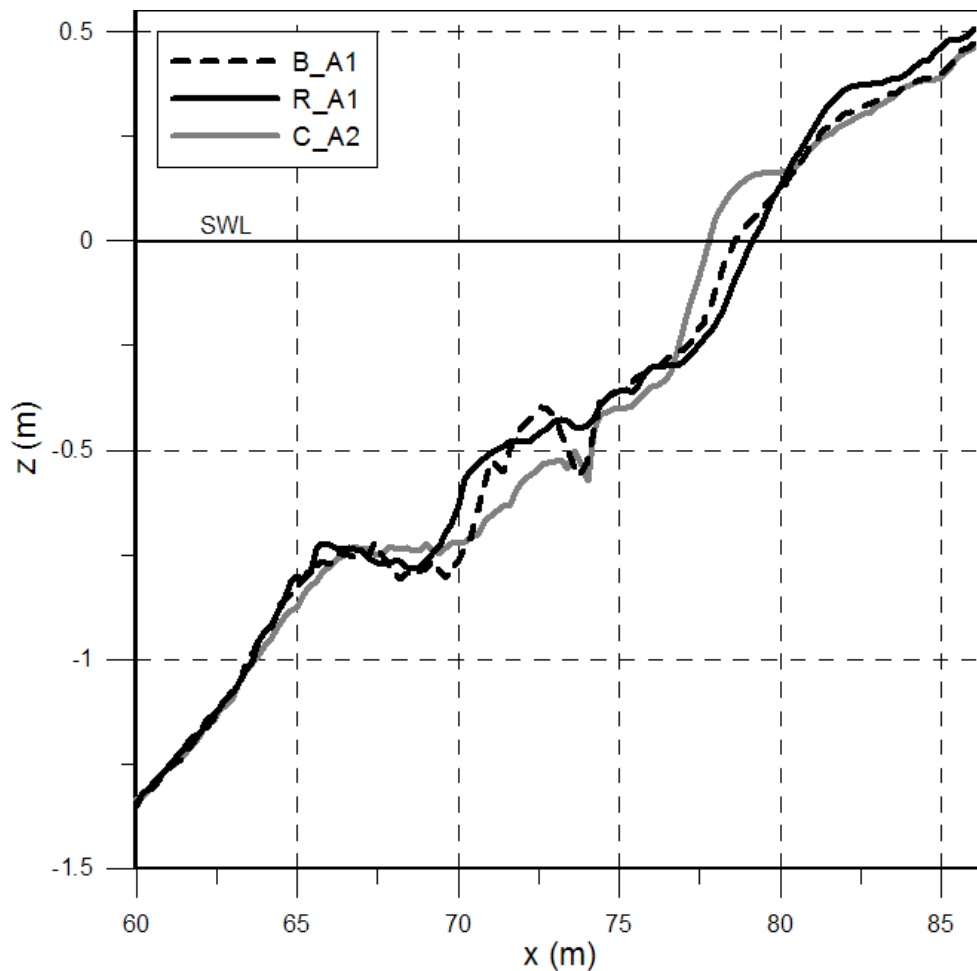


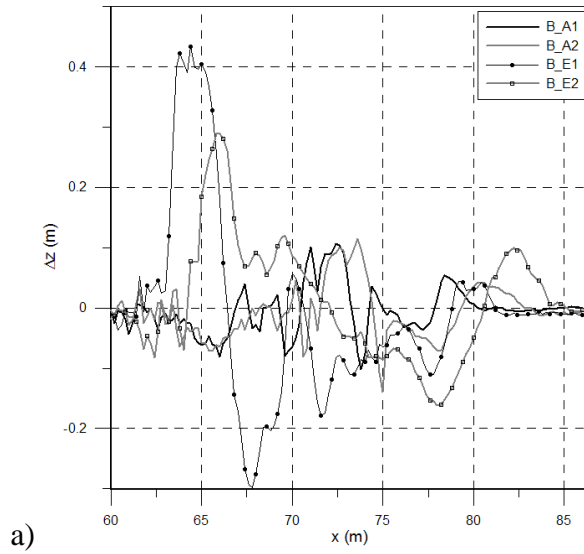
Figure 4.12. Beach profile comparison for tests B\_A1, R\_A1 and C\_A2.

#### 4.3.2.3 Morphological pattern

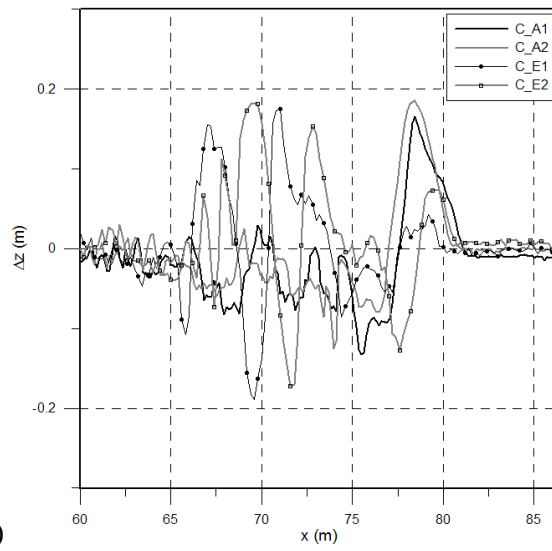
In Figure 4.13 a detailed analysis of relative cross-shore vertical variation  $\Delta z$  between the initial and final profile of each test is reported. This analysis is useful to highlight where each wave condition is able to give larger changes to the profile.

Increases in the bandwidth in the bichromatic wave groups, both for erosive as accretive cases (from B\_E1 to B\_E2 and from B\_A1 to B\_A2), results in an onshore shift of the bed forms (Fig. 4.13a). In particular, in erosive conditions, the accretion of the bar for case B\_E1 is 0.4 m, followed by a trough of about 0.3 m, while in condition B\_E2 the maximum accretion is about of 0.3 m but no trough is observed. The greatest change of the SZ is obtained from the bichromatic case with large bandwidth (B\_E2), for which berm elevation of 0.1 m occurs. The comparison of bichromatic tests for accretive conditions shows that the narrower bandwidth case (B\_A1) gives a similar behaviour in terms of  $\Delta z$  to the broader

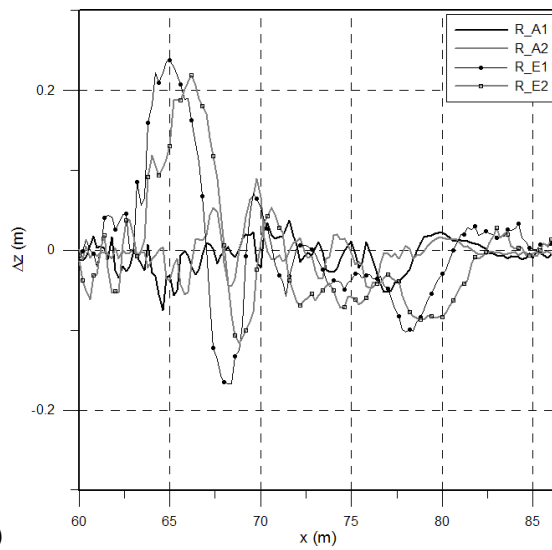
bandwidth case (B\_A2) but is shifted offshore about 1.3 m. The bed form shifting effect is also noticeable in the erosive cases for combination tests. Here, the monochromatic wave perturbed with the larger long waves (C\_E1) gives the same vertical variation of the case with smaller long waves (C\_E2) but shifting offshore of about 2.5 m (Fig. 4.13b). In accretive conditions, not much difference in the  $\Delta z$  pattern is observed. Figure 4.13c contrasts the vertical variation pattern for pairs of random waves R\_E1-R\_E2 and R\_A1-R\_A2. The pattern for each case is very similar, with a small shift in cross-shore position, in particular in the outer surf and SZ, in which the maximum  $\Delta z$  on the bar and on the swash berm are realized in the R\_E1 case (GF = 1) about 1.3m offshore of that in the R\_E2 case (GF = 1.1). In accretive conditions, the relative cross-shore variation in the beach profile for case R\_A1 is quite similar to that for case R\_A2.



a)



b)



c)

Figure 4.13. Relative cross-shore vertical variation from initial and final profile of: a) bichromatic cases; b) Combination cases; c) random cases.

### 4.3.3 Sediment dynamic results

#### 4.3.3.1 Cross-shore Sediment transport patterns

Comparison of case M\_E and case C\_E2 shows how the sediment transport pattern is very similar within the bar-trough region of the profile and within the inner surf zone (Fig. 4.14). Figure 4.15a contrasts the beach evolution and net sediment transport pattern for monochromatic case M\_E and bichromatic wave group case B\_E1. Figure 4.15b shows a similar comparison for case B\_E2, and cases B\_E1 and B\_E2 are compared with each other in figure 4.15c. For case B\_E1, the maximum seaward transport occurs at the bar crest, which is similar to the monochromatic case. However, for case B\_E2, the seaward transport is spread more widely, the maximum seaward transport rate is lower, and the maximum occurs in the mid-surf zone. A swash berm also forms for case B\_E2, and this forms higher on the beach than the monochromatic case, reflecting the larger maximum runup during the bichromatic wave conditions. These trends are very consistent with those observed during small-scale tests by Baldock et al. (2010). In those tests, the bichromatic waves generated larger net offshore transport rates, and larger bars that were further offshore in comparison to the equivalent monochromatic cases. In addition, with increasing bandwidth, the offshore transport rate maxima reduced in magnitude, the bars formed further landward, and greater onshore transport occurred in the SZ, with the formation of more pronounced swash berms. This is consistent with figure 4.15c and the different morphological response for case B\_E1 and B\_E2. Figures 4.16a-4.16c compare for case M\_E with that for the two random wave cases R\_E1 and R\_E2. Consistent with the morphological response, the variation in groupiness between the two random wave cases does not significantly affect the transport pattern. However, the more broad-banded random waves, R\_E1, appear to generate a widening of the sediment transport domain than the more narrow banded waves, R\_E2.

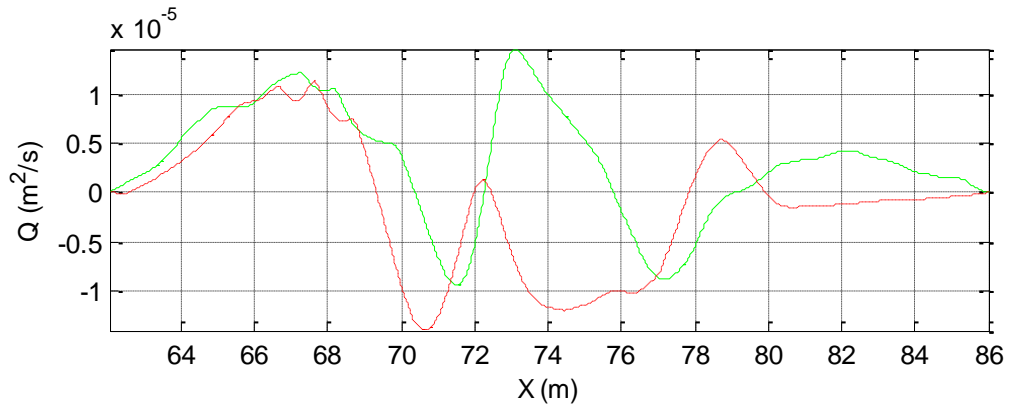


Figure 4.14. Integral corrected net sediment transport between monochromatic case M\_E and combination case C\_E2. Green solid line, t=96min, case M\_E, red dashed line; t=96min, case C\_E2.

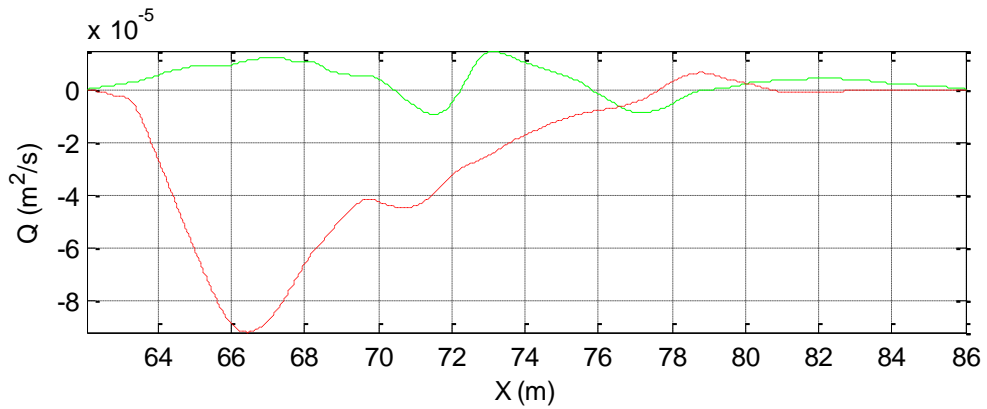


Figure 4.15a. Integral corrected net sediment transport between monochromatic case M\_E and bichromatic case B\_E1. Green solid line, t=96min, case M\_E, red dashed line; t=96min, case B\_E1.

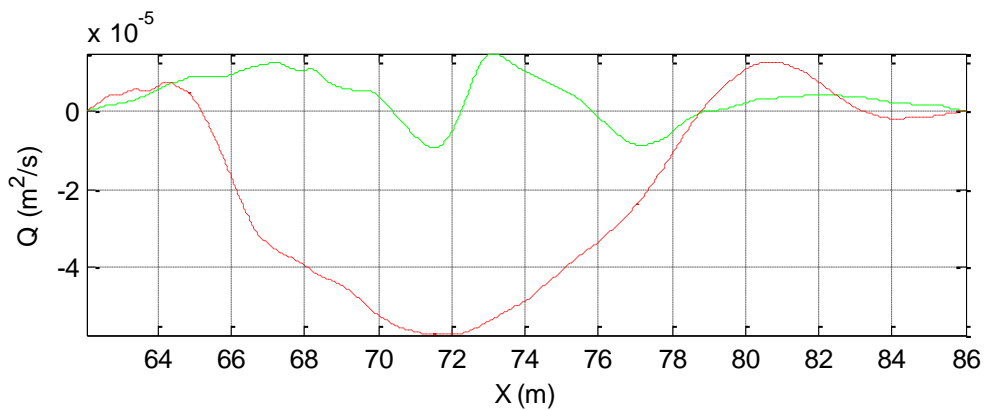


Figure 4.15b. Integral corrected net sediment transport between monochromatic case M\_E and bichromatic case B\_E2. Green solid line, t=96min, case M\_E, red dashed line; t=96min, case B\_E2.

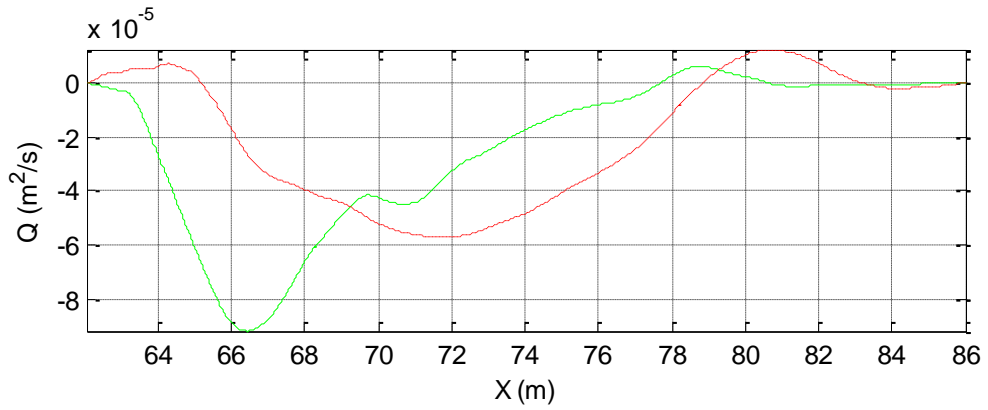


Figure 4.15c. Integral corrected net sediment transport between bichromatic cases B\_E1 and B\_E2. Green solid line,  $t=96\text{min}$ , case B\_E1, red dashed line;  $t=96\text{min}$ , case B\_E2.

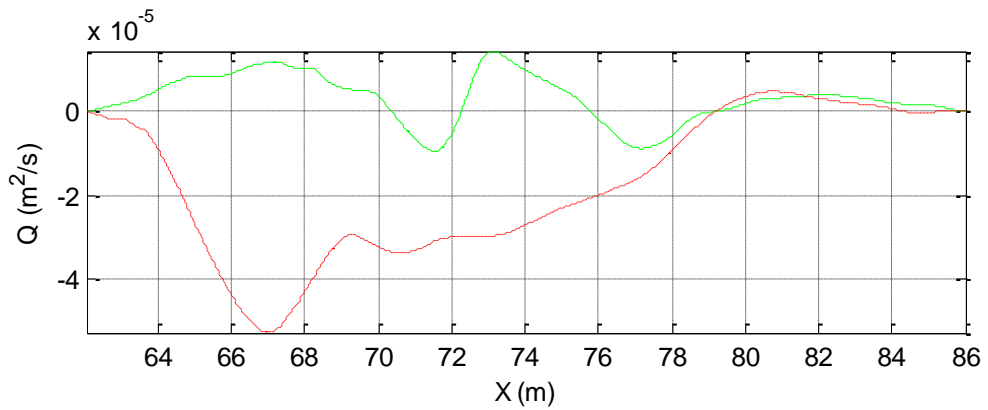


Figure 4.16a. Integral corrected net sediment transport between monochromatic case M\_E and random wave case R\_E1. Green solid line,  $t=96\text{min}$ , case M\_E, red dashed line;  $t=96\text{min}$ , case R\_E1.

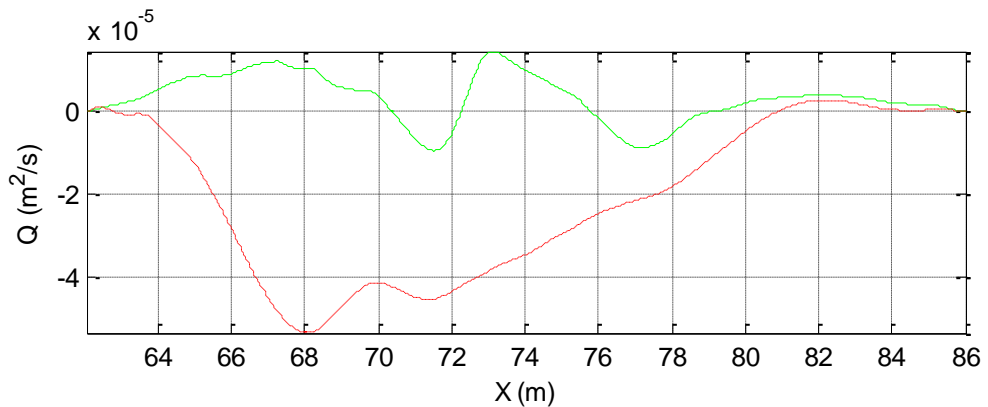


Figure 4.16b. Integral corrected net sediment transport between monochromatic case M\_E and random wave case R\_E2. Green green solid line,  $t=96\text{min}$ , case M\_E, red dashed line;  $t=96\text{min}$ , case R\_E2.

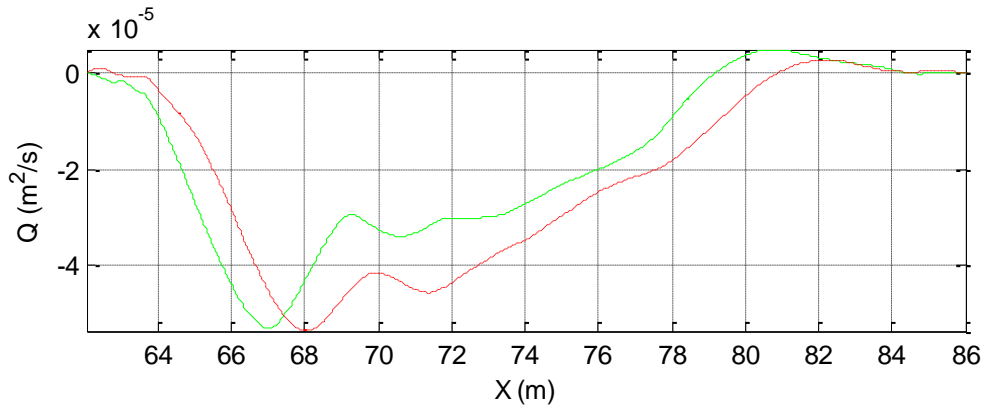


Figure 4.16c. Integral corrected net sediment transport between random wave cases with different groupiness, R\_E1 and R\_E2. Green solid line,  $t=96\text{min}$ , case R\_E1, red dashed line;  $t=96\text{min}$ , case R\_E2.

For erosive conditions, since the wave heights and wave periods for case M\_A are not similar to those of cases C\_A1 and C\_A2, the results cannot be directly compared. However, even though cases C\_A1 and C\_A2 have a larger wave height than case M\_A, they produce greater landward transport and shift the location of the maximum transport shoreward. (Fig. 4.17a and 4.17b). Figure 4.17c shows very similar results for the two combination cases (which have the correct wave height), which gives further confidence in the sediment transport measurements.

The sediment transport patterns for the two bichromatic wave groups are very similar (Fig. 4.18c), but quite distinct from that induced by the monochromatic wave (Fig. 4.18a-4.18b) and the equivalent combination cases (Fig. 4.18d). In comparison to cases C\_A1 and C\_A2, in fact, the bichromatic groups generate significantly less shoreward transport, or even offshore transport, in the mid-inner surf zone region, with significant gradients in  $Q(x)$  around the breakpoint which lead to formation of a small breaker bar because strong landward sediment transport on the seaward flank is reduced by the offshore directed undertow in the surf zone. Landward transport still occurs in the SZ, and the swash berm is again built to a higher elevation on the beachface, consistent with greater runup for the largest waves in the group. Swash overtopping remains important in the berm growth process. The same influence of the bichromatic wave groups was observed by Baldock et al. (2010), i.e. a clear trend to reduced onshore transport or a change to offshore transport across the surf zone in comparison to monochromatic conditions, and a larger swash berm at a higher elevation. Hence, there is a different effect in the surf and swash zones. This effect may be related to differences in the

degree of swash-swash interaction between monochromatic conditions and bichromatic conditions, and which is greater for more monochromatic wave conditions. Van Wellen et al. (2000) suggested that greater interaction curtailed the swash backwash and hence helped promote onshore transport, which is consistent with the observations.

For random waves, as noted previously, the data from R\_A2 cannot be compared directly. It is clear that reshaping of the profile is essential to distinguish the effects of the wave groups or random waves over the short duration of the tests, since the beach is moving rapidly toward an approximate equilibrium profile and the sediment transport rates reduce rapidly as the total run-time increases. However, it is noteworthy that the cross-shore variation in sediment transport for case R\_A2 is still quite similar to that for case R\_A1 (Fig. 4.19a), with maxima and minima at the same cross-shore locations, despite the much smaller magnitude of the transport rates for case R\_A2. Overall, random cases generate significantly less shoreward/offshore transport than equivalent combination cases (Fig. 4.19b).

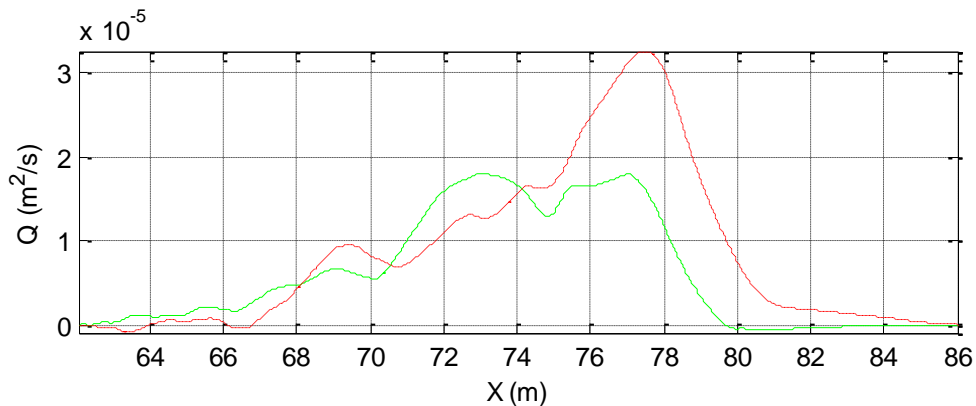


Figure 4.17a. Integral corrected net sediment transport between monochromatic case M\_A and combination case C\_A2. Green solid line, t=96min, case M\_A, red dashed line; t=96min, case C\_A1.

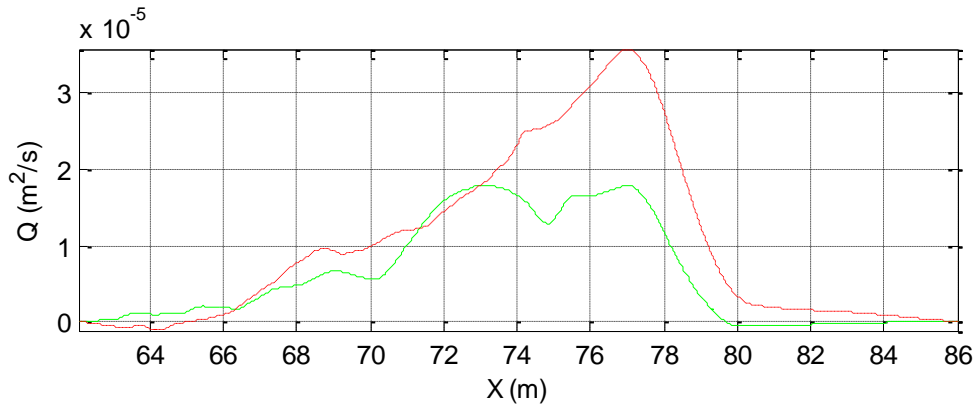


Figure 4.17b. Integral corrected net sediment transport between monochromatic case M\_A and combination case C\_A2. Green solid line,  $t=96\text{min}$ , case M\_A, red dashed line;  $t=96\text{min}$ , case C\_A2.

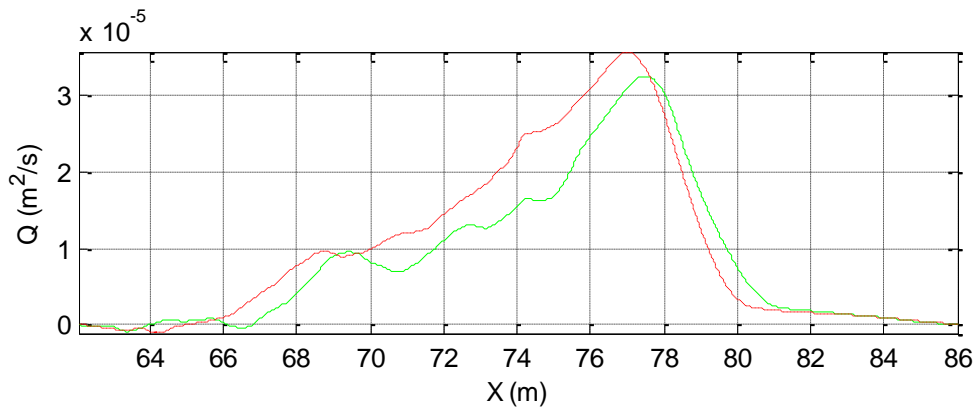


Figure 4.17c. Integral corrected net sediment transport between combination case C\_A1 and C\_A2. Green solid line,  $t=96\text{min}$ , case C\_A1, red dashed line;  $t=96\text{min}$ , case C\_A2.

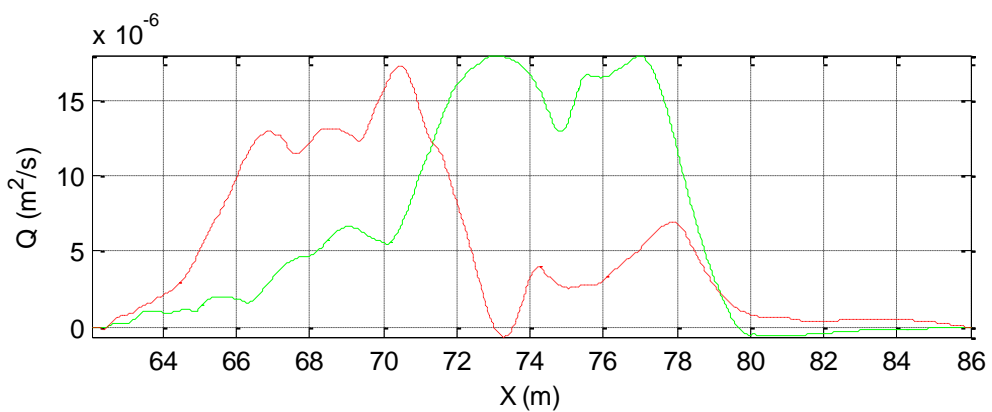


Figure 4.18a. Integral corrected net sediment transport between monochromatic case M\_A and bichromatic case B\_A1. Green solid line,  $t=96\text{min}$ , case M\_A, red dashed line;  $t=96\text{min}$ , case B\_A1.

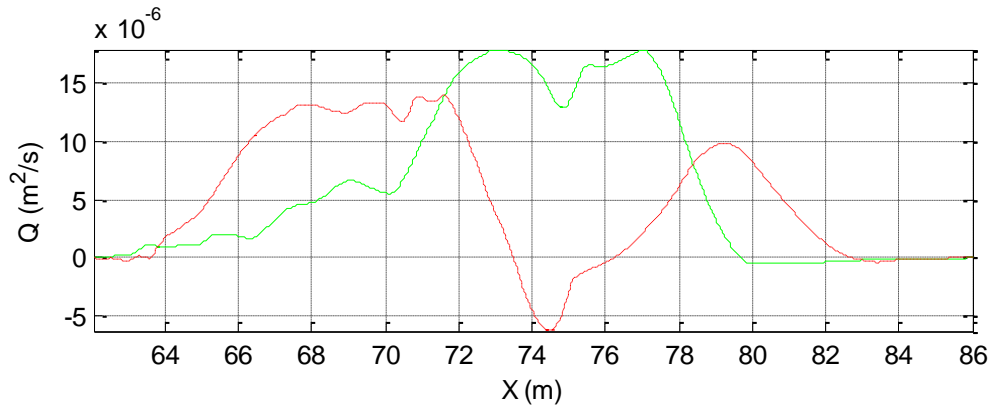


Figure 4.18b. Integral corrected net sediment transport between monochromatic case M\_A and bichromatic case B\_A2. Green solid line,  $t=96\text{min}$ , case M\_A, red dashed line;  $t=96\text{min}$ , case B\_A2.

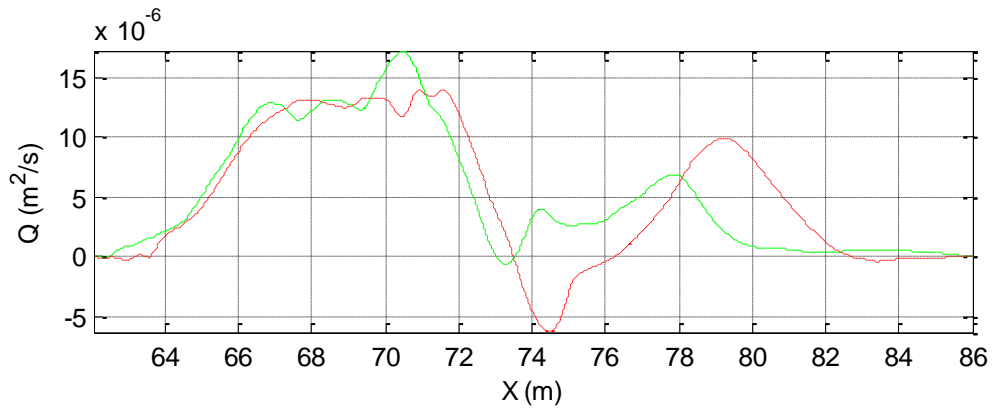


Figure 4.18c. Integral corrected net sediment transport between bichromatic cases B\_A1 and B\_A2. Green solid line,  $t=96\text{min}$ , case B\_A1, red dashed line;  $t=96\text{min}$ , case B\_A2.

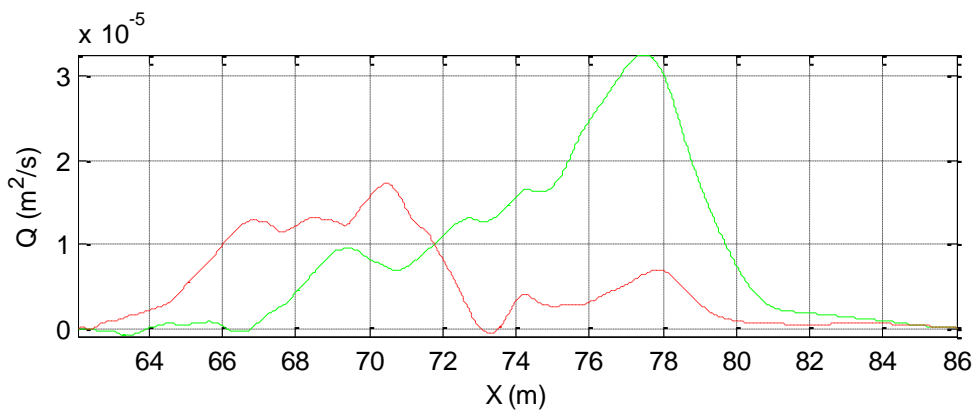


Figure 4.18d. Integral corrected net sediment transport between combination case C\_A1 and bichromatic case B\_A1. Green solid line,  $t=96\text{min}$ , case C\_A1, red dashed line;  $t=96\text{min}$ , case B\_A1.

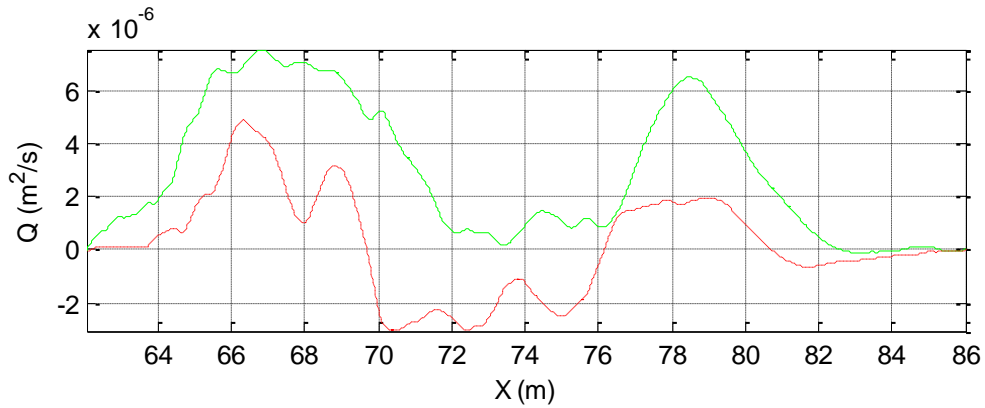


Figure 4.19a. Integral corrected net sediment transport between random wave cases with different groupiness, R\_A1 and R\_A2. Green solid line,  $t=96\text{min}$ , case R\_A1, red dashed line;  $t=96\text{min}$ , case R\_A2. Note case R\_A2 was not reshaped prior to testing.

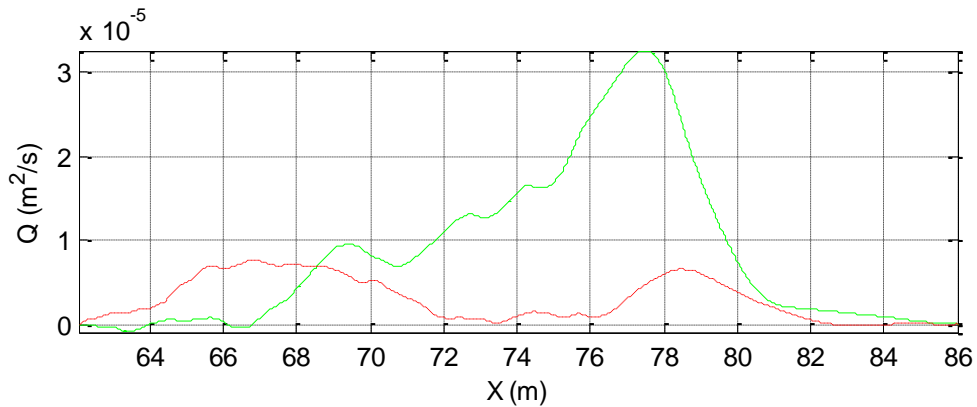


Figure 4.19b. Integral corrected net sediment transport between monochromatic case C\_A1 and random wave case R\_A1. Green solid line,  $t=96\text{min}$ , case C\_A1, red dashed line;  $t=96\text{min}$ , case R\_A1.

#### 4.3.3.2 Total net sediment transport direction and magnitude

Figure 4.20 provides a quantitative summary of the differences in normalized net transport,  $\zeta_t$ , between the different wave cases, obtained from integrating the local sediment transport rates,  $Q(x)$ , across the whole active beach profile. The local transport rates themselves are obtained from integrating the sediment continuity equation along the beach profile, using the changes in bed elevation between the start and end of the test. Note that  $Q(x)$  is a transport vector and can be negative (offshore transport dominant) or positive (onshore transport dominant) and does not integrate to zero unless onshore and offshore transport magnitudes are equal. A positive total transport rate represents net landward transport and a

negative rate indicates net offshore transport. The data have been normalised by the maximum total transport rate observed in any one test (case B\_E1), so the magnitude of the bars indicates the relative transport, or percentage difference, between tests. The bichromatic and random wave cases generate much greater offshore sediment transport than the corresponding monochromatic wave case M\_E. In particular,  $\zeta_t$  for the bichromatic waves with narrower bandwidth (B\_E1) is 12 times greater than case M\_E, while bichromatic waves with larger differences between the frequencies of the components (B\_E2) is 10 times greater. It is noteworthy that relative to combination case C\_E2,  $\zeta_t$  of M\_E test is about 2 times greater. However, the absence of data for case C\_E1 makes it difficult to identify a clear influence of the long waves for the erosive conditions. The slight reduction in offshore transport is however consistent with the long wave influence observed in small-scale tests (Baldock et al., 2010).

For the accretive conditions, because the short wave height was incorrect for case M\_A, it is again difficult to draw firm conclusions. However the short-wave energy in the remaining cases was very similar. The addition of a longer free wave period (C\_A1) produces less net shoreward transport than case with a smaller free long wave period (C\_A2) by a factor of about 1.2. The influence of the free long wave is again very consistent with the small-scale tests of Baldock et al. (2010), who also found a strong increase in the landward sediment transport and the growth of larger swash berms when a free long wave was added to monochromatic waves. This effect appears quantitatively more important for the accretive conditions than for the erosive conditions, possibly because the long wave is larger relative to the short waves. Bichromatic cases B\_A1 and B\_A2 reduce the landward transport of sediment in comparison to cases M\_A, C\_A1 and C\_A2. Finally, the random wave cases show the same trends as the bichromatic cases, i.e., a greatly increased offshore transport during erosive conditions and a reduced landward transport during accretive conditions.

Hence, overall, the presence of wave groups, and any long waves induced by the groups, tends to bias sediment transport in the offshore direction compared to monochromatic conditions.

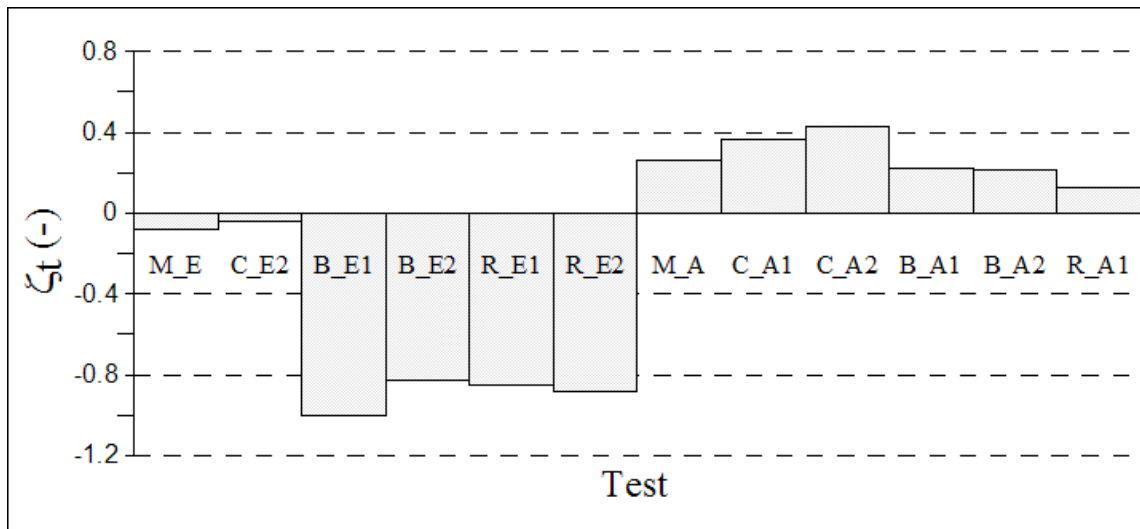


Figure 4.20. Normalised net sediment transport across whole active profile for each test, positive values represent accretion or landward transport, negative values represent erosion or seaward transport.

Figure 4.21 summarises the differences in net transport in the SZ region,  $\zeta_s$ , between the different wave cases, obtained from integrating the local sediment transport rates above  $z = 0$ . The data have been normalised by the maximum total net transport in the SZ observed in any one test (case C\_A1). For the erosive cases, there is no clear pattern because the runup can build swash berms even though the more shoreward part of the profile is eroding. It should be noted that tests with initial conditions incorporating a dune would probably show different results in the SZ region.

$\zeta_s$  of monochromatic condition is 2.5 time greater than that one of the case B\_E1 but is 1.6 time smaller than case B\_E2.

For the accretive tests the influence of the long waves is clear, with much greater shoreward transport in the SZ than for the monochromatic test or the wave group tests.  $\zeta_t$  of combination case C\_A2 is 1.2 times greater than that one with larger free long waves, C\_A1 (Fig. 4.20). Focusing on only the emerged part of the beach, an inverted trend is observed, with a  $\zeta_s$  of C\_A1 equal to 1.13 times  $\zeta_s$  of C\_A2 (Fig. 4.21).

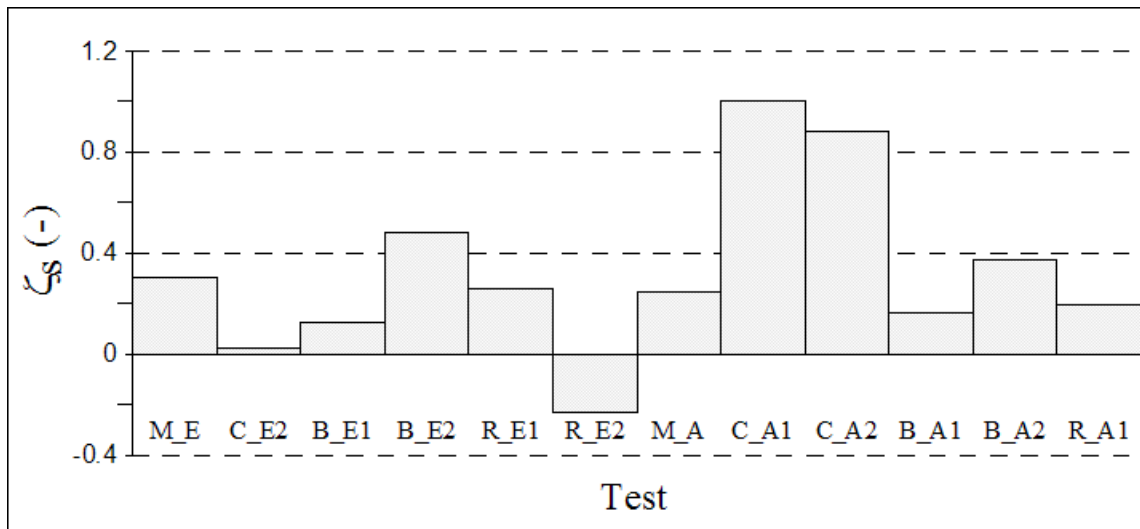


Figure 4.21. Normalised net sediment transport in the SZ ( $z > 0$ ) for each test, positive values represent accretion or landward transport, negative values represent erosion or seaward transport.

Although the experimental design was not followed exactly, with data missing for two cases, overall, the quantitative total sediment transport data and the qualitative results illustrated by the profile changes agree with the small-scale data presented by Baldock et al. (2010). Baldock et al. (2010) discussed sediment scaling issues at length and sought to maintain similar relative fall velocity between the small scale models and prototypes, as recommended by Hattori and Kawamata (1985) and Dean (1985). Their conclusion that the free long waves tend to promote more landward transport and that the bichromatic groups tend to promote offshore transport is supported by these large scale experiments, and possible reasons for this are discussed further below. The present experiments further suggest that the profile response to random waves is very similar to that for bichromatic wave groups with the same mean energy flux. For the erosive tests, while the free long waves in the combination cases have some influence on the profile evolution, it is a weak effect compared to that induced by the wave groups and random waves. For the accretive tests, the influence of the free long waves is significant in the inner surf and swash zones and of similar influence to the wave group induced long waves.

The role of the short waves, mean currents, and long waves inside the surf zone, is briefly examined at a micro-scale level by considering the net suspended sediment fluxes measured in the outer and inner surf zone, i.e.,  $\langle u.c \rangle$  obtained from the OBS and ADV records (figures 4.22a and 4.22b). The estimated net transport induced by the mean flow and

the long waves (low frequency component) is always directed offshore in the lower water column, and both components are very similar. In contrast, the estimated net transport by the short waves is minimal near the bar, and small and onshore in the inner surf zone. For case B\_E2, the local sediment flux data suggests that offshore sediment transport should be larger in the inner surf zone compared to that further offshore, which is contrary to the net transport derived from the morphology (figure 4.15b). In addition, the sediment flux data show a similar magnitude of offshore transport at  $x=74\text{m}$  for both cases C\_E2 and B\_E2 (figure 4.22a), but the morphological data suggest a factor four difference. For case C\_E1 the long wave component of the transport is more negative than for case B\_E1 in the outer surf zone, again in contrast to the trend suggested by the profile evolution. Given the sparseness of the data and the uncertainty in the relative elevation and cross-shore location of the instruments for the different tests, it is difficult to compare the magnitudes of the transport between the different test series and this is not pursued further here. It is noted that the total sediment transport converges at the bars for all the erosive cases (figures 4.15-4.17), in contrast to the diverging sediment suspended sediment transport observed for long waves by Aagaard and Greenwood (2008).

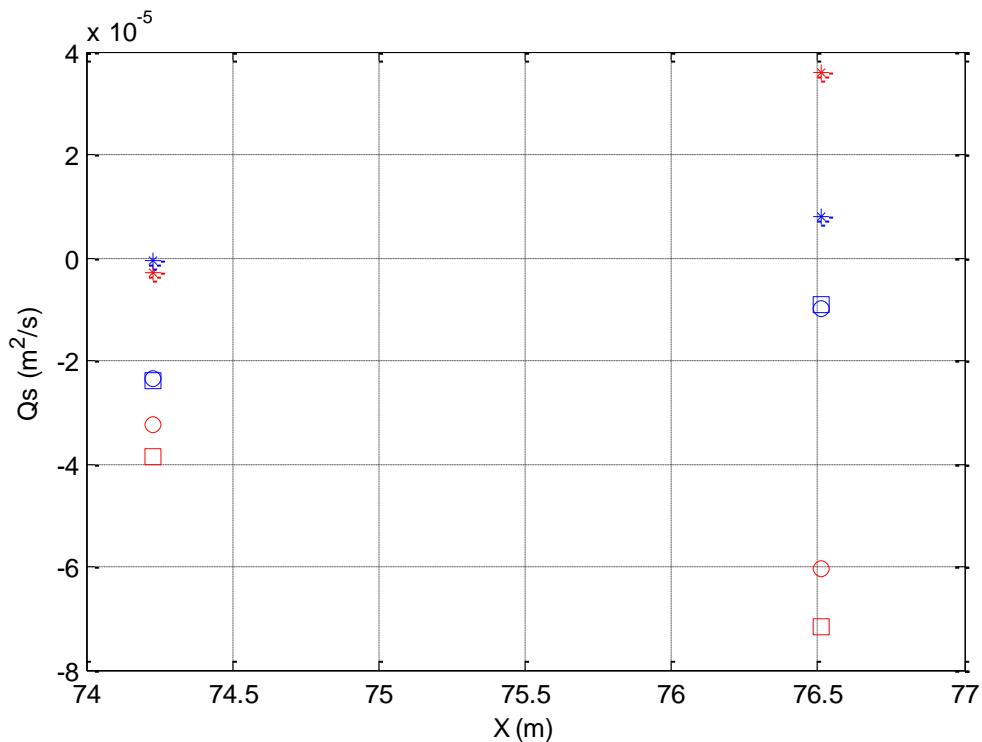


Figure 4.22a. Computed net suspended sediment flux at  $z \approx 3\text{cm}$  above the bed for erosive test cases C\_E4 (blue symbols) and B\_E2 (red symbols). Circles - mean component; star – short wave component; square - long wave component (from Baldock et al., 2011).

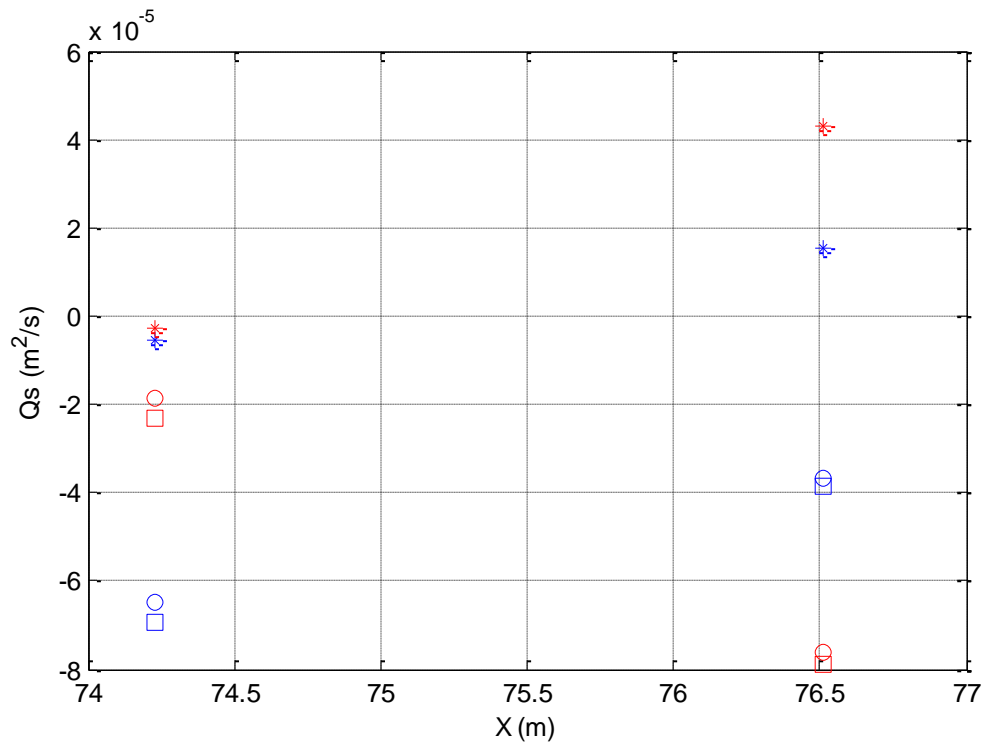


Figure 4.22b. Computed net suspended sediment flux at  $z \approx 3\text{cm}$  above the bed for erosive test cases C\_E1 (blue symbols) and B\_E1 (red symbols). Circles - mean component; star – short wave component; square - long wave component (from Baldock et al., 2011).

## 5. Discussion and Conclusions

### 5.1 Discussion

#### 5.1.1 Large experiment at GWK

It is worth to remind that grain size, beach slope and drain configurations used in these experiments are fully comparable to the field installations present in the literature, at least at Italian level (Ciavola et al., 2008).

This work can be taken as a demonstration that in/exfiltration acting on a medium-grained sandy beach does not play a significant role in controlling the beachface morphology. The cause is recognizable in the small hydraulic conductivity. Indeed, the evident conflict which was observed in the literature regarding the net effect of infiltration–exfiltration on the sediment transport appears to be resolved by grain size control. How the combined effects of stabilisation–destabilization (due to effective normal stress variations) and boundary layer modification (at which increasing/decreasing in shear stress is related) are balanced, was quantified by Nielsen (1998), Turner and Masselink (1998) and Butt et al., (2001). Nielsen (1998) found that boundary layer effects are only likely to dominate at grain sizes above  $D_{50} = 0.58$  mm. Butt et al., (2001) found that there is a critical grain size at which the influence of infiltration-exfiltration changes from offshore to onshore. They suggested a  $D_{50} = 0.55$  mm, with a dominance of stabilisation–destabilisation below this value and a dominance of boundary layer effects above it. However, the exact value of this grain size is highly sensitive to the method used to estimate the friction factor. The results of the works cited above confirm a previous study carried out by Oldenzil and Brink (1974) which established that infiltration always decreased the rate of sand transport for a range of sizes  $0.13 \div 0.57$  mm. Moreover, in the observations of Masselink and Li (2001) from numerical modelling and other older literature (Bagnold, 1940; Dubois, 1972) a critical sediment hydraulic conductivity of 1 cm/s was suggested, which corresponds to a grain size threshold of 1.5 mm (coarse sand). Therefore, the infiltration process would have negligible effects on most sandy beaches where the sand grain size is usually finer than 1 mm. Furthermore, recent results of Bakhtyar et al. (2011) obtained from comparison between process-based modelling and laboratory experiments (data from Horn et al, 2007), substantiates that for fine sand the accretion effects of swash infiltration is not sufficiently large because of the low hydraulic conductivity. In any case, the grain size used in our experiments ( $D_{50} = 0.33$  mm) seems to be always under the

thresholds aforementioned in all the literature studies cited above. Our suggestion is that the idea that a positive balance of transport onshore due to changed infiltration-exfiltration could be produced by lowering the water table, is only reasonable if a large water volume is drained. Hence, much more details on the hydraulic performances of drains, as well as on their spatial positioning, are required.

The presence of a hydraulic discontinuity in the groundwater-drain system implies that the internal flow of the drains occurred as an open-channel flow allowing low drained flows. From a morphological viewpoint, in fact, it seems that whatever the wave conditions were during the experiment, the beach was still evolving towards an equilibrium shape. This did not affect the results of the experiment because its aim was to analyze the efficacy of the drainage system on beach stabilization under different wave condition also in a transition regime context, regardless of the initial beach configuration for each test.

### 5.1.2 Large experiment at CIEM

The analyses of morphological changes, cross-shore sediment patterns and net sediment transport rates (seen in Section 4) suggested that the large change in the beach response between monochromatic conditions and wave groups is a result of the wave groupiness, not the presence of the forced and free long waves induced by the groupiness. An explanation for this can be formulated in terms of the variation in short-wave height within the bichromatic waves and random waves, as compared to the steady short-wave height for the monochromatic waves (Baldock et al., 2010). The maximum wave height is larger for the bichromatic and random wave groups (figure 5.1a and 5.1b), and the significant wave height is also greater than  $H_{rms}$  for wave groups and random waves. Assuming a Shields model relationship between transport and shear stress, the gross sediment transport can be expected to be a function of  $u^n$  or  $H^n$ , with  $n$  likely to be in the range  $2 < n < 3$ . Consequently, the larger waves in the groups dominate the transport process and can be expected to tend to increase offshore transport, particularly as the undertow largely follows the instantaneous wave height (Svendsen, 1984). This is consistent with the use of the significant wave height in defining  $\Omega$ , as it is usual, rather than the rms or mean wave height. Therefore, it is proposed that the *effective* relative fall velocity,  $\Omega = H/w_s T$ , increases for the bichromatic waves and random waves, compared to monochromatic waves with the same energy flux.

With reference to the sediment transport direction as a function of the effective relative fall velocity, there is a potential natural asymmetry in the net transport under wave groups, since the transport by the smaller waves cannot cancel, or reverse, that of the larger waves because the energy levels are much lower in magnitude (Baldock et al., 2010, 2011). This can be regarded to be similar to the different time-scales between storm erosion and long term beach recovery. Storm waves can erode sediment more intensively and rapidly than swell waves can return the sediment back onshore, because the energy levels are lower during the accretive phase. However, such a simple explanation can be complicated by the presence of swash overtopping, morphological-hydrodynamic feedback and how much the beach profile differs from some quasi-steady equilibrium condition. Nevertheless, if the effective relative fall velocity is considered a robust overall predictor of beach profile response to different forcing conditions and the tendency of a beach to erode or accrete (e.g. Gourlay, 1968; Dean, 1973; Wright et al., 1985; Larson and Kraus, 1989; Dalrymple, 1992), then this model is consistent with the present data. A different effective fall velocity for wave groups and monochromatic waves may also explain some of the variation in erosive/accretive thresholds in the literature.

This form of model provides a simple heuristic explanation for the different profile evolution between the cases considered in these experiments, and since the profile evolution commences from an approximately planar profile, variations in  $\Omega$  also indicate the influence of the perturbations to the wave climate on sediment transport magnitude and direction. However, some caution is required when considering shoreward transport, because the net cross-shore transport,  $Q$ , cannot be a monotonic function of  $\Omega$ . Consider the likely form of  $Q(\Omega)$ , illustrated on figure 4.24.  $Q$  must be zero for zero wave height, should be small and positive (onshore) for moderate  $\Omega$ , and becomes large and negative (offshore) for large  $\Omega$ . Following Wright et al. (1985) and Yates et al. (2009) an equilibrium-state model for  $Q$  can be written as

$$Q = A_c (\Omega_e(b) - \Omega) \Omega^n \quad [5.1]$$

where  $A_c$  is an arbitrary constant,  $n$  is some power, and  $\Omega_e(s)$  is the value of  $\Omega$  for equilibrium conditions (no net cross-shore transport) and a given beach width,  $b$ . Previous conditions could also be represented by parameters other than the beach width, e.g. a beach volume. Differentiating with respect to  $\Omega$  shows that the maximum shoreward transport will occur when

$$\Omega = \Omega_{\max} = \frac{i_n \Omega_e(b)}{i_n + 1} \quad [5.2]$$

Taking, for simplicity,  $i_n$  as an integer in the range 1-3 suggests that the rate of maximum accretion will occur when

$$\frac{1}{2} \Omega_e(b) < \Omega_{\max} < \frac{3}{4} \Omega_e(b) \quad [5.3]$$

which is quite a narrow range, and  $\Omega_{\max} \approx 2/3 \Omega_e$  appears most likely. Eq. [5.2] also shows that  $n \neq 0$ , as suggested by Wright et al. (1985). This relationship may be useful in estimating beach recovery times under changing wave climates, and could be tested with laboratory or field data. More importantly, (2) shows that the shoreward transport will decrease for perturbations in wave height when  $\Omega \approx \Omega_{\max}$ . Hence, around this value of  $\Omega$ , the simple heuristic equilibrium state model shows that small perturbations to the relative fall velocity can lead to either increased or decreased shoreward transport, depending whether  $\Omega$  is greater or less than  $\Omega_{\max}$ .

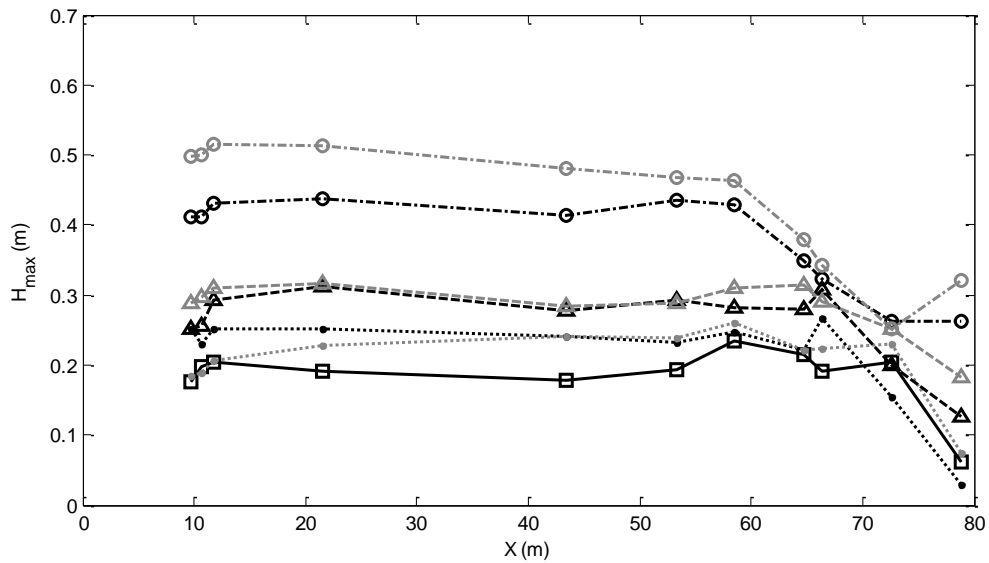


Figure 5.1a. Cross-shore distribution of  $H_{\max}$  for erosive tests: M\_E,  $\square$ ; C\_E2,  $\bullet$ ; C\_E4,  $\bullet$ ; B\_E1,  $\Delta$ ; B\_E2,  $\Delta$ ; R\_E1,  $\circ$ ; R\_E2,  $\circ$  (from Baldock et al., 2011).

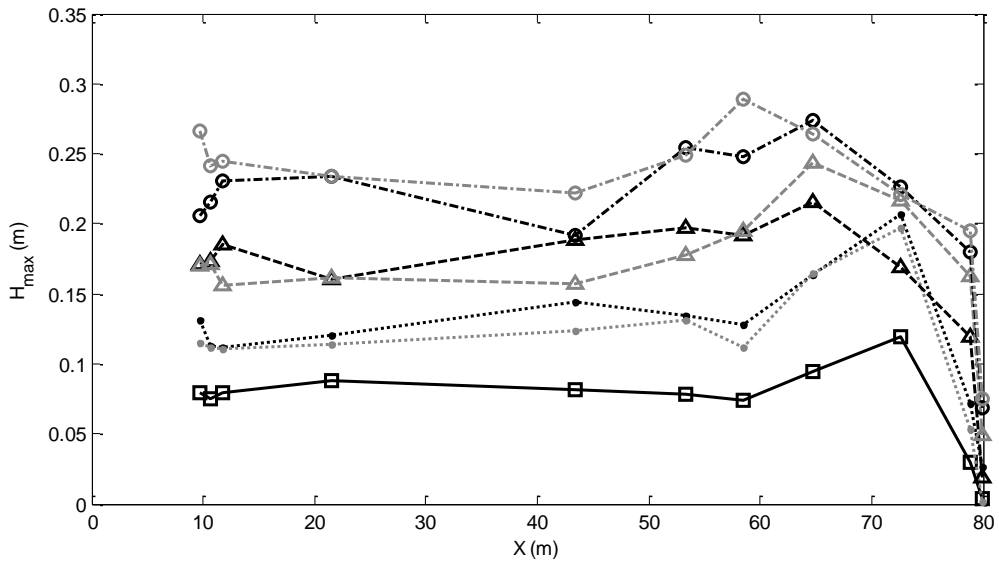


Figure 5.1b. Cross-shore distribution of  $H_{\max}$  for accretive tests: M\_A,  $\square$ ; C\_A2,  $\bullet$ ; C\_A4,  $\bullet$ ; B\_A1,  $\Delta$ ; B\_A2,  $\Delta$ ; RA\_1,  $\circ$ ; R\_A2,  $\circ$  (from Baldock et al., 2011).

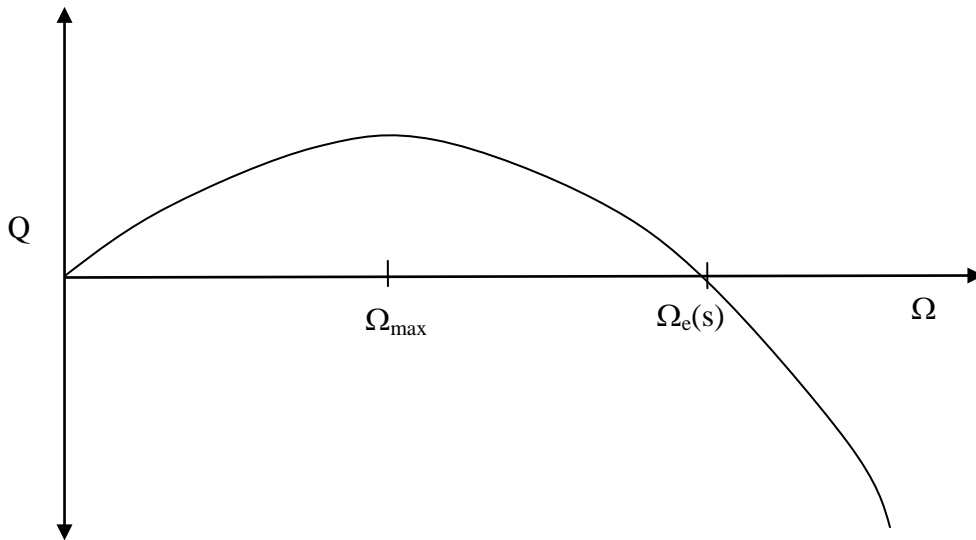


Figure 5.2. Conceptual sketch of relationship between transport magnitude and direction and  $\Omega$ . The maximum rate of accretion (total net shoreward transport) occurs at  $\Omega_{\max}$ . Equilibrium (no net transport) occurs at  $\Omega = \Omega_e(b)$  (Baldock et al., 2011).

### 5.1.3 Implication on SZ modelling

Although well developed, numerical models use some assumptions which limit their capabilities of reproducing natural flow conditions. One of the most crucial shortcomings concerns the treatment of the boundary between the wet and dry domains, i.e., the definition of the shoreline boundary conditions. Simplified shoreline boundary conditions (SBCs) are often used in enforcing at the inshore boundary of the computational domain, i.e. perfect absorption (Wei et al., 1999; Johnson et al., 2005) or perfect reflection (Bradford, 2005). Both of them are clearly incorrect as they prescribe the wrong magnitude and shape of LFWs radiating out to sea (Brocchini, 2006). A third type of SBC, i.e., a SZ condition, is required. However, implementation of such SBCs is not an easy task due to the wide range of scales to be linked.

Recalling the conceptual scheme presented in Section 1, the SZ system represents a very special boundary layer in which not only must small scales be properly resolved and their influence fed into the larger-scale dynamics, but the connection between small and large scales must be performed (Brocchini and Baldock, 2008). From this point of view, the physical processes that have been investigated through the present research could significantly provide to process knowledge. Further, the data provide a comprehensive and controlled series of tests for evaluating numerical models.

In the context of the micro-scale processes, despite good conceptual models of the influence of infiltration/exfiltration and beach groundwater on the boundary layer and swash hydrodynamics, quantitative measurements were prime requirement for future work, as prospected by some authors (Elfrink and Baldock, 2002). In this perspective, the tests carried out at GWK experiment explored the beach response induced by various groundwater regimes, where groundwater regimes were modified by a dewatering system. The beach dewatering can be treated as a local hydrodynamic process and considered as a SZ boundary condition. On the other hand, the scope of the tests carried out at CIEM was to derive information in the changes in the beach response as a direct result of the wave groupiness. Wave grouping can be addressed to the global hydrodynamic processes and considered as an inner surf zone boundary condition. Following this concept, significant considerations can be addressed to this large scale experiment.

A local dewatering of the watertable may affect large-scale hydrodynamic processes also in the inner surf zone. The analysis of the energy density spectra measured by the

pressure transducers inside the beach, shows significant influence of the BDS on wave setup, undertow current profiles and surf beat oscillations. This, again, is counter intuitive and interesting, particularly in view of the range of scales to be bridged for the implementation of the SZ Shoreline Boundary Conditions (SBCs). Note that up to now the beach groundwater-inner surf hydrodynamic feedback has not yet been analyzed, probably due to the small scale of the experiments where scale effects could be significant in influencing the results.

The considered wave conditions give surf similarity parameters such that  $\xi_0 < 1.5$  (Aristodemo et al., 2010). In this case the infragravity waves prove to be generally dominant in the SZ processes with respect to the high-frequency wave bores, due to wave grouping remaining in the inner surf zone (Elfrink and Baldock, 2002). The drain activation leads to an additional increase of the infragravity energy components. This processes is linked to the stabilization of the reflection coefficients induced by the drainage leading the beach towards a more dissipative character. As recently observed by Baldock *et al.* (2010), on dissipative beaches long period infragravity waves were found to account for significant sediment suspension in the SZ and the drains could tend to enhance the onshore sediment flux. On the other hand, sediment suspension events are correlated to the incident short breaking waves on reflective beaches (Bakhtyar *et al.*, 2009). In addition the analyses highlight that the pressure spectra  $S_p(f)$  tend to be proportional about to  $f^{-2}$  in undrained conditions (Kaihatu *et al.*, 2007), showing changes in the spectral slope under drained tests. Therefore, the progressive tendency to the possible saturation of swash spectra could be influenced by the rise in the unsaturated zone inside the beach due to the activation of the BDS.

In summary, three different mechanisms have been identified by which artificial element acting in the nearshore, such as a BDS, aims to interact with the swash sediment dynamics by favouring the deposition of sediments transported by waves during the uprush phase and contrasting their offshore movement during the backwash phase. These are:

- *direct hydrodynamic influence on vertical swash flows;*
- *indirect hydrodynamic aspects concerning wave setup, undertow and surf beat;*
- *related feedback processes (e.g. wave reflection, longshore bar morphology).*

Nevertheless, the direct effects such as the net result of the combined normal/shear stress variation induced by lowering the watertable, are dominant in the morphological change. In addition, they could contribute to some general aspects of the aforementioned indirect mechanisms, through feedback processes. Indeed, the observed variation in wave reflection

for drained and undrained conditions due to the progressive beach saturation (Aristodemo et al., 2010), is in strong agreement with experimental and field observations of natural beaches (Baquerizo *et al.*, 1997). This means that influence of drainage on reflection coefficient is the result of the morphological change in the active infiltration zone, rather than direct influence on saturation level. On the other hand, BDS lead to a reduction of wave set up (Damiani et al., 2011). This, in turn, leads to reduction in the undertow velocity profile. Since undertow is the dominant bar forming mechanism (Dally, 1987) significant modification in sediment transport patterns in the SZ could be observed, due to relevant hydro-morphodynamic feedback.

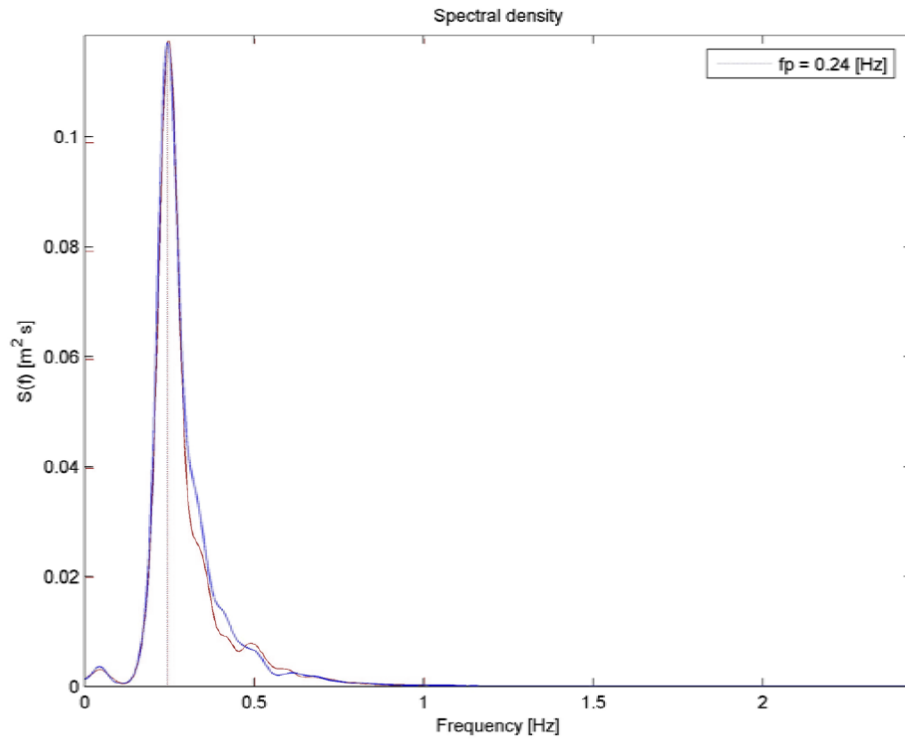
The detailed dependence of BDS on inner surf hydrodynamics requires further work because the role of the test duration increases. In fact, to appreciate these indirect and feedback mechanisms, particularly evident in low energy conditions, the test should be run for larger time. This is also confirmed by the SUSCO experiment. During low energy condition (also defined “accretive”) the addition of a free long wave to monochromatic case produced significant changes, building a larger swash berm at higher elevation on the beachface. Observations during the course of the experiment showed that swash overtopping is particularly important in this growth process, as observed in the field (Weir et al., 2006), and that overtopping of the growing berm is assisted and increased by the modulation of the short wave runup by the long wave. There is a strong feedback between the morphology and sediment transport rate under these conditions; the long waves promote overtopping, which changes the backwash flows and enhances the landward sediment transport seaward of the SZ (Baldock et al., 2005).

Nevertheless, the results presented here prove that the BG hydrodynamic influences on the swash flows should be modelled not only at micro and intermediate scales (i.e. in/exfiltration and wave induced phenomena) but also considering Low Frequency Waves and currents kinematics (large-scale processes, see Brocchini and Baldock, 2008 for a review).

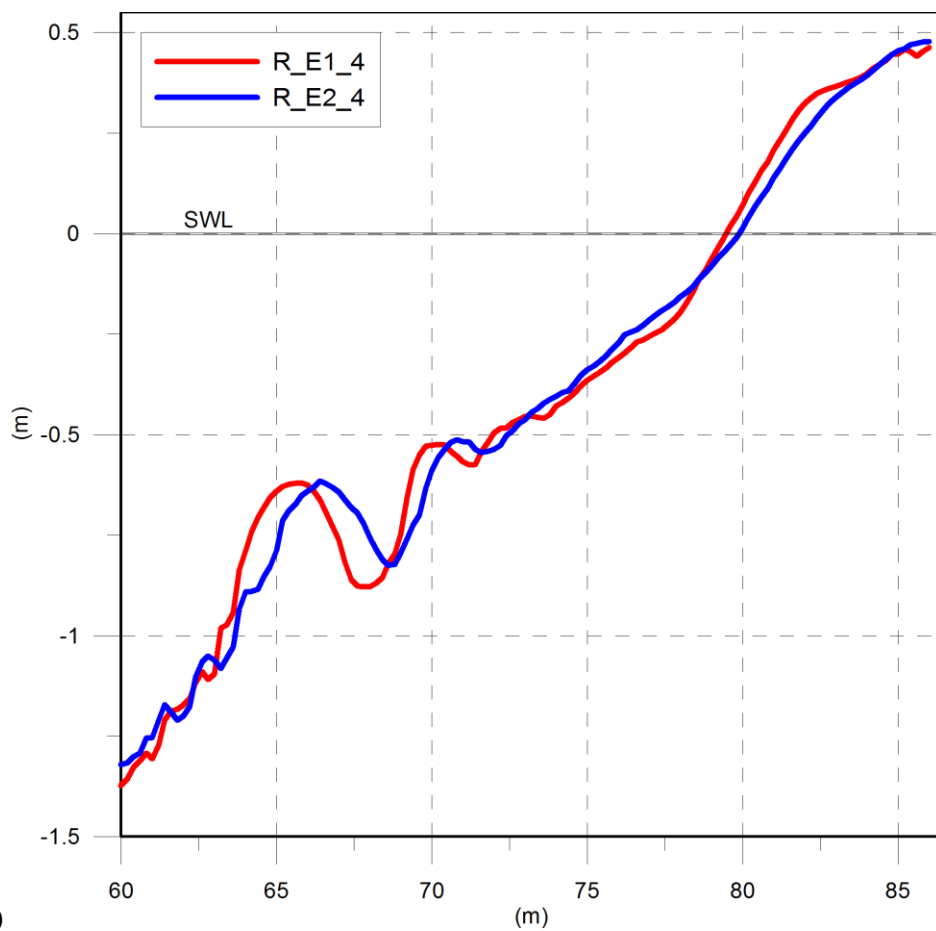
The hydro-morphodynamic results obtained from CIEM experiments, show how the characterization of sea states in terms of spectral characteristics (i.e. in the frequency domain) may be insufficient. The random wave cases were designed to have the same mean energy flux and characterized by different groupiness factors. The groupiness factor can be taken as a measure of the correlation between following higher waves in a given sea state. In other words, the random waves had the only difference in the time domain. Indeed, Figure 5.3a contrasts the two energy spectra calculated by the third offshore wave gauge (wg3, located at 10.7m from the wave paddle) for the erosive random cases, R\_E1 and R\_E2: only small

discrepancies can be found. In contrast, comparing their morphological response, significant influences on longshore bar development may be appreciated (Fig. 5.3b). In more detail, consistent with the observations for the bichromatic groups, the broader banded random waves (R\_E2) appear to generate a bar that is further landward than for the narrower banded waves. Hence, it seem that the groupiness factor has the same effect of the phase correlation for bichromatic waves. Note, however, that energy spectra for bichromatic wave cases was significantly different (Fig. 5.4a,b).

This results lead to significant implications for modelling purposes, because random waves are usually employed for real sea state simulations. Hence, as suggested by Brocchini and Baldock (2008), instead of choosing a single representative swash based on a representative wave height and wave period, future broad-scale modelling should follow a deterministic-probabilistic approach to account for random wave runup.

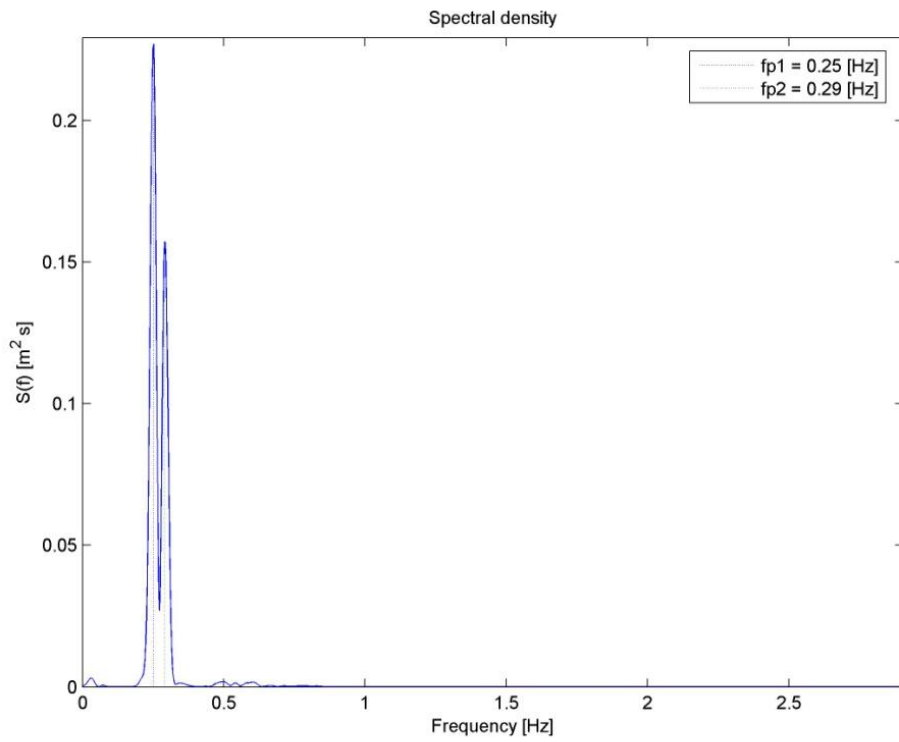


a)

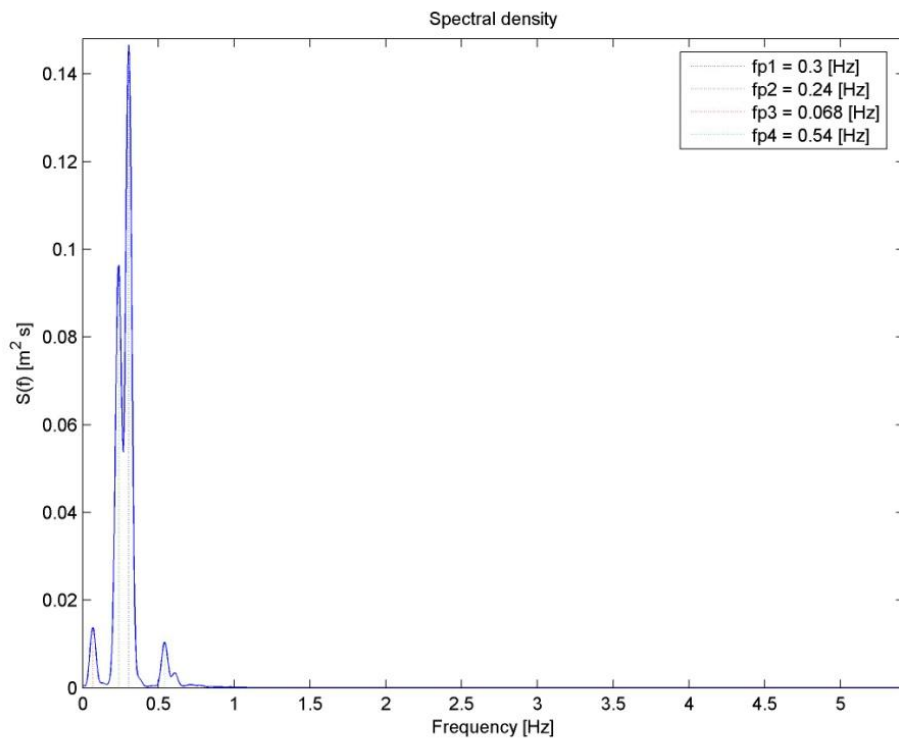


b)

Figure 5.3. a) Comparison of energy density spectra by wg3 for random wave cases; b) Beach profile comparison. Red line, R\_E1; Blue line, R\_E2;



a)



b)

Figure 5.4. Comparison of energy density spectra for bichromatic wave cases; a) Bichromatic waves with narrower bandwidth (B\_E1); b) Bichromatic waves with broader bandwidth (B\_E2).

## 5.2 Summary of key results and Conclusion

The modelling of SZ hydrodynamics and sediment transport and the resulting morphodynamics has been an area of very active research over the last decade. However, many details are still to be understood, whose knowledge will be greatly advanced by the collection of high-quality data obtained under controlled large-scale laboratory conditions. The advantage of using a large wave flume is that scale effects that affected previous laboratory experiments are minimized.

This Thesis presents new large-scale laboratory data from two sets of experiments. Physical models testing were performed in the large-scale wave flumes at Grosser Wellen Kanal (GWK) in Hannover and at Catalonia University of Technology (UPC) in Barcelona, within the Hydralab III program.

The tests carried out at the GWK aimed at improving the knowledge of the hydrodynamic and morphodynamic behaviour of the beach containing a Beach Drainage System. The approach taken in this study entails a program of experiments that fill gaps left by previous studies with significant scale effects. Indeed, previous laboratory experiments undertaken to understand groundwater dynamics and hydrodynamic phenomena resulting from the presence of a drainage by investigators in Australia and Europe, had limitations with respect to the scale effects (e.g. grain size and hydraulic conductivity). In this sense, the complexity of the infiltration-induced stability problem suggested the need to obtain and operate on data acquired through high quality laboratory investigations at large scale.

Experiments were undertaken using a set of multiple drains, up to three working simultaneously, located below the beach and at variable distances from the shoreline. The experimental program was organized in series of tests with variable wave energy. The duration of the opening of the drains (1 h) during each test represented a time interval to achieve quasi-stationary conditions of the water table evolution inside the beach in which the beach follows, more slowly, a proper equilibrium configuration.

The results of the present experimental investigation reveal that for HE (High Energy) wave conditions the opening of drains exhibited a local stabilization effect in correspondence of the cone of depression. When two drains (D1+D2) were operative, the stabilized area was doubled in size with respect to that induced by drain D1 only. In any case, the drainage system was not able to have a proper overall effect on the beach stabilization. The

comparisons of relative vertical variation of bed level ( $\Delta z$ ) in tests with drains D1 and D3 operative highlights that drainage acting in the saturated zone (under exit point), D1, and in the unsaturated zone (above the exit point), D3, have similar effects.

For ME (Medium Energy) wave conditions drainage generated by a single drain in any position (D1, D2 or D3) seemed to be inadequate to produce a global stabilization effect. The simultaneous opening of drains D1 and D2 generated, after three hours of test, a good stabilization of the beach. The simultaneous opening of drains D1, D2 and D3 surprisingly triggered again the original erosive trend. The asymmetric increases of normal shear stresses due to the increasing of infiltration and the decreasing of exfiltration could provide a heuristic explanation about the inefficacy of 3 drains working simultaneously.

For LE (Low Energy) wave conditions the drainage system with one (D1) or two (D1 and D2) drains generated an increase in the natural accretive trend of the beach.

In conclusion, under HE wave condition the drainage system seemed to be inadequate to give any stabilizing effect; the largest benefits were visible with the simultaneous operation of two adjacent drains, simulating an unique drain of double diameter, for ME and LE tests, where a global beach stabilization and an increased accretion were respectively observed. The results obtained under ME conditions with 3 drains operative was undefined.

The poor performance of the system observed in the laboratory under different kinds of wave attacks proves to be dependent on the characteristics of the used sand and the drains, as well as their position. In particular, the failure of the installation was evident when the system was exposed to HE conditions. The better performance, in terms of beach stabilization, obtained during the ME and LE tests marks a threshold for an effective draining of the beach and suggests combining BDS with other coastal defences such as breakwaters to partially dissipate high waves and consequently prevent strong shoreline variations during storm conditions.

On the basis of the present results a better design for field installations may be achieved. However, further laboratory investigations could be performed to test a drainage system with an improved efficacy in terms of beach stabilization.

The tests carried out in the large wave flume at UPC had the intent to investigate the SZ under storm conditions. Physical model testing was performed in the large-scale CIEM wave flume at UPC, Barcelona, as part of the SUSCO (Swash zone response Under grouping Storm COnditions) experiment. Fourteen different wave conditions were used, encompassing

monochromatic waves, bichromatic wave groups and random waves. However, two tests contained errors due to a problem in wave generation and cross-tank asymmetry of the evolving beach profile. The experiments compared variations in beach profile evolution between monochromatic waves and unsteady waves with the same mean energy flux, and used both erosive and accretive conditions. The effect of groupiness has been examined using random waves with varying groupiness factor and bichromatic wave groups with different bandwidth. Furthermore, considering that free long waves are present in the surf zone, a comparison has been made among monochromatic conditions, monochromatic conditions perturbed with free long waves and wave conditions in which free and forced long waves are generated by wave groups .

The data demonstrate that increasing differences in the spectral wave components, through perturbations of monochromatic waves with very long waves, or enlarging the bandwidth in bichromatic wave groups, or decreasing the grouping factor in random waves, promotes the offshore shifting of bed forms, in particular the bar and the swash berm. The greatest relative vertical variations in the surf zone are obtained in the erosive bichromatic case with narrow bandwidth (B\_E1), while those ones in the SZ are observed in the accretive combination case with smaller long waves (C\_E2). Considering that free long waves are generated from grouping, and that the bed form shifting effect is really strong in the combination cases, it is suggested that the offshore shifting is due to the larger long waves, while the greatest changes in the beach profile is strongly related to the waves grouping. Some of the relevant morphodynamic results are:

- during erosive conditions, bichromatic waves and random waves generate much greater erosion and offshore transport than an equivalent monochromatic wave with the same mean energy flux;
- accretive random wave conditions having different grouping factor (R\_A1 and R\_A2) show only slight differences in beach profile;
- the maximum topographical gradient in accretive condition was generated in test C\_A2 in which the backshore profile shows a large swash berm;
- during accretive conditions, bichromatic waves and random waves generate much less accretion and landward sediment transport than the equivalent combination wave cases with the same mean short-wave energy flux;
- the long-wave effect is the widening of the region where sediment transport takes place, through a modulation of the breakpoint and the modulation of the short wave runup;

- random waves and bichromatic waves generate very similar changes in beach morphology and similar sediment transport rates.

Net cross-shore transport rates were calculated from beach profile measurements made at half-hourly and hourly intervals. Consistent with recent small-scale experiments (Baldock et al., 2010), the data suggest that free long waves in combination with monochromatic waves promote onshore sediment transport compared to monochromatic waves only, although the lack of data for two cases makes it difficult to provide firm conclusions. Very clearly, the bichromatic wave groups greatly increase offshore transport during erosive conditions, and generate breaker bars that are larger and further offshore. Similarly, the bichromatic wave groups reduce onshore transport during accretive conditions. The random waves have a similar influence to the bichromatic wave groups, promoting offshore transport in comparison to the monochromatic conditions. The data indicate that including sediment transport effects induced by wave groups is important for improved nearshore morphological modelling of cross-shore beach profile evolution. It is suggested that the large change in the beach response between monochromatic conditions and wave groups is a result of the wave groupiness, rather than the presence of the forced and free long waves induced by the groupiness. It is suggested that an equilibrium-state model provides a heuristic explanation of the influence of wave groups, in that the effective relative fall velocity is larger than for monochromatic waves with the same incident energy flux. These general trends are very consistent with those observed by Baldock et al. (2007) and Baldock et al. (2010) in small scale tests.

Finally, the data provide a comprehensive and controlled series of tests for evaluating numerical models.

## REFERENCES

- Aagaard, T. (1990). Infragravity waves and nearshore bars in protected, storm-dominated coastal environments, *Marine Geology*, 94(3), 181-203.
- Aagaard, T., et al. (1994). Cross-shore structure of infragravity standing-wave motion and morphological adjustment - an example from northern Zealand, Denmark, *Journal of Coastal Research*, 10(3), 716-731.
- Aagaard, T. and Greenwood, B., 2008. Infragravity wave contribution to surf zone sediment transport - the role of advection. *Marine Geology*, 251(1-2): 1-14
- Agnon, Y. (1993). On a uniformly valid model for surface wave interaction. *Fluid Mech.* 247 : pp 589-601
- Alsina, J., T. Baldock, M. Hughes, F. Weir, and J. Sierra (2005), Sediment transport numerical modelling in the swash zone, paper presented at the Coastal Sediments 2007, Am. Soc. of Civ. Eng., New Orleans, La.
- Alsina, J.M. and Cáceres, I., 2010. Sediment suspension events in the nearshore. Measurements in large scale and high energy conditions. *Coastal Engineering* (submitted)
- Ang, L.S., Sum, C.H.-Y., Baldock, T.E., Li, L., Nielsen, P., December 13–17 2004. Measurement and Modelling of Controlled Beach Groundwater Levels Under Wave Action. 15th Australasian Fluid Mechanics Conference, The University of Sydney, Sydney, Australia.
- Anfuso, G. 2005. Sediment-activation depth values for gentle and steep beaches. *Marine Geology* 220 (2005) 101–112
- Anthony, E.J., 1998. Sediment-wave parametric characterization of beaches. *J. Coast. Res.* 14, 347–352.
- Archetti, R., Brocchini, M., 2002. An integral swash zone model with friction: an experimental and numerical investigation. *Coastal Engineering* 45, 89–110.
- Bagnold, R.A., 1940. Beach formation by waves: some model experiments in a wave tank. *Journal of the Institution of Civil Engineers* 15, 27–52.
- Bagnold, R.A., 1954. Experiments on a gravity-free dispersion of large solid sphere in a Newtonian fluid under shear. *Proc. R. Soc. London A*225, 49^63.
- Bagnold, R. A. (1956), The flow of cohesionless grains in fluid, *Philos. Trans. R. Soc. London, Ser. A*, 249(964), 235– 297.
- Bagnold, R.A., 1963. Mechanics of marine sedimentation. In: M.N. Hill (Ed.), *The Sea*, Vol. 3, Wiley- Interscience, New York, pp. 507–528.
- Bagnold, R.A., 1966. An Approach to the Sediment Transport Problem from General Physics. 422-I, US Geological Survey, Washington, DC.
- Barnes, T., 1996. The generation of low-frequency water waves on beaches, Ph.D. Thesis, University of Bristol, U.K.
- Bakhtyar, R., Barry, D.A., Li, L., Jeng, D.S., Yeganeh-Bakhtiary, A., 2009. Modeling sediment transport in the swash zone: a review. *Ocean Engrg.*, 36, 767-783.

- Bakhtyar, R., Brovelli, A., Barry, D.A., Li, L., 2011. Wave-induced water table fluctuations, sediment transport and beach profile change: Modeling and comparison with large-scale laboratory experiments. *Coastal Engineering* 58 (2011) 103–118.
- Bailard, J.A., Inman, D.L., 1981. An energetics bedload model for a plane sloping beach. *J. Geophys. Res.* 86, 2035–2043
- Baird, A.J., Horn, D.P., 1996. Monitoring and modelling ground water behaviour in sandy beaches. *Journal of Coastal Research* 12 (3), 630–640.
- Baird, A.J., Mason, T.E., Horn, D.P., 1998. Validation of a Boussinesq model of beach ground water behaviour. *Marine Geology* 148, 55–69.
- Baldock, T.E., 2009. Bound wave release induced by short wave breaking - true or false? In: M. Mizuguchi and S. Sato (Editors), *Proceedings of Coastal Dynamics 2009*.
- Baldock, T. (2009). Discussion of “Measurement of wave-by-wave bed-levels in the swash zone” by Turner, I.L., Russell, P.E., Butt, T. *Coastal Engineering*, 56, pp. 380-381
- Baldock, T. E., Alsina, J., Caceres, I., Vicinanza, D., Contestabile, P., Power, H., Sanchez-Arcilla, A. (2011). “Large-scale experiments on beach profile evolution and sediment transport induced by long waves, wave groups and random waves”, *Coastal Engineering*, ISSN 0378-3839, vol. 58, pp. 214-227.
- Baldock, T.E., Holmes, P., Horn, D.P. 1997. Low frequency swash motion induced by wave grouping. *Coastal Engineering* 32, pp. 197-222.
- Baldock, T.E., Huntley, D.A., Bird, P.A.D., O'Hare, T.J. and Bullock, G.N., 2000. Breakpoint generated surf beat induced by bichromatic wave groups. *Coastal Engineering*, 39(2-4), pp. 213-242.
- Baldock, T. E. and Huntley D. A. (2002). Long-wave forcing by the breaking of random gravity waves on a beach. *Proceedings of the Royal Society, A*, 458: 2177 - 2201.
- Baldock, T. E., and O'Hare T. J. (2004), Energy transfer and dissipation during surf beat conditions. *Proc. 29th Int. Conf. Coastal Engineering*. pp. 1212–1224. Lisbon, ASCE.
- Baldock, T.E., Hughes, M.G., Day, K. and Louys, J., 2005. Swash overtopping and sediment overwash on a truncated beach. *Coastal Engineering*, 52(7): 633-645.
- Baldock, T. E., Manoonvoravong, P. and Pham K. S., 2007. Beach face morphology and surf beat sediment transport. *Journal of Coastal Research*, SI 50 (Proceedings of the 9th International Coastal Symposium), 631-635. Gold Coast, Australia, ISSN 0749.0208.
- Baldock, T. E., Manoonvoravong, P. and Kim Son Pham, (2010). Sediment transport and beach morphodynamics induced by free long waves, bound long waves and wave groups. *Coastal Engineering*, 57, 898-916.
- Baldock, T.E., Swan, C., Taylor, P.H., 1996. A laboratory study of nonlinear surface waves on water. *Philos. Trans. R. Soc. Lond., A* 354, 649–676.
- Bagnold, R.A. (1940). Beach formation by waves: some model experiments in a wave tank. *J. Inst. Civil Eng.* 15, 27–53.

- Barry, D.A., Barry, S.J., Parlange, J.-Y., 1996. Capillarity correction to periodic solution of the shallow flow approximation. In: Pattiaratchi, C.B. (Ed.), *Mixing Processes in Estuaries and Coastal Seas*. Coastal and Estuarine Studies 50. American Geophysical Union, Washington, DC, pp. 496–510.
- Bascom, W.H., 1951. The relationship between sand size and beach face slope. *Transactions, American Geophysical Union* 32, 866–874.
- Battjes, J.A., 1974. Surf similarity. In: *Proceedings of the 14th International Conference on Coastal Engineering ASCE*, pp. 466–480.
- Battjes, J. A. 1988 Surf zone dynamics. *A. Rev. Fluid Mech.* 20, 257-293.
- Battjes, J. A., H. J. Bakkenes, T. T. Janssen and A. R. van Dongeren (2004). Shoaling of subharmonic gravity waves. *Journal of Geophysical Research*. 109, C02009, doi:10.1029/2003JC001863.
- Baquerizo, A., Losada, M.A., Smith, J.M., and Kobayashi, N., 1997. Cross-shore variation of wave reflection from beaches. *J. of Waterway, Port, Coastal, and Ocean Engrg.*, 123(5), 274-279.
- Bauer, B.O., Greenwood, B., 1988. Surf-zone similarity. *Geogr. Rev.* 78, 137–147.
- Beach, R.A., and Sternberg, R.W., 1991. Infragravity driven suspended sediment transport in the swash, inner and outer-surf zone. *Proceedings Coastal Sediments 1991*. American Society of Civil Engineers, New York, pp 114-128.
- Bejan, A., 1997. *Advanced Engineering Thermodynamics*, Chapter 13, second ed. Wiley, New York.
- Bellotti, G., R. Archetti, and M. Brocchini (2003), Experimental validation of mean swash zone boundary conditions, *J. Geophys. Res.*, 108(C8), 3250, doi:10.1029/2002JC001510.
- Bellotti, G., and M. Brocchini (2005), Swash zone boundary conditions for long wave models, *Coastal Eng.*, 52, 971–976.
- Blewett, J.C., Holmes, P., Horn, D.P., 2000. Field measurements of swash hydrodynamics on sand and shingle beaches: implications for sediment transport. In: *Proceedings of the 27th International Conference on Coastal Engineering*. American Society of Civil Engineers, New York, pp. 597–609.
- Bodge, K.R., Dean, R.G., 1987. Short-term impoundment of longshore transport. In: Kraus, N.C. (Ed.), *Coastal Sediments '87*. American Society of Civil Engineers, New York, pp. 468–483.
- Borthwick, A.G.L., Hunt, A.C., Feng, T., Taylor, P.H., Stansby, P.K., 2006. Flow kinematics of focused wave groups on a plane beach in the U.K. *Coastal Research Facility. Coastal Engineering* 53 (2006) 1033–1044
- Bowen, A. J. (1980). Simple models of nearshore sedimentation: beach profiles and longshore bars. In: McCann, S. B. (Ed.). *The Coastline of Canada*, Geological Survey of Canada.80-10: 1-11.

- Bowen, A. J., and D. L. Inman, Edge waves and crescentic bars, *J. Geophys. Res.*, 76, 8662–8671, 1971.
- Bowen, A. J. and D. A. Huntley (1984). Waves, long waves and nearshore morphology. *Marine Geology* 60, 1-13.
- Bowman, D., Ferri, S., Pranzini, E. (2007). Efficacy of beach dewatering-Alassio, Italy. *Coastal Engineering*, 16, pp. 197-208.
- Bradshaw, M.P., 1980. Topographic control of run-up variability. *Proc. 17th Int. Conf. Coastal Eng.*, ASCE, pp. 1091–1105.
- Bradshaw, M.P., 1982. Bores and swash on natural beaches. *Coastal Studies Unit Technical Report No. 82/4*, University of Sydney, 107 pp.
- Brocchini, M., Peregrine, D.H., 1996. Integral flow properties of the swash zone and averaging. *Journal of Fluid Mechanics* 317, 241– 273.
- Brocchini, M. 1997. Eulerian and Lagrangian aspects of the longshore drift in the surf and swash zones. *Journal of Geophysical Research – Oceans* 102(C10), pp. 23155-23169.
- Brocchini, M. and Bellotti, G. 2002. Integral flow properties of the swash zone and averaging. Part 2. Shoreline boundary conditions for wave-averaged models. *Journal of Fluid Mechanics* 458, pp. 269-281.
- Brocchini, M. and Baldock, T.E., 2008. Recent advances in modeling swash zone dynamics: Influence of surf-swash interaction on nearshore hydrodynamics and morphodynamics. *Rev. Geophys.*, 46, RG3003.
- Bruun, P. (2005). Beach drain. In: Schwartz, M.L. (Ed.), *Encyclopedia of Coastal Science*. Springer, pp. 138–140
- Butt, T., Russell, P., 1999. Suspended sediment transport mechanisms in high energy swash. *Mar. Geol.* 161, 361–375.
- Butt, T., and P. Russell (2000), Hydrodynamics and cross-shore sediment transport in the swash-zone of natural beaches: A review, *J. Coastal Res.*, 16, 255–268.
- Butt, T., Russell, P., Puleo, J.A., Miles, J., Masselink, G., 2004. The influence of bore turbulence on sediment transport in the swash and inner surf zones. *Continental Shelf Research* 24, 757–771.
- Butt, T., Russell, P., Puleo, J.A., Masselink, G., 2005. The application of Bagnold-type sediment transport models in the swash zone. *Journal of Coastal Research* 21, 887–895.
- Cáceres, I., J.M. Alsina and A. Sánchez-Arcilla (2009). Mobile bed experiments focused to study the swash zone evolution. *ICS 2009, Journal of Coastal Research*, SI 56, 1736-1740
- Carlson, C., Field studies of run-up on dissipative beaches, paper presented at 19th International Conference of Coastal Engineering, Am. Soc. of Civ. Eng., Reston, Va., 1984.
- Carstens, M.R, Neilson, F.M., Altinbilek, H.D. 1969. Bedforms generated in the laboratory under an oscillatory flow, *CERC Tech Memo* 28.

- Carter, T. G., P. L.-F. Liu and C. C. Mei (1973). Mass transport by waves and offshore sand bedforms. *J. Wtrwy. Hrbrs. and Coast. Eng. Div., Proc. American Society of Civil Engineers*, 99, 165-183.
- Carter, R.W.G., 1988. *Coastal Environments*. Academic Press. 617 pp.
- Cartwright, N., Nielsen, P., and Jessen, O.Z., 2002. Swash zone and near-shore watertable dynamics. *Proc. of 28th ICCE, Cardiff*, 1006-1015.
- Cartwright, N., Nielsen, P., 2003. Dynamics of the salt–freshwater mixing zone in ocean beaches. In: *Proceedings of the Second International Conference on Saltwater Intrusion and Coastal Aquifers, Merida, Mexico, CD-ROM*.
- Cartwright, N., Li, L., Nielsen, P., 2004a. Response of the salt–freshwater interface in a coastal aquifer to a wave induced groundwater pulse: field observations and modelling. *Advances in Water Resources* 27, 297–303.
- Cartwright, N., Nielsen, P., Li, L., 2004b. Experimental observations of watertable waves in an unconfined aquifer with a sloping boundary. *Advances in Water Resources* 27, 991–1004.
- Cartwright, N., Nielsen, P., Li, L., 2004c. The influence of offshore storm waves on groundwater dynamics and salinity in a sandy beach. In: *Proceedings of the 29th International Conference on Coastal Engineering, World Scientific, Singapore*, pp. 1841–1850.
- Cartwright, N., Baldock, T.E., Nielsen, P., Jeng, D.-S., Tao, L. 2005 forthcoming. Swash–aquifer interaction in sandy beaches. *Coasts and Ports, 17th Australasian Coastal and Ocean Engineering Conference, Adelaide, Australia, September 2005*.
- Cartwright, N. Jessen, O.Z., Nielsen, P., In press. Application of a coupled ground–surface water flow model to simulate periodic groundwater flow influenced by a sloping boundary, capillarity and vertical flows. *Environmental Modelling and Software*.
- Chappel, J., Eliot, I.G., Bradshaw, M.P., Lonsdale E. (1979). Experimental Control of beach face dynamics by watertable pumping, *Engineering Geology*, 14, 29-41.
- Chiaia, G., Damiani, L., Ranieri, G. (2005). Experimental analysis of the water table of a beach equipped with a drainage system. *Proc. 31th IAHR Congress Seoul*, E12(4), 5919–5929.
- Ciavola, P., Ferreira, G., Taborda, R., Alveirinho Dias, J., 1995. Field assessment of longshore transport at Culatra Island (Portugal) using sand tracers. In: *Sodre Borges, F., Marques, M.M. (Eds.), Resumos alargados do IV Congresso Nacional de Geologia. Mem. Mus. Lab. Mineral. Geol. Univ. Port0 4*, 905-909.
- Ciavola, P., Taborda, R., Ferreira, O. and Dias, J.M.A. (1997). Field observations of sand-mixing depths on steep beaches. *Marine Geology*, 141, 147-156.
- Ciavola, P., Nadalini, F. and Ardone, V. (2006). Depth of sand activation on protected and non-protected nourished beaches: a laboratory study in a large-scale wave flume. *Proceedings of Coastal Dynamics 2005, ASCE, New York, USA (CD-ROM)*.

- Ciavola, P., Vicinanza, D., Fontana E. (2008). Beach drainage as a form of shoreline stabilization: case studies in Italy. Proceedings of 31 International Conference on Coastal Engineering, pp. 2646-2658.
- Ciavola, P., Fontana, E., Vicinanza D. (2009). Performance of a beach drainage system at Lido Adriano (Ravenna – Italy). Proceedings of the 33 International Association of Hydraulic Engineering & Research (IAHR) Biennial Congress, Vancouver, Canada, pp. 7312-7319.
- Ciavola, P., Vicinanza, D., Aristodemo, F., and Contestabile, P., 2010. Full scale experiments on a Beach Drainage System: morphodynamic analysis. Journal of Hydr. Res., SI P3974.
- Ciavola P., Vicinanza D., Aristodemo F., Contestabile P., (2011). “Large-scale morphodynamic experiments on a Beach Drainage System”, Journal of hydraulic research, Vol. 49, n. 4, pp. 523-528.
- CIRIA (1996). Beach management manual. Report 153. Construction Industry Research and Information Association, London.
- Clarke, D.J., Eliot, I.G., Frew, J.R., 1984. Variation in subaerial beach sediment volume on a small sandy beach over a monthly lunar cycle. Marine Geology 58, 319– 344.
- Coco, G., D. A. Huntley, and T. J. O’Hare, 2000. Investigation of a self-organisation model for beach cusp formation and development, J. Geophys. Res., 105, 21,991– 22,002.
- Conley, D. C., Falchetti, S., Lohmann, I. P., and Brocchini, M., 2008. The effects of flow stratification by non-cohesive sediment on transport in high-energy wave-driven flows. J. Fluid Mech. (2008), vol. 610, pp. 43–67. 2008 Cambridge University Press
- Contestabile, P., Aristodemo, F., Vicinanza, D., Ciavola, P. (2011). “Laboratory study on a beach drainage system”, Coastal Engineering, ISSN 0378-3839, vol. ??, pp. ???-??? (submitted).
- Conley, D.C., Beach, R.A., 2003. Cross-shore sediment transport partitioning in the nearshore during a stormevent. J. Geophys. Res.108 (C3). doi:10.1029/2001JC001230.
- Conley, D.C., Falchetti, S., Lohmann, I.P., Brocchini, M. (2008) The effects of flow stratification by non-cohesive sediment on transport in high-energy wave-driven flows. J. Fluid Mech., 610, 43-67.
- Conley, D.C., Griffin, J.G., 2004. Direct measurements of bed stress under swash in the field. Journal of Geophysical Research 109, C03050.
- Conley, D.C., Inman, D.L., 1992. Field observations of the fluid-granular boundary layer under near-breaking waves. J. Geophys. Res. 97, 9631^9643.
- Conley, D.C., Inman, D.L., 1994. Ventilated oscillatory boundary- layers. Journal of Fluid Mechanics 273, 261–284.
- Cowen, E.A., Sonu, I.M., Liu, P.L.-F., Raubenheimer, B., 2003. PIV measurements within a laboratory generated swash zone. Journal of Engineering Mechanics 129, 1119–1129.
- Cox, D.T., Hobensack, W.A., Sukumaran, A., 2000. Bottom stress in the inner surf and swash zone. Proceedings 27<sup>th</sup> International Conference on Coastal Engineering, ASCE, pp. 108–119.

- Dally, W. R. (1987). Longshore bar formation-surf beat or undertow? Proceedings of Special Conference on Coastal Sediments. American Society of Civil Engineers. 71-86.
- Dally, W. R. (1991). Long wave effects in laboratory studies of cross-shore transport. Proceedings of Special Conference on Quantitative Approaches to Coastal Sediment Processes. American Society of Civil Engineers. 85-99.
- Dally, W. R. & Dean, R. G. 1986 Transformation of random breaking waves on surf beat. In Proc. 20th Int. Conf. Coastal Engineering, pp. 109-123. New York: American Society of Civil Engineers.
- Dalrymple, R.A., 1992. Prediction of Storm/Normal Beach Profiles. Journal of Waterway, Port, Coastal, and Ocean Engineering, 118(2): 193-200.
- Damiani, L., Aristodemo, F., Saponieri, A., Verbeni, B., Veltri, P., and Vicinanza, D., 2010. Full scale experiments on a Beach Drainage System: hydrodynamic effects inside the beach. Journal of Hydr. Res., SI Hydralab III.
- Damiani, L., Ranieri, G., Rossetti, R. (2003). Coastal protection with BMS: the first experience in Italy. Proceedings of the 6 Conference on Coastal Engineering, pp. 568-576.
- Damiani, L., Petrillo, A., Saponieri, A. (2009) Beach Dewatering Systems: modelling coastal ground-water flow. Proceedings of the 33 International Association of Hydraulic Engineering & Research (IAHR) Biennial Congress, Vancouver, Canada
- Damiani, L., Vicinanza, D., Aristodemo, F., Saponieri, A., Corvaro, S., 2011. Experimental investigation on wave set-up and nearshore velocity field in presence of a BDS. Journal of Coastal Research, SI 64 (Proc. of 11<sup>th</sup> ICS), Szczecin, 1-5.
- Dean, R. G. (1973). Heuristic models of sand transport in the surf zone. Proc. Conf. on Engineering Dynamics in the Surf Zone. Sydney. N.S.W. 208-214.
- Dean, R. G. (1985), Physical modeling of littoral processes, in Physical Modelling in Coastal Engineering, edited by R. A. Dalrymple, pp. 119-139, Balkema, Rotterdam.
- Dean, R.G. (1990). Independent analysis of beach changes in the vicinity of the Stabeach system at Sailfish Point, Florida. Unpublished report prepared for Coastal Stabilization Inc. (16 pp).
- Dean and Dalrymple, Water Wave Mechanics for Engineers and Scientists, 2002 (Handbook).
- Deigaard, R., Fredsøe, J., Hedegaard, I.B., 1986. Suspended sediment in the surf zone. J. Waterw., Port, Harbors Coastal Ocean Eng., Am. Soc. Civ. Eng. 112 (1), 115– 128.
- Deigaard, R., J. B. Jakobsen and J. Fredsøe (1999). Net sediment transport under wave groups and bound long waves. Journal of Geophysical Research-Oceans. 104(C6): 13559-13575.
- Dolphin. T.J., Hume, T.M., Parnell, K.E., 1995. Oceanographic processes and sediment mixing on a sand flat in an enclosed sea, Manukau Harbour. New Zealand. Mar. Geol. 128.1699181.
- Drake, T., and J. Calantoni (2001), Discrete particle model for sheet flow sediment transport in the nearshore, J. Geophys. Res., 106, 19,859–19,868.

- Duncan Jr. J.R. (1964). The effects of watertable and tide cycle on swash-backwash sediment distribution and beach profile development, *Marine Geology*, 2 (3), 186-197.
- Elfrink, B. and Baldock, T., 2002. Hydrodynamics and sediment transport in the swash zone: a review and perspectives. *Coastal Engineering*, 45(3-4), pp. 149-167.
- Elgar, S., Herbers, T.H.C., Okihiro, M., Oltman-Shay, J., Guza, R.T., 1992. Observations of infragravity waves. *J. Geophys. Res.* 97, 15573–15577
- Eliot, I.G., Clarke, D.J., 1986. Minor storm impact on the beachface of a sandy beach. *Marine Geology* 73, 61– 83.
- Eliot, I.G., Clarke, D.J., 1988. Semi-diurnal variation in beach face aggradation and degradation. *Marine Geology* 79, 1– 22.
- Emery, K.O., Foster, J.F., 1948. Water tables in marine beaches. *Journal of Marine Research* 7, 644–654.
- Engelund, F. and Hansen, E. 1972. A monograph on sediment transport in alluvial streams. Teknisk Forlag, Copenhagen.
- Erikson, L., Larson, M., Hanson, H., 2005. Prediction of swash motion and run-up including the effects of swash interaction. *Coastal Engineering* 52, 285–302.
- Ferreira, O., Ciavola, P., Taborda, Rr., Bairros, M. and Dias J.M.A. (2000). Sediment mixing depth determination for steep and gentle foreshores. *Journal of Coastal Research*, 16, 830-839.
- Fredsøe, J., Deigaard, R., 1992. Mechanics of coastal sediment transport. Advanced series on Ocean Engineering, vol. 3. World Scientific. 366 pp.
- Fredsøe, J., Sumer, B.M., 1997. Scour at the round head of a rubble mound breakwater. *Coast. Eng.* 29 (3–4), 231– 262.
- Fredsøe, J., Sumer, B.M., Kozakiewicz, A., Chua, L. H.C., Deigaard, R. Effect of externally generated turbulence on wave boundary layer. *Coastal Engineering* 49 (2003) 155–183.
- Freeze, R.A., Cherry, J.A., 1979. *Groundwater* Prentice-Hall, Englewood Cliffs, NJ.
- Fucella, J.E., Dolan, R.E., 1996. Magnitude of subaerial beach disturbance during northeast storms. *J. Coastal Res.* 12 (2), 420-429.
- Gallagher, B., 1971. Generation of surf beat by non-linear wave interactions. *J. Fluid Mech.* 49, 1–20.
- Gómez-Pujol, L., Orfila, A., Cañellas, B., Alvarez-Ellacuria, A., Méndez, F.J., Medina, R., Tintoré, J., 2007. Morphodynamic classification of sandy beaches in low energetic marine environment. *Mar. Geol.* 242, 235–246.
- Goda, Y. 1975. Irregular wave deformation in the surf zone. *Coastal Engineering in Japan* 18, pp. 13-26.
- Goda, Y. and Suzuki, Y., 1976. Estimation of incident and reflected waves in random wave experiments. *Proc. of 15<sup>th</sup> ICCE, Honolulu*, 1, 828-845.

- Goda, Random Seas and Design of Maritime Structures, 2002. (Handbook).
- Goring, D.G. and Nikora, V.I., 2002. Despiking acoustic Doppler velocimeter data. *Journal of Hydraulic Engineering*, 128(1): 117-126.
- Gourlay, M.R., 1992. Wave set-up, wave run-up and beach water table: interaction between surf zone hydraulics and groundwater hydraulics. *Coastal Engineering* 17, 93– 144.
- Gourlay, M.R., 1968. Beach and Dune Erosion Tests. Delft Hydraulics Laboratory, Report no. M935/M936.
- Grant, U.S., 1946. Effects of groundwater table on beach erosion. *Geological Society of American Bulletin* 57, 1952 (abstract).
- Grant, U.S. (1948). Influence of the water table on beach aggradation and degradation, *Journal of Marine Research*, 7, 655-660.
- Greenwood, B., Hale, P.B.. 1980. Depth of activity. sediment flux and morphological change in a barred nearshore environment, In: McCann, S.B. (Ed.). *The Coastline of Canada*. Pap. 80-10. *Geol. Surv. Can.*, Halifax. pp. 89 109.
- Greenwood, B., and Osborne, 1990. Vertical and horizontal structure in cross-shore flows: An example of undertow and wave set up on a barred beach. *Coastal Engng.*, 14, 543-580.
- Guard, P., and T. Baldock (2007), The influence of seaward boundary conditions on swash zone hydrodynamics, *Coastal Eng.*, 54, 321–331.
- Guy, H.P., Simons, D.B., and Richardson, E.V. 1966. Summary of alluvial channel data from flume experiments, 1956-1961, U.S. Geographical Survey, Prof paper 462-I, Washington DC.
- Guza, R.T., Inman, D.L., 1975. Edge waves and beach cusps. *J. Geophys. Res.* 80, 2997–3012
- Guza, R.T., Thornton, E.B., 1982. Swash oscillations on a natural beach. *J. Geophys. Res.* 87 (C1), 483– 491
- Guza, R., and E. Thornton (1985), Observations of surf beat, *J. Geophys. Res.*, 90, 3161–3172.
- Hamm, L., Madsen, P. A. & Peregrine, D. H. 1993 Wave transformation in the nearshore: a review. *Coastal Engng* 21, 5-39.
- Hanes, D. M., and D. L. Inman (1985b), Experimental evaluation of a dynamic yield criterion for granular-fluid flow, *J. Geophys. Res.*, 90(B5), 3670– 3674.
- Hansen, J.B., Svendsen, I.A. (1984). A theoretical and experimental study of undertow. *Proc.19th Conf. Coastal Eng.*, 2246–2262. ASCE, New York.
- Hald, T. (1995). Wave group analysis by means of the Hilbert transform technique. *Hydraulics & Coastal Engineering Laboratory, Aalborg University*. Internal note.
- Hardisty, J., 1990. *Beaches: Form and Process* Unwin Hyman, London.

- Hardisty, J., Collier, J., Hamilton, D., 1984. A calibration of the Bagnold beach equation. *Marine Geology* 61, 95-101.
- Hattori, M., and R. Kawamata (1980), Onshore-Offshore transport and beach profile change, in *Proc. 17th Coastal Engineering Conference*, 2, 1175-1193, ASCE.
- Hegge, B.J., Masselink, G., 1991. Groundwater-table responses to wave run-up: an experimental study from Western Australia. *Journal of Coastal Research* 7 (3), 623–634.
- Herbers, T.H.C., Elgar, S., Guza, R.T., 1995a. Generation and propagation of infragravity waves. *J. Geophys. Res.* 100, 24863–24872.
- Herbers, T.H.C., Elgar, S., Guza, R.T., O'Reilly, W.C., 1995b. Infragravity frequency (0.005–0.05 Hz) motions on the shelf: II. Free waves. *J. Phys. Oceanogr.* 25, 1063–1079.
- Hibberd, S., Peregrine, D.H., 1979. Surf and run-up on beaches: a uniform bore. *J. Fluid Mech.* 95, 323– 345.
- Hoefel, F., and S. Elgar (2003), Wave-induced sediment transport and sandbar migration, *Science*, 299, 1885– 1887.
- Holland, K.T., Holman, R.A., 1999. Wavenumber-frequency structure of infragravity swash motions. *J. Geophys. Res.* 104 (C6), 13479– 13488.
- Holland, K.T., Puleo, J.A., 2001. Variable swash motions associated with foreshore profile change. *Journal of Geophysical Research* 106, 4613–4623.
- Holland, K.T., Raubenheimer, B., Guza, R.T., Holman, R.A., 1995. Runup kinematics on a natural beach. *J. Geophys. Res.* 100 (C3), 4985–4993.
- Holman, R. A. and A. J. Bowen (1982). Bar, bumps and holes: models for the generation of complex beach topography. *Journal of Geophysical Research.* 87, 457-468.
- Holman, R.A., 1986. Extreme value statistics for wave run up on a natural beach. *Coast. Eng.* 9, 527–544.
- Horn D. P., 2002. Beach groundwater dynamics, *Geomorphology* 48, pp. 121-146.
- Horn, D.P., Walton, S.M. (2004). Sediment-level oscillations in the swash zone of a mixed sand and gravel beach. *Proceedings of 29 International Conference on Coastal Engineering*. ASCE, vol. 3, pp. 2390-2402.
- Horn, D. (2006), Measurements and modelling of beach groundwater flow in the swash-zone: A review, *Cont. Shelf Res.*, 26, 622–652.
- Horn, D.P., Baldock, T.E., Li, L., 2007. The influence of groundwater on profile evolution of fine and coarse sand beaches. *Proceedings of Coastal Sediments '07*, New Orleans, ASCE, pp. 506–519.
- Howd, P.A., Holman, R.A. (1987). A simple model of beach foreshore response to long period waves. *Marine Geology*, 78, pp. 11-22.
- Hsiao, S.-C., Hwung, H.-H. and Lin, Y.-H., 2009. Swash motion driven by bichromatic wave groups over sloping bottoms. In: P. Lynett (Editor), *Nonlinear wave dynamics. Selected*

- papers of the Symposium held in honor of Philip I-F Liu's 60th birthday. World Scientific, pp. 223-246.
- Huang, N.E., Long, S.R., Shen, Z., 1996. The Mechanism for Frequency Downshift in Nonlinear Wave Evolution. *Advances in Applied Mechanics* Volume 32, 1996, Pages 59-117, 117A, 117B, 117C.
- Hughes, M.G., 1992. Application of a non-linear shallow water theory to swash following bore collapse on a sandy beach. *J. Coast. Res.* 8, 562– 578.
- Hughes, M.G., 1995. Friction factors for wave uprush. *J. Coastal Res.* 11, 1089– 1098.
- Hughes, M.G., Masselink, G., Hanslow, D., Mitchell, D., 1997a. Toward a better understanding of swash zone sediment transport. *Proc. Coastal Dynamics '97*. ASCE, Plymouth, pp. 804– 813.
- Hughes, M.G., Masselink, G., Brander, R.W., 1997b. Flow velocity and sediment transport in the swash zone on a steep beach. *Mar. Geol.* 138, 91– 103.
- Hughes, M.G., Moseley, A.S., 2007. Hydrokinematic regions within the swash zone. *Continental Shelf Research* 27 (15), 2000–2013.
- Hughes, M.G., Turner, I., 1999. The beach face. In: Short, A.D. (Ed.), *Handbook of Beach and Shoreface Morphodynamics*. Wiley, Chichester, pp. 119–144.
- Hunt, I. (1959), Design of seawalls and breakwaters, *J. Waterw. Harbors Coastal Eng. Div. Am. Soc. Civ. Eng.*, 85(WW3), 123– 152.
- Huntley, D.A., Guza, R.T., Bowen, A.J., 1977. A universal form for shoreline run-up spectra. *J. Geophys. Res.* 82, 2577– 2581.
- Huntley, D.A., Guza, R.T., Thornton, E.B., 1981. Field observations of surf beat: 1. Progressive edge waves. *J. Geophys. Res.* 86, 6451–6466.
- Iribarren, C.R., Nogales, C., 1949. Protection des ports. Sect. 2, comm. 4, 17th Int. Nav. Cong., Lisbon, p. 31– 80
- Jannat, M. R. A. and T. Asano (2007). External forces of sediment transport in surf and swash zones induced by wave groups and their associated long waves. *Coastal Engineering*. 49(2): 205-227.
- Jackson, D.W.T., Cooper, J.A.G., del Rio, L., 2005. Geological control of beach morphodynamic state. *Mar. Geol.* 216, 297–314.
- Jago, C.F., Hardisty, J., 1984. Sedimentology and morphodynamics of a macrotidal beach, Pendine Sands, SW Wales. *Marine Geology* 60, 123-154.
- Jiménez , J. A., Guillén, J., Falqués, A., 2008. Comment on the article “Morphodynamic classification of sandy beaches in low energetic marine environment” by Gómez-Pujol, L., Orfila, A., Cañellas, B., Alvarez-Ellacuría, A., Méndez, F.J., Medina, R. and Tintoré, J. *Marine Geology*, 242, pp. 235–246, 2007. *Marine Geology* 255 (2008) 96–101

- Johannessen, T., Swan, C., 2001. A laboratory study of the focusing of transient and directionally spread surface water waves. *Proc. R. Soc. Lond., A* 457, 971–1006.
- Jonsson, I.G., 1966. Wave boundary layers and friction factors, *Proc 10<sup>th</sup> Int Conf. Coastal Engineering*, Tokyo, 127-148.
- Kaihatu, J.M., Veeramony, J., Edwards, K.L., and Kirby, J.T., 2007. Asymptotic behavior of frequency and wave number spectra of nearshore shoaling and breaking waves. *J. Geophys. Res.*, 112(C06016), 1-15.
- Kajiura, K., 1968. A model of the bottom boundary layer in water waves, *Bulletin Earthquake Res, Institute*, 46, 75-123.
- Kang, H.-Y., Nielsen, P., 1996. Watertable dynamics in coastal areas. *Proceedings of the 25th International Conference on Coastal Engineering*. American Society of Civil Engineers, New York, pp. 4601–4612.
- Karambas, T.V., 2003. Modelling of infiltration–exfiltration effects of cross-shore sediment transport in the swash zone. *Coastal Engineering Journal of Japan* 45, 63–82.
- Karambas, T.V. (2009). Numerical study of the beach profile evolution due to a ‘coastal drain system’. *Proc. 33th IAHR Congress Vancouver* 12315, 1–8.
- Karunaratna, H., Chadwick, A., Lawrence, J., 2005 Numerical experiments of swash oscillations on steep and gentle beaches. *Coastal Engineering* 52 (2005) 497–511
- Kemp, P.H., Plinston, D.T., 1968. Beaches produced by waves of low phase difference. *Journal of the Hydraulics Division, ASCE* 94, 1183–1195.
- Kemp, P.H. 1975. Wave asymmetry in the nearshore zone and breaker area. In: Hails, J., Carr, A. (Eds.), *Nearshore Sediment Dynamics and Sedimentation*. Wiley-Interscience, London, pp. 47-67.
- Kirk, R.M., 1980. Mixed sand and gravel beaches: morphology, processes and sediments. *Progress in Physical Geography* 4, 189– 210.
- Kirkham, D., 1967. Explanation of paradoxes in Dupuit–Forchheimer seepage theory. *Proceedings of the Soil Science Society of America* 10, 58–68.
- Komar, P.D., 1998. *Beach Processes and Sedimentation*. Prentice-Hall, Englewood Cliffs, NJ.
- Kobayashi, N., DeSilva, G.S., Watson, K.D., 1989. Wave transformation and swash oscillation on gentle and steep slopes. *J. Geophys. Res.* 94, 951– 966.
- Kobayashi, N., A. K. Otta and I. Roy (1987). Wave reflection and run-up on rough slopes. *Journal of Water, Port, Coastal, and Ocean Engineering*. ASCE 113; 282-298.
- Kraus, N.C., 1992. Engineering approaches to cross-shore sediment transport processes. *Proc. of Short Course on Design and Reliability of Coastal Structures*, Venice, 175-209.
- Kraus, N. C., M. Larson, And D. I. Kriebel. 1991. Evaluation of beach erosion and accretion predictors, p. 572-587. In *Coastal Sediments '91*. American Society of Civil Engineers, Seattle, Washington.

- Kubota, S., Mizuguchi, M., Takezawa, M., 1993. Prediction of field swash and reflected wave distribution. *Coast. Eng. Jpn.* 36 (2), 111– 131.
- Lake, B. M. & Yuen, H. C. 1978 A new model for nonlinear wind waves. P a r t 1 : Physical model and experimental evidence. *J. Fluid Mech.* 88, 33-62
- Lambert, A., Rey, V., Samat, O., Provansal, M., 2005. Watertable monitoring on a beach equipped with a dewatering system: relationship between watertable elevation and beach morphology, preliminary results, Proceedings of the 4<sup>th</sup> IAHR symposium on River, Coastal and Estuarine Morphodynamics, 2005, Illinois, USA, pp. 1-10.
- Larson, M. and Kraus, N.C., 1989. SBEACH: Numerical model for simulating storm-induced beach change. . CERC 89-9, Coastal Engineering Research Centre, USACE, Vicksburg.
- Larson, M., Kubota, S., Erikso, L. (2004). Swash-zone sediment transport and foreshore evolution: field experiments and mathematical modelling. *Marine Geology*; 212, pp. 61-79.
- Larson, M., Sunamura, T., 1993. Laboratory experiment on flow characteristics at a beach step. *Journal of Sedimentary Petrology* 63, 495–500.
- Lewandowski, A., Zeidler, R.B., 1978. Beach ground-water oscillations. In: Proceedings of the 16th Conference on Coastal Engineering, pp. 2051-2065.
- Levoy, F., Anthony, E.J., Monfort, O., Larsonneur, C., 2000. The morphodynamics of megatidal beaches in Normandy, France. *Mar. Geol.* 171, 39–59.
- Li, L., Barry, D.A., Stagnitti, F., Parlange, J.-Y., 2000a. Groundwater waves in a coastal aquifer: a new governing equation including vertical effects and capillarity. *Water Resources Research* 36 (2), 411–420.
- Li, L., Barry, D.A., Stagnitti, F., Parlange, J.-Y., Jeng, D.-S., 2000b. Beach water table fluctuations due to spring-neap tides: moving boundary effects. *Advances in Water Resources* 23, 817–824.
- Li, L., Barry, D.A., Parlange, J.-Y., Pattiaratchi, C.B., 1997a. Beach water table fluctuations due to wave run-up: capillarity effects. *Water Resources Research* 33, 935–945.
- Li, L., Barry, D.A., Pattiaratchi, C.B., Masselink, G., 2001. BeachWin: modelling groundwater effects on swash sediment transport and beach profile changes, *Environmental Modelling & Software*, 17, pp. 313-320.
- Lippmann, T.C., Holman, R.A., Bowen, A.J., 1997. Generation of edge waves in shallow water. *J. Geophys. Res.* 102, 8663– 8679.
- List, J.H., 1991. Wave groupiness variations in the nearshore. *Coast. Eng.* 15, 475– 496.
- Lofquist, K.E.B. 1986. Drag on naturally rippled beds under oscillatory flows, Misc Paper CERC-86-13.
- Longo, S., M. Petti, and I. Losada (2002), Turbulence in the swash and surf zones: A review, *Coastal Eng.*, 45, 129–147.

- Longuet-Higgins, M. S. and R. W. Stewart (1962). Radiation stress and mass transport in gravity waves, with application to 'surf beats. *Journal of Fluid Mechanics*.13: 481-504.
- Longuet-Higgins, M.S., Stewart, R.W., 1964. Radiation stresses in water waves: a physical discussion, with applications. *Deep-Sea Research* 11, 259– 562.
- Longuet-Higgins, M.S., 1974. Breaking waves in deep or shallow water. *Proc. 10th Conf. On Naval Hydrodynamics*, Cambridge, MA, USA, pp. 597–605.
- McArdle, S., McLachlan, A., 1992. Sand beach ecology: swash features relevant to the macrofauna. *J. Coast. Res.* 8 (2), 398– 407.
- Machemehl, J.L., French, T.J., Huang, N.E. (1975). New method for beach erosion control. *Proceedings of Engineering in the Oceans*, ASCE, 142-160.
- Madsen, P.A., Sørensen, H.A., Schaffer, H.A., 1997. Surf zone dynamics simulated by a Boussinesq-type model. Part I. Model description and cross-shore motion of regular waves. *Coastal Eng.* 32, 255–287.
- Madsen, P.A., Svendsen, I.A., 1983. Turbulent bores and hydraulic jumps. *J. Fluid Mech.* 129, 1 –25.
- Makaske, B., Augustinus, P.G.E.F., 1998. Morphologic changes of a micro-tidal, low wave energy beach face during a spring-neap tide cycle, Rhone-Delta, France. *Journal of Coastal Research* 14, 632–645.
- Mansard, E.P.D. and Funke, E.R., 1980. The measurements of incident and reflected wave spectra using a least square method. *Proc. of 17<sup>th</sup> ICCE*, Sydney, 1, 154-172.
- Martin, C S (1970): Effect of a porous sand bed on incipient sediment motion. *Water Resources Res*, Vol 6, No 4, pp 1162-1174.
- Makaske, B., Augustinus, P.G.E.F., 1998. Morphologic changes of a micro-tidal, low wave energy beach face during a springneap tide cycle, Rhone-Delta, France. *Journal of Coastal Research* 14, 632–645.
- Mase, H. (1988), Spectral characteristics of random wave run-up, *Coastal Eng.*, 12, 175–189.
- Mase, H. (1995), Frequency down-shift on swash oscillations compared to incident waves, *J. Hydraul. Res.*, 33, 397–411.
- Massa, D.P. (1999a). Choosing an ultrasonic sensor for proximity or distance measurement, part 1: acoustic considerations. *Sensors*, Vol. 16 (2).
- Massa, D.P., (1999b). Choosing an ultrasonic sensor for proximity or distance measurement, part 2: optimizing sensor selection. *Sensors*, Vol. 16 (3).
- Masselink, G., Hughes, M.G., 1998. Field investigation of sediment transport in the swash zone. *Cont. Shelf Res.* 18, 1179– 1199.
- Masselink, G., Hegge, B.J., Pattiaratchi, C.B., 1997. Beach cusp morphodynamics. *Earth Surf. Processes Landforms* 22, 1139 - 1155.

- Masselink, G., Li, L. (2001). The role of swash infiltration in determining the beach face gradient: a numerical study. *Marine Geology*, 176, pp. 139–156
- Masselink, G., Pattiaratchi, C.B., 2001. Seasonal changes in beach morphology along the sheltered coastline of Perth, western Australia. *Mar. Geol.* 172, 243– 264.
- Masselink, G., Puleo, J. A. 2006. Swash-zone morphodynamics. *Continental Shelf Research* 26, pp. 661-680.
- Masselink, G. and Russell, P., 2006. Flow velocity, sediment transport and morphological change in the swash zone of two contrasting beaches. *Marine Geology*, 227, 227-240.
- Michallet, H., F. Grasso and E. Barthelemy (2007). Long waves and beach profile evolutions. *Journal of Coastal Research*. Special Issue 50: 221-225.
- Miche, R., 1951. Le pouvoir re'fle'chissant des ouvrages maritimes expose's a` l'action de la houle. *Ann. Ponts Chaussees* 121, 285– 319.
- Miles, J.R., Russell, P.E., and Huntley, D.A., 2001. Field measurements of sediment dynamics in front of a seawall. *J. of Coastal Research*, 17(1), 195-206.
- Miller, J.K. and Dean, R.G., 2004. A simple new shoreline change model. *Coastal Engineering*, 51(7): 531-556.
- Morton, R.A., Speed, F.M., 1998. Evaluation of shorelines and legal boundaries controlled by water levels on sandy beaches. *J. Coast. Res.* 14 (4), 1373–1384.
- Munk, W.H., 1949. Surf beats. *Trans. Am. Geophys. Union* 30, 849–854.
- Nelson, C.L. and Miller, R.L., 1974. The Interaction of Fluid and Sediment on the Foreshore. Univ. Chicago, Dep. Geophys. Sci., Fluid Dynamics and Sediment Transport Labor. Tech. Rep., 15, 175 pp.
- Nielsen, P., 1988b. Towards modeling coastal sediment transport. *Coastal Engineering*, Vol. 12, pp 43-62.
- Nielsen, P., 1989. Wave setup and runup: an integrated approach. *Coastal Eng.* 13, 1 – 9.
- Nielsen, P., 1992. Coastal bottom boundary layers and sediment transport. *Advanced Series on Ocean Engineering*, vol. 4. World Scientific, Singapore. 324 pp.
- Nielsen, P., 1999. Groundwater dynamics and salinity in coastal barriers. *J. Coast. Res.* 15 (3), 732– 740.
- Nielsen, P., 2002. Shear stress and sediment transport calculations for swash zone modelling. *Coast. Eng.* 45, 53– 60.
- Nielsen, P., 2009. *Coastal and Estuarine Processes*. World Scientific, 343 pp.
- Nielsen, P., Perrochet, P., 2000b. Errata: Watertable dynamics under capillary fringes: experiments and modelling. *Advances in Water Resources* 23, 907–908.
- Nielsen, P., Turner, I.L., 2000. Groundwater waves and water exchange in beaches. *Proc. 27th Int. Conf. Coastal Eng. ASCE*, New York, pp. 2356–2363.

- Obhrai, C., P. Nielsen, Vincent, C.E. (2002). "Influence of infiltration on suspended sediment under waves." *Coastal Engineering* 45(2): 111-123.
- Ogden, M.R., Weisman, R.N., 1991. Beach stabilization using drains—an experimental model study. In: Kraus, N.C., Gingerich, K.J., Kriebel, D.L. (Eds.), *Coastal Sediments '91*, pp. 1955– 1969.
- Oh, T.-M., Dean, R.G., 1994. Effects of controlled water table on beach profile dynamics. *Proceedings of the 24th International Conference on Coastal Engineering*, 2449– 2460.
- O'Hare, T. J., and D. A. Huntley (1994), Bar formation due to wave groups and associated long waves, *Marine Geology*, 116(3-4), 313-325.
- Oldenziel, D.M., Brink, W.E., 1974. Influence of suction and blowing on entrainment of sand particles. *Journal of the Hydraulics Division, ASCE* 100, pp. 935– 949.
- Oltman-Shay, J., Guza, R.T., 1987. Infragravity edge wave observations on two California beaches. *J. Phys. Oceanogr.* 17, 644– 663.
- Osborne, P.D. and Greenwood, B., 1992. Frequency-dependent cross-shore suspended sediment transport .2. A barred shoreface. *Marine Geology*, 106(1-2): 25-51.
- Osborne, P.D. and Rooker, G.A., 1997. Surf zone and swash zone sediment dynamics on high energy beaches: West Auckland, New Zealand. *Proceedings Coastal Dynamics, ASCE*, pp. 814–823.
- Osborne, P.D., Rooker, G.A., 1999. Sand resuspension events in a high energy infragravity swash zone. *Journal of Coastal Research* 15 (1), 74–86.
- Otvos, E.G., 1965. Sedimentation – erosion cycles of single tidal periods on Long Island Sound beaches. *Journal of Sedimentary Petrology* 35, 604– 609.
- Packwood, A.R., 1983. The influence of beach porosity on wave uprush and backwash. *Coastal Engineering* 7, 29–40.
- Plant, N. G., K. T. Holland, J. A. Puleo and E. L. Gallagher (2004). Prediction skill of nearshore profile evolution models. *Journal of Geophysical Research*. 109, C01006.
- Plant, N.G., Holman, R.A., Freilich, M.H. and Birkemeier, W.A., 1999. A simple model for interannual sandbar behavior. *Journal of Geophysical Research-Oceans*, 104(C7): 15755-15776.
- Peregrine, D. (1972), Equations for water waves and the approximations behind them, in *Waves on Beaches and the Resulting Sediment Transport*, edited by R. Meyer, pp. 95–121, Academic, New York.
- Peregrine, D. (1974), Surface shear waves, *J. Hydraul. Div. Am. Soc. Civ. Eng.*, 100(HY9), 1215–1227.
- Peregrine, D. H. 1983 Breaking waves on beaches. *A. Rev. Fluid Mech.* 15, 149-178.
- Peregrine, D., and S. Williams (2001), Swash overtopping a truncated plane beach, *J. Fluid Mech.*, 440, 391–399.

- Petti, M., and S. Longo (2001), Turbulence experiments in the swash zone, *Coastal Eng.*, 43, 1–24.
- Price, M., 1985. *Introducing Groundwater*. George Allen & Unwin, London.
- Pritchard, D., and A. Hogg (2005), On the transport of suspended sediment by a swash event on a plane beach, *Coastal Eng.*, 52, 1–23
- Power, H.E., Hughes, M.G., Aagaard, T. and Baldock, T.E., 2010. Nearshore wave height variation in unsaturated surf. *J. Geophys. Res.*, 115(C8): C08030.
- Puleo, J.A., Holland, K.T., 2001. Estimating swash zone friction coefficients on a sandy beach. *Coastal Engineering* 43, 25–40.
- Puleo, J.A., Beach, R.A., Holman, R.A., Allen, J.S., 2000. Swash zone sediment suspension and transport and the importance of bore-generated turbulence. *Journal of Geophysical Research* 105, 17021–17044.
- Puleo, J.A., Slinn, D.N., Holland, K.T., Smith, E. and Webb, B.M., 2002. Numerical modelling of swash zone hydrodynamics. *Proceedings 28th International Conference on Coastal Engineering*, ASCE, pp. 968–979.
- Puleo, J.A., Holland, K.T., Plant, N., Slinn, D.N., Hanes, D.M., 2003. Fluid acceleration effects on suspended sediment transport in the swash zone. *Journal of Geophysical Research* 108, 3350.
- Quick, M.C., 1991. Onshore–offshore sediment transport on beaches. *Coastal Engineering* 15, 313–332.
- Ramamonjiarisoa, A. and Mollo-Christensen, E. 1979 Modulation characteristics of sea surface waves. *J. Geophys. Res.* 84, 7769–7775.
- Ranasinghe, R., Symonds, G., Black, K., Holman, R., 2004. Morphodynamics of intermediate beaches: a video imaging and numerical modelling study. *Coast. Eng.* 51, 629–655.
- Ranieri, G. (2005). Studio sperimentale degli effetti del drenaggio della watertable sul processo erosivo del profilo di spiaggia. *Ingegneria del Agua*, 12 (2).
- Rapp, R.J., Melville, W.K., 1990. Laboratory measurements for deep water breaking waves. *Philos. Trans. R. Soc. Lond., A* 331, 735–800.
- Reis, A. H., Gama. C., 2010. Sand size versus beachface slope — An explanation based on the Constructal Law. *Geomorphology* 114 (2010) 276–283
- Raubenheimer, B., R.T. Guza, S. Elgar, and N. Kobayashi, Swash on a gently sloping beach, *J. Geophys. Res.*, 100, 8751–8760, 1995.
- Raubenheimer, B., Guza, R.T., 1996. Observations and predictions of run-up. *J. Geophys. Res.* 101, 25575– 25587.
- Raubenheimer, B., 2002. Observations and predictions of fluid velocities in the surf and swash zones. *Journal of Geophysical Research*, 107.

- Robinson, C., Gibbes, B., Li, L., 2006. Driving mechanisms for groundwater flow and salt transport in a subterranean estuary, *Geophys. Res. Lett.*, 33, pp. L03402.
- Roelvink, J. A. (1993). Surf Beat and Its Effect on Cross-Shore Profiles. PhD Thesis, TU Delft, Netherlands: 116p.
- Roelvink, J. A. and M. J. F. Stive (1989). Bar-generating cross-shore flow mechanisms on a beach. *Journal of Geophysical Research*. 94(C\_E4): 4785-800.
- Roos, A., Battjes, J.A., 1994. Characteristics of flow in run-up of periodic waves. *Proc. 15th Intl. Conf. Coastal Eng. - ASCE 1*, pp. 781– 795.
- Ruessink, B. G., and Y. Kuriyama (2008), Numerical predictability experiments of cross-shore sandbar migration, *Geophys. Res. Lett.* 35, L01603, doi: 10.1029/2007GL032530.
- Ruessink, B.G., Houwman, K.T. and Hoekstra, P., 1998. The systematic contribution of transporting mechanisms to the cross-shore sediment transport in water depths of 3 to 9 m. *Marine Geology*, 152(4): 295-324.
- Sallenger, A.H., Richmond, B.M. (1984). High-frequency sediment level oscillations in the swash zone. *Marine Geology*, 60, pp. 155-164.
- Savitzky, A., Golay, M.J.E. (1964). Smoothing and differentiation of data by simplified least squares procedures. *Analytical Chemistry*, 36 (8), pp. 1627-1639.
- Sato, S., 1992. Sand transport under grouping waves, *Proc. International Conf. Coastal Engineering*. ASCE, pp. 2411-2423.
- Schaffer, H.A., 1993. Infragravity waves induced by short wave groups. *J. Fluid Mech.* 247, 551–588.
- Schlichting, H., 1979. *Boundary Layer Theory*, McGraw-Hill, New York, USA, 7th edition.
- Schoones, J.S., Theron, A.K., 1995. Evaluation of ten cross-shore sediment transport oblique morphological models. *Coastal Engineering* 25, 1 –41.
- Schwartz, M.L., 1967. Littoral zone tidal-cycle sedimentation. *Journal of Sedimentary Petrology* 37 (2), 677–683.
- Seymour, R.J., 1986. Results of cross-shore transport experiments. *Journal of the Waterway, Port, Coastal and Ocean Division, ASCE* 112 (WW1), 168– 173.
- Shah, A.M., Kamphuis, J.W., 1996. The swash zone: a focus on low frequency motion. *Proceedings of the 25th International Conference on Coastal Engineering*, pp. 1431–1442.
- Shen, M., and R. Meyer (1963), Climb of a bore on a beach part 3. Run-up, *J. Fluid Mech.*, 16, 13–125.
- Sherman, D.J., Short, A.D., Takeda, I., 1993. Sediment mixingdepth and bedform migration in rip channels. *J. Coastal Res., Spec. Iss.* 15. 39948.
- Sherman, D.J., Lyons, W., 1994. Beach-state controls on Aeolian sand delivery to coastal dunes. *Physical Geography* 15, 381–395.

- Sherman, D.J., Jackson, D.W.T., Namikas, S.L., Wang, J.K., 1998. Wind-blown sand on beaches: an evaluation of models. *Geomorphology* 22, 113– 133.
- Shields, A., 1936. Anwendung der Ähnlichkeitsmechanik und Turbulenzforschung auf die Geschiebebewegung. Mitt Preuss Versuchsanstalt für Wasserbau und Schiffbau, No 26, Berlin.
- Short, A.D., 1991. Macro–meso tidal beach morphodynamics—an overview. *Journal of Coastal Research* 7 (2), 417– 436.
- Strahler, A.N., 1966. Tidal cycle of changes in an equilibrium beach, Sandy Hook, New Jersey. *Journal of Geology* 74, 247– 268.
- Shi, N. C. and L. H. Larsen (1984). Reverse sediment transport induced by amplitude modulated waves. *Marine Geology*. 54: 181-200.
- Short, A. J. (1975). Multiple offshore bars and standing waves. *Journal of Geophysical Research*. 80: 3838-3840.
- Sonu, C.J., van Beek, J.L., 1971. Systematic beach changes on the Outer Banks, North Carolina. *Journal of Geology* 79, 416–425.
- Sonu, C.J., James, W.R., 1973. A Markov model for beach profile changes. *Journal of Geophysical Research* 78, 1462–1471.
- Stive, M.J.F., 1980. Velocity and pressure field of spilling breakers. Proc. 17th Int. Conf. Coastal Eng., ASCE, pp. 547– 566.
- Sunamara, T., 1984. Quantitative prediction of beach-face slopes. *Geological Society of America Bulletin*, 95: 242-245.
- Svendsen, I.A., 1984. Mass flux and undertow in a surf zone. *Coastal Engineering*, 8(4): 347-365.
- Symonds, G., D. A. Huntley and A. J. Bowen (1982). Two-dimensional surf beat: long wave generation by a time-varying breakpoint. *Journal of Geophysical Research*. 87: 492-498.
- Symonds, G. and Bowen, A.J., 1984. Interactions of nearshore bars with incoming wave groups. *Journal of Geophysical Research-Oceans*, 89(NC2): 1953-1959.
- Stockdon, H., R. Holman, P. Howd, and A. J. Sallenger (2006), Empirical parameterization of setup, swash, and runup, *Coastal Eng.*, 53, 573–588.
- Svendsen, I.A., Putrevu, U., 1996. Surf zone hydrodynamics. In: Liu, P.L.-F. (Ed.), *Advances in Coastal and Ocean Engineering*. World Scientific, pp. 1 –78.
- Suhayda, J.N., 1974. Standing waves on beaches. *J. Geophys. Res.* 79, 3065–3071.
- Thornton, E.B., Humiston, R.T., and Birkemeier, W., 1996. Bar/ trough generation on a natural beach. *J. Geophys. Res.*, 101, 12097-12110.
- Ting, F.C.K., 2002. Laboratory study of wave and turbulence characteristics in narrow-band irregular breaking waves. *Coastal Engineering*, 46(4): 291-313.

- Ting, F.C.K. and Kirby, J.T., 1995. Dynamics of surf-zone turbulence in a strong plunging breaker. *Coastal Engineering*, 24(3-4): 177-204.
- Ting, F.C.K., Kirby, J.T., 1996. Dynamics of surf-zone turbulence in a spilling breaker. *Coast. Eng.* 27, 131– 160.
- Tucker, M.J., 1950. Surf beats: sea waves of 1 to 5 min. period. *Proc. R. Soc. London, Ser. A* 202, 565–573.
- Turner, I.L., 1993a. The total water content of sandy beaches. *Journal of Coastal Research Special Issue* 15, 11– 26.
- Turner, I.L., 1993b. Water table outcropping on macro-tidal beaches: a simulation model. *Marine Geology* 115, 227–238.
- Turner, I.L., 1993c. Beach face permeability, the groundwater effluent zone, and intertidal profiles of macro-tidal beaches: a conceptual model. In: Thomas, M. (Ed.), *Catchments and coasts of eastern Australia*. Department of Geography, University of Sydney Monograph Series, vol. 5, 88– 99.
- Turner, I.L., 1995a. Simulating the influence of groundwater seepage on sediment transported by the sweep of the swash zone across the intertidal profile of macrotidal beaches. *Marine Geology* 125, 153–174.
- Turner, I.L., 1995b. Simulating the time-varying extent of groundwater seepage on tidal beaches. *Software and Technical Bulletin, Earth Surface Processes and Landforms* 20, 833–843.
- Turner, I.L., 1998. Monitoring groundwater dynamics in the littoral zone at seasonal, storm, tide and swash frequencies. *Coastal Engineering* 35, 1 – 16.
- Turner, I.L., Leatherman, S.P. (1997). Beach Dewatering as a ‘Soft’ Engineering Solution to Coastal Erosion-A History and Critical Review. *Journal of Coastal Research*, 13 (4), 1050-1063.
- Turner, I.L., Nielsen, P., 1997, Rapid water table fluctuations within the beach face: Implications for swash zone sediment mobility?, *Coastal Engineering*, 32, pp. 45-59.
- Turner, I., Masselink, G., 1998, Swash infiltration-exfiltration and sediment transport. *J. Geophys. Res.*, 103, pp. 13-24.
- Turner, I.L., Russell, P.E., Butt, T. (2008). Measurement of wave-by-wave bed-levels in the swash zone. *Coastal Engineering*, 55, pp. 1237-1242..
- Turcotte, D.L., 1960. A sublayer theory for fluid injection into the incompressible turbulent boundary layer. *J. Aerospace Sci.*, 27(9): 675-678.
- Uchiyama, Y. and Kawahara, T.: *Wave Motion* 20 (1994) 99

- Van Wellen, E., Baldock, T. E., Chadwick, A. J. and Simmonds, D., 2000. STRAND – a model for longshore sediment transport in the swash zone. Proc. 27th Int. Conf. Coastal Eng, Sydney, June 2000, 3139-3150.
- Van Wellen, E., Chadwick, A.J., Mason, T., 2000. A review and assessment of longshore sediment transport equations for coarsegrained beaches. Coastal Engineering 40 (3), 243–275.
- Vesterby, H. (1991). Coastal drain system: a new approach to coastal restoration, Proceedings of GEO-Coast '91, 651-654.
- Vesterby, H. (1994). Beach face dewatering-the European experience. Alternative Technologies in Beach Preservation. Proceedings of the 1994 National Conference on Beach Preservation Technology, 53-68.
- Vesterby, H. (2000). Modelling groundwater flow in beach profiles for optimising stabilising measures. Int. Coastal Symp. Rotorua NZ, 1–7.
- Vicinanza, D., Baldock, T. E., Contestabile, P., Alsina, J., Cáceres, I., Brocchini, M., Conley, D., Andersen, T. L., Frigaard, P., Ciavola, P. (2010). "Swash Zone Response Under Grouping Storm Conditions", Journal of Hydraulic Research, ISSN 0022-1686 (under review).
- Vicinanza, D., Ciavola, P., Biagi, S. (2009). Field experiment to control coastline subsidence: a unique case study at Lido Adriano (Italy)., Journal of Coastal Research, SI 56, pp. 1105-1109.
- Vicinanza, D., Contestabile, P., Power, H., Alsina, J., Cáceres, I. 2009. Swash zone response Under grouping Storm Conditions (SUSCO), Internal Report EC contract no. 022441 (RII3), HYIII-WAVELAB-6, Canal d'Investigació i Experimentació Marítima (CIEM).
- Vicinanza, D., Contestabile P., Baldock T., Power H., Cáceres I., Alsina J., Brocchini M., Postacchini M., Conley D., Lykke Andersen T., Frigaard P., Ciavola P. 2010. Large-scale experiments on the Swash zone response under grouping storm conditions. Proceedings of the Hydralab III Joint User Meeting, Hannover, Germany.
- Vicinanza, D., Guida, A., Ferrante, V., Ciavola, P. (2010). Performance of a Beach Drainage System at Chiaiolella Beach (Procida Island, Italy). Journal of Coastal Research, in press.
- Voulgaris, G., Collins, M.B., 2000. Sediment resuspension on beaches: response to breaking waves. Marine Geology 167, 167–187.
- Waddell, E., 1976. Swash–groundwater– beach profile interactions. In: Davis, R.A., Etherington, R.L. (Eds.), Beach and Nearshore Sedimentation. Society of Economic and Paleontological Mineralogists Special Publication, 24, pp. 115– 125.
- Watson, G., Peregrine, D.H., Toro, E.F., 1992. Numerical solution of the shallow-water equations on a beach using the weighted average flux method. In: Hirsh, Ch., et al. (Eds.), Computational Fluid Dynamics '92, vol. 1. Elsevier, Amsterdam.

- Watson, G., Barnes, T.C.D., Peregrine, D.H., 1994. The generation of low frequency waves by a single wave group incident on a beach. *Proc. 24th Intl. Conf. Coast. Engng. - ASCE* 1, pp. 776– 790.
- Weir, F.M., Hughes, M.G. and Baldock, T.E., 2006. Beach face and berm morphodynamics fronting a coastal lagoon. *Geomorphology*, 82(3-4): 331-346.
- Werner, A.D., Lockington, D.A., 2003. Influence of hysteresis on tidal capillary fringe dynamics in a well-sorted sand *Advances in Water Resources* 26 (11), 1199–1204.
- Wijnberg, K.M., Kroon, A., 2002. Barred beaches. *Geomorphology* 48, 103–120.
- Whitham, G. (1958), On the propagation of shock waves through regions of non-uniform area or flow, *J. Fluid Mech.*, 4, 337–360.
- Wright, L.D., Short, A.D., 1983. Morphodynamics of beaches and surf zones in Australia. In: Komar, P.D. (Ed.), *Handbook of Coastal Processes and Erosion*. CRC Press, Boca Raton, FL, pp. 35– 64.
- Wright, L.D., Short, A.D., 1984. Morphodynamic variability of surf zones and beaches: a synthesis. *Mar. Geol.* 56, 93– 118.
- Wright, L.D., Short, A.D. and Green, M.O., 1985. Short-term changes in the morphodynamic states of beaches and surf zones: An empirical predictive model. *Marine Geology*, 62(3-4): 339-364.
- Wright, L.D., Short, A.D., Boon III, J.D., Hayden, B., Kimball, S., List, J.H., 1987. The morphodynamic effects of incident wave groupiness and tide range on an energetic beach. *Mar. Geol.* 74, 1 –20.
- Yates, M.L., Guza, R.T. and O'Reilly, W.C., 2009. Equilibrium shoreline response: Observations and modeling. *Journal of Geophysical Research-Oceans*, 114: 16.
- Yeh, H.H., Ghazali, A., 1988. On bore collapse. *J. Geophys. Res.*96, 6930– 6936.
- Yeh, H.H., Ghazali, A., Marton, I., 1989. Experimental study of bore run-up. *J. Fluid Mech.* 206, 563– 578.
- Yu, X., Hsu, T.J. and Hanes, D.M., 2010. Sediment transport under wave groups: Relative importance between nonlinear waveshape and nonlinear boundary layer streaming. *Journal of Geophysical Research-Oceans*, 115: 18.
- Yu, J . amd Mei, C. C. 2000 Formation of sand bars under surface waves. *J. Fluid Mech.* 416, 315-348.